UNIVERSITÀ
DEGLI STUDI
DI PADOVA

Sede Amministrativa: Università degli Studi di Padova

Dipartimento di Scienze Chimiche

---

CORSO DI DOTTORATO DI RICERCA IN: SCIENZE MOLECOLARI
CURRICOLO: SCIENZE CHIMICHE
CICLO XXXV

# Bio-inspired foldamers: from catalysis to supramolecular applications

**Coordinatore:** Ch.mo Prof. Leonard Prins
**Supervisore**: Ch.mo Prof. Alessandro Moretto

**Dottorando** : Matteo Pollastrini

# Index

# Abstract

This thesis focuses on the uses of organized foldamers for the development of interisting catalytic activities. To this aim, a set of different procedures were taken in account and developed by chemical and supramolecular approaches.

## Light mediated catalytic activity in a foldamer mimic of proteases

The design of synthetic equivalents of hydrolytic enzymes in both activity and range of chemical transformations continues to be a major challenge. A foldamer-based catalyst is reported as an attractive alternative to the well-developed strategies involving small molecules or conventional peptides. A catalytic foldamer was developed in which a fumaramide chromophore links a Ser residue to a helical domain that contains within its sequence the residues His and Asp. Photoisomerization of the fumaramide chromophore (with *E* geometry) to the corresponding maleamide (with *Z* geometry) brings together a "catalytic triad" of Ser, His, and Asp. A detailed conformational study confirmed the helical conformation of the foldamer and the formation of a contact between the two peptide segments. The ability of the foldamer to catalyse the hydrolysis of ester substrates versus control peptides was evaluated and revealed that the fumaramide/maleamide linker thus acts as a light-sensitive switchable cofactor for the in-situ assembly of the catalytic triad of reactive side chains, enabling the photo-control of catalytic activity in short foldamers.

## Helical peptide foldamers with three dimensional catalytic centres

A reductive amination approach is reported for the assembly of helical catalytic peptide foldamers containing a -$CH_2$-NH- moiety as replacement of one peptide bond. A detailed ECD, NMR and crystallographic conformational study was performed on (L-Ala-Aib)-based foldamers of increasing length. Over a certain length, the -$CH_2$-NH- moiety is compatible with a fully developed $3_{10}/\alpha$-helical conformation. This reductive amination approach was then used to synthesize a set of peptide foldamers built principally from Aib residues, containing a primary amine and another possible reactive group in proximity of the new-formed secondary amine for the creation of catalytic triads. The foldamers were tested in the catalysis of C-C bond macrocyclization of a linear dialdehyde precursor, mediated by primary/secondary amine via imine-enamine chemistry. The high efficiency

of the system can be related to the rigid foldamer conformation, which allows spatial control of the relative positioning of the catalytic diads and triads.

## A set of multivalent catalysts from a single peptide sequence inspired by hydrolytic enzymes

Various approaches to the synthesis of multivalent hydrolytic catalysts were explored starting from a common peptide sequence containing a "catalytic triad" of Ser, His, and Asp.

In a first attempt, the incorporation of a versatile 1,3-dimercaptobenzene core to the peptide sequence was essential to the exploration of dynamic combinatorial libraries to obtain a multivalent catalytic foldamer. Interestingly, the formation of a 16-mer foldamer containing the triad was observed, while the effect of (L-Ala-Aib)$_4$ ordered domains on the composition of the library was also explored. In a second attempt, we investigated the synthesis of silver nanoparticles with a modified *p*-mercaptobenzoic acid as ligands to exploit the spatial organization of the ligands in these systems. The change in the nature of the ligand was shown to affect the optical properties of the nanoparticles, but various elements suggest a successful synthesis. As the last attempt, we investigated an amphiphilic N-teminal lipidated tetratrapeptide that was able to self-assemble producing a hydrogel with very low concentration of organogelator. The systems obtained with these approaches were compared in the hydrolysis of an activated ester substrate and revealed that silver nanoparticles containing peptide ligands are a promising approach in the development of multivalent peptide-based catalytic systems.

## Self- and co-assembly of amphiphilic peptide foldamers

The possibility to create self-assembled microstructures with different characteristics and shapes from (L-Ala-Aib)$_4$ based foldamers was explored. A set of amphiphilic peptides were synthesized characterized by polar heads and a common domain which consists in a helicoidal spacer made of an -(L-Ala-Aib)$_4$-octapeptide and N-terminal lipophilic tail. The peptides were able to self-assemble producing different structures, from fibres to liposomal-like structures, depending on the nature of the heads. Co-assembly studies suggested highly efficient recognition phenomena between peptides with different binding heads.

# Abbreviations

Ac = acetyl

$Ac_2O$ = acetic anhydride

AcOH = acetic acid

Aib = α-amino*iso*butyric acid

Ala = Alanine

AgNPs = silver nanoparticles

Arg = Arginine

Asp = Aspartic acid

Bn = benzyl

Boc = *tert*-butyloxycarbonyl

$Boc_2O$ = di-*tert*-butyl dicarbonate

CC = coiled coil

CD = cyclodextrin

COSY = COrrelation SpectroscopY

CTAB = cetyl trimethyl ammonium bromide

Cy = cyclohexyl

CyPA = cyclophilin A

Cys = cysteine

Dap = 2,3-Diaminopropionic Acid

DBU = 1,8-diazabicyclo[5.4.0]undec-7-ene

DCL = dynamic combinatorial library

DCM = dichloromethane

DIC = N,N'-di*iso*propylcarbodiimide

DIPEA = N,N-di*iso*propylethylamine

DMAP = 4-dimethylaminopyridine

DMBA = 3,5-dimercaptobenzoic acid

DMF = N,N-dimethylformamide

DMSO = dimethylsulphoxyde

ECD= electronic circular dichroism

EDC = N-ethyl-N'-(3-dimethylamino)propyl-carbodiimide

ESI = electrospray ionization

Et = ethyl

$Et_2O$ = diethyl ether

EtOH = ethanol

Fmoc = (9*H*-fluoren-9-yl)methoxycarbonyl

FDA = fluorescein diacetate

FT-IR = Fourier transform infrared spectroscopy

FUM = fumaramide

GFP = green fluorescent protein

Glu = Glutamic acid

Gly = Glycine

HATU = *O*-(7-aza-1,2,3-benzotriazol-1-yl)-N,N,N',N'-tetramethyluronium hexafluorophosphate

HFIP = 1,1,1,3,3,3-hexafluoro-2-propanol

His = histidine

HOAt = 1-hydroxy-7-azabenzotriazol

HPLC = high performance liquid chromatography

Leu = Leucine

Lys = Lysine

MAL = maleamide

MALDI = Matrix-Assisted Laser Desorption/Ionization

# Abbreviations

*p*-MBA= *p*-mercaptobenzoic acid

*p*-NPA = 4-Nitrophenyl acetate

*p*-NPB = 4-Nitrophenyl butyrate

Me = methyl

MeOH = methanol

NCA = *N*-carboxyanhydride

NMR = nuclear magnetic resonance

NOESY = nuclear Overhauser effect spectroscopy

OMe = methoxy

O*t*Bu = *tert*-butoxy

Phe = phenylalanine

Pro = Proline

ROESY = rotating frame Overhauser enhancement spectroscopy

Ser = serine

SPPS = solid phase peptide synthesis

TEA = trimethylamine

TEM = transmission electron microscopy

tBu = *tert*-butyl

TFA = trifluoro acetyl

TGA = thermogravimetric analysis

THF = tetrahydrofuran

TIS = triisopropylsilane

TOF = time-of-flight

Tyr = Tyrosine

Trt = triphenylmethyl

UV-Vis = ultraviolet-visible spectroscopy

Val = valine

Z = benzyloxycarbonyl

# Project aims

The main purpose of this Ph.D. project is the development of new sets of foldamers, built on chemically modified peptides, and their application in organocatalysis pursuing different chemical and supramolecular approaches to enable their catalytic activity.

In recent years, foldamers, oligomers with a strong tendency to adopt a specific conformation in solution, have found applications in various scientific areas from the generation of self-assembled structures to the development of enzyme mimics. In this context, conformationally restrained peptides may offer attractive features related to their ability to fold into defined helical conformations and their ease of functionalization. Moreover, amphiphilic peptides offer an attractive scaffold for the fabrication of new supramolecular architectures, due to their modular nature and simple structure.

Applications therefore will explore (i) assembly of catalytic sites in helical foldamers, (ii) multivalent catalysts, (iii) self-assembly.

(i) Assembly of catalytic sites in helical foldamers. A central paradigm in enzymology is the relationship between the functions of enzymes and their three-dimensional structure. In this work, we will explore the use of a stimulus-controlled catalytic foldamer system. We want to explore the possibility to synthetize a catalytic helical foldamer in which the photo-isomerization of a fumaramide linker assembles a "catalytic triad" and triggers esterase activity. The fumaramide/maleamide linker thus acts as a light-sensitive switchable cofactor for activation of catalytic activity in short foldamers (Chapter 2).

Additionally, a methodology for the synthesis of mixed amine/amide foldameric systems will be investigated. This approach will be then used for the construction of catalytic diads and triads in a set of helical peptide foldamers for the catalysis of a, difficult to achieve, C-C bond macrocyclization (Chapter 3).

(ii) Multivalent catalysts. The building up of the contributions of several weakly binding units into a strong binding is a process well-exploited by natural systems. With the aim of employing multivalency in peptide catalytic systems, we will explore various peptide based

multivalent catalysts featuring a common "catalytic triad" and their efficiency in the hydrolysis of activated esters (Chapter 4).

(iii) Self-assembly. Supramolecular catalysis has become a field subject to numerous investigations in recent years. With the aim of finding a modular platform for the development of supramolecular catalysts, we want to explore the possibility of a modular approach to the synthesis of peptide amphiphiles. For this purpose, we will study the self- and co-assembly behaviour of peptide amphiphiles .characterized by polar heads, a common helical domain with alternating α-aminoisobutyric acid (Aib) and L-Ala residues, and a N-terminal lipophilic tail (Chapter 5). We thought that the study of this model system could guide the future development of supramolecular catalytic systems through the insertion of prosthetic polar heads able to exert a catalytic function.

The results in this thesis were obtained by combining knowledge of organic synthesis and supramolecular chemistry, and I was responsible for the synthetic design, the synthesis, and the characterization of all the studied compounds, guided by my Ph.D. supervisor, Prof. Alessandro Moretto.

All the work wouldn't have been possible without the collaboration and the efforts of other people, with whom I worked, and which have helped me for the completion of this Ph.D. thesis. In particular, all the X-Ray diffraction structures reported have been resolved by Dott. Marco Crisma and Dott. Marzio Rancan.

# 1. Introduction

The close relationship between chemical structures and macromolecular properties of biopolymers is one of the most important mechanisms of Nature to manifest itself.

In Nature, the folding of long polypeptide chains provides the 3D globular morphologies of proteins, and this allow proteins to display explicit chemical functions. Proteins continually reconfigure their shape, and consequently their function, under the supervisory of specific molecular interactions that sense, process and transmit informations from the surrounding environment to the proteins. The study and development of biomimetic chemistry and materials is of great impact in the development of new drugs and materials for bio-medical application, as well as new catalytic systems.

## 1.1 Self- and co-assembly of amphiphilic peptides

The tendency of natural peptides and proteins to achieve hierarchical complexity has inspired the development of synthetic peptide systems that similarly achieve hierarchical morphologies.

Peptides are popular building blocks for the design of functional nanostructures given their modular and programmable nature, their conformational and functional diversity, and ease of preparation through well-established methods. Peptide materials can also be highly biocompatible and biodegradable, given the nature of their building blocks. Most notably, the self-assembly of peptides with various conformations and at different length scales can generate a variety of ordered structures such as nanospheres, nanotubes, nanofibrils, nanotapes, fiber bundles and others.[1–3]

An important goal is to achieve structurally complex assemblies from short peptide building blocks. Thus, controlling interactions among primary assemblies of homogeneous short peptide systems has been proven useful in programming the assembly of hierarchical structures. Yet, we need a better understanding of how intermolecular interactions among peptides within the assemblies affect superstructure formation. This can help to explain the complex assembly of proteins and to direct the design of synthetic peptide systems. The cooperative action of various non-covalent interactions is essential to determine a thermodynamically stable supramolecular structure. The most common types of non-covalent interactions involved in peptide self-assembly are hydrogen-bonding, $\pi-\pi$, electrostatic, hydrophobic, and van der Waals interactions. Amide groups of the peptide backbone

and amino and carboxyl groups of the sidechains provide several H-bond donor and acceptor groups. The strength of this directional interaction has a varied range, and it is mainly 5–10 $kT$ (~10–40 kJ $mol^{-1}$) per bond. H-bonding is probably the most ubiquitous and important non-covalent interaction in peptide self-assembly and can induce the conversion of peptides into diverse 1-dimensional (1-D), 2-D, and 3-D nanostructures.

$\pi-\pi$ interactions are important in the self-assembly of aromatic peptides and, depending on the environment, their strength can be changed by two to three times (~2-50 kJ $mol^{-1}$).

Electrostatic interactions based on Coulombic forces are relative strong if compared to H-bonds ([ion-ion (~100-350 kJ $mol^{-1}$), ion-dipole (~50-200 kJ $mol^{-1}$), dipole-dipole (~5-50 kJ $mol^{-1}$)]). Electrostatic interactions are usually employed to induce specificity between different charged self-assembling peptides.

The hydrophobic effect is one of the main driving forces for the association of amphipathic molecules in water. Despite the attractive force-like effects, the hydrophobic effect is an umbrella term that describes a series of self-sorting phenomena: it depends on the inability of the solvent to make sufficiently strong interactions with a solute, resulting in self-association of water molecules (and non-polar solutes consequently also self-associate, forming aggregates).[4-6]

Van der Waals forces arise from fluctuations in the electron density of the molecules and are ubiquitous. They are nondirectional and of relatively weak intensity ($< 5$ kJ $mol^{-1}$). Van der Waals forces provide important contributions to other non-covalent interactions, but their nature hinder their use as a driving force in the in the self-assembly process.

One of the most employed recognition motifs for peptide self-assembly is the Phe-Phe zipper. Key motif of the Alzheimer's β-amyloid polypeptide, Phe-Phe promotes self-assembly mainly through highly organized $\pi$-$\pi$ stacking and Phe-Phe-inspired peptides have been engineered to form several complex nanostructures.[1,2,7–9]

An additional example of peptide-based supramolecular architecture is given by amphipathic peptides. These peptides are made by alternating hydrophobic and hydrophilic amino acid residues

that possess strong propensities to form β-sheets. The sequence displays hydrophilic and hydrophobic sides that can further assemble into fibrillar structures.

A broad class of peptide amphiphile (PA) molecules consists of a peptide sequence conjugated to a fatty acid that in aqueous solution has been proved to self-assemble into nanoscale filamentous assemblies. These systems can be programmed to form nanofibers that mimic extracellular filaments and have emerged as a promising biomaterials platform for regenerative medicine therapies.[10–14]

Dynamics within these assemblies depend partly on hydrogen bonding among PA molecules, and the addition of strongly cohesive $\beta$-sheet forming peptide sequences adjacent to the hydrophobic segment can further slow internal motion. Improved solubility, responsiveness to environmental changes and tailored function can be added with short sequences of charged amino acids and peptide epitopes following the hydrophobic peptide portion. A short spacer is usually employed between the epitope and the rest of the molecule to limit possible negative effects on the assembly behaviour of PA molecules and to improve the epitope availability.[15]

Multicomponent peptide supramolecular co-assembly is recently emerging as a promising broad approach able to further expand the conformational space of peptide assemblies in terms of structural and functional complexity.

## 1.2 Catalytic foldamers

Chemists have synthesized countless compounds to achieve "biomimetic chemistry", taking various inspiration from biological molecules and mimicking, in some way, both structure and function. Function may span from binding, recognition interactions, and specificity to the unparalleled ability of enzymes to catalyse chemical reactions.

In the context of chemical catalysis, many types of enzymes mimics have been developed to overcome the limitation of natural systems, such as instability under non-physiological environment and narrow substrate scope, while retaining their proficiency. To this date, powerful and competent catalysts for many reactions have arisen from a reductionist approach in constructing catalytic sites.

## Catalytic foldamers

Short artificial peptides sequences have been proven to be reliable catalysts and helped to shed light on to the mechanistic features of effective organocatalysts, often shared between enzymes and synthetic catalysts.[16–19]

Like enzymes, short peptides catalysts are modular in nature and exploit sequences of simple building blocks to access high structural and functional diversity. Noncovalent interactions are fundamental in the creation of folded three-dimensional structures, displaying arrays of functional groups for cooperative and selective substrate activation. These characteristics have made short peptides well-suited to enable novel, multifunctional and asymmetric catalysis. However, short peptides usually adopt an ensemble of conformations in solution being conformationally dynamic if not inherently flexible. Dynamic and cooperative noncovalent interactions could be beneficial in a catalyst: in recent years, flexible peptide catalysts are under study due to their potential ability to maximize these interactions and operate in an induced-fit-type manner.[20] However, peptide flexibility can also hinder catalytic efficiency.

For instance, enzymatic catalysis often depends on the close relationship between structure and function: the folding of the polypeptide chains allows the proper spatial organization of functional groups and the creation of an active site within the folded topology. Tight control of folding propensity also encodes functionally important dynamics, such as cooperative motions to form catalytic pockets.[21,22]

Among the chemical approaches developed over the last years, the foldamer-based approach for catalyst development represents an attractive alternative to those involving small molecules or conventional peptides.[23,24] Foldamers are synthetic short oligomers with the strong tendency to adopt a defined conformation in solution, i.e., non-natural conformationally defined mimics of proteins and other biopolymers.[25] Oligomeric structures possess manifold degrees of freedom, and their conformational space could in principle comprise several conformations. On the other hand, numerous factors are known to play a role in the narrowing of the conformational space of short linear strands: solvophobic effects, local conformation restrictions, specific interactions between oligomer functionalities (e.g., periodic H-bond networks) and combinations of the three.[26] Unnatural monomers

and backbones have been studied and their conformational preference have been used to create helical scaffolds, as well as turns and strand-like conformations.[27,28]

The exploration of new moieties and new geometries for set of reactive side chains is enabled by the modular nature of foldamers at the covalent level. Exploring the capabilities of predictable secondary structures that are very stable at short lengths as scaffolds for multifunctional catalysis represents a first step toward the development of larger foldamers, discrete tertiary structures and the approach of enzyme-like reactivities.

### 1.2.1 Secondary structures of catalytic foldamers

As previously mentioned, most of the investigated foldamer scaffolds possess helical secondary structures and the relationship between helix parameters and monomer identity are well established. Formation of stable and regular helical structure in $\alpha$-peptides is usually maintained by intermolecular C=O···HN H-bonds between non-adjacent residues. The most common helical structures among helical $\alpha$-peptides are the classical $\alpha$-helix, and to a much lower extent the $3_{10}$-helix (Figure 1).[29] These two types of helical conformations have different C=O···HN intramolecular hydrogen bond patterns, torsion angles, pitch and number of residues per turns (3.63 for the $\alpha$-helix and 3.24 for the $3_{10}$-helix).[30,31] The $\alpha$-helix is stabilized by an $i \leftarrow i + 4$ hydrogen bonding pattern, where a pseudo-cycle of 13 atoms ($C_{13}$-structure or $\alpha$-turn) is formed through the intramolecular H-bonds between the C=O group of the residue at $i$ position and the N-H group at the $i + 4$ position. In the $3_{10}$-helix, the pseudo-cycle is composed of 10 atoms ($C_{10}$-structure or type-III-beta-turn) and it is formed between residues at the $i$ *and* $i + 3$ positions.

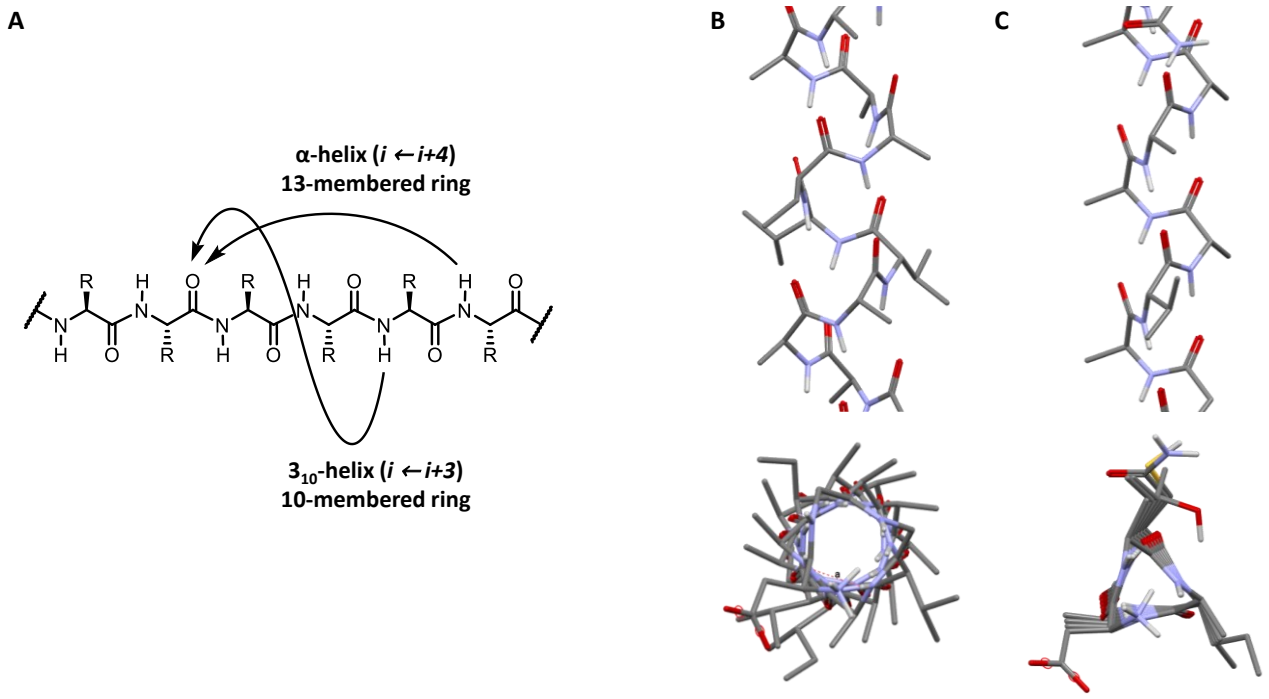


*Figure 1: (A) Intramolecular C=O···H–N H-bonds pattern: $i \leftarrow i+3$ for the $3_{10}$-helix and $i \leftarrow i+4$ for the α-helix. (B) Side view and top view of the theoretical α-helix (left) and $3_{10}$-helix (right).*

In natural proteins and peptides in solution, the interconversion barriers between the more tightly bound and more elongated $3_{10}$-helix and the α-helix are small; the higher abundance of α-helix content in proteins is probably due to the lower H-bond distortion for the $i \leftarrow i + 4$ ring formation, compared to $i \leftarrow i + 3$.[32,33] $3_{10}$-Helical conformations are usually found in short peptides (≤6 residues) mainly located as a N- or C-terminal extension of an α-helix, and are usually absent in higher-order tertiary and quaternary interactions.[29,34,35]

The formation of these helical H-bond networks requires the spatial proximity of otherwise distant H-bond donor and acceptor groups (NH and CO of the amide bond, respectively) through pre-organization of the peptide backbone. In α-peptides this pre-organization of the backbone is mainly due to factors restricting the rotation around the phi and psi torsion angles, such as minimization of pseudo-allylic strain and Newman and Pitzer strain as well. Various approaches can be developed to promote the occurrence of helical α-peptide fold. The most extensively used approach to restrict the accessible conformational space of polypeptide chains is the use of the Thorpe-Ingold effect, introducing α,α-disubstituted α-amino acids (Figure 2) in the sequence. α-Aminoisobutyric acid

(Aib) is the simplest $C^{\alpha}$-tetrasubstituted amino acid, with two methyl groups at the alpha carbon, and have restricted $\Psi$ and $\beta$ values around ($\pm 60°$,$\pm 30°$).[31]

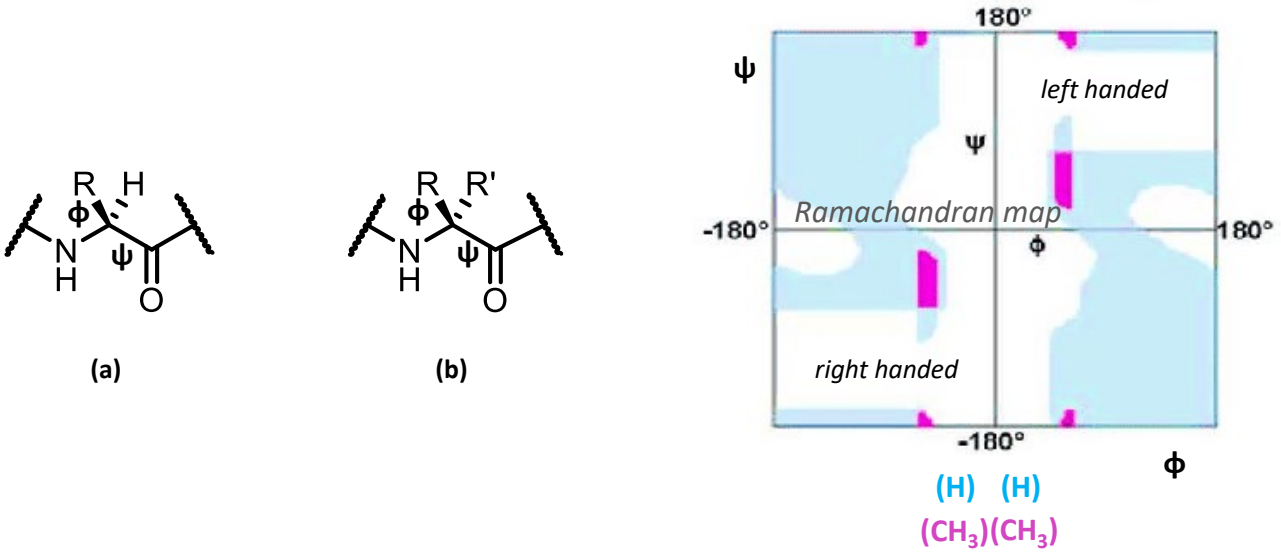


*Figure 2: (A) Chemical structures of $C_{\alpha}$-(a) and $C_{\alpha,\alpha}$-(b) substituted amino acids residues; (B) Overlapped Ramachandran maps for Ac-L-Ala-NHMe and Ac-D-Ala-NHMe. The magenta regions are the stereochemically allowed regions for Aib.*

Oligomers of Aib have a strong preference for adopting helical conformations (in particular $3_{10}$-helices[33,36]) and the strategic incorporation of Aib and related $C^{\alpha,\alpha}$-dialkyl amino acid in peptide sequences is strongly helix stabilizing. A large body of crystallographic studies have shown that peptides containing Aib residues can exhibit $3_{10}$-helices, $\alpha$-helices, and mixed helical structures. The preference towards a specific type of helix is governed by several factors including chain length, Aib content and amino acid sequence.

The $\alpha$-helix (as well as the $3_{10}$-helix) is polarized from the N to the C terminus. Therefore, the incorporation of appropriate capping groups or neighbouring side chains can enhance its stability by electrostatic interaction.[37,38] Macrocycle formation through the stapling of residues in a $i/i+n$ relationship can also stabilize the helical conformation.[39–43]

Besides $C^{\alpha}$-tetrasubstituted amino acids, one of the most common unit to create helical foldamers consists in $\beta$-amino acid (Figure 3). Homologation of $\alpha$-amino acids by insertion of one methylene group forms $\beta$-peptides with a stable helical fold, in which the side chains of residues in the $i/i+3$ relationship are placed nearly on top of each other (in a similar fashion to the $\alpha$-helix).[44,45] The folding is stabilized by a $NH_i \cdots CO_{i+2}$ hydrogen bonding pattern, forming a pseudo-cycle of 14 atoms

($3_{14}$-helix or 14-helix). The most common $\beta$-amino acid employed is the cyclic $\beta^{2,3}$-amino acid, *trans*-2-aminocyclohexyl carboxylic acid (*trans*-ACHC), that is ideally pre-organized for $3_{14}$-helix formation ($\theta \pm 60°$).[46–48] The other most common adopted helical conformation in $\beta$-peptides is 12-helix, with a (1←4) H-bonding pattern and promoted by the cyclic trans-2-aminocyclopentyl carboxylic acid (trans-ACPC).[49]

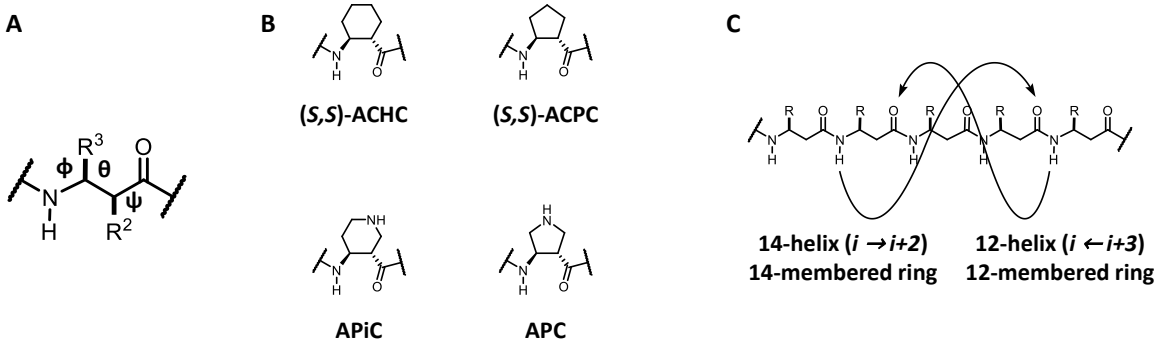


*Figure 3: (A) General formula of $\beta^{2,3}$-amino acid residue and its torsional angles; (B) (S,S)-ACHC residue (top left), a 14-helix stabilizer, the related five-membered ring analogue ACPC (top right) and their amino-functionalized analogues APiC and APC (bottom). (C) Comparison of $\beta^3$-peptide 14- and 12-helical hydrogen bonding patterns.*

Considerable efforts have been undertaken in the study of the folding pattern of $\beta$-peptides through the study of $\alpha/\beta$-peptides derived from the incorporation of α-amino acids and the development of amino-functionalized versions of ACHC and ACPC to increase water solubility (Figure 3B).[50–52] The pyrrolidine-containing APC unit shows conformational properties similar to the parent ACPC and with α-amino acid tends to form helical secondary structure with $CO_i \cdots HN_{i+3}$ or $CO_i \cdots HN_{i+4}$ H-bonding patterns.[50,53,54]

### 1.2.2 Design of catalytic foldamers

The design of potential foldameric organocatalyst has been achieved following different strategies.

The foldamer can be used as a simple scaffold, conjugating a prosthetic group to enable the catalytic activity. In this case, the foldameric scaffolds provides a recognition element and a chiral environment for the catalytic action of the embedded prosthetic group. This approach was first used by Kirshenbaum et al. for the oxidative kinetic resolution of racemic 1-phenyl-ethanol with N-(1-phenylethyl)glycine peptoid oligomers bearing a nitroxyl group derived from TEMPO at various sites.[55] The 1-phenylethyl substitution is a strong cis-amide inducer and N-(1-phenylethyl)glycine oligomers adopt a polyproline I-like conformation, even though the peptoid backbone is achiral.[56] The authors found a strong correlation between the position of the TEMPO cofactor, the handedness and degree of conformational order of the scaffold, and the enantioselectivity of the reaction. Covalent attachment of the cofactor was shown to be essential to the performance of the catalytic system, highlighting a synergistic effect between the chiral peptoid scaffold and the TEMPO catalytic activity (Figure 4A).

Webb et al. recently reported the use of Aib foldamers terminated with rhodium(I) NHC complexes for the hydrosilylation of alkynes, ketones, and aldehydes.[57] An ethylene bridge was used to attach a Rh(NHC) complex to the C-terminus of an Aib tetramer, while the N-termini was functionalized with chiral residues with differing abilities to induce an helical excess through the Aib portion. The foldamer scaffold resulted compatible with the metal complex and it did not hamper the catalytic performance of the system, however poor stereochemical communication through the ethylene bridge resulted in poor diastomeric execess of the reactions.

Indolocarbazole-naphthyridine (IN) aromatic helical foldamers bearing a 4-(*N*,*N*-dimethylamino)pyridine (DMAP) moiety at one end of the strands were used by Jeong et al. as catalysts for the regioselective acetylation of octyl $\beta$-d-glucopyranoside (Figure 4B).[58] IN oligomers fold into helical conformations due to dipole-dipole interactions between the aromatic subunits, further stabilized by $\pi$-stacking between the helical turns, and their internal cavity is capable of binding octyl $\beta$-d-glucopyranoside.[59] These foldamers were able to catalyse the acetylation of octyl $\beta$-d-glucopyranoside at the 6-OH group with low yields but good regioselectivity (up to 90 %). The

authors suggest that the proximity between the acylium DMAP intermediate and the 6-OH group of octyl β-d-glucopyranoside could be the cause of the selectivity, even if formation of multiple complexes of different binding modes was observed by NMR spectroscopy.

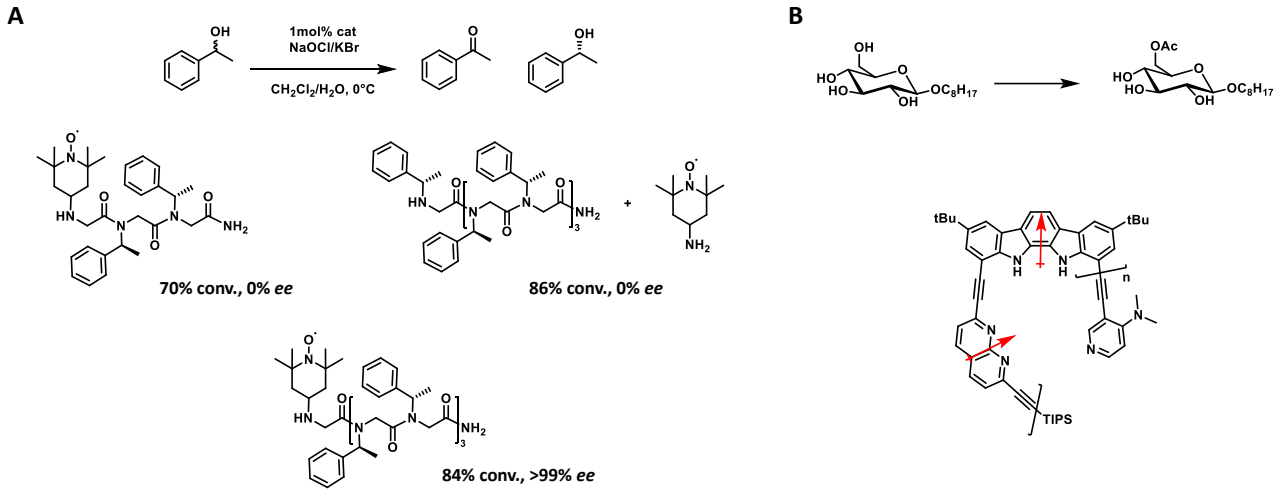


*Figure 4: (A) Catalytic enantioselective oxidation of 1-phenylethanol by TEMPO–peptoid hybrids: Conversion, enantioselectivities and enantiomeric excess. (B) Regioselective acetylation of octyl β-d-glucopyranoside (top) with indolocarbazole-naphthyridine (IN) aromatic helical foldamers (bottom). Dipole-dipole interactions stabilize the syn conformation of the IN monomer.*

As a second approach, the H-bond network of the foldamer main chain can be used to perform H-bond catalysis. Poly(L-amino acids) catalysts for asymmetric epoxidation of electron poor double bonds fall in this category (Figure 5A). A historical example is the Julià-Colonna epoxidation: in the '80s Julià (Paris)[60] and Colonna (Milan)[61] reported, almost at the same time, the asymmetric epoxidation of calcones catalysed by poly(L-alanine) and poly(L-leucine) (Figure 5A). This reaction is an asymmetric variant of the Weitz-Scheffer reaction and over the years its mechanistic aspects have been systematically investigated and the substrate scope expanded.[62] The folding of the polypeptide chain into a helical structure proved to be essential to the enantioselectivity of the reaction: in the folded structure, the N-terminal N-H groups are available for H-bonding with the enone and the peroxide anion, while the helix macrodipole stabilize the peroxide enolate intermediate.[63] Other helical foldamers catalyse the asymmetric epoxidation of chalcone (Figure 5A),[64,65] and the same principles have been used to catalyse different reactions (i.e., enantioselective carbon-carbon bond formation reactions) in recent years.

Tanaka et al. employed helical peptides to catalyse Michael addition reactions of nitro-alkane or dialkyl malonate to $\alpha,\beta$-unsaturated ketones,[66,67] while Guichard er al. employed oligourea-based foldamers to catalyse the enantioselective addition of malonates to nitro-olefins (Figure 5B).[68] In both cases, the amide or urea H-bond donor groups act as oxyanion hole mimics, activating the nucleophile through H-bonding coordination in a similar manner to the Julià-Colonna epoxidation. Also in this case, the charge stabilization by the directional H-bond network of the foldamer enhances the reactivity of these hydrogen bond donor sites. N,N'-linked thioureas have propensity to fold into a helix with 2.5 residues per turn through a series of $C{=}O_i{\cdots}HN'_{i+2}$ and $C{=}O_i{\cdots}HN_{i+3}$ hydrogen bonds, which stabilize the structure (Figure 5B).[69–71] The helical foldamer of Tanaka et al. are poly(L-Leu)-based peptide foldamers in which the helical conformation is stabilized by $\alpha,\alpha$-disubstituted $\alpha$-amino acid components, such as Aib and aminocyclopentane-1-carboxylic acid (Ac5c).

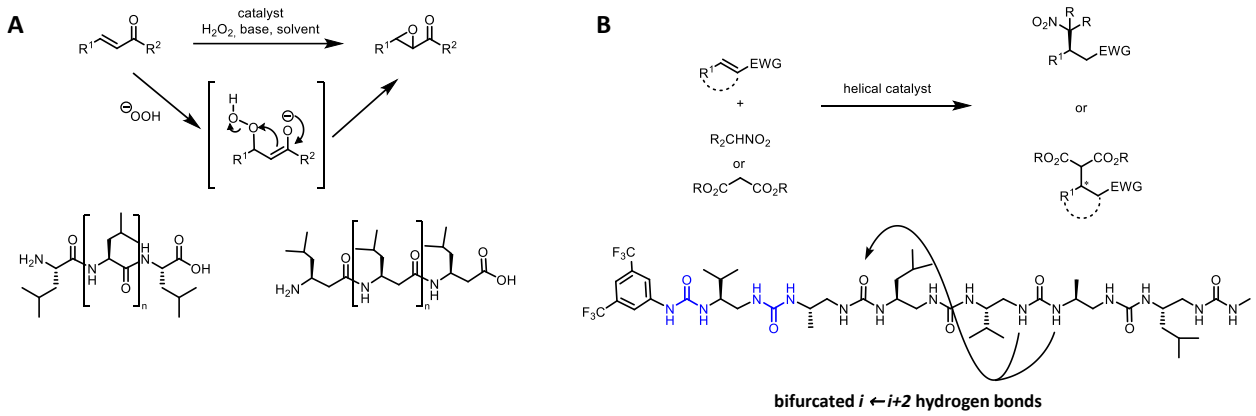


*Figure 5: (A) Scheme of the oxidation of α, β-unsaturated ketones by hydrogen peroxide under basic conditions (Julia-Colonna epoxidation), with the reaction proceeding through a peroxide-enolate intermediate, and examples of poly-L-leucine and poly-L-β³-Leucine catalysts. (B) General scheme of Michael addition reactions catalysed by helical foldamers (top) and intramolecular C=O···H–N H-bonds pattern of N,N'-linked oligoureas reported by Guichard et al. (bottom), with hydrogen-bonding sites for catalysis highlighted in blue.*

The main limitation of these reactions, however, is that their enantioselectivity is strongly influenced by the asymmetric folding of the oligomeric catalyst. The asymmetric folding depends on the chirality of the monomers and in order to switch the selectivity, the configuration of all the monomers has to be inverted. To overcome this challenge, Clayden et al. have used an Aib achiral oligomer, inducing the symmetry breaking by an external stimulus.[72] An amino-thiourea catalytic moiety was appended to the N-terminus of a right-handed helical structure bearing a C-terminal

photoswitchable Bni residue (5-bromo-7-nitroindoline) ligated to an Ala residue. The photochemical deprotection was sufficient to refold the helical oligomer, interconverting the screw-sense preference and changing the enantioselectivity of the addition reaction of diethylmalonate to β-trans-nitrostyrene.

Another approach is the incorporation of unnatural foldameric portions into a natural enzyme to enhance or modify its catalytic activity. One of the drawbacks of synthetic foldamers is the lack of well-defined binding pockets, having the side chains mainly exposed to the solvent. A top-down approach with the insertion of non-natural foldameric "protheses" within a natural enzyme is a potential strategy to obtain highly effective hybrid catalysts. Gellman et al. developed a functional heterodimeric chorismate mutase (CM): foldamer prostheses made of $\alpha/\beta$-peptides were used to complement an inactive three-helix domain of the enzyme.[73] The number, location and/or type of $\beta^3$-residues substitutions were varied along the helix domain, providing helpful guidelines: preorganization with conformationally constrained building blocks is beneficial to the foldamer-protein assembly and solvent-exposed sites are the most tolerant towards modifications, while modifications at the sites involved in protein-protein interactions or at the active site are far less. A similar demonstration is given by Wilson et al. where a segment of RNase S is replaced by an aromatic oligoamide foldamer mimicking an $\alpha$-helix.[74] The helical foldamer successfully replaced an $\alpha$-helix segment of the catalytic site through non-covalent association, restoring the catalytic activity. The "topographical mimic", however, lacked one of the two histidine residues required for acid-base catalysed hydrolysis of RNA and therefore the S-protein/proteomimetic complex showed an efficiency $10^4$-fold lower than the fully functional RNase S-protein/S-peptide complex.

The most studied approach for developing catalytic foldamers is the use of the foldamer scaffold to achieve cooperative catalysis. The predictable architecture and stability of foldamers allows to design linear sequences that will bring two or more reactive functional groups into proximity upon helical folding. Natural enzymes achieve the proper spatial positioning of functional groups through their specific tertiary structures, and they offer much more possibilities in terms of numbers and geometric relationships between catalytic groups. However, from the point of view of a purely rational design of catalysts, foldamers can display predictable secondary structures at short lengths. This predictability

allows organic chemists to achieve a predetermined spatial organization between reactive groups in a simplified manner by the careful design of simple short sequences.

An elegant example of foldamer design is reported by Matile et al. in the study of synergistic effects between $\pi$-$\pi$ stacking and anion-$\pi$ interactions in catalysis, using $\pi$-stacked foldamer to catalyse conjugate addition of malonic acid monothioester to nitroalkenes.[75] A series of foldamers based on the face-to-face stacking of naphthalenediimide units and of increasing length were used to investigate the selectivity for conjugate addition over decarboxylation. Conjugate addition selectivity increased with the length of the foldamers in a roughly linear manner, while optoelectronic properties of the foldamers followed the sublinear power laws of oligomer chemistry, suggesting long-range, synergistic anion-$\pi$ catalysis.

Tri-functional catalysts for transesterification reactions (i.e., methanolysis of vinyl trifluoroacetate) were developed by Houk, Schafmeister et al. using "spiroligozymes".[76] These are spiro-fused oligomers (bis-peptides) obtained from the coupling of cyclic building blocks through pairs of amide bonds.[77] The concave shape of these spirocyclic peptidomimetics in solution was used to present a catalytic triad composed of an urea acting as an oxyanion hole, a pyridine as a general base catalyst and an alcohol as nucleophile (Figure 6A). Another set of spiroligozymes were designed as Ketosteroid Isomerase mimics for the aromatic Claisen rearrangement of a 1,1-dimethylallyl coumarin.[78] Anchoring of two hydrogen bonding donor groups onto the conformationally defined spirocyclic scaffold generated a competent catalyst, able to stabilize the transition state through a two-point H-bonding stabilization (Figure 6B).

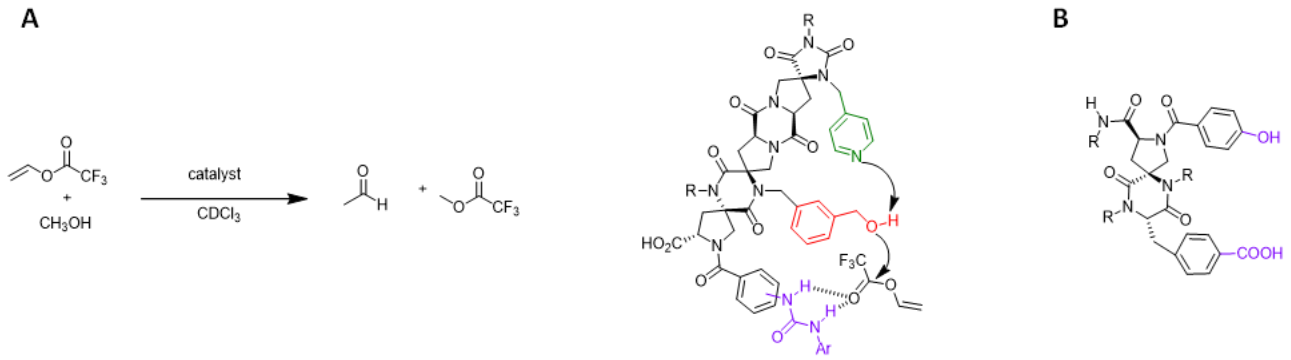


*Figure 6: (A) Transesterefication of trifluorovinylacetate to trifluoromethylacetate catalysed by Schafmeister spiroligozymes (left) and mode of action of the trifunctional catalyst (right). (B) Bifunctional spiroligozyme for two-point H-bond catalysis of the aromatic Claisen rearrangement of a 1,1-dimethylallyl coumarin.*

Despite important advances, the de novo rational design and synthesis of protein catalysts have not yet been realized. However, in recent years $\alpha$-helical coiled coils peptides emerged as useful building blocks for the design of biomimetic catalysts with hydrolytic, ligase, transferase or redox activity.[79] Protein-like helix-bundle quaternary structures were also designed and obtained from $\beta$-peptides and oligourea foldamers.

A notable example is provided by the $\beta^3$-peptide bundle reported by Schepartz et al. for the hydrolysis of 8-acetoxypyrene-1,3,6-trisulfonate.[80] Catalytic activity was achieved engineering a previously reported thermally and kinetically stable $\beta^3$-peptide bundle characterized by a set of parallel and antiparallel 14-helices, a $\beta^3$-Leu core and several $\beta^3$-homoornithines salt-bridges (high-charge density).[81] A histidine residue at the N-terminus of the peptide, $\beta^3$-homoornithines residue were replaced with $\beta^3$-homoarginine for better substrate binding and two monomers were joined via a tetra- $\beta$-homoglycine linker to enhance the bundle self-assembly. The resulting foldamer catalysed the reaction with a Michealis-Menten kinetic at low substrate concentration, while showing substrate inhibition phenomena at higher concentrations.

Enamine and iminium catalysis are between the most studied methodologies for functionalization of carbonyl compound through organocatalysis (e.g., foldamer catalysis). In the 90s, Alleman and Benner designed L-Lys-rich amphiphilic $\alpha$-helical peptides as minimal aldolase (i.e., oxaloacetate decarboxylase) mimics,[82] followed by Hilvert et Gellman with a $\beta^3$-Lys-rich 14-helical $\beta$-peptide decamer (**1-3**, Figure 7).[83] In both systems, the catalytic activity is strongly related to the folding propensity and the clustering of amine/ammonium side chains on one side of the helical cylinder.

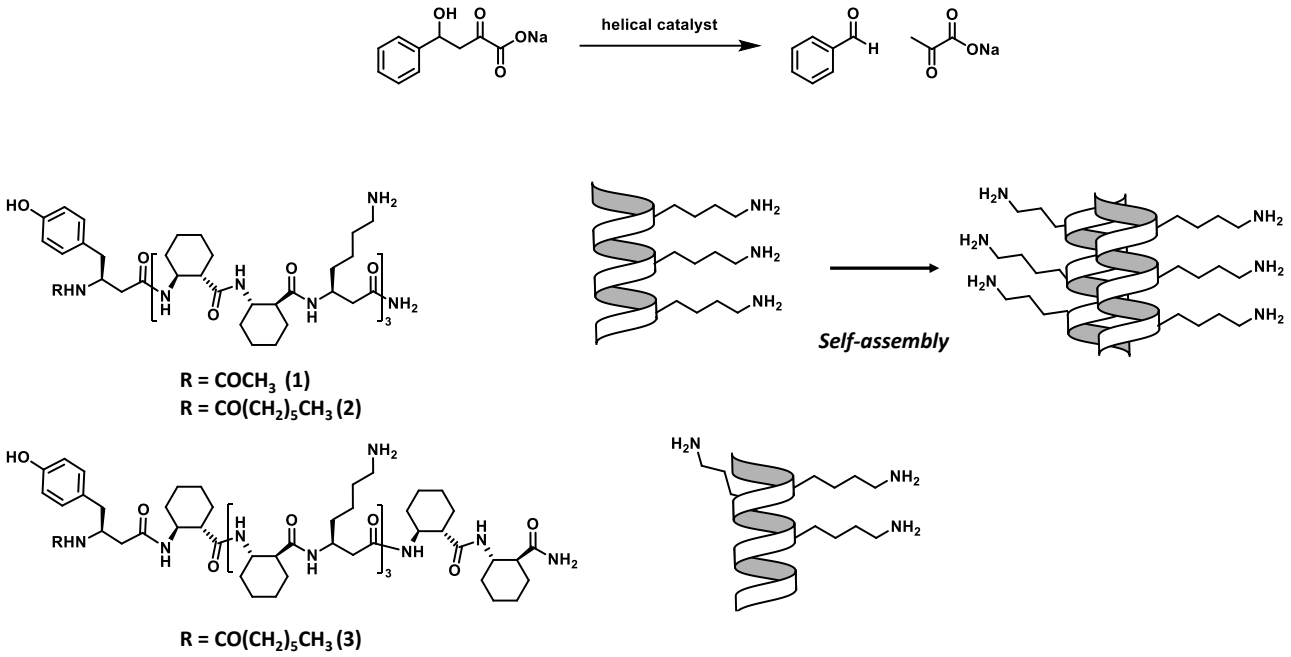


*Figure 7: (**top**) Retroaldol reaction catalysed by the β-peptides **1-3**. (bottom left) Sequences of β-peptides **1-3**: ($\beta^3$-hLys) residues at i, i + n*3 positions lead to alignment of the amine-containing side chains. (bottom right) Cartoon representation of the 3D-organization and self-assembly of β-peptides **1-3**.*

$\beta$-peptide **1** was proficient in the catalysis of the retro-aldol reaction of 4-phenyl-4-hydroxy-2-oxobutyrate with a Michaelis–Menten behaviour, while $\beta$-peptide **3,** where the ammonium side chains were scattered around the helix circumference, was a poor catalyst. The proximity of positive side chains enhances catalysis, depressing the $pK_a$ of at least one side chain due to coulombic interactions. Likewise, the addition of a long chain tail at the N-terminus enhanced the catalytic activity of the peptide (20-times higher than the N-termini unfunctionalized peptide), suggesting the benefit of self-assembly to increase the positive-charge density and hydrophobicity of the environment around the catalytic moiety.

In recent years, de Figueiredo, Maillard, et al. explored a class of helical heterocyclic γ-peptides, built around a thiazole ring (i.e., ATC, 4-amino(methyl)-1,3-thiazole-5-carboxylic acids), to catalyse the Michael-addition of cyclohexanone and *β-trans*-nitrostyrene (**4**, Figure 8).[84] ATC oligomers tend to adopt a nine-helix structure, stabilized by a stable $C_9$ hydrogen-bonding pattern, thanks to the planar conformation of the $C^{\gamma}$-$C^{\beta}$-$C^{\alpha}$-C(O) torsion angle imposed by the heterocycles.[85] The two reactive groups for the bifunctional catalysis were inserted on a single ATC unit, with a nucleophilic pyrrolidine in position 2 of the thiazole core and a propanoic chain on the γ carbon. ATC **5** could be viewed as a structural analogue of the H–D–Pro–Pro–Glu–$NH_2$ tripeptide (**6**), an efficient catalyst for this kind of chemistry previously reported by the Wennemers group.[86–89] Including **5** into a folded γ-peptide increased modestly both yield and stereoselectivity of the reaction, suggesting an influence of the helical structure.

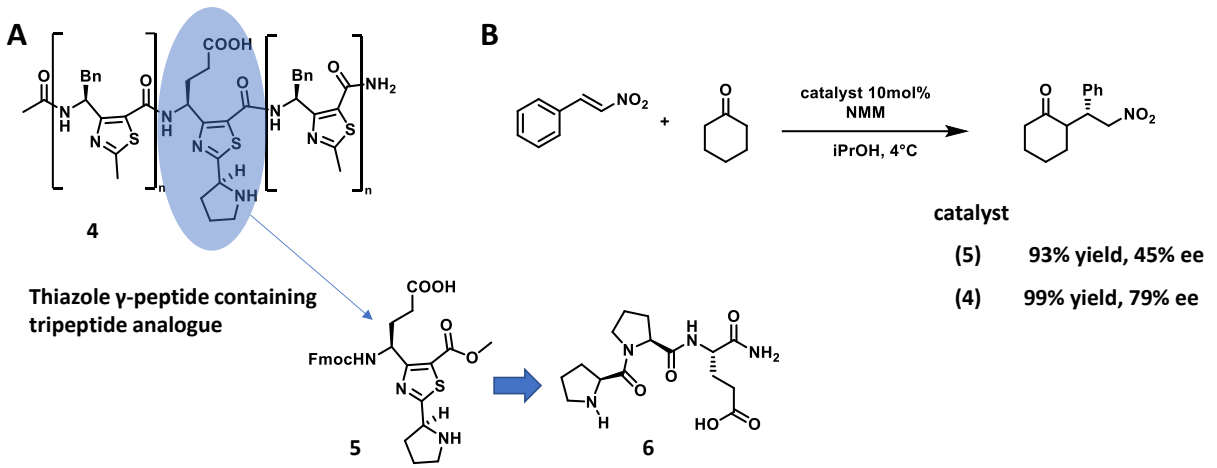


*Figure 8: (A) ATC (4-amino(methyl)-1,3-thiazole-5-carboxylic acids)-based catalyst (**4**) incorporating a functional monomer (**5**) mimicking the tri-α-peptide d-Pro-Pro-Glu-$NH_2$ (**6**). (B) Nitro-Michael addition reaction of cyclohexanone to β-trans-nitrostyrene using ATC-based catalysts.*

Helical foldamers were used as scaffolds for the development of bifunctional catalyst for Diels-Alder reactions of 2-butenal and a carbamate functionalized diene by Michaelis, Price et al.[90] The two catalytic groups (an imidazolidinone and a thiourea) were inserted as side chains in an α-helical Aib-rich peptide. The imidazolidinone was intended to activate the 2-butenal (via iminium formation), while the thiourea H-bond donor group was placed along the helix side to hold the diene near the iminium dienophile. These hypotheses were verified disrupting the helical conformation by the insertion of proline residues. Loss of helical folding was followed by a loss of catalytic activity. A second control experiment instead highlighted the cooperative nature of the catalyst, employing a

diene with carbamate (able to bind to thiourea) and one without (cyclopentadiene). Using the functionalized foldamer, a strong selectivity towards the diene with carbamate was found, which was not the case with a simple imidazolidinone catalyst.

Michaelis et al. have also investigated the effect of the local chemical environment on the performance of a bifunctional helical peptide catalyst in the conjugate addition of cyclohexanone to nitroolefins (Figure 9).[91]

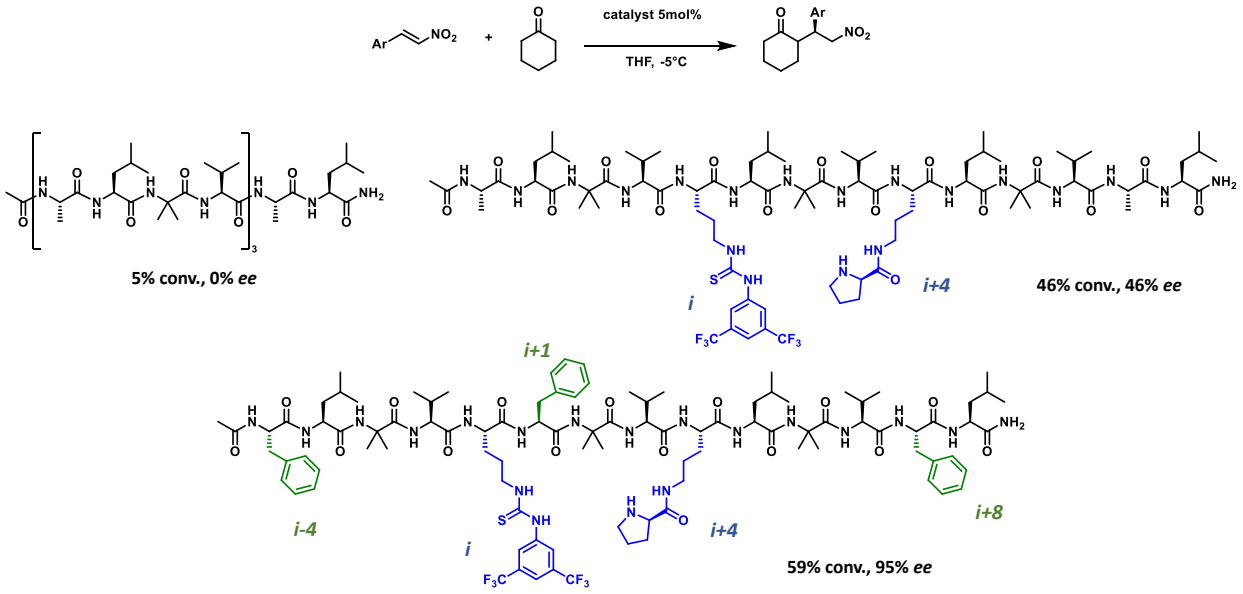


*Figure 9: Michael addition reaction between cyclohexanone and β-nitrostyrene catalysed by bifunctional helical catalysts. Chemical structures and catalytic performances of parent peptide, bifunctional catalyst with the two catalytic moieties (in blue) in the optimal i/i+4 relationship, and catalyst with optimized surrounding environment due to hydrophobic Phe residues (in green).*

The helical scaffold was obtained from repeating a helicogenic tetrapeptide sequence (Aib-Val-Ala-Leu) and a prolinamide and thiourea side chains were inserted respectively for enamine and hydrogen bonding catalysis. The authors then evaluated the catalytic efficiency of a series of foldamers with different positioning of the catalytic side chains and where phenylalanine residues were placed at strategic positions along the helix, for possible $\pi$-stacking or other steric interactions with the catalysts and substrate. Placing the enamine and thiourea hydrogen bonding catalyst one turn apart on the helix resulted in enhanced catalytic activity: the folding of the catalyst into a helical conformation is crucial to bring the catalytic residues in to proximity. The insertion of phenylalanine residues at several positions enhanced the enantioselectivity (95% ee) of the catalyst, suggesting the importance of the environment around the catalytic residues. However, increased foldamer

aggregation was observed after Phe introduction, suggesting that this increased selectivity may derive from the self-assembly of the foldamers.

A notable example of enamine/iminium chemistry is the α-methylenation reactions of aldehydes with formaldehyde catalysed by pyrrolidine. As shown by Erkkilä and Pihko in the 2000s,[92] the reaction proceeds following a Knoevenagel–Mannich-type mechanism, where the nucleophilic aldehyde is activated via enamine formation, while the electrophilic one via iminium formation. Helical foldamers bearing two properly spaced amine diads were therefore investigated by Gellman et al. as bifunctional catalysts for aldol reactions.[93] The secondary amine moiety was derived from a pyrrolidine-derived β-amino acid residue (APC) and a series of bisAPC-containing $\alpha/\beta$-peptides were evaluated in their catalytic efficiency by varying the positioning of catalytic residues as well the ratio between $\alpha$-amino acid and cyclic $\beta$-amino acids residues. Remarkably, the best catalysts candidate was characterized by a 1:2 $\alpha/\beta$-ratio leading to a helix with 3 residues per turn and two APC residue spaced by a turn along the helix (*i+3* spacing): this arrangement was proved essential to provide bifunctional catalysis (Figure 10A). A notable application of APC-containing $\alpha/\beta$-peptide foldamer has been then reported by the Gellman group in the catalysis of intramolecular aldol macrocyclization of bis-aldehydes compounds in order to form 14-to18-membered rings (Figure 10B).[94]

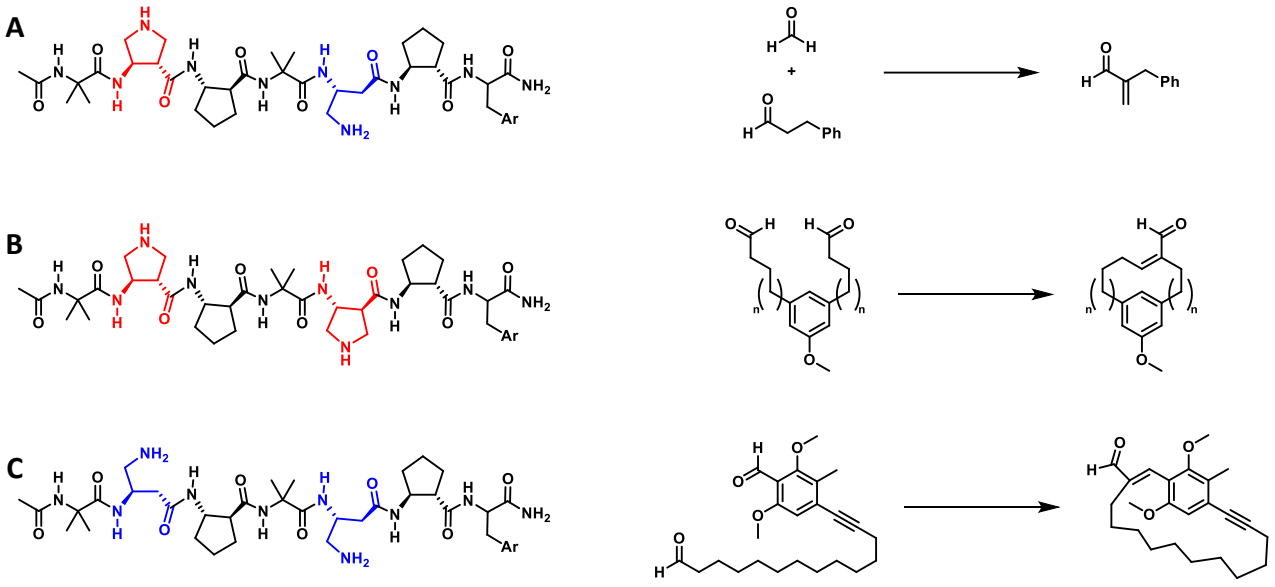


*Figure 10: Overview of the distinct reaction catalysed by α/β-peptide helical foldamers displaying different amine diads.*

The catalytic diad was modified and one of the two APC catalytic units was replaced by a primary amine, required for iminium activation of one of the two carbonyls. The enamine/iminium activation was effective in catalyse the macrocyclization reaction, thanks to the templating effect of the foldamer which, activating both carbonyls and conformational pre-organizing the substrate, overcome the entropic cost of the intramolecular cyclization.[95] More recently, the potential of this catalytic $\alpha$/$\beta$-peptide foldamers was further expanded when replacement of both the APC residues with two primary amine groups allowed the crossed aldol macrocyclization with aryl aldehydes as the electrophile (Figure 10C).[96]

## 1.3 Synthetic catalysts inspired by serine proteases

Hydrolytic processes found applications in many industrial chemical reactions and hydrolytic enzymes (hydrolases) are displaying growing relevance given their ability to catalytically hydrolyse a range of chemical bonds in lipids, starches, and proteins. Several families of hydrolases have been developed by evolution, each with a different role. Among the most interesting hydrolases for chemists, proteases are enzymes able to break down the peptide (amide) bonds in proteins.[97] Hydrolysis of amide bonds is a thermodynamically favourable process, but its kinetic is very slow at physiological conditions with a half-life of around 500 years.[98,99] Proteases speed up the process to outstanding rates (diffusion-limited),[99,100] and chemists have long tried to design simple synthetic catalysts that could perform hydrolase-inspired chemistry.[101] The design of simple organic catalyst that mimic the chemistry of hydrolytic enzymes generally stems from imitation of specific structural features of the natural enzymes.[102,103] This can be seen in the case of synthetic mimics of serine proteases, where the key aspects usually mimicked are the active site, the oxyanion hole for TS stabilization, and the hydrophobic pocket, as well as combinations of these features. The active site is the common example of interplay of a nucleophile, a general base, and an acid: this "catalytic triad" is generally composed of serine, histidine, and aspartic acid residues (Figure 11A).[104,105] The $pK_a$ of the His imidazole is increased by hydrogen bonding to the Asp carbonyl. The imidazole nitrogen, acting as a general base, deprotonates the Ser residue, enhancing its nucleophilicity. The nucleophilic attack by the Ser residue on the carbonyl of the substrate results in an acyl-enzyme intermediate. Subsequent hydrolysis of the acyl-intermediate regenerate the catalytic triad and ejects the product, through a substitution-elimination reaction with water as the nucleophile and the His imidazole as a general acid. Hydrogen bonding donor groups, such a backbone amide groups and serine or aspartate residues, constitute the "oxyanion hole" that stabilizes the charged intermediate and reduces the activation energy of the reaction.[106] Many studies on the development of serine proteases mimics have a reductionist approach, focusing on the most investigated and attractive aspect of these enzymes, the "catalytic triad".

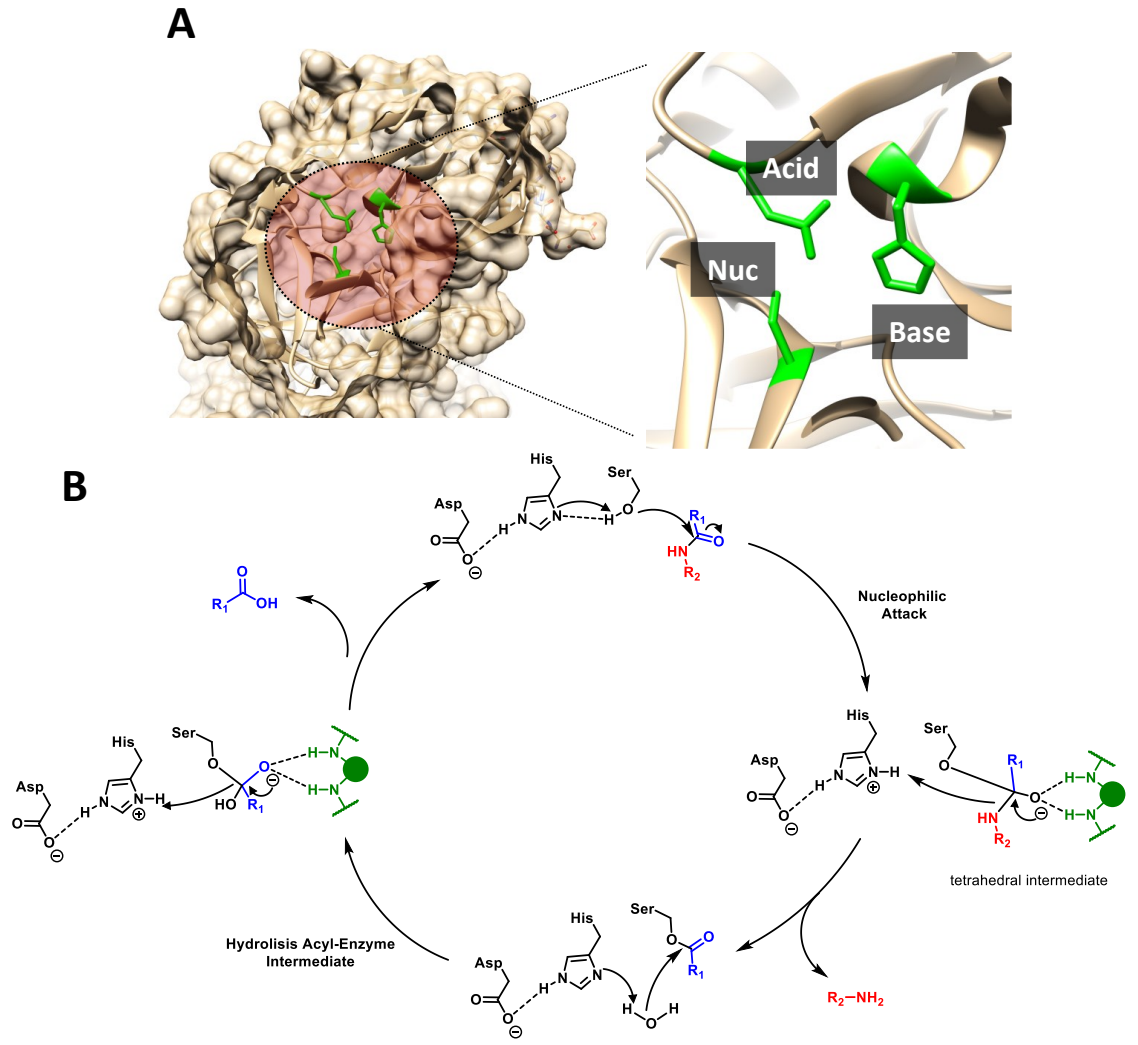


*Figure 11: (A) Detail of the catalytic site of a serine protease. (B) General mechanism of hydrolysis of an amide substrate catalysed by a Ser-His-Asp catalytic triad (black) through Ser addition-elimination to the substrate carbonyl moiety and subsequent hydrolysis of the acyl-enzyme intermediate; (dashed lines represent hydrogen-bonding). The "oxyanion hole" (green) of nearby peptide N–H bonds stabilize the charged tetrahedral transition states.*

A notable example is the trifunctional catalytic "spiroligomer" cited in Section 1.2, Figure 6. Another similar example of a trifunctional catalyst was previously reported by Ema et al. with catalyst containing a thiourea group as an oxyanion hole mimic, an hydroxyl group as a nucleophile, and a pyridine group as a base, but without the directing scaffold provided by the "spiroligomer";[107] nevertheless impressive rate enhancement ($3.8\times10^6$ $k_{cat}/k_{uncat}$) was observed in the transesterification reaction of vinyl trifluoroacetate. Fuentes de Arriba et al. also developed small-molecule artificial catalysts which mimic the active centres of hydrolases (Figure 12). The combination of a 1,2-amino alcohol with a suitable oxyanion hole mimic was used to recreate the action of N-terminal hydrolases, in which the Ser-His-Asp residues are replaced by a terminal serine or threonine.[108,109] A rigid

cyclohexane skeleton (tetralin) was used to place the base, the nucleophilic hydroxyl group, and the oxyanion hole in the appropriate spatial organization; the oxyanion moiety was optimized in various generations of the catalyst and the authors found a naphthalene scaffold with carboxamide and sulfonamide as hydrogen bond donors to be the best performing the transesterification of unactivated ester (i.e., acetylcholine and ethyl acetate).

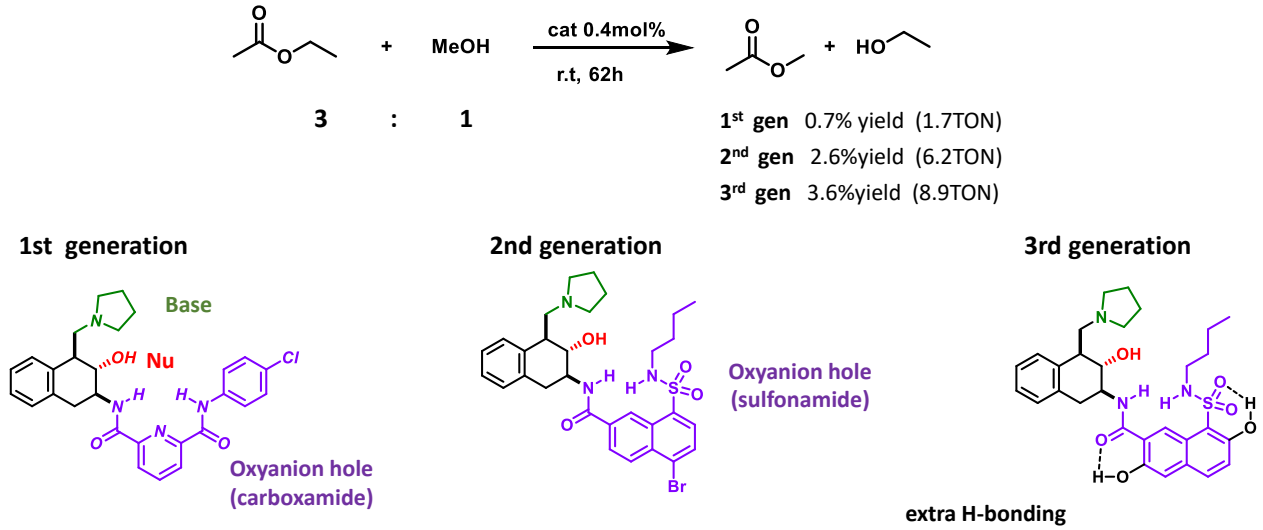


*Figure 12: Transesterification of ethyl acetate promoted by small molecules mimicking N-terminal hydrolases. First generation catalysts featured base (green), nucleophile (red), and oxyanion hole (purple) moieties on a tetralin scaffold; second generation ones feature a shorter and adaptable oxyanion hole and the third generation of catalysts provides extra hydrogen bonds for further stabilization of the transition state.*

The internal cavity of cyclodextrins offers the possibility to pre-organize the reactive groups to develop macrocyclic protease mimics, presenting at the same time a hydrophobic environment.[110,111] On the other hand, it is difficult to selectively functionalize cyclodextrins and they require high concentrations for optimal complexation with the substrate; thus, alternative macrocyclic approaches have been sought, such as cucurbituril-based mimic[112] and functionalized cavitands.[113,114]

Rebeks et al. investigated the ability of a pyridone functionalized cavitand in the aminolysis of cationic activated esters.[115] The synergistic action between the well-defined binding pocket provided by the cavitand (recognition) and the pyridine moiety on the cavitand rim (catalysis) resulted in aminolysis of the substrate. As for cyclodextrins, high concentrations of the catalyst (2 eq.) are required to observe noticeable catalytic effects. An alternative example of cyclodextrin-enabled hydrolytic catalysts was reported by Ueno et al. using a series of cyclodextrin−peptide hybrid (CD−peptides) catalysts.[116] These CD−peptides adopt stable α-helix conformations where a β-

cyclodextrin, an imidazole, and a carboxylate moiety are positioned on the same side of the $\alpha$-helix. The topological aspect of the functional groups was found to be important, with the order of the functional groups on the α-helix peptide affecting the enantioselectivity of the binding: the catalyst with $\beta$-CD, imidazole, and carboxylate from N-terminus or C-terminus showed 7-fold higher $k_{cat}/K_M$ value for Boc-D-Ala-*para*-nitrophenate than for the L-enantiomer.

One of the most notable examples of minimalistic protease mimic has been reported in the 2000s by Chen et al: the proteolytic and esterolytic activity of the simple dipeptide Ser-His.[117] This essential protease model contains the three functional groups of the catalytic triad in proximity within a very simple molecule. Despite the reports of its activity,[118] follow-up studies by Gellman et al. questioned the ability of Ser-His to catalyse the hydrolysis of amides or unactivated ester.[119] Further studies by Szostak et al. showed how the ability of the Ser-His dipeptide to catalyse the inverse reaction (i.e., peptide condensation) requires localization in a hydrophobic environment,[120] in a similar manner to the native enzyme. In serine proteases, the binding pocket is composed of hydrophobic residues; the hydrophobic environment enhances H-bonding and electrostatic interactions in the active site, while enhancing the binding of substrates and release of products. Self-assembled systems, polymers and dendrimers are the most used approach to recreate a hydrophobic environment. The nature of these nano-systems also favours the development of multivalent catalytic systems.[121,122]

### 1.3.1 Multivalent hydrolytic catalysts

Multivalency is an intriguing characteristic of many biological processes and over the years many efforts have been spent to investigate and mimic the enhancement in function obtained from the controlled sum of multiple weak interactions. The use of multiple similar interactions (homovalency) and different interactions (heterovalency) often led to enhanced selectivity and specificity in recognition, and multivalent systems are often found to guide protein-protein, protein-cell, and cell-cell interactions.[123,124] Catalysis requires the binding of the transition state of a reaction to lower its energy, thus catalytic systems should benefit from multivalency: from enhanced interaction to the transition states to cooperative interactions of different functional groups.[125,126] In synthetic systems, this multivalent display of functional groups may originate from the repetition of identical building

blocks held together by weak interactions (e.g., micellar aggregates) or by covalent bonding of a catalytic system to a multivalent scaffold such as dendrimers and polymeric or metal nanoparticles.[121]

A large corpus of protease-inspired multifunctional surfactants was developed from the 60s.[127,128] Self-assembled structures from surfactants containing one or more of the catalytic triad functional groups could provide compartmentalized hydrophobic environment (for partitioning and concentration of the substrates) and tune chemical reactivity by the functionalized headgroups. Potential interactions between the functional groups were investigated, by the functionalization of the amphiphilic head groups with both hydroxyl- and imidazolyl-functional groups, as well as co-assembly of hydroxyl- and imidazolyl-containing surfactants (Figure 13A-D).[129–137] The most recent example of minimalist surfactant hydrolase mimic was reported by Connal et al:[138] an imidazole, a hydroxyl, and a carboxylate group were placed in close proximity as the head group (ACT) of a surfactant with an hexadecyl ($C_{16}$) hydrophobic chain (Figure 13E).

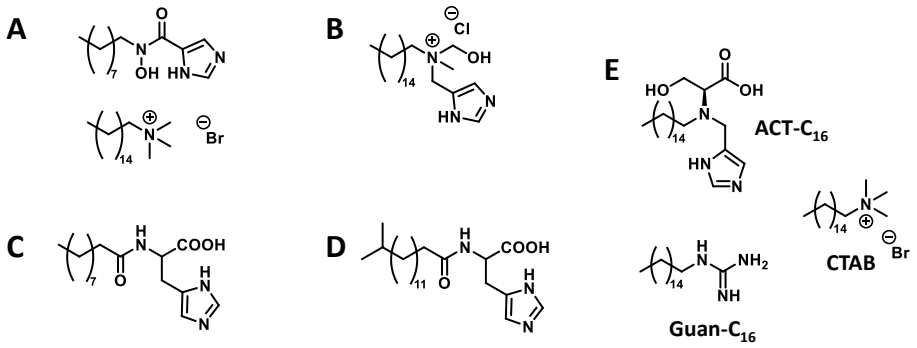


*Figure 13: Selection of surfactant-based catalytic system for hydrolysis of esters, containing one or more moieties of the catalytic triad at their head groups. (A) The bifunctional surfactant (imidazole and -OH) with enhanced performance through co-assembly with CTAB. (B) Bifunctional cationic surfactant which operate through intermolecular interaction of its functional groups (C,D) Examples of bifunctional surfactants explored by Tonellato and Ihara (E) Tri-functional surfactant reported by Connal, that through co-assembly with hexadecyl guanidinium hydrochloride (Guan-$C_{16}$) and CTAB yields catalytically active micelles.*

The catalyst was obtained via a simple, modular synthesis starting from L-Serine and the co-assembly with CTAB and guanidinium-$C_{16}$ (Guan-$C_{16}$) enabled its self-assembly and catalytic activity (Figure 13E). While the three-component system showed great rate enhancement in the hydrolysis of *p*-nitrophenylbenzoate compared to the uncatalysed reaction, supporting the concerted action of the Guan-$C_{16}$ and ACT headgroups, CTAB was essential in maintaining the solubility of the system. Moreover, the exclusion the Guan-$C_{16}$ from the co-surfactant system resulted in a drop in catalytic

activity, and the Guan-$C_{16}$/CTAB cosurfactant system revealed a higher catalytic effect than for the ACT-$C_{16}$/CTAB system.

A large corpus of studies has also been focused on the development of amino acid-containing hydrolytic catalysts that could mimic enzymatic mechanisms to introduce efficiency and selectivity toward a variety of substrates.[139,140] In recent years, a series of lipopeptides was designed by Déjugnat et al.,[141] by grafting fatty chains on histidine-containing tripeptides either at the C-terminal position or at the N-terminal extremity (Figure 14A). Various self-assembled aggregates (from globular objects to fibers) were obtained varying the peptide sequence and the hydrophobic character. Nevertheless, the lipopeptides presented a more efficient catalytic activity as monomers than in aggregates: a retention of the substrate in the hydrophobic region of the aggregates and exclusion from the hydrolytic nucleophiles generated an overall protecting effect of the aggregates on the substrate.

An elegant example of a peptide-based artificial hydrolase has been presented by Zhao et al., with the incorporation of photo-responsive azobenzene units into a self-assembling His-containing peptide, to achieve light-mediated assembly/disassembly resulting in modulation of catalytic activity (Figure 14B).[142]

He et al. developed an artificial hydrolytic enzyme by combining the self-assembling motif Fmoc-Phe-Phe with the components of the catalytic Ser-His-Asp triad (Figure 14C),[143] followed by co-assembly of the peptides to generate catalytically active nanofibers (CoA-HSD). CoA-HSD showed enhanced activity compared with the nanofibers containing only the catalytic histidine residue (doubled $k_{cat}$/Km), suggesting the synergistic effect of histidine, serine, and aspartate residues.

Enhancement of catalytic activity through co-assembly was also observed by Liang et al.,[144] in the study of amphipathic peptides functionalized at the N-terminus with a Ser-His diad (for the catalytic activity) or Ser-Gly and Ser-Arg diads (for the control and stabilization of the transition state)(Figure 14D). The activity in the hydrolysis of *p*-nitrophenilacetate (*p*-NPA) of the His-containing peptide was improved through co-assembly with the Arg-containing one, reaching a maximum (1.67 times) with the Arg/His ratio was 1/10.

Marchesan et al. investigated the effect of C- and N- capping on the self-assembly and catalytic activity of His-D-Phe–D-Phe (or the enantiomer) tripeptides (Figure 14E).[145,146] All the compounds self-organized into nanofibrils, showed modest catalytic activity and the terminal carboxylic acid moiety was shown to not significantly assist in the catalysis.

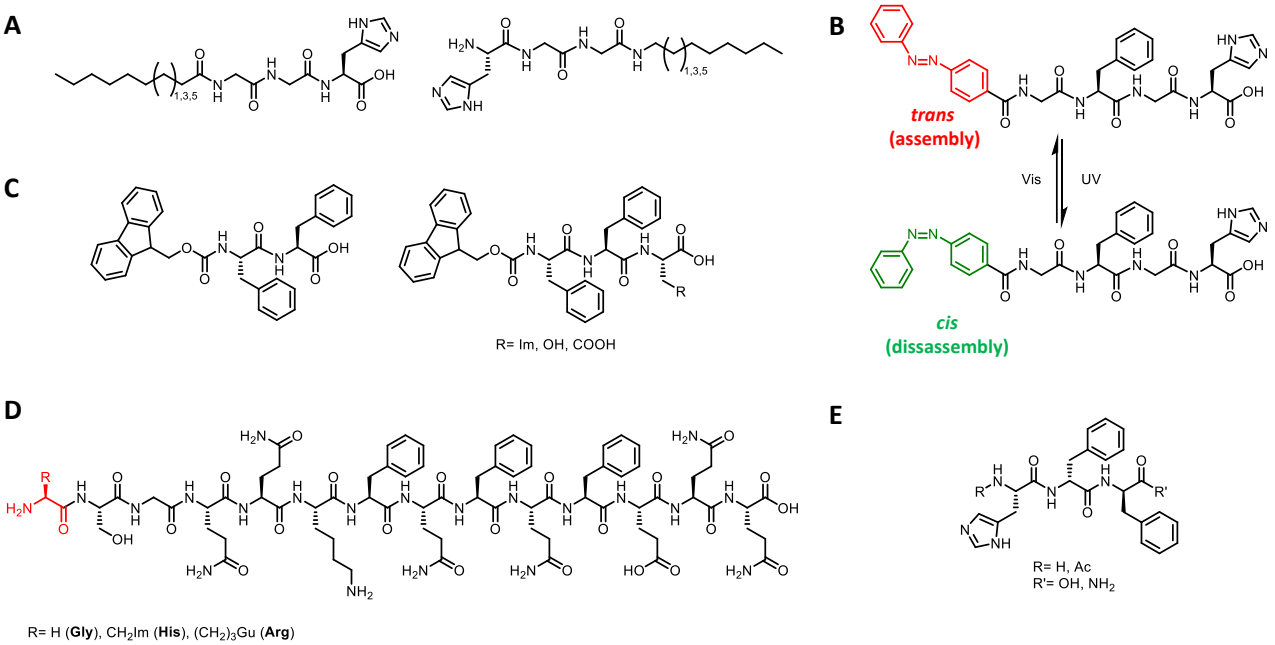


*Figure 14: Selection of chemical structure of peptides for the creation of catalytically active supramolecular architectures. (A) Examples of N-terminal and C-terminal lipopeptides reported by Déjugnat, (B) Photoresponsive peptide catalyst reported by Zhao. The catalytic activity (His residues) is modulated by the (dis)assembly of the peptide nanofiber through isomerization of a photoresponsive azobenzene unit. (C) Short Fmoc-Phe-Phe peptides for the co-assembly of nanofibers containing residues of the catalytic triad. (D) Amphipatic peptides for the co-assembly of catalytic nanofibers. (E) His-Phe-Phe tripeptide investigated by Marchesan.*

Baltzer et al. reported the first example of CC-based hydrolase mimic. The designed antiparallel helix-loop-helix hairpin dimer (KO-42) catalysed acyl-transfer reactions of *p*-nitrophenyl esters through the cooperative action of surface exposed unprotonated/protonated histidines aligned on a helix side and acting as nucleophilic and general acid catalysts.[147] The same group developed analogues of KO-42 by the replacement of some histidine residues with charged residues such as arginine and lysine.[148] These peptides showed great rate enhancements, as well as substrate recognition, chiral discrimination, and saturation kinetics for the hydrolysis of p-nitrophenyl esters. The presence of the new positive charged residues was proposed to generate charge-charge repulsion with the amine-moiety of the norleucine activated ester substrate, destabilizing the transition state for attack on one enantiomer, thus generating enantioselectivity.

Liu et al. reported a CC-scaffold based on a subunit of the envelope glycoprotein of HIV-1.[149] The reactive site contains six His residues. His residues were engineered on the surface of a parallel coiled-coil trimer (N36) stabilized by antiparallel association of three outer alfa-helices (C34). The most active variant ($C34_{H13/20}/N36_{H15/22}$) showed 600-fold rate enhancement ($k_{cat}/k_{uncat}$) in the hydrolysis of *p*-NPA. Another interesting metal-free CC scaffold was reported by the Woolfson group, using an α-helical barrel (CC-Hept) in which a catalytic triad of Cys (or homocysteine, hCys), His and Glu was installed in the hydrophobic channel of the four-heptad CC-heptamer.[150]

Supramolecular aggregates share several properties with dendrimers such as multivalency, binding of substrates and creation of nano-environments different from the bulk; thus, dendrimers can be seen as "unimolecular micelles".[151] These macromolecules are highly symmetrical and made of branched monomer units, extending in layers (generations) from a core. The layered architecture of dendrimers allows the precise functionalization of monomer units and then control of the environment surrounding the catalytic moieties and their positioning.

Reymond et al. studied the effects of the structure and composition in the esterase activity of peptide-based dendrimers.[152,153] Dendrimers endowed with a catalytic site at the core were investigated as well as dendrimers with competent catalytic branches. A combinatorial approach was used for the first type: the outcome of the combinatorial library was characterised by species containing His and positive charged residues (Arg) in the catalytic core, and aromatic residues in the outer shell. These findings highlight the similarity between native enzymes and dendritic enzyme-mimics. For the second type, a systematic series of Ser-His-containing peptide-dendrimers of increasing generation number was studied. All dendrimers catalysed the hydrolysis of active esters with Michaelis–Menten profiles and a positive dendritic effect was observed with up to a 100-fold increase in reactivity between the series. The strong dendritic effect was traced back to the cooperativity between binding and catalysis.

Metal nanoparticles passivated with functionalized organic molecules have properties between dendrimers and micellar aggregates. Their large surface area qualifies them as good supports for catalytic species, where the catalyst is assembled as multiple catalytic ligands strongly bonded to a structuring metal core.

Scrimin et al. studied the mechanism of esterolytic catalysts based on small gold nanoparticles (AuNPs) functionalized with short peptide sequences. N-methylimidazole-functionalized AuNPs (**7**, Figure 15)[154] similarly to dendrimers reported by Reymonds, graph of the hydrolysis rate of 2,4-dinitrophenyl acetate *vs.* pH showed bell-shaped profile, indicating that two imidazoles were involved in the catalytic process with complementary roles. Later, the same group investigated AuNPs functionalized with thiols terminating with a HisPhe-OH dipeptide (**8**, Figure 15).[155] A tris-ethylenglycol methyl ether-containing thiol was used in combination with the dipeptide ligand to increase the water solubility of the system. The surface-confined peptide showed a different operating mechanism with respect to the free peptide, showing a 300-fold increase in catalytic efficiency at low pH values thanks to the cooperative action of the carboxylate (general base) and protonated imidazole (general base). The same mechanism was observed with the dodecapeptide Leu-Gly-Tyr-Lys-Ala-His-Phe-Ala-Gly-Arg-Gly-Arg-OH (**9**, Figure 15),[156] with the pH-rate profile accounting for specific cooperative contributions playing different roles at different pH values. The group reported also catalytically active peptide–Au nanoparticle complexes, obtained by assembling small negatively charge His-containing peptide sequences on the surface of cationic self-assembled monolayers on gold NPs (**10**, Figure 15).[157] When self-assembled on the surface of the AuNPs, the peptides were able to accelerate the transesterification of Z-protected amino acid activated esters by more than two orders of magnitude. Here, a linear correlation was observed between the number of His-residues and the second-order rate constant, with the pH-rate profile suggesting a role as the nucleophile for the imidazole moiety.

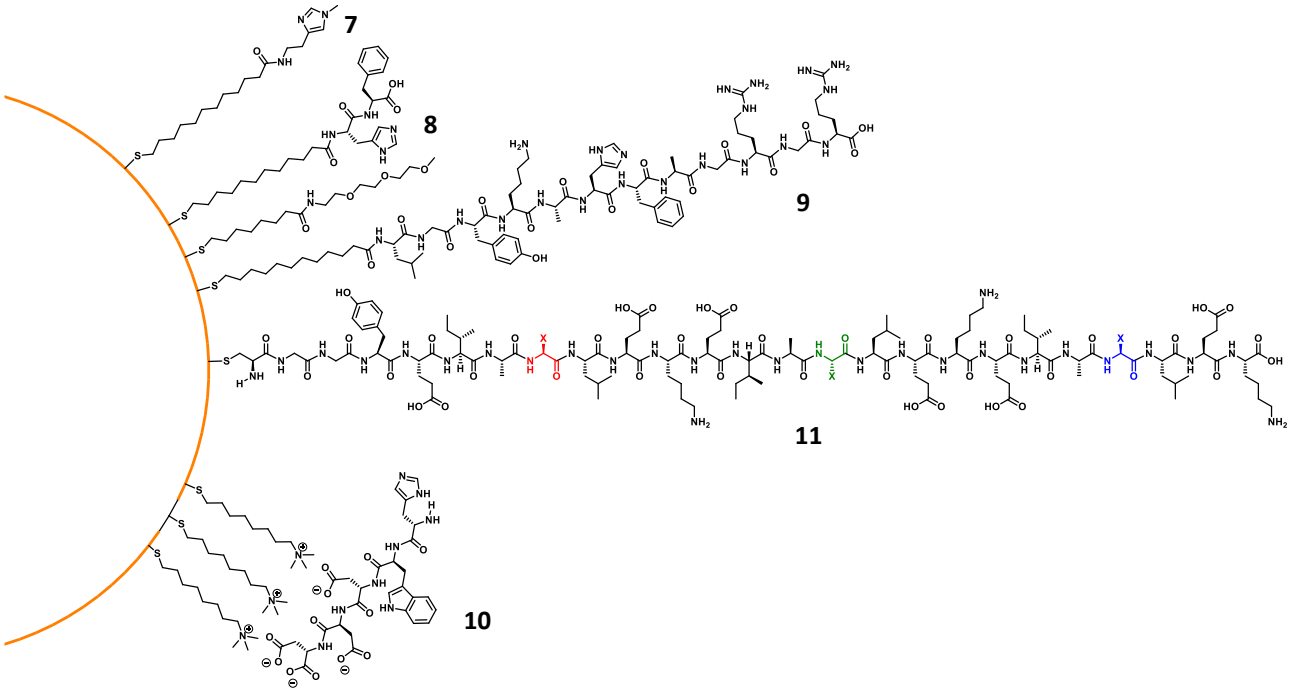


*Figure 15: Schematic representation of a gold nanoparticle (AuNP) with different passivating thiols for esterase mimicking.*

The AuNP acts as a multivalent scaffold for bringing the catalyst and substrate into close proximity, but also creates a change in the local microenvironment. The possibility to modulate the microenvironment through the self-assembly of other species was also highlighted by Koksch et al.,[158] whereby a catalytically active peptide-NP was inhibited by the addition of a complementary helical peptide to form coiled-coil aggregates and induce a conformational change in the grafted peptide. The same authors also investigated the effect that the location of the catalytic group within the peptide monolayer has on the catalytic activity and substrate specificity.[159,160] Peptide-functionalized AuNps were prepared with a series of three 25-mer peptides that consisted of three repeated heptads that differed only in the position of the replacement of an Ala with a His (**11**, Figure 15). The esterolytic activity against activated esters of Z-protected amino acids of different hydrophobicity was compared and the more hydrophilic ones were best cleaved in the intermediate region: while the proximity to the solvent reduce the cooperativity in substrate binding, due to the increased flexibility of the peptide ends, a higher water content is related to a higher activity. These results display how peptide-functionalized metallic-NP could provide a unique environment for catalysis through the balance between solvation of functional groups, rigidity of the peptide scaffold and cooperativity.

# References


1 E. Gazit, *Chem. Soc. Rev.*, 2007, **36**, 1263–1269.

2 P. Makam and E. Gazit, *Chem. Soc. Rev.*, 2018, **47**, 3406–3420.

3 R. V. Ulijn and A. M. Smith, *Chem. Soc. Rev.*, 2008, **37**, 664–675.

4 N. T. Southall, K. A. Dill and A. D. J. Haymet, *J. Phys. Chem. B*, 2002, **106**, 521–533.

5 D. Chandler, *Nature*, 2005, **437**, 640–647.

6 P. S. Cremer, A. H. Flood, B. C. Gibb and D. L. Mobley, *Nat. Chem.*, 2018, **10**, 8–16.

7 P. Tamamis, L. Adler-Abramovich, M. Reches, K. Marshall, P. Sikorski, L. Serpell, E. Gazit and G. Archontis, *Biophys. J.*, 2009, **96**, 5020–5029.

8 C. Guo, Z. A. Arnon, R. Qi, Q. Zhang, L. Adler-Abramovich, E. Gazit and G. Wei, *ACS Nano*, 2016, **10**, 8316–8324.

9 Y. Chen, A. A. Orr, K. Tao, Z. Wang, A. Ruggiero, L. J. W. Shimon, L. Schnaider, A. Goodall, S. Rencus-Lazar, S. Gilead, I. Slutsky, P. Tamamis, Z. Tan and E. Gazit, *ACS Nano*, 2020, **14**, 2798–2807.

10 K. Sato, M. P. Hendricks, L. C. Palmer and S. I. Stupp, *Chem. Soc. Rev.*, 2018, **47**, 7539–7551.

11 A. N. Edelbrock, T. D. Clemons, S. M. Chin, J. J. W. Roan, E. P. Bruckner, Z. Álvarez, J. F. Edelbrock, K. S. Wek and S. I. Stupp, *Adv. Sci.*, 2021, 2004042.

12 T. J. Moyer, F. Chen, D. J. Toft, Y. Ruff, V. L. Cryns and S. I. Stupp, *ACS Biomater. Sci. Eng.*, 2019, **5**, 6046–6053.

13 H. Cui, M. J. Webber and S. I. Stupp, *Biopolymers*, 2010, **94**, 1–18.

14 E. T. Pashuck, H. Cui and S. I. Stupp, *J. Am. Chem. Soc.*, 2010, **132**, 6041–6046.

15 S. Sur, F. Tantakitti, J. B. Matson and S. I. Stupp, *Biomater. Sci.*, 2015, **3**, 520–532.

16 A. J. Metrano, A. J. Chinn, C. R. Shugrue, E. A. Stone, B. Kim and S. J. Miller, *Chem. Rev.*, 2020, **120**, 11479–11615.

17 K. Akagawa and K. Kudo, *Acc. Chem. Res.*, 2017, **50**, 2429–2439.

18 C. R. Shugrue and S. J. Miller, *Chem. Rev.*, 2017, **117**, 11894–11951.

19 H. Wennemers, *Chem. Commun.*, 2011, **47**, 12036–12041.

20 J. Crawford and M. Sigman, *Synthesis*, 2019, **51**, 1021–1036.

21 O. C. Redfern, B. Dessailly and C. A. Orengo, *Curr. Opin. Struct. Biol.*, 2008, **18**, 394–402.

22 M. I. Freiberger, A. B. Guzovsky, P. G. Wolynes, R. G. Parra and D. U. Ferreiro, *Proc. Natl. Acad. Sci.*, 2019, **116**, 4037–4043.

23 Z. C. Girvin and S. H. Gellman, *J. Am. Chem. Soc.*, 2020, 142, 17211–17223.

24 B. Legrand, J. Aguesseau-Kondrotas, M. Simon and L. Maillard, *Catalysts*, 2020, **10**, 700.

25 S. H. Gellman, *Acc. Chem. Res.*, 1998, **31**, 173–180.

26 I. Huc and S. Hecht, *Foldamers*, 2007.

27 T. A. Martinek and F. Fülöp, *Chem. Soc. Rev.*, 2012, **41**, 687–702.

## References


28 G. Guichard and I. Huc, *Chem. Commun.*, 2011, **47**, 5933–5941.

29 D. J. Barlow and J. M. Thornton, *J. Mol. Biol.*, 1988, **201**, 601–619.

30 G. N. Ramachandran, C. Ramakrishnan and V. Sasisekharan, *J. Mol. Biol.*, 1963, **7**, 95–99.

31 M. Crisma, F. Formaggio, A. Moretto and C. Toniolo, *Biopolymers*, 2006, **84**, 3–12.

32 C. Toniolo and E. Benedetti, *Trends Biochem. Sci.*, 1991, **16**, 350–353.

33 A. Bavoso, E. Benedetti, B. Di Blasio, V. Pavone, C. Pedone, C. Toniolo and G. M. Bonora, *Proc. Natl. Acad. Sci.*, 1986, **83**, 1988–1992.

34 P. Kumar, N. G. Paterson, J. Clayden and D. N. Woolfson, *bioRxiv*, 2021, 2021.12.11.471898.

35 J. S. Richardson and D. C. Richardson, *Science*, 1988, **240**, 1648–1652.

36 V. Pavone, B. di Blasio, A. Santini, E. Benedetti, C. Pedone, C. Toniolo and M. Crisma, *J. Mol. Biol.*, 1990, **214**, 633–635.

37 A. Chakrabartty and R. L. Baldwin, in *Advances in Protein Chemistry Volume 46*, Elsevier, 1995, pp. 141–176.

38 R. L. Baldwin, *Biophys. Chem.*, 1995, **55**, 127–135.

39 M. R. Ghadiri and C. Choi, *J. Am. Chem. Soc.*, 1990, **112**, 1630–1632.

40 D. Y. Jackson, D. S. King, J. Chmielewski, S. Singh and P. G. Schultz, *J. Am. Chem. Soc.*, 1991, **113**, 9391–9392.

41 H. E. Blackwell and R. H. Grubbs, *Angew. Chemie Int. Ed.*, 1998, **37**, 3281–3284.

42 A. K. Boal, I. Guryanov, A. Moretto, M. Crisma, E. L. Lanni, C. Toniolo, R. H. Grubbs and D. J. O'Leary, *J. Am. Chem. Soc.*, 2007, **129**, 6986–6987.

43 L. D. Walensky and G. H. Bird, *J. Med. Chem.*, 2014, **57**, 6275–6288.

44 D. Seebach, M. Overhand, F. N. M. Kühnle, B. Martinoni, L. Oberer, U. Hommel and H. Widmer, *Helv. Chim. Acta*, 1996, **79**, 913–941.

45 D. H. Appella, L. A. Christianson, I. L. Karle, D. R. Powell and S. H. Gellman, *J. Am. Chem. Soc.*, 1996, **118**, 13071–13072.

46 T. L. Raguse, J. R. Lai and S. H. Gellman, *J. Am. Chem. Soc.*, 2003, **125**, 5592–5593.

47 J. J. Barchi, X. Huang, D. H. Appella, L. A. Christianson, S. R. Durell and S. H. Gellman, *J. Am. Chem. Soc.*, 2000, **122**, 2711–2718.

48 D. H. Appella, L. A. Christianson, I. L. Karle, D. R. Powell and S. H. Gellman, *J. Am. Chem. Soc.*, 1999, **121**, 6206–6212.

49 D. H. Appella, L. A. Christianson, D. A. Klein, D. R. Powell, X. Huang, J. J. Barchi and S. H. Gellman, *Nature*, 1997, **387**, 381–384.

50 X. Wang, J. F. Espinosa and S. H. Gellman, *J. Am. Chem. Soc.*, 2000, **122**, 4821–4822.

51 M. Schinnerl, J. K. Murray, J. M. Langenhan and S. H. Gellman, *Eur. J. Org. Chem.*, 2003, **2003**, 721–726.

52 L. M. Johnson and S. H. Gellman, in *Methods in Enzymology*, ed. A. E. Keating, Academic Press, 2013, pp. 407–429.

53 M. A. Schmitt, S. H. Choi, I. A. Guzei and S. H. Gellman, *J. Am. Chem. Soc.*, 2006, **128**, 4538–4539.

54 S. H. Choi, I. A. Guzei, L. C. Spencer and S. H. Gellman, *J. Am. Chem. Soc.*, 2008, **130**, 6544–6550.

55 K. Kirshenbaum, A. E. Barron, R. A. Goldsmith, P. Armand, E. K. Bradley, K. T. V. Truong, K. A. Dill, F. E. Cohen and R. N. Zuckermann, *Proc. Natl. Acad. Sci.*, 1998, **95**, 4303–4308.

56 C. W. Wu, T. J. Sanborn, K. Huang, R. N. Zuckermann and A. E. Barron, *J. Am. Chem. Soc.*, 2001, **123**, 6778–6784.

57 D. P. Tilly, W. Cullen, H. Zhong, R. Jamagne, I. Vitórica-Yrezábal and S. J. Webb, *Chem. – A Eur. J.*, , DOI:10.1002/chem.202104293.

58 G. Song and K. Jeong, *Chempluschem*, 2020, **85**, 2475–2481.

59 J. Y. Hwang, H.-G. Jeon, Y. R. Choi, J. Kim, P. Kang, S. Lee and K.-S. Jeong, *Org. Lett.*, 2017, **19**, 5625–5628.

60 S. Juliá, J. Masana and J. C. Vega, *Angew. Chem., Int. Ed. Engl.*, 1980, **19**, 929–931.

61 S. Juliá, J. Guixer, J. Masana, J. Rocas, S. Colonna, R. Annuziata and H. Molinari, *J. Chem. Soc., Perkin Trans. 1*, 1982, 1317–1324.

62 G. Carrea, S. Colonna, D. R. Kelly, A. Lazcano, G. Ottolina and S. M. Roberts, *Trends Biotechnol.*, 2005, **23**, 507–513.

63 D. R. Kelly and S. M. Roberts, *Chem. Commun.*, 2004, 2018.

64 P. E. Coffey, K.-H. Drauz, S. M. Roberts, J. Skidmore and J. A. Smith, *Chem. Commun.*, 2001, 2330–2332.

65 A. Berkessel, N. Gasch, K. Glaubitz and C. Koch, *Org. Lett.*, 2001, **3**, 3839–3842.

66 T. Umeno, A. Ueda, M. Doi, T. Kato, M. Oba and M. Tanaka, *Tetrahedron Lett.*, 2019, **60**, 151301.

67 A. Ueda, T. Umeno, M. Doi, K. Akagawa, K. Kudo and M. Tanaka, *J. Org. Chem.*, 2016, **81**, 6343–6356.

68 D. Bécart, V. Diemer, A. Salaün, M. Oiarbide, Y. R. Nelli, B. Kauffmann, L. Fischer, C. Palomo and G. Guichard, *J. Am. Chem. Soc.*, 2017, **139**, 12524–12532.

69 L. Fischer, P. Claudon, N. Pendem, E. Miclet, C. Didierjean, E. Ennifar and G. Guichard, *Angew. Chemie Int. Ed.*, 2009, **49**, 1067–1070.

70 V. Semetey, D. Rognan, C. Hemmerlin, R. Graff, J.-P. Briand, M. Marraud and G. Guichard, *Angew. Chemie Int. Ed.*, 2002, **41**, 1893–1895.

71 V. Diemer, L. Fischer, B. Kauffmann and G. Guichard, *Chem. - A Eur. J.*, 2016, **22**, 15684–15692.

72 B. A. F. Le Bailly, L. Byrne and J. Clayden, *Angew. Chemie Int. Ed.*, 2016, **55**, 2132–2136.

73 C. Mayer, M. M. Müller, S. H. Gellman and D. Hilvert, *Angew. Chemie Int. Ed.*, 2014, **53**, 6978–6981.

74 Z. Hegedus, C. M. Grison, J. A. Miles, S. Rodriguez-Marin, S. L. Warriner, M. E. Webb and A. J. Wilson, *Chem. Sci.*, 2019, **10**, 3956–3962.

75 A.-B. Bornhof, A. Bauzá, A. Aster, M. Pupier, A. Frontera, E. Vauthey, N. Sakai and S. Matile, *J. Am. Chem. Soc.*, 2018, **140**, 4884–4892.

76 M. Kheirabadi, N. Çelebi-Ölçüm, M. F. L. Parker, Q. Zhao, G. Kiss, K. N. Houk and C. E. Schafmeister, *J. Am. Chem. Soc.*, 2012, **134**, 18345–18353.

77 C. E. Schafmeister, Z. Z. Brown and S. Gupta, *Acc. Chem. Res.*, 2008, **41**, 1387–1398.

78 M. F. L. Parker, S. Osuna, G. Bollot, S. Vaddypally, M. J. Zdilla, K. N. Houk and C. E. Schafmeister, *J. Am. Chem. Soc.*, 2014, **136**, 3817–3827.

79 W. M. Rink and F. Thomas, *Chem. - A Eur. J.*, 2019, **25**, 1665–1677.

80 P. S. P. Wang, J. B. Nguyen and A. Schepartz, *J. Am. Chem. Soc.*, 2014, **136**, 6810–6813.

81 C. J. Craig, J. L. Goodman and A. Schepartz, *ChemBioChem*, 2011, **12**, 1035–1038.

82 K. Johnsson, R. K. Allemann, H. Widmer and S. A. Benner, *Nature*, 1993, **365**, 530–532.

83 M. M. Müller, M. A. Windsor, W. C. Pomerantz, S. H. Gellman and D. Hilvert, *Angew. Chemie Int. Ed.*, 2009, **48**, 922–925.

84 J. Aguesseau-Kondrotas, M. Simon, B. Legrand, J. Bantigniès, Y. K. Kang, D. Dumitrescu, A. Van der Lee, J. Campagne, R. M. de Figueiredo and L. T. Maillard, *Chem. – A Eur. J.*, 2019, **25**, 7396–7401.

85 L. Mathieu, B. Legrand, C. Deng, L. Vezenkov, E. Wenger, C. Didierjean, M. Amblard, M.-C. Averlant-Petit, N. Masurier, V. Lisowski, J. Martinez and L. T. Maillard, *Angew. Chemie Int. Ed.*, 2013, **52**, 6006–6010.

86 M. Wiesner, G. Upert, G. Angelici and H. Wennemers, *J. Am. Chem. Soc.*, 2010, **132**, 6–7.

87 M. Wiesner, J. D. Revell, S. Tonazzi and H. Wennemers, *J. Am. Chem. Soc.*, 2008, **130**, 5610–5611.

88 M. Wiesner, M. Neuburger and H. Wennemers, *Chem. - A Eur. J.*, 2009, **15**, 10103–10109.

89 T. Schnitzer and H. Wennemers, *Helv. Chim. Acta*, , DOI:10.1002/hlca.201900070.

90 M. J. Kinghorn, G. A. Valdivia-Berroeta, D. R. Chantry, M. S. Smith, C. C. Ence, S. R. E. Draper, J. S. Duval, B. M. Masino, S. B. Cahoon, R. R. Flansburg, C. J. Conder, J. L. Price and D. J. Michaelis, *ACS Catal.*, 2017, **7**, 7704–7708.

91 A. X. Wayment, M. Rodriguez Moreno, C. J. Jones, G. J. Smith, P. Jarman, N. J. Garcia Morin, M. J. Coombs, J. A. Parkman, C. D. Barlow, S. Allington Smith, S. R. Burt and D. J. Michaelis, *Org. Lett.*, 2022, **24**, 2983–2988.

92 A. Erkkilä and P. M. Pihko, *Eur. J. Org. Chem.*, 2007, **2007**, 4205–4216.

93 Z. C. Girvin and S. H. Gellman, *J. Am. Chem. Soc.*, 2018, **140**, 12476–12483.

94 Z. C. Girvin, M. K. Andrews, X. Liu and S. H. Gellman, *Science*, 2019, **366**, 1528–1531.

95 V. Martí-Centelles, M. D. Pandey, M. I. Burguete and S. V. Luis, *Chem. Rev.*, 2015, **115**, 8736–8834.

96 M. K. Andrews, X. Liu and S. H. Gellman, *J. Am. Chem. Soc.*, 2022, **144**, 2225–2232.

97 N. D. Rawlings and G. Salvesen, *Handbook of Proteolytic Enzymes*, Elsevier Ltd, 2013, vol. 1–3.

98 D. Kahne and W. C. Still, *J. Am. Chem. Soc.*, 1988, **110**, 7529–7534.

99 R. Wolfenden, *Chem. Rev.*, 2006, **106**, 3379–3396.

100 R. Wolfenden and M. J. Snider, *Acc. Chem. Res.*, 2001, **34**, 938–945.

101 M. D. Nothling, Z. Xiao, A. Bhaskaran, M. T. Blyth, C. W. Bennett, M. L. Coote and L. A. Connal, *ACS Catal.*, 2019, **9**, 168–187.

102 X. Zhang and K. N. Houk, *Acc. Chem. Res.*, 2005, **38**, 379–385.

103 M. Raynal, P. Ballester, A. Vidal-Ferran and P. W. N. M. van Leeuwen, *Chem. Soc. Rev.*, 2014, **43**, 1734–1787.

104 L. Polgár, *Cell. Mol. Life Sci.*, 2005, **62**, 2161–2172.

105 A. R. Buller and C. A. Townsend, *Proc. Natl. Acad. Sci.*, 2013, **110**, E653–E661.

106 L. Hedstrom, *Chem. Rev.*, 2002, **102**, 4501–4524.

107 T. Ema, D. Tanida, T. Matsukawa and T. Sakai, *Chem. Commun.*, 2008, 957–959.

108 J. J. Garrido-González, M. M. Iglesias Aparicio, M. M. García, L. Simón, F. Sanz, J. R. Morán and Á. L. Fuentes

de Arriba, *ACS Catal.*, 2020, **10**, 11162–11170.

109 J. J. Garrido-González, E. Sánchez-Santos, A. Habib, Á. V. Cuevas Ferreras, F. Sanz, J. R. Morán and Á. L. Fuentes de Arriba, *Angew. Chemie Int. Ed.*, , DOI:10.1002/anie.202206072.

110 R. Breslow and S. D. Dong, *Chem. Rev.*, 1998, **98**, 1997–2012.

111 D.-Q. Yuan, Y. Kitagawa, K. Aoyama, T. Douke, M. Fukudome and K. Fujita, *Angew. Chemie Int. Ed.*, 2007, **46**, 5024–5027.

112 K. I. Assaf and W. M. Nau, *Chem. Soc. Rev.*, 2015, **44**, 394–418.

113 B. W. Purse and J. Rebek, *Proc. Natl. Acad. Sci.*, 2005, **102**, 10777–10782.

114 D. J. Cram, H. E. Katz and I. B. Dicker, *J. Am. Chem. Soc.*, 1984, **106**, 4987–5000.

115 A. Gissot and J. Rebek, *J. Am. Chem. Soc.*, 2004, **126**, 7424–7425.

116 H. Tsutsumi, K. Hamasaki, H. Mihara and A. Ueno, *J. Chem. Soc. Perkin Trans. 2*, 2000, 1813–1818.

117 Y. Li, Y. Zhao, S. Hatfield, R. Wan, Q. Zhu, X. Li, M. McMills, Y. Ma, J. Li and K. L. Brown, *Bioorg. Med. Chem.*, 2000, **8**, 2675–2680.

118 Y. Ma, X. Chen, M. Sun, R. Wan, C. Zhu, Y. Li and Y. Zhao, *Amino Acids*, 2008, **35**, 251–256.

119 M. J. Macdonald, L. D. Lavis, D. Hilvert and S. H. Gellman, *Org. Lett.*, 2016, **18**, 3518–3521.

120 K. Adamala and J. W. Szostak, *Nat. Chem.*, 2013, **5**, 495–501.

121 L. Gabrielli, L. J. Prins, F. Rastrelli, F. Mancin and P. Scrimin, *Eur. J. Org. Chem.*, 2020, **2020**, 5044–5055.

122 L. Prins, F. Mancin and P. Scrimin, *Curr. Org. Chem.*, 2009, **13**, 1050–1064.

123 A. Barnard and D. K. Smith, *Angew. Chemie Int. Ed.*, 2012, **51**, 6572–6581.

124 R. Haag, *Beilstein J. Org. Chem.*, 2015, **11**, 848–849.

125 J. Huskens, L. J. Prins, R. Haag and B. J. Ravoo, Eds., *Multivalency*, Wiley, 2018.

126 C. A. Hunter and H. L. Anderson, *Angew. Chemie Int. Ed.*, 2009, **48**, 7488–7499.

127 *Catalysis in Micellar and Macromolecular Systems*, Elsevier, 1975.

128 S. Ta§cioğlu, *Tetrahedron*, 1996, **52**, 11113–11152.

129 U. Tonellato, *J. Chem. Soc. Perkin Trans. 2*, 1977, 821–827.

130 R. Fornasier and U. Tonellato, *J. Chem. Soc. Perkin Trans. 2*, 1982, 899–902.

131 L. Anoardi, R. Fornasier and U. Tonellato, *J. Chem. Soc. Perkin Trans. 2*, 1981, 260–265.

132 U. Tonellato, *J. Chem. Soc. Perkin Trans. 2*, 1976, 771–776.

133 Y. Ihara, M. Nango, Y. Kimura and N. Kuroki, *J. Am. Chem. Soc.*, 1983, **105**, 1252–1255.

134 T. Kunitake, Y. Okahata and T. Sakamoto, *J. Am. Chem. Soc.*, 1976, **98**, 7799–7806.

135 R. A. Moss, R. C. Nahas and S. Ramaswami, *J. Am. Chem. Soc.*, 1977, **99**, 627–629.

136 J. M. Brown, R. L. Elliott, C. G. Griggs, G. Helmchen and G. Nill, *Angew. Chem., Int. Ed. Engl.*, 1981, **20**, 890–892.

137 T. Kunitake and S. Shinkai, in *Advances in Physical Organic Chemistry*, eds. V. Gold and D. Bethell, Academic Press, 1980, pp. 435–487.

138 M. D. Nothling, Z. Xiao, N. S. Hill, M. T. Blyth, A. Bhaskaran, M.-A. Sani, A. Espinosa-Gomez, K. Ngov, J. White, T. Buscher, F. Separovic, M. L. O'Mara, M. L. Coote and L. A. Connal, *Sci. Adv.*, , DOI:10.1126/sciadv.aaz0404.

139 E. A. C. Davie, S. M. Mennen, Y. Xu and S. J. Miller, *Chem. Rev.*, 2007, **107**, 5759–5812.

140 M. O. Guler and S. I. Stupp, *J. Am. Chem. Soc.*, 2007, **129**, 12082–12083.

141 M. Bélières, N. Chouini-Lalanne and C. Déjugnat, *RSC Adv.*, 2015, **5**, 35830–35842.

142 Y. Zhao, B. Lei, M. Wang, S. Wu, W. Qi, R. Su and Z. He, *J. Mater. Chem. B*, 2018, **6**, 2444–2449.

143 M. Wang, Y. Lv, X. Liu, W. Qi, R. Su and Z. He, *ACS Appl. Mater. Interfaces*, 2016, **8**, 14133–14141.

144 C. Zhang, X. Xue, Q. Luo, Y. Li, K. Yang, X. Zhuang, Y. Jiang, J. Zhang, J. Liu, G. Zou and X.-J. J. Liang, *ACS Nano*, 2014, **8**, 11715–11723.

145 M. Kurbasic, A. M. Garcia, S. Viada and S. Marchesan, *Molecules*, 2020, **26**, 173.

146 A. M. Garcia, M. Kurbasic, S. Kralj, M. Melchionna and S. Marchesan, *Chem. Commun.*, 2017, **53**, 8110–8113.

147 K. S. Broo, H. Nilsson, J. Nilsson, A. Flodberg and L. Baltzer, *J. Am. Chem. Soc.*, 1998, **120**, 4063–4068.

148 K. S. Broo, H. Nilsson, J. Nilsson and L. Baltzer, *J. Am. Chem. Soc.*, 1998, **120**, 10287–10295.

149 Y. Bai, Y. Ling, W. Shi, L. Cai, Q. Jia, S. Jiang and K. Liu, *ChemBioChem*, 2011, **12**, 2647–2658.

150 A. J. Burton, A. R. Thomson, W. M. Dawson, R. L. Brady and D. N. Woolfson, *Nat. Chem.*, 2016, **8**, 837–844.

151 X. Fan, Z. Li and X. J. Loh, *Polym. Chem.*, 2016, **7**, 5898–5919.

152 N. Maillard, R. Biswas, T. Darbre and J.-L. Reymond, *ACS Comb. Sci.*, 2011, **13**, 310–320.

153 E. Delort, T. Darbre and J.-L. Reymond, *J. Am. Chem. Soc.*, 2004, **126**, 15642–15643.

154 L. Pasquato, F. Rancan, P. Scrimin, F. Mancin and C. Frigeri, *Chem. Commun.*, 2000, 2253–2254.

155 P. Pengo, S. Polizzi, L. Pasquato and P. Scrimin, *J. Am. Chem. Soc.*, 2005, **127**, 1616–1617.

156 P. Pengo, L. Baltzer, L. Pasquato and P. Scrimin, *Angew. Chemie Int. Ed.*, 2007, **46**, 400–404.

157 D. Zaramella, P. Scrimin and L. J. Prins, *J. Am. Chem. Soc.*, 2012, **134**, 8396–8399.

158 D. J. Mikolajczak, J. L. Heier, B. Schade and B. Koksch, *Biomacromolecules*, 2017, **18**, 3557–3562.

159 D. J. Mikolajczak, J. Scholz and B. Koksch, *ChemCatChem*, 2018, **10**, 5665–5668.

160 D. J. Mikolajczak, A. A. Berger and B. Koksch, *Angew. Chemie Int. Ed.*, 2020, **59**, 8776–8785.

# 2. Light-mediated catalytic activity in foldamer mimic proteases

Serine proteases are some of the most well-studied and ubiquitous enzymes in biology. These proteases are characterized by a catalytic triad composed of Ser-His-Asp (Figure 1A). This triad accelerates the rate of amide or ester bond hydrolysis by factors of $10^8$ to $10^{10}$ compared to the spontaneous hydrolysis rate of the same substrate in neutral aqueous solution (see Section 1.3).

The amino acids Ser and His are conserved as key amino acids in the catalytic site of a wide range of hydrolytic enzymes and self-splicing sequences. Therefore, it was hypothesized that an extremely minimalistic version of this catalytic sites (a Ser/His diad) free of any secondary and tertiary structural elements could be capable of ester or amide bond hydrolysis. Seryl-histidine dipeptide (Ser-His, Figure 1B) is the shortest peptide sequence reported to catalyse the hydrolysis of a wide range of substrates, including bovine serum albumin (BSA), DNA and *p*-nitrophenyl acetate (*p*-NPA) at various pH and temperature. The development of simple synthetic catalysts for challenging hydrolysis reaction is a fascinating goal for synthetic chemists; the performances of this dipeptide sequence are impressive and inspiring for the development of simple enzyme-mimetic catalysts. However, despite the reports of Ser-His being able to cleave proteins and other substrates by promoting their hydrolysis, serious concerns were raised on the actual performances of the catalyst. In the work of Li et al.,[1] the hydrolytic performance of Ser-His dipeptide was tested incubating BSA in Britton–Robinson buffer at 50°C with or without Ser-His (50 mM). The performance of the catalytic system was analysed by silver-stained 10% reducing PolyAcrylamide Gel Electrophoresis (PAGE), in which the peptide bond hydrolysis of BSA into smaller peptide fragments was deducted from the appearance of a smear of fragments with progressively higher mobility. Ser-His dipeptide was also found also to be competent in the hydrolysis of the model ester substrate *p*-nitrophenyl acetate (*p*-NPA). The catalytic activity was said to be dependent on the concentration of Ser-His, as well as on pH and temperature. The report however lacked any sort of characterization for the BSA degradation and data on the pH dependence of *p*-NPA hydrolysis, thus its findings were reviewed by Gellmann and co-workers.[2] The catalytic activity of the Ser-His dipeptide was re-evaluated under the previously reported conditions with a set of ester and amide substrates (Figure 1C).

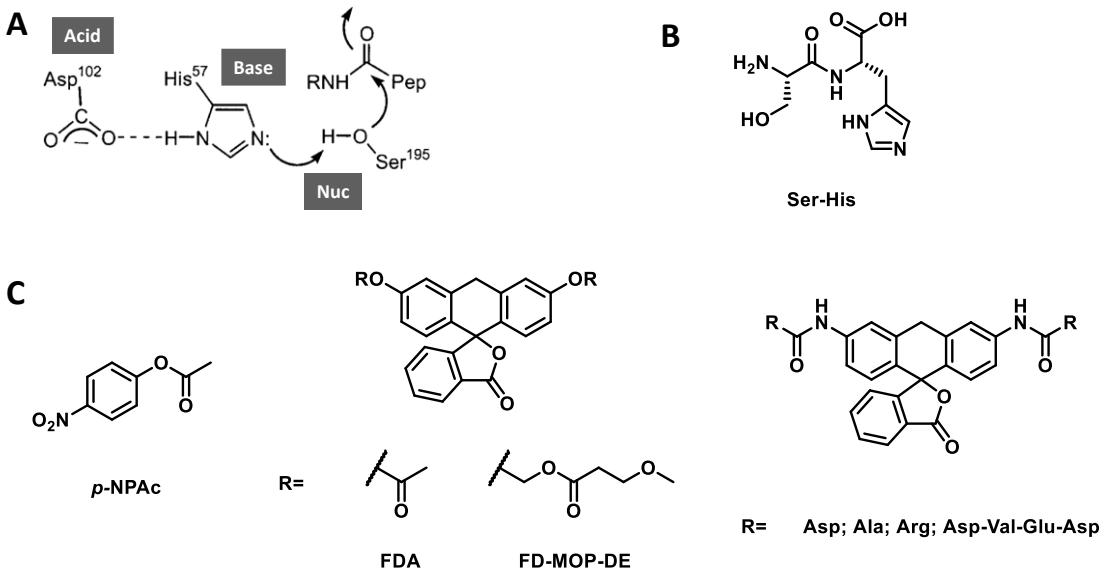


*Figure 1: (A) Detail of the catalytic triad and chemical mechanism for the hydrolysis of ester and amide bonds by serine proteases. (B) Chemical structure of Ser-His dipeptide. (C, left) p-nitrophenyl acetate (p-NPA); (C, centre) fluorogenic ester substrates: fluorescein diacetate (FDA) and fluorescein di(3-methoxy-propanoxymethyl ether) (FD-MOP-DE); (C, right) fluorogenic amide substrates: diacylated derivative of rhodamine 110 with Asp, Ala, Arg and Asp-Val-Glu-Asp tetrapeptide.*

The hydrolysis of *p*-NPA was investigated at pH 4, 6 and 8 (10 mM Ser-His, 2 mM *p*-NPA and 40 mM Britton–Robinson buffer). In contrast to the earlier findings, no evidence of significant *p*-NPA hydrolysis was detected at acidic pH. At pH 8, however, substantial difference in extent of hydrolysis between the catalyzed and uncatalyzed reaction was observed. Thus, the catalytic activity reported at pH 6 is probably the result of a higher pH than the reported one. The Ser-His dipeptide also did not show any catalytic activity on two more challenging fluorogenic ester substrates at pH 6 (Figure 1C, centre). Fluorescein diacetate (FDA) and fluorescein di(3-methoxy-propanoxymethyl ether) (FD-MOP-DE) both hydrolyse to fluorescein and their hydrolysis can be followed through fluorescence intensity measurements. While FDA as an activity similar to *p*-NPA in term of hydrolysis, the acyloxymethyl ether containing substrate can be considered an un-activated ester. The rate of hydrolysis for both of these substrates in the presence of Ser-His were comparable to the background reaction.

A set of four amide rhodamine derivatives was also tested (Figure 1C, right). The acyl fragment consists of an acidic (Asp), basic (Arg) or neutral (Ala) side chain an Asp-Val-Glu-Asp tetrapeptide, employed to detect caspase-3 activity. In conditions like the ones originally employed for the BSA hydrolysis, no increase in the hydrolysis rate was observed in the reaction containing Ser-His relative

to the control experiments. Overall, this study was unable to confirm the role of Ser-His dipeptide as a general catalyst of amide or ester hydrolysis.

In a follow-up report the authors of the original paper expanded the protein substrate scope to GFP, CyPA and myoglobin (Mb).[3] The study was centred on the cleavage efficiency and cleavage propensity of Ser-His ag at both the primary and secondary sequence levels of the protein substrates. Protein samples were incubated with and without Ser-His dipeptide in buffer at pH 6.0 and 50°C for GFP, Mb and BSA, and in a buffer consisting of 10 mM KAc and 10 mM $KH_2PO_4$ (pH 6.0), 5 mM DTT, 0.02% $NaN_3$ at 37 °C for CyPA due to its thermal instability. The product distribution of the reaction was analysed by high-resolution MALDI-TOF/TOF mass spectrometry for GFP and CyPA and by nanoLC–ESI–MS for BSA and Mb. The cleavage sites were determined by mapping the HRMS data (peptide fragments) back to the protein sequences. Based on the reported structures, it was shown that while the cleavage efficiencies vary (Mb > CyPA > GFP/BSA), there is no intrinsic preference for a particular secondary structure. The amino acid specificity of the cleavage site was low with no consistency. Only a set of three amino acids (Tryptophan, Asparagine and Phenylalanine) were found to be easily cleaved; it should be noted that these amino acids are rarely present in the protein samples, thus accidental cleavage could result in a high cleavage propensity value. This article was not devoid of criticism either. It is interesting to note that the assays were performed in a single experimental condition and the article lacks any evaluation of the structure of the four proteins in this set up. Moreover, while the four proteins have a resolved structure, the Accessible Surface Area (ASA) of the residues was not calculated. The lack of comparison between the proteins in their native forms and under denaturing conditions hinders a meaningful analysis of the actually available cleavage sites for hydrolysis.

Therefore, while the catalytic activity of a simple molecule as Ser-His would be an impressive achievement in the design of minimalistic enzyme-mimetic catalysts, these findings suggest that the discovery of such a catalyst is still an open challenge in molecular catalyst design. Aside from the chemical identity of the reactive side chains involved in the catalytic site, several factors should be taken in consideration during the design of a protease mimic.

The precise orientations of the catalytic groups and their chemical environment are also of paramount importance for catalytic activity; thus, disorder or slight perturbations in the structure of the active site can have enormous effects on activity. Artificial mimicry of the structure-forming propensity of biomolecules over short distances can be achieved using foldamers. Foldamer structures allow chemists to broaden and diversify the more limited range of structural components that build up natural proteins and a foldamer-based approach to enzyme mimics is becoming an attractive alternative to well-developed strategies in recent years (see Section 1.2). In the work presented in this chapter, we developed a short catalytic helical foldamer in which the proper disposition of Ser-His-Asp side chains and a fumaramide/maleamide chromophore allow the use of light as a cofactor for esterase activity.

Photosensitive fumaramide/maleamide linkers were shown to be particularly compatible with the hydrogen-bonded structures of peptide foldamers. In a previous work of the the group where I carried out my PhD, it was showed that foldamers containing a fumaramide (*E*) or a maleamide (*Z*) residue display conformationally "insulating" or "conducting" properties.[4] An (*E*) unsaturated fumaramide linkage introduced into Aib peptide foldamer structures was photoisomerized to its (*Z*) (maleamide) isomer by irradiation with UV light. As a result of the photoisomerization, a new hydrogen-bonded contact becomes possible between the peptide domains located on either side of the unsaturated (*E*) linkage. Importantly, this new folded structure places in close contact the two-side chains of the two amino acids linked to the *maleamide* (Figure 2).

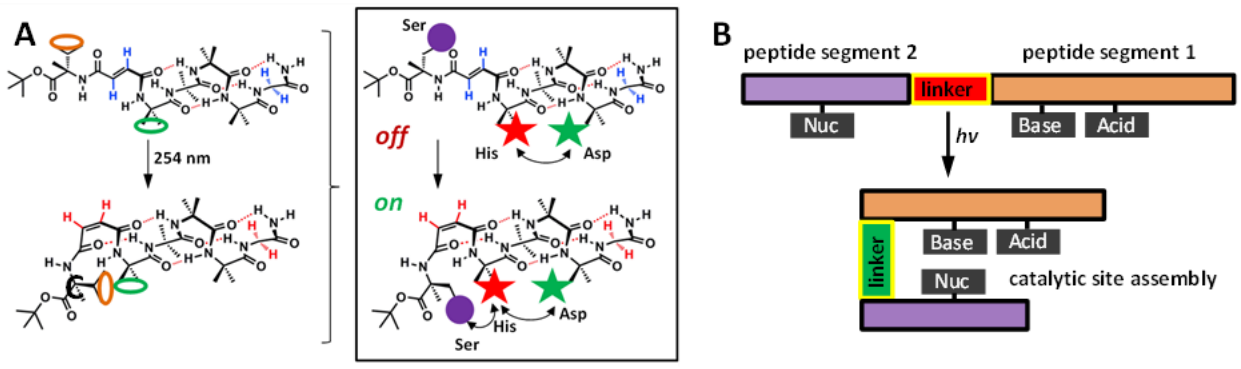


*Figure 2: (A) Helical foldamers incorporating photoswitchable residues: the photoswitch allows the contact between the two selected side chains. (B) Schematic representation of the catalytic site assembly in the functional photo-responsive foldamer reported in this work.*

In particular, we planned to mimic protease activity by the use of helical foldamers able to place in right distance and geometry Asp and His residues. Ser is introduced in a faraway position and only after activation by light (foldamer *E* to *Z* isomerization) it will be sited closely to His residue. In this way, the catalytic performance of the triad will be activated on demand (Figure 2). This feature resembles that of the protease, where the triad is activated by chemical reactions (i.e, phosphorylation) which allow a protein conformational change, thus to locate Ser-His-Asp in the right spatial confinement and hence to allow triad to work.

As a starting point a set of peptide foldamers was synthesized, built principally from Aib residues (Figure 3).

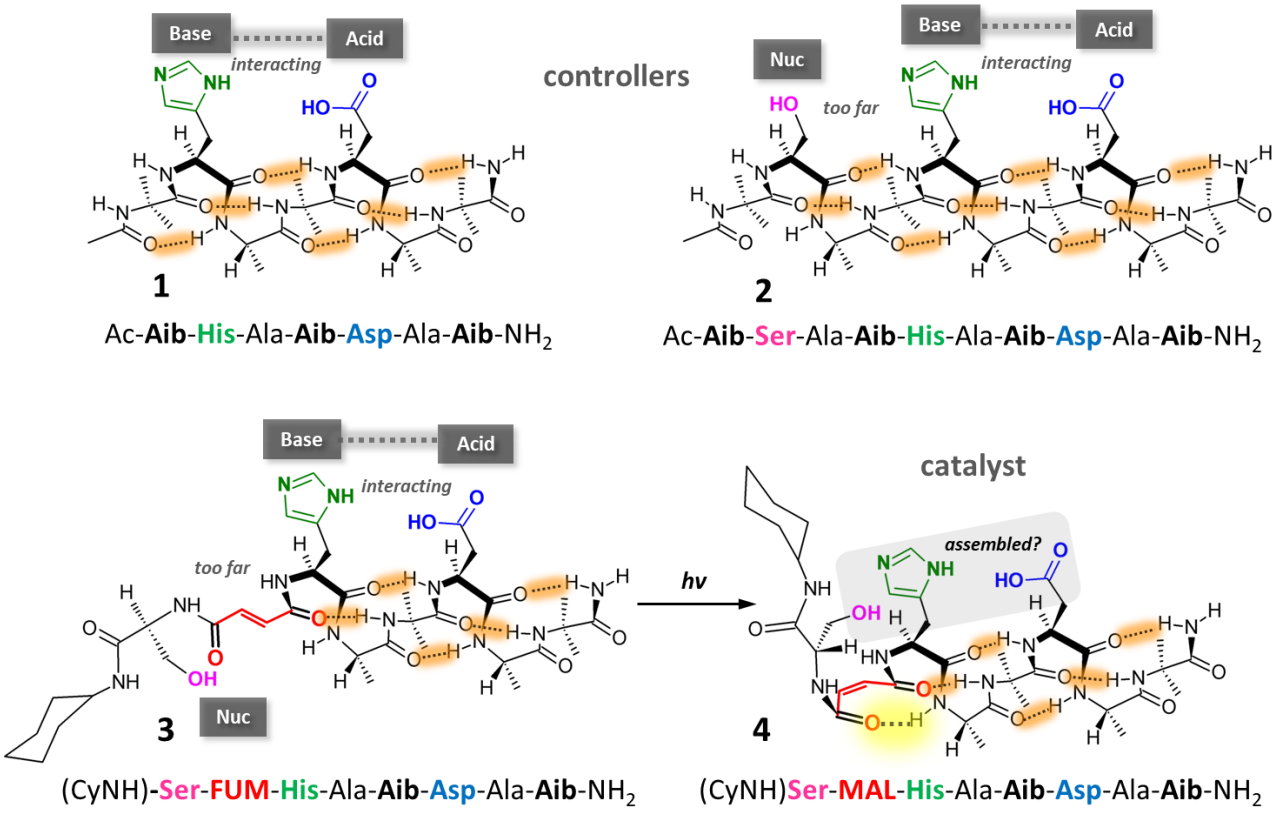


*Figure 3: Chemical structures and foldamer composition sequences of helical foldamers presented in this work (CyNH = cyclohexyl amide; FUM = fumaramide; MAL = maleamide).*

Based on the $3_{10}$-helix scaffold, the foldamers were synthesized in a way that places sequentially, at residue separations of *i*/*i*+3, His and Asp and, analogously, Ser, His and Asp (Figure 4, compounds **1** and **2**). Next, a second set of molecules was synthesized, related to foldamer **1** but the N-terminal Aib was replaced by a fumaramide linked to an appropriately modified Ser residue (**3**) and the

foldamer capped as a cyclohexylamide to improve local hydrophobicity. Foldamer **4** is the *Z* geometrical isomer of foldamer **3** (Figure 4, compounds **3** and **4**).

Foldamers **1** and **2** were synthesized on a Rink-amide resin by solid phase peptide synthesis with from Fmoc protected monomers. Solid phase peptide synthesis was also used to obtain foldamer **3**. In this case, with the Fmoc-protecting group removed from the N-terminus His(Trt) residue, the free amino group was allowed to react with activated Cy-NH-Ser(OtBu)-NH-FUM-COOH (**I**, Figure 4A and B). Cleavage from the resin afforded foldamer **3**, which was isomerized to its corresponding maleamide (*Z*) isomer **4** by irradiation at 254 nm in a diluted MeOH/$CH_3CN$ mixture (Figure 4).

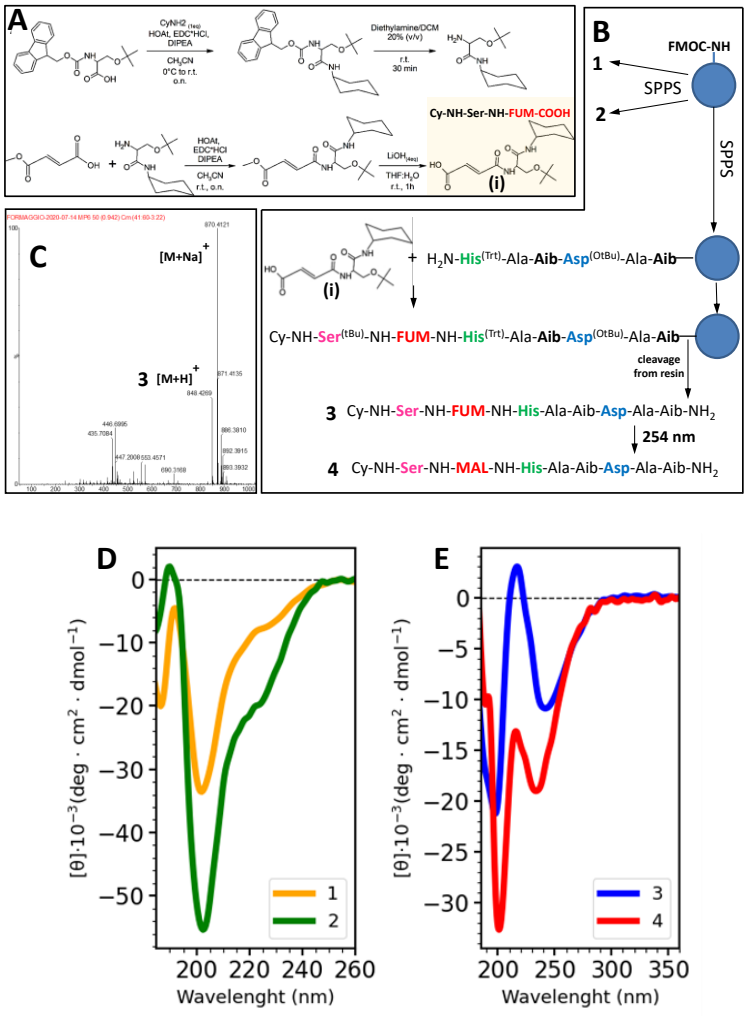


*Figure 4: (A and B) synthetic routes for foldamers* ***1-4****. (****C****) HRMS spectrum of foldamer* ***3*** *after cleavage from the resin. (D) Comparison of ECD spectra of compound* ***1*** *and* ***2*** *in water (0.3 mM). (E) Comparison of ECD spectra of Compound* ***3*** *and* ***4*** *in water (0.3 mM).*

The ECD spectra of foldamers **1** and **2** in water are consistent with the expected $3_{10}$-helical structure of Aib-rich peptides (Figure 4D). Foldamers **3** and **4** displays similar, but distinct, ECD profiles to previously reported maleamide/fumaramide containing peptides (Figure 4E).[4] *E* isomer **3** displays a moderately intense negative band with maximum at 198 nm followed by two weak bands of opposite sign, one positive at 216 nm and one negative at 240 nm, respectively (Figure 4E, blue line). The *Z* isomer **4** displays two negative maxima at 200 nm (having a shoulder at 188 nm) and at 234 nm (Figure 4E, red line). Thus, the presence of the maleamide/fumaramide chromophore hinders a conformational analysis in foldamers **3** and **4** by comparison of the ECD profiles alone.

Therefore, the consequences of isomerizing the *E* double bond of **3** to the *Z* double bond of **4** were studied using 2D NMR (ROESY) experiments in $D_2O/H_2O$ and comparing 1D $^1$H-NMR in different solvents. Comparison of the 1D $^1$H-NMR spectra of peptides **3** and **4** in $CD_3CN$ reveals significantly different chemical shifts for the NH signals of His(1) ($\Delta\delta_{E/Z} \approx 0.57$ppm) and Ala(2) ($\Delta\delta_{E/Z} \approx 0.74$ppm) in the two isomers, suggesting the formation of new intramolecular H-bonds in this solvent (Figure 5D). The same comparison in $D_2O/H_2O$, DMSO-$d_6$ and $CD_3OH$ is reported in Figure 4A, B and C respectively. Although the effects of proton solvation do not allow significantly difference in the chemical shifts to be seen, Ala(2) seems to be involved in a new intramolecular H-bond also in these more challenging solvents (orange circle, Figure 5).

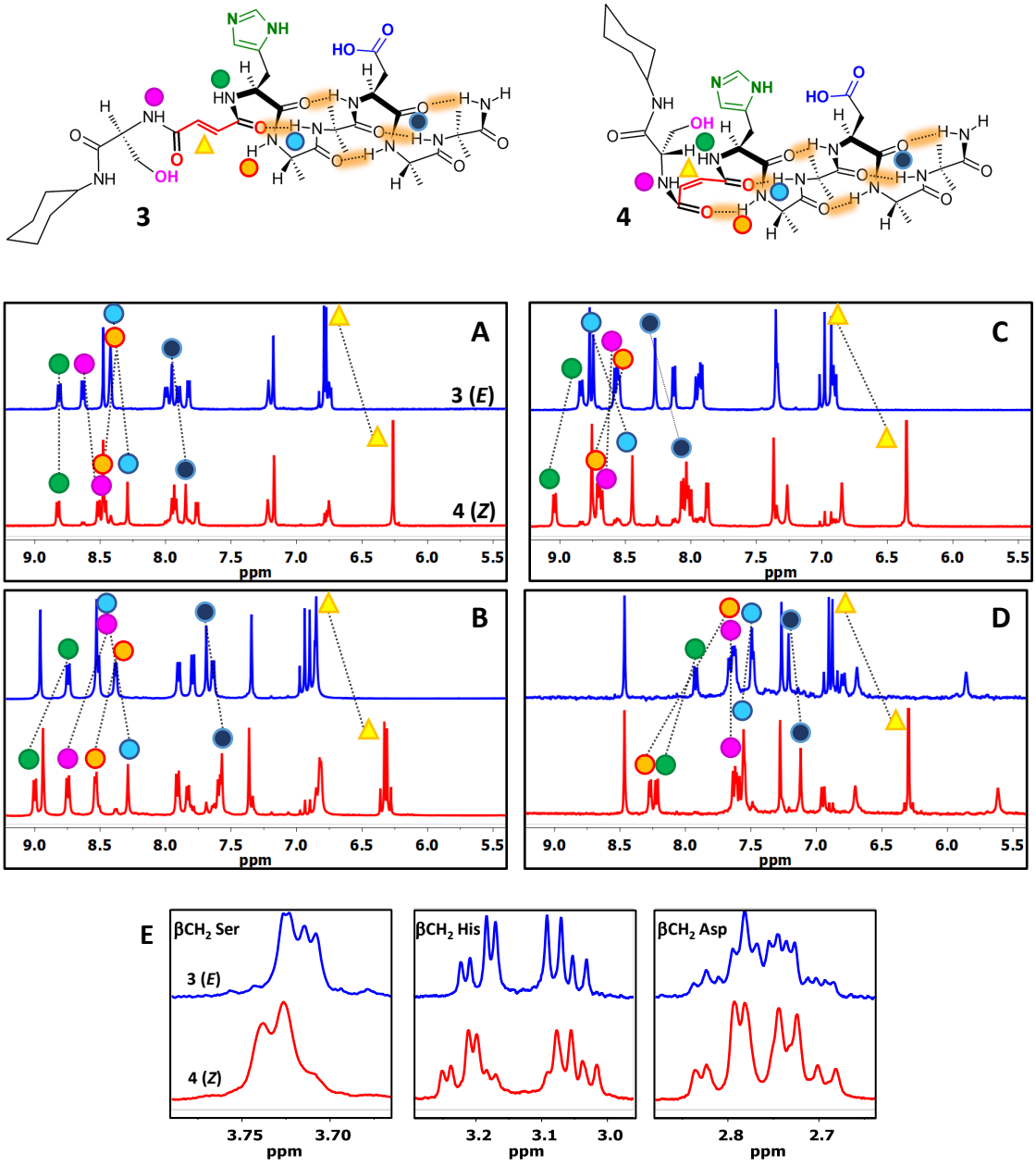


*Figure 5: (A-D) $^1$H-NMR traces in the region of the NH amide proton resonance of **3**(E, blue line) and **4**(Z, red line) in $D_2O/H_2O$ (A), DMSO-d6 (B), $CD_3OH$ (C) and $CD_3CN$ (D). (E) $^1$H-NMR traces comparing $\beta CH_2$ protons resonance of Ser, His and Asp of **3** and **4**.*

More importantly, in the $\beta CH_2$ resonance region all the three amino acids Ser, His and Asp show geometry-dependent differences in chemical shift and/or coupling constants (Figure 5E). In particular, the Ser $\beta CH_2$ signals in foldamer **4** displayed a slight up-field shift together with a different coupling constant with respect to foldamer **3**, which may suggest a hydrogen bond contact involving the Ser hydroxyl.

ROESY spectra of both **3** and **4** shows a series of sequential $\alpha$NH $i \rightarrow \alpha$NH$(i+1)$ and $\beta$CH$_3$ $i \rightarrow \alpha$NH$(i+1)$ correlations suggesting that the -His-Ala-Aib-Asp-Ala-Aib-NH$_2$ segment is indeed folded into a helical conformation, as expected, and that the helix remains almost unchanged by the isomerization process. ROESY experiments also show for foldamer **4** a spatial proximity between the Ser $\beta$CH$_2$ protons and the $\delta$CH proton of the imidazole ring, an interaction that is absent in foldamer **3**. These results are consistent with the proposal that foldamer **4** adopts a conformation that allows communication between Ser and His side chains (Figure 6).

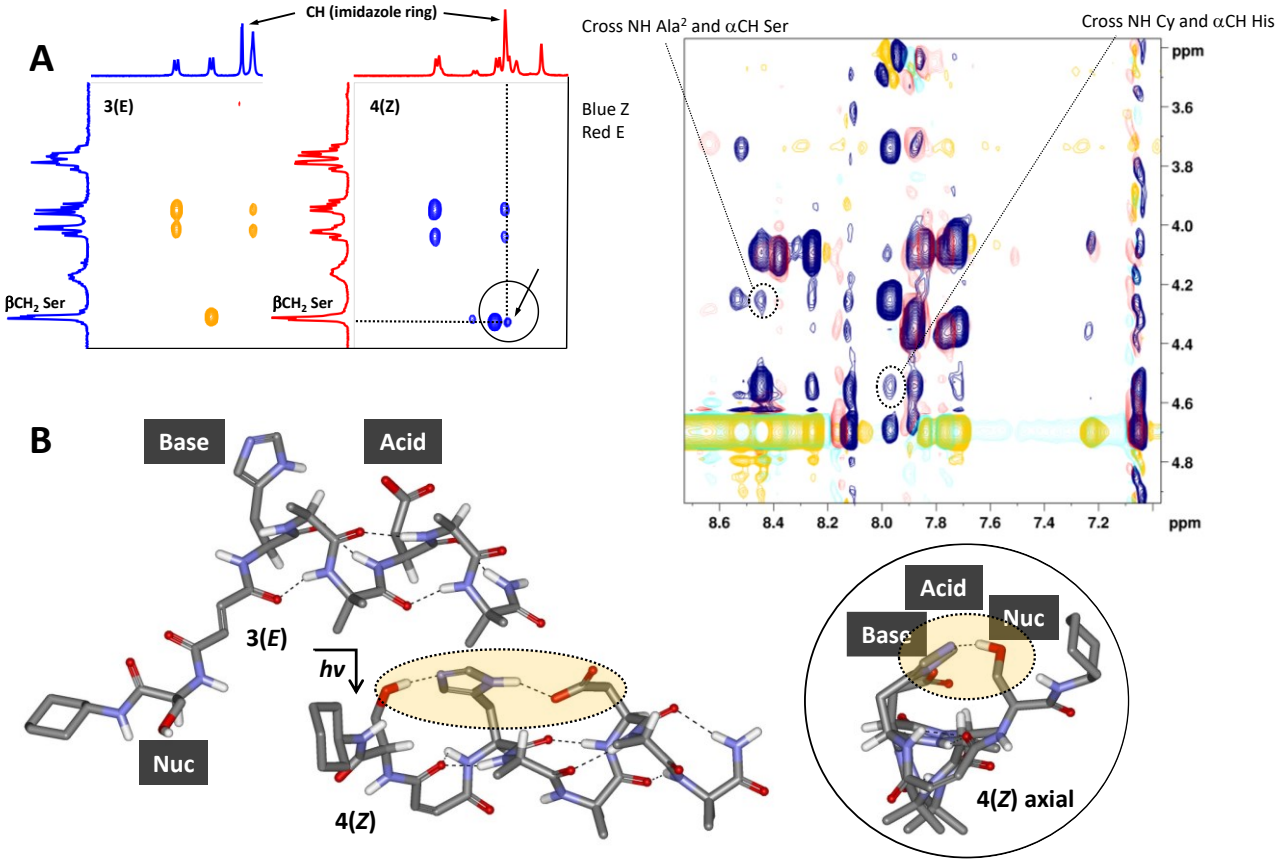


*Figure 6: (A) Sections of ROESY spectra and signals comparison for foldamer **3** and **4**. (B) Force field (CHARMM parameters) optimized models of 3D-structure in the case of foldamer **3** and **4**.*

Evaluation of foldamer **1-4** as catalyst with esterase-like activity were performed by observing the hydrolysis of activated esters. As a starting point, an estimate of the ability of the peptides to catalyse ester hydrolysis was done using the ester substrate *p*-NPA (para-nitrophenyl acetate) hydrolysis at pH 6.2 and 7.3 (40 mM Britton–Robinson buffer, titrated to the appropriate pH with NaOH). All experiments were run in a quartz cuvette and followed by UV-Vis spectroscopy, at 25°C under stirring, with a foldamer concentration of 2 mM and substrate concentration of 30 mM. *p*-

NPA is an activated ester, having the good leaving group 4-nitrophenolate, and is a common model compound to study catalytic activity of synthetic systems. In these conditions, the data indicated a difference in extent of hydrolysis of *p*-NPA in the presence versus the absence of the various foldamers. The two photoswitchable-peptides showed different activities in the hydrolysis of *p*-NPA depending on the geometry of their double bond and its positioning.

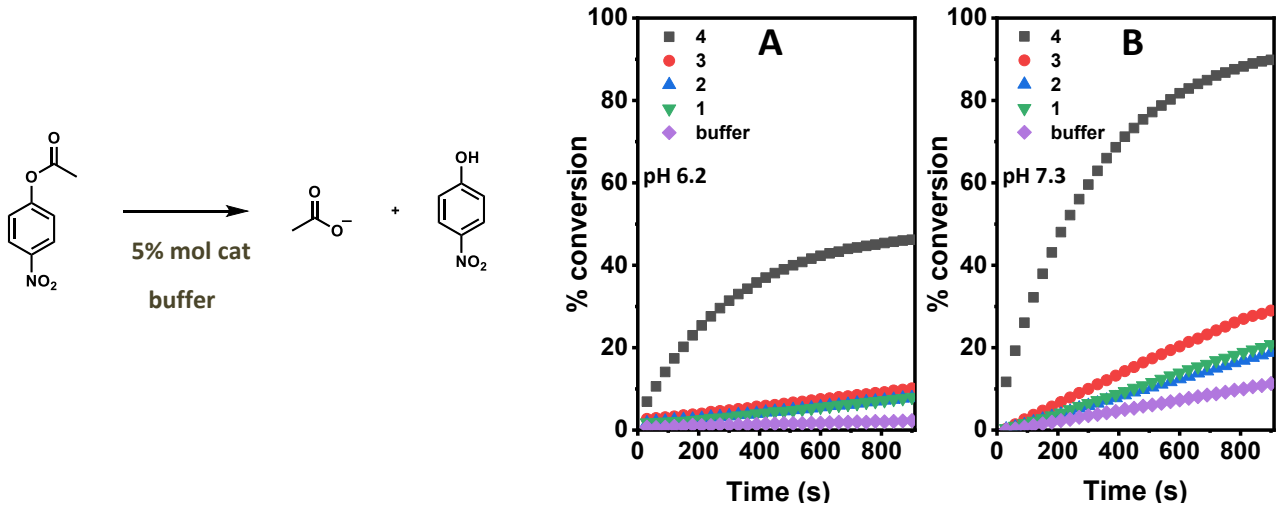


*Figure 7: Evaluation of foldamer* ***1-4*** *in p-NPA hydrolyses at pH 6.2 (A), 7.3 (B)(40 mM Britton–Robinson buffer, titrate to the corresponding pH with NaOH).*

The reaction was followed for 15 min (900 s). For hydrolysis at pH 6.2 (Figure 3A) we observed <5% conversion to product in the absence foldamers (buffer effect), and <10% in presence of foldamers **1-3**. In the case of foldamer **4**, our data showed a 45% conversion (Figure 7A). Kinetic experiments run at pH 7.3 (Figure 7B) showed an increase in the hydrolyses rates for all the samples. Considerable hydrolysis of the *p*-NPA substrate was observed under these conditions with foldamer **4** (almost 90% conversion after 15 min), but the presence of foldamer **1-3** did not lead to a significant enhancement in the extent of reaction compared to the background hydrolysis rate.

Similar striking results were obtained in the case para-nitrophenyl butyrate (*p*-NPB) as substrate at pH 8.80. In contrast to the traditional para-nitrophenyl acetate model system, *p*-NPB was significantly more stable under the assay conditions, thus making *p*-NPB a more representative substrate. Experiments were run at pH 8.80 (no catalytic activity was noted at pH 6 or 7.8) and followed by UV-Vis spectroscopy at 25 °C for 65 min.

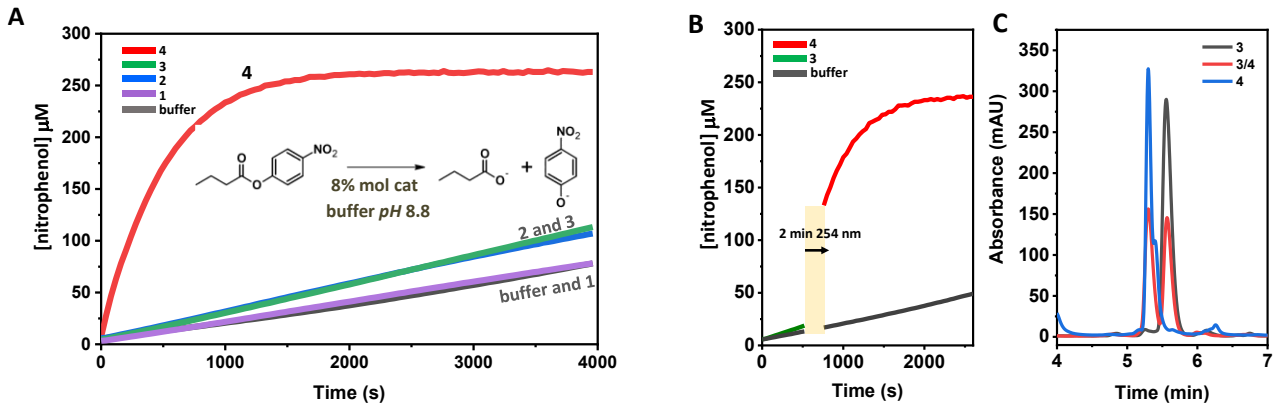


*Figure 8: (A) Evaluation of foldamers* ***1–4*** *(8% mol) for the hydrolysis of p-NPB at pH 8.80 (40 mM Britton–Robinson buffer, titrated to the corresponding pH with NaOH). (B) Effect of photoisomerization on the rate of reaction. (C): HPLC profile showing the consequence of E to Z isomerization.*

Significantly, esterase-like catalysis was observed only with foldamer **4** (quantitative conversion after 2000 s, TON 12.5 and TOF at $t_{1/2}$ of 0.015 $s^{-1}$), with much lower catalytic activity from control structures **1**–**3** (Figure 8A). In foldamer **1**, the presence of His and Asp has no effect on the rate of hydrolysis of the substrate beyond that of buffer alone. The additional Ser residue of foldamers **2** and **3** may be the reason for the small increase (8%) in the rate of hydrolysis relative to foldamer **1**. Thus, the catalytic effect of foldamer **4** seems be related to the novel disposition of the Ser–His–Asp which allows catalytic cooperativity between side chains. None of these experiments showed the burst phase characteristic of natural esterases. This may be due to a Ser residue that is significantly less nucleophilic than in the natural enzyme, requiring high pH to show any activity at all. It is possible that with the foldamer catalysts, the initial acylation step is rate-determining, but it is nonetheless dependent on the proximity of His and Asp for activity. Finally, to prove the effect of the cofactor-mediated photoswitch on the rate of hydrolyses, compound **3** was isomerized by irradiation during its reaction (*p*-NPB hydrolysis at pH 8.8) after 520 sec for 2 min. The reaction was monitored for additional 800 seconds showing an evident enhancement of the hydrolysis rate (Figure 8B). Proof of the **3** to **4** isomerization is reported in Figure 8C which shows the HPLC profile of compound **3**, mixture **3**/**4** resulting from 1 min irradiation (red line, 45 : 55 ratio of **3** : **4**) and 2 min irradiation (blue line, 05 : 95 ratio of **3** : **4**).

In summary, we have demonstrated the light-induced in situ assembly of a catalytic triad of reactive side chains – Ser, His and Asp – in a photo-responsive helical foldamer. The incorporation of the

switchable fumaramide linker allows to reorganize the conformation of the foldamer simply upon irradiation with UV-light. Only in the maleamide-containing foldamer generated by switching the linker from *E* to *Z* geometry can the triad function cooperatively catalyse the hydrolysis of an ester bond. The foldamer appears to function by a two-step mechanistic pathway, analogous to that exhibited by their enzyme equivalents, that involves successive acylation and deacylation steps mediated by hydroxyl–imidazole–carboxyl group interactions.

# Experimental Section

## Materials and Methods

All starting materials and reagents were purchased from Sigma-Aldrich. Monomethyl fumarate was synthesized based on the literature.[5] $^{1}$H NMR, $^{13}$C NMR, and 2D-NMR spectra were recorded at 25°C on Bruker Avance 400 MHz instruments. $^{1}$H and $^{13}$C spectra were referenced relative to the solvent residual peaks and chemical shifts (δ) reported in ppm downfield of tetramethylsilane ($CDCl_3$ δ H: 7.26 ppm, δ C: 77.16 ppm; $CD_3CN$ δ H: 1.94 ppm; $CD_3OH$ δ H: 3.30 ppm DMSO δ H: 2.50 ppm) and *J* values are given in Hz. The multiplicity of a signal is indicated as br, broad; s, singlet; d, doublet; t, triplet; m, multiplet. Mass spectra by electrospray ionization (ESI), collected in the positive mode, were performed on Perseptive Biosystem Mariner ESI-ToF5220 spectrometer. The HPLC measurements were performed using an Agilent 1200 apparatus equipped with a UV detector at various wavelength and a column Agilent extend-C18 (stationary phase). Eluants: A= 9:1 $H_2O/CH_3CN$, 0.05 % TFA; B= 1:9 $H_2O/CH_3CN$, 0.05 % TFA.

## Synthesis of Fmoc-Ser($^{t}$Bu)-NH-Cy

Fmoc-Ser($^{t}$Bu)-OH (3 g, 7.8 mmol) and HOAt (1.06 g, 7.8 mmol) were dissolved in dry $CH_3CN$ (35 mL) and the solution cooled to 0°C. EDC·HCl (1.50 g, 7.8 mmol) was added. After complete dissolution, cyclohexylamine (0.89 mL, 7.8 mmol) was added dropwise to the reaction mixture, and DIPEA was used to reach basic pH. The reaction mixture was diluted with $CH_3CN$ (90 mL) and stirred at r.t. overnight. The solvent was removed under reduced pressure and the residue dissolved in EtOAc. The organic phase was washed with $KHSO_4$(aq) (5%), $NaHCO_3$(aq) (5%) and brine, dried over $Na_2SO_4$, filtered, and concentrated to dryness. The residue was triturated in cold $Et_2O$.

Yield 3.52 g (97%) of white solid. $^{1}$H NMR (400 MHz, $CDCl_3$) δ 7.77 (d, J = 7.5 Hz, 2H), 7.60 (d, J = 7.5 Hz, 2H), 7.40 (t, J = 7.4 Hz, 2H), 7.31 (t, J = 7.4 Hz, 2H), 6.56 (s, 1H), 5.81 (d, J = 6.0 Hz, 1H), 4.39 (d, J = 7.0 Hz, 2H), 4.23 (t, J = 7.2 Hz, 1H), 4.19 - 4.09 (m, 1H), 3.78 (dt, J = 9.1, 4.4 Hz, 2H), 3.33 (t, J = 8.7 Hz, 1H), 1.90 (dt, J = 12.9, 4.2 Hz, 2H), 1.65 (m, 5H), 1.51 – 1.30 (m, 2H), 1.21 (s, 13H). $^{13}$C NMR (101 MHz, $CDCl_3$) δ 169.3, 144.0, 143.9, 141.4, 141.4, 127.9, 127.2, 125.3, 120.1, 77.2(CDCl3), 74.3, 62.1, 48.4, 47.3, 33.1, 27.6, 25.7, 24.8. MS (ESI-TOF): $[M+H]^+$ m/z calcd. for $C_{28}H_{36}N_2O_4$, 465.2749; found 465.2752. FT-IR $\tilde{\nu}_{max}$ ($cm^{-1}$) 3324, 3302, 3064, 2976, 2934, 2853, 1697,

1650, 1602, 1544, 1478, 1447, 1392, 1364, 1320, 1277, 1238, 1192, 1158, 1133, 1104, 1088, 1054, 992, 936, 900,869, 808, 798, 768, 759, 738.

Synthesis of $H_2N$-Ser($^t$Bu)-NH-Cy

Fmoc-Ser($^t$Bu)-NH-Cy (2.3 g, 4.95 mmol) was dissolved in a solution of diethylamine in DCM (20% v/v). The reaction was stirred at room temperature for 30 min. The solvent was removed under reduced pressure and the residue was redissolved in a solution of diethylamine in DCM (20% v/v) and stirred at r.t. for 30 min. The solvent was then removed under reduced pressure and the residue purified by flash chromatography with a DCM/MeOH eluant mixture, by increasing the polarity from only DCM to 9:1 DCM/MeOH. Yield 1.02 g (83%) of yellow oil.

Synthesis of MeO-Fum-Ser($^t$Bu)-NH-Cy

Monomethyl fumarate (1.0 g, 7.7 mmol) and HOAt (1.05 g, 7.7 mmol) were dissolved in dry $CH_3CN$ (25 mL) and EDC·HCl (1.48 g, 7.7 mmol) was added. After 10 min, $H_2N$-Ser($^t$Bu)-NH-Cy (1.25 g, 5.1 mmol) was to the reaction mixture and DIPEA was used to reach basic pH. The reaction mixture stirred at r.t. overnight. The solvent was removed under reduced pressure and the residue dissolved in EtOAc. The organic phase was washed with $KHSO_{4(aq)}$ (5%), $NaHCO_{3(aq)}$ (5%) and brine, dried over $Na_2SO_4$, filtered, concentrated to dryness and precipitated from EtOAc/hexane.

Yield 1.13 g (61%) of white solid. $^1$H NMR (400 MHz, $CDCl_3$) δ 7.01-6.92 (m, 2H), 6.82 (d, J = 15.4 Hz, 1H), 6.62 (d, J = 8.0 Hz, 1H), 4.46-4.36 (m, 1H), 3.85 - 3.73 (m, 1H), 3.79 (s, 3H), 3.28 (t, J = 8.8 Hz, 1H), 1.88 (dt, J = 12.4, 4.1 Hz, 2H), 1.77 (s, 3H), 1.73-1.57 (m, 3H), 1.45-1.29 (m, 2H), 1.26 (s, 1H), 1.21 (s, 9H), 1.21-1.09 (m, 2H). $^{13}$C NMR (101 MHz, $CDCl_3$) δ 168.8, 166.0, 163.4, 136.2, 130.6, 74.6, 61.3, 53.1, 52.4, 48.5, 33.1, 33.0, 27.6, 25.6, 24.7, 24.7.

MS (ESI-TOF): $[M+Na]^+$ m/z calcd. for $C_{18}H_{30}N_2O_5$, 377.2047; found 377.2043. FT-IR $\tilde{\nu}_{max}$ ($cm^{-1}$) 3277, 3080, 2975, 2934, 2856, 1731, 1647, 1635, 1533, 1475, 1437, 1448, 1392, 1364, 1337, 1262, 1193, 1167, 1127, 1097, 1025, 983, 922, 893, 873, 779, 708, 653, 603.

Synthesis of HO-Fum-Ser($^t$Bu)-NH-Cy

MeO-Fum-Ser($^t$Bu)-NH-Cy (586 mg, 1.65 mmol) was dissolved in THF (12 mL) and a solution of LiOH·$H_2O$ (277 mg, 6.6 mmol) in water (12 mL) was added. The solution was stirred at r.t. for 1 h.

The mixture was then acidified with solid $KHSO_4$, saturated with brine and extracted with EtOAc. The organic phase was dried over $Na_2SO_4$, filtered and concentrated to dryness.

Yield 423 mg (75%) of white solid. $^1$H NMR (400 MHz, DMSO-$d_6$) δ 8.61 (d, J = 8.3 Hz, 1H, $\mathbf{NH_{Ser}}$), 7.87 (d, J = 7.9 Hz, 1H, Cy-NH), 7.13 (d, J = 15.5 Hz, 1H, fumarate =CH-), 6.51 (d, J = 15.5 Hz, 1H, fumarate =CH-), 4.43 (m, 1H, $H^{\alpha}_{Ser}$), 3.54 (m, 1H, Cy-CH), 3.43 (m, 2H, $H^{\beta}_{Ser}$), 1.79-1.61 (m, 4H, Cy), 1.60-1.48 (m, 1H,Cy), 1.10 (m, 14H, $^t$Bu and Cy). $^{13}$C NMR (101 MHz, DMSO-$d_6$) 168.2, 166.5, 162.9, 137.0, 129.9, 72.8, 62.0, 53.6, 47.6, 39.5 (DMSO), 32.4, 32.2, 27.2, 25.2, 24.6, 24.5. MS (ESI-TOF): $[M+Na]^+$ m/z calcd. for $C_{17}H_{28}N_2O_5$, 363.1890; found 363.1922. FT-IR $\tilde{\nu}_{max}$ (cm$^{-1}$) 3283, 3091, 2973, 2932, 2855, 2669, 1705, 1644, 1633, 1552, 1476, 1448, 1410, 1393, 1364, 1333, 1253, 1192, 1153, 1125, 1097, 1023, 994, 931, 899, 893, 874, 779, 755, 705, 653, 603.

General procedure for solid phase peptide synthesis.

Rinke-amide resin (0.65 mmol/g) was added to a vessel. The resin was swelled in DMF and then Fmoc-protecting group was removed with 20% piperidine solution in DMF (40 min). After filtering, the resin was washed with DMF, DCM and DMF. A solution of the amino acid Fmoc-AA-OH (3 eq.), HATU (3 eq.), HOAt (2.7 eq) and DIPEA (5 eq.) in DMF was added to the peptide synthesis vessel and shaken for 1h and 30 minutes. The resin was filtered, and washed with DMF, DCM and DMF. Iterative cycles of Fmoc deprotection and coupling were carried out with 20% piperidine solution in DMF. Unreacted sites were capped by treatment with an 18:4:1 DMF/$Ac_2O$/DIPEA mixture for 20 minutes. After filtering, the resin was washed with DCM. Then, the resin was treated with DMF and then with 20% piperidine solution in DMF and shaken for 20 minutes twice. After filtering, the resin was washed with DMF, DCM and DMF. For the last coupling of **3,** on the resin a solution of HO-Fum-Ser($^t$Bu)-NH-Cy (2.3 eq.), HATU (2.3 eq.), HOAt (2 eq) and DIPEA (2.3 eq.) in DMF was added to the peptide synthesis vessel and shaken for 1h and 30 minutes. The resin was filtered, and washed with DMF, DCM and DMF. The resin was acetylated prior to cleavage. Cleavage of the peptide sequence from the resin was performed with a mixture of TFA:$H_2O$:TIS 95:2.5:2.5 (15 mL) standing for 1 h and washing with DCM; the filtrated was collected and

evaporated under reduced pressure. The residue was triturated in cold $Et_2O$, centrifuged and lyophilized.

(**1**) Yield 370 mg (96%) of white solid. $^1$H NMR (400 MHz, DMSO-*d*$_6$) δ 8.67 (s, 1H, $\mathbf{Ar_{His}}$), 8.42 (s, 1H, $\mathbf{NH_{Aib}}$), 8.27 (s, 1H, $\mathbf{NH_{Aib}}$), 8.16 (d, J = 7.7 Hz, 1H, $\mathbf{NH_{His}}$), 7.89 (d, J = 7.0 Hz, 1H, $\mathbf{NH_{Asp}}$), 7.78 (d, J = 6.2 Hz, 1H, $\mathbf{NH_{Ala}}$), 7.62 (d, J = 6.8 Hz, 1H, $\mathbf{NH_{Ala}}$), 7.54 (s, 1H, $\mathbf{NH_{Aib}}$), 7.21 (s, 1H, $\mathbf{Ar_{His}}$), 6.80 (s, 2H, $CONH_2$), 4.46 – 4.29 (m, 2H, $H^{\alpha}_{Asp}$ and $H^{\alpha}_{His}$), 4.11 (m, 2H, $H^{\alpha}_{Ala}$), 3.18 (dd, J = 15.2, 4.3 Hz, 1H, $H^{\beta}_{His}$), 3.02 (dd, J = 15.2, 9.9 Hz, 1H, $H^{\beta}_{His}$), 2.75 (dd, J = 16.7, 4.7 Hz, 1H, $H^{\beta}_{Asp}$), 2.64 (dd, J = 16.7, 8.5 Hz, 1H, $H^{\beta}_{Asp}$), 1.87 (s, 3H, $CH_3$-acetamide), 1.40 – 1.15 (m, 24H, Ala and Aib $CH_3$). $^{13}$C NMR (101 MHz, DMSO-*d*$_6$) δ 176.3, 174.5, 174.5, 173.4, 172.2, 171.4, 170.7, 170.6, 170.6, 134.1, 55.9, 55.8, 55.7, 49.2, 49.1, 39.5 (DMSO), 35.0, 25.7, 25.4, 25.2, 24.6, 24.5, 24.4, 23.1, 17.1, 16.6. MS (ESI-TOF): $[M+H]^+$ m/z calcd. for $C_{30}H_{48}N_{10}O_{10}$, 709.3628; found 709.3666. FT-IR $\tilde{\nu}_{max}$ ($cm^{-1}$) 3314, 3055, 2989, 2940, 2878, 2640, 1663, 1540, 1458, 1388, 1366, 1299, 1255, 1201, 1137.

(**2**) Yield 568 mg (92%) of white solid. $^1$H NMR (400 MHz, DMSO-*d*$_6$) 1H NMR (400 MHz, DMSO-d6) δ 8.81 (s, 1H, $\mathbf{Ar_{His}}$), 8.55 (s, 1H, $\mathbf{NH_{Aib}}$), 8.22 (s, 1H, $\mathbf{NH_{Aib}}$), 8.01 (d, J = 6.1 Hz, 1H, $\mathbf{NH_{Ser}}$), 7.92 (d, J = 6.4 Hz, 1H, $\mathbf{NH_{Ala}}$), 7.84 (d, J = 6.7 Hz, 1H, $\mathbf{NH_{Asp}}$), 7.79 – 7.56 (m, 5H, 2· $\mathbf{NH_{Ala}}$,2· $\mathbf{NH_{Aib}}$, $\mathbf{NH_{His}}$), 7.32 (s, 1H, $\mathbf{Ar_{His}}$), 6.78 (s, 2H, $CONH_2$), 5.10 (bs, 1H, Ser-OH), 4.42 (m, 1H, $H^{\alpha}_{His}$), 4.34 (m, 1H, $H^{\alpha}_{Asp}$), 4.18 – 3.96 (m, 4H, $H^{\alpha}_{Ala}$ and $H^{\alpha}_{Ser}$), 3.78 – 3.62 (m, 2H, $H^{\beta}_{Ser}$), 3.21 (dd, J = 15.3, 4.4 Hz, 1H, $H^{\beta}_{His}$ ), 2.99 (dd, J = 15.3, 10.2 Hz, 1H, $H^{\beta}_{His}$), 2.79 – 2.59 (m, 2H, $H^{\beta}_{Asp}$), 1.89 (s, 3H, $CH_3$-acetamide), 1.37 – 1.21 (m, 33H, Ala and Aib $CH_3$). $^{13}$C NMR (101 MHz, DMSO-*d*$_6$) δ 176.3, 175.6, 174.6, 173.6, 173.4, 172.0, 171.4, 171.2, 170.9, 170.7, 170.5, 133.9, 116.9, 72.9, 60.4, 57.5, 56.0, 55.9, 55.8, 55.8, 52.6, 50.6, 50.0, 49.6, 49.2, 39.5 (DMSO), 35.1, 27.2, 26.2, 25.6, 25.4, 25.3, 24.6, 24.1, 24.1, 24.0, 23.1, 17.0, 16.6, 16.4. MS (ESI-TOF): $[M+H]^+$ m/z calcd. for $C_{40}H_{65}N_{13}O_{14}$, 952.4847 m/z; found 952.4841. FT-IR $\tilde{\nu}_{max}$ ($cm^{-1}$) 3319, 2988, 2940, 1664, 1541, 1458, 1389, 1366, 1300, 1203, 1138.

(**3**) Yield 449 mg (92%) of white solid. $^1$H NMR (400 MHz, DMSO-*d*$_6$) δ 12.39 (bs, 1H) 8.96 (s, 1H, $\mathbf{Ar_{His}}$), 8.74 (d, J = 8.0 Hz, 1H, $\mathbf{NH_{His}}$), 8.53 (m, 2H, $\mathbf{NH_{Aib}}$ and $\mathbf{NH_{Ser}}$), 8.38 (d, J = 5.8 Hz, 1H, $\mathbf{NH_{Ala}}$), 7.90 (d, J = 7.3 Hz, 1H, $\mathbf{NH_{Asp}}$), 7.79 (d, J = 7.9 Hz, 1H, Cy-NH), 7.69 (s, 1H, $\mathbf{NH_{Aib}}$), 7.64 (d, J = 6.6 Hz, 1H, , $\mathbf{NH_{Ala}}$), 7.35 (s, 1H, $\mathbf{Ar_{His}}$), 7.01 – 6.83 (m, 4H, $CONH_2$ and fumarate =CH-), 4.73 (td, J = 8.1, 5.2 Hz, 1H, $H^{\alpha}_{His}$), 4.36 (m, 2H, $H^{\alpha}_{Ser}$ and $H^{\alpha}_{Asp}$), 4.21 (m, 1H, $H^{\alpha}_{Ala}$), 4.09 (m, 1H,

$H^{\alpha}_{Ala}$), 3.53 (m, 3H, Cy-CH and $H^{\beta}_{Ser}$), 3.13 (dd, J = 15.4, 5.1 Hz, 1H, $H^{\beta}_{His}$), 2.99 (dd, J = 15.4, 8.3 Hz, 1H, $H^{\beta}_{His}$), 2.81 – 2.60 (m, 2H, $H^{\beta}_{Asp}$), 1.74 – 1.51 (m, 6H), 1.42 – 0.92 (m, 22H). $^{13}$C NMR (101 MHz, DMSO-$d_6$) δ 176.4, 174.3, 173.3, 172.3, 171.6, 170.7, 169.9, 168.5, 164.0, 163.52,133.8, 133.4, 132.3, 129.2, 116.9, 61.9, 55.9, 55.8, 55.5, 51.6, 50.2, 49.2, 47.6, 39.5 (DMSO), 35.1, 32.4, 32.3, 27.1, 25.6, 25.3, 25.2, 24.6, 24.6, 24.6, 24.4, 17.14, 17.0. MS (ESI-TOF): $[M+H]^+$ m/z calcd. for $C_{37}H_{57}N_{11}O_{12}$, 848.4261; found, 848.4269. FT-IR $\tilde{\nu}_{max}$ ($cm^{-1}$) 3306, 3054, 2936, 2858, 1657, 1535, 1452, 1389, 1365, 1252, 1202, 1139.

$^1$H NMR (400 MHz, $H_2O/D_2O$) δ 8.81 (d, J = 7.4 Hz, 1H, $\mathbf{NH_{His}}$), 8.63 (d, J = 6.9 Hz, 1H, $\mathbf{NH_{Ser}}$), 8.48 (d, J = 1.5 Hz, 1H, $\mathbf{Ar^{C2}_{His}}$), 8.45 – 8.37 (m, 2H, $\mathbf{NH_{Aib1}}$ and $\mathbf{NH_{Ala1}}$), 8.02 – 7.97 (m, 1H, $\mathbf{NH_{Asp}}$), 7.95 (s, 1H, $\mathbf{NH_{Aib2}}$), 7.90 (d, J = 8.6 Hz, 1H, Cy-NH), 7.83 (d, J = 6.1 Hz, 1H, $\mathbf{NH_{Ala2}}$), 7.21 (s, 1H, $CONH_2$), 7.18 (s, 1H, $\mathbf{Ar^{C4}_{His}}$), 6.85 – 6.71 (m, 3H, $CONH_2$ and fumarate =CH-), 4.30 (m, 1H, $H^{\alpha}_{Ser}$), 4.18 – 4.02 (m, 1H, $H^{\alpha}_{Ala}$), 3.77 – 3.65 (m, 2H, $H^{\beta}_{Ser}$), 3.54 – 3.39 (m, 1H, Cy-CH), 3.26 – 3.01 (m, 2H, $H^{\beta}_{His}$), 2.86 – 2.67 (m, 2H, $H^{\beta}_{Asp}$), 1.71 – 1.40 (m, 6H, Cy), 1.34 – 1.28 (m, 12H, Aib $CH_3$), 1.24 (d, J = 7.2 Hz, 6H, Ala $CH_3$), 1.21 – 0.96 (m, 4H, Cy).

$^1$H NMR (400 MHz, $CD_3OH$) δ 8.84 (d, J = 7.9 Hz, 1H, $\mathbf{NH_{His}}$ ), 8.77 (s, 1H, $\mathbf{Ar_{His}}$), 8.75 (s, 1H, $\mathbf{NH_{Aib}}$), 8.61 – 8.52 (m, 2H, $\mathbf{NH_{Ser}}$ and $\mathbf{NH_{Ala}}$ ), 8.27 (s, 1H, $\mathbf{NH_{Aib}}$), 8.13 (d, J = 7.3 Hz, 1H, $\mathbf{NH_{Asp}}$), 7.99 – 7.89 (m, 2H, $\mathbf{NH_{Ala}}$ and Cy-NH), 7.38 – 7.31 (m, 2H,), $\mathbf{Ar_{His}}$ and $CONH_2$) 7.04 – 6.85 (m, 3H, fumarate =CH- and $CONH_2$), 4.45 (m, 2H, $H^{\alpha}_{Ser}$ and $H^{\alpha}_{Asp}$), 4.25 (m, 1H, $H^{\alpha}_{Ala}$ ), 3.79 (d, J = 5.6 Hz, 1H, $H^{\beta}_{Ser}$), 3.72 – 3.59 (m, 1H, Cy-CH), 3.41 – 3.29 (m, 8H, $H^{\beta}_{His}$ and $CD_3OH$ residual peak), 3.24 – 3.13 (m, 1H, $H^{\beta}_{His}$), 3.04 – 2.81 (m, 2H, $H^{\beta}_{Asp}$), 1.93 – 1.57 (m, 6H, Cy), 1.50 – 1.43 (m, 12H, Aib $CH_3$), 1.42 – 1.36 (m, 6H, Ala $CH_3$), 1.36 – 1.17 (m, 4H, Cy).

$^1$H NMR (400 MHz, Acetonitrile-$d_3$) δ 8.46 (d, J = 1.4 Hz, 1H), 7.91 (d, J = 7.6 Hz, 1H), 7.63 (m, 3H), 7.49 (m, 2H), 7.27 (s, 1H), 7.21 (s, 1H), 6.97 – 6.83 (m, 2H), 6.82 – 6.77 (m, 1H), 6.69 (s, 1H), 5.86 (s, 1H), 4.81 – 4.71 (m, 1H), 4.42 – 4.26 (m, 2H), 4.20 – 4.08 (m, 2H), 3.85 – 3.58 (m, 4H), 3.38 (m, 1H), 3.14 (m, 1H), 3.00 – 2.78 (m, 2H), 1.85 – 1.56 (m), 1.52 – 1.38 (m), 1.38 – 1.24 (m), 1.28 – 1.17 (m).

(**4**) obtained quantitatively from isomerization of (**3**), of white solid. $^{1}$H NMR (400 MHz, DMSO-$d_6$) δ 9.00 (d, J = 7.2 Hz, 1H, $\mathbf{NH_{His}}$), 8.94 (s, 1H, $\mathbf{Ar_{His}}$), 8.75 (d, J = 7.8 Hz, 1H, $\mathbf{NH_{Ser}}$), 8.54 (d, J = 5.9 Hz, 1H, $\mathbf{NH_{Ala}}$), 8.29 (s, 1H, $\mathbf{NH_{Aib}}$), 7.91 (d, J = 7.9 Hz, 1H, Cy-NH), 7.81 (d J = 6.9 Hz, 1H, $\mathbf{NH_{Asp}}$), 7.60 (m, 2H, $\mathbf{NH_{Aib}}$ and $\mathbf{NH_{Ala}}$ ), 7.36 (s, 1H, $\mathbf{Ar_{His}}$), 6.88 – 6.79 (m, 1H, $CONH_2$), 6.32 (dd, J = 12.4 Hz, 2H, maleate =CH-), 4.95 (bs, 1H), 4.52 (td, J = 9.2, 7.2, 4.8 Hz, 1H, $H^{\alpha}_{His}$), 4.41 – 4.31 (m, 1H, $H^{\alpha}_{Asp}$ ), 4.19 – 4.00 (m, 2H, $H^{\alpha}_{Ala}$), 3.62 (d, J = 5.5 Hz, 2H, $H^{\beta}_{Ser}$), 3.55 – 3.31 (m, 27H, Cy-CH and $H_2O$), 3.22 – 2.95 (m, 2H, $H^{\beta}_{His}$), 2.78 – 2.58 (m, 2H, $H^{\beta}_{Asp}$), 1.65 (m, 5H, Cy), 1.59 – 1.47 (m, 1H, Cy), 1.38 – 1.05 (m, 22H, Ala and Aib $CH_3$ and Cy). $^{13}$C NMR (101 MHz, DMSO-$d_6$) δ 176.4, 174.6, 173.7, 172.1, 171.6, 171.6, 170.8, 170.5, 168.2, 166.4, 164.8, 133.9, 132.0, 129.5, 129.2, 117.0, 61.7, 56.0, 55.9, 55.9, 55.8, 55.7, 52.5, 50.5, 49.9, 49.3, 47.8, 39.5 (DMSO), 35.1, 32.4, 32.3, 25.6, 25.2, 25.2, 24.7, 24.7, 24.0, 17.0, 16.7. FT-IR $\tilde{\nu}_{max}$ ($cm^{-1}$) 3311, 3054, 2989, 2936, 2857, 1657, 1541, 1453, 1390, 1366, 1254, 1202, 1138.

$^{1}$H NMR (400 MHz, $H_2O/D_2O$) δ 8.82 (d, J = 7.1 Hz, 1H, $\mathbf{NH_{His}}$), 8.51 (d, J = 6.9 Hz, 1H, $\mathbf{NH_{Ser}}$), 8.49 – 8.45 (m, 2H, $\mathbf{Ar^{C2}_{His}}$ and $\mathbf{NH_{Ala1}}$), 8.29 (s, 1H, $\mathbf{NH_{Aib1}}$), 7.98 – 7.89 (m, 2H, $\mathbf{NH_{Asp}}$ and Cy-NH), 7.85 (s, 1H, $\mathbf{NH_{Aib2}}$), 7.76 (d, J = 6.0 Hz, 1H, $\mathbf{NH_{Ala2}}$) 7.22 (s, 1H, $CONH_2$), 7.17 (s, 1H, $\mathbf{Ar^{C4}_{His}}$), 6.75 (s, 1H, $CONH_2$), 6.26 (s, 1H, maleate =CH-), 4.25 (s, 1H, $H^{\alpha}_{Ser}$), 4.15 – 3.99 (m, 2H, $H^{\alpha}_{Ala}$), 3.76 – 3.68 (m, 1H, $H^{\beta}_{Ser}$), 3.51 – 3.39 (m, 1H, Cy-CH), 3.26 – 2.98 (m, 2H, $H^{\beta}_{His}$), 2.86 – 2.65 (m, 2H, $H^{\beta}_{Asp}$), 1.68 – 1.40 (m, 6H, Cy), 1.34 – 1.21 (m, 18H, Ala and Aib $CH_3$), 1.21 – 0.99 (m, 4H, Cy).

$^{1}$H NMR (400 MHz, $CD_3OH$) δ 9.04 (d, J = 7.1 Hz, 1H, $\mathbf{NH_{His}}$), 8.76 (s, 1H, $\mathbf{Ar^{C2}_{His}}$), 8.72 – 8.66 (m, 2H, $\mathbf{NH_{Ala1}}$ and $\mathbf{NH_{Ser}}$), 8.45 (s, 1H, $\mathbf{NH_{Aib1}}$), 8.16 – 7.97 (m, 3H, $\mathbf{NH_{Asp}}$, Cy-NH and $\mathbf{NH_{Aib2}}$), 7.88 (d, J = 5.9 Hz, 1H, $\mathbf{NH_{Ala2}}$), 7.36 (s, 1H, $\mathbf{Ar^{C4}_{His}}$), 7.26 (s, 1H, $CONH_2$), 6.85 (s, 1H, $CONH_2$), 6.35 (s, 1H, maleate =CH-), 4.48 – 4.37 (m, 2H, $H^{\alpha}_{Asp}$ and $H^{\alpha}_{Ser}$), 4.26 – 4.10 (m, 1H, $H^{\alpha}_{Ala}$), 3.82 (d, J = 5.3 Hz, 2H, $H^{\beta}_{Ser}$), 3.72 – 3.58 (m, 1H, Cy-CH), 3.44 – 3.30 (m, 9H, $H^{\beta}_{His}$ and $CD_3OH$ residual peak), 3.24 – 3.11 (m, 1H, $H^{\beta}_{His}$), 3.01 – 2.81 (m, 2H, $H^{\beta}_{Asp}$), 1.90 – 1.59 (m, 5H, Cy), 1.52 – 1.40 (m, 18H, Ala and Aib $CH_3$), 1.40 – 1.18 (m, 5H, Cy).

$^1$H NMR (400 MHz, Acetonitrile-$d_3$) δ 8.47 (m, 1H, $\mathbf{Ar_{His}}$), 8.27 (d, J = 5.4 Hz, 1H, $\mathbf{NH_{Ala}}$), 8.22 (d, J = 6.8 Hz, 1H, $\mathbf{NH_{His}}$), 7.67 – 7.56 (m, 2H, $\mathbf{NH_{Ala}}$ and), 7.57 – 7.52 (m, 2H, $\mathbf{NH_{Aib}}$ and), 7.28 (s, 1H), 7.12 (s, 1H), 6.95 (d, J = 8.1 Hz, 1H), 6.70 (s, 1H), 6.33 – 6.25 (m, 2H), 4.65 – 4.55 (m, 1H, $H^{\alpha}_{His}$), 4.40 – 4.26 (m, 2H, $H^{\alpha}_{Asp}$ and $H^{\alpha}_{Ser}$), 4.17 – 3.99 (m, 2H, $H^{\alpha}_{Ala}$), 3.85 – 3.70 (m, 2H, $H^{\beta}_{Ser}$), 3.70 – 3.59 (m, 1H Cy-CH), 3.36 (dd, J = 15.3, 4.5 Hz, 1H, $H^{\beta}_{His}$), 3.11 (dd, J = 15.3, 9.4 Hz, 1H, $H^{\beta}_{His}$), 2.87 (d, J = 6.8 Hz, 2H, $H^{\beta}_{Asp}$), 1.84 – 1.56 (m, 16H, Cy and $CD_3CN$ residual peak), 1.48–1.34 (m, Aib and Ala $CH_3$),1.28 – 0.99 (m, Cy).

## General procedure for hydrolysis experiments

Substrates solutions for hydrolysis experiments were prepared dissolving 2.5 mol of the selected ester (*p*-NPA or *p*-NPB) in 10 ml of a 3% v/v DMSO/$H_2O$ solution. Experiments were run in a quartz cuvette at pH 6.2, 7.3 and 8.8 (40 mM Britton–Robinson buffer, titrated to the appropriate pH with NaOH) and followed by UV-Vis spectroscopy at 25°C while stirring, with substrate (*p*-NPA and *p*-NPB) concentration of 250 µM and foldamers concentration of 20 µM (8%mol). The cuvette was placed in a Shimadzu model UV-2501 PC spectrophotometer and the hydrolysis of the substrates was monitored at 400 nm, acquiring the UV-Vis spectra every 30 seconds under stirring.

## References

1 Y. Li, Y. Zhao, S. Hatfield, R. Wan, Q. Zhu, X. Li, M. McMills, Y. Ma, J. Li and K. L. Brown, *Bioorg. Med. Chem.*, 2000, **8**, 2675–2680.

2 M. J. Macdonald, L. D. Lavis, D. Hilvert and S. H. Gellman, *Org. Lett.*, 2016, **18**, 3518–3521.

3 Y. Liu, Y. Li, X. Gao, Y. Yu, X. Liu, Z. Ji, Y. Ma, Y. Li and Y. Zhao, *Amino Acids*, 2018, **50**, 69–77.

4 D. Mazzier, M. Crisma, M. De Poli, G. Marafon, C. Peggion, J. Clayden and A. Moretto, *J. Am. Chem. Soc.*, 2016, **138**, 8007–8018.

5 M. Dymicky, *Org. Prep. Proced. Int.*, 1983, **15**, 233–238.

## Acknowledgement

The content of the chapter is reproduced from Ref. M. Pollastrini, G. Marafon, J. Clayden and A. Moretto, *Chem. Commun.*, 2021, **57**, 2269–2272. with permission from the Royal Society of Chemistry.

# 3. Helical peptide foldamers with three dimensional catalytic centres

Macrocyclic compounds (containing a ring of 12 or more atoms) are frequent and spread evenly among natural products, both from terrestrial and marine sources. Several macrocyclic compounds are of pharmacological interest and possesses high bio-medicinal efficacy or cytotoxic properties.[1] The conformational constraints generated by the macrocyclization can increase the metabolic stability or enhance the binding affinity and selectivity of pharmaceutical compounds. Their application, however, is often limited by the difficulty of their synthesis, often involving complex and long routes in order to obtain the desired macrocyclic structure in good yield. Thus, macrocyclic structures and their synthesis have received considerable increasing attention as synthetic targets in the organic and medicinal chemistry community. From a physical chemistry point of view, every synthetic macrocyclization approach must face a delicate balance of thermodynamic and kinetic factors, such as ring strain, the common entropic penalty to ring closure or the competition between the possible intra- and intermolecular pathways. For example, the common use of high-dilution conditions is aimed to use the kinetical advantage of intramolecular versus intermolecular reactions. Moreover, the use of reversible reactions can lead to macrocyclic structures under thermodynamic control when these are more stable than the acyclic oligomeric ones.

Pre-organization of the open-chain substrate is also an effective approach to macrocyclization, and it can be achieved through two approaches. A first approach is the proper design of the precursor to obtain an open-chain substrate with an intrinsically favourable pre-organization (conformational or configurational). An important alternative is the use a template element to externally induce a favourable pre-organization even if not present in the substrate.

Recently, Gellman and co-workers, reported the foldamer templated macrocyclization of di-aldehydes compounds through carbon-carbon bond formation via iminine/enamine catalysis. The authors, exploiting a combination of α- and β-amino acids, developed a set of foldamers carrying on their surface one primary amine and one secondary amine functions at varying sequence positions. The high efficiency of the system was related to the rigid foldamer conformation, which allowed spatial

control of the relative positioning of the catalytic diad: the foldamer featuring the two functionalities spaced by one helical turn proved to be a potent catalyst.[2]

We speculated that if one of the functionalities of the catalytic diad could be placed directly into the backbone of a helical foldamer rather than at a side-chain position, then the versatility of the system could be expanded, possibly opening the way to catalytic triads. To this aim, peptide-based foldamers containing a -$CH_2$-NH- moiety as replacement of one peptide bond ( **Ψ**[$CH_2$NH] in the notation for peptide bond surrogates) represent suitable candidates. Concerning the helical foldameric scaffold, we relied on the well documented ability of $\alpha$-aminoisobutyric acid (Aib), to promote stable and highly populated $\alpha$-/$3_{10}$-helical conformations when combined with protein amino acids in $\alpha$-peptides even of limited main-chain length.

As a preliminary step of the study, we explored the conformational effects of the **Ψ**[$CH_2$NH] backbone modification in selected model compounds. Imine formation followed by reduction (reductive amination) is a powerful and reliable strategy for the formation of C–N bonds and an attractive feature of the reductive amination chemistry is that the coupling chemistry can be carried out sequentially in two steps. The formation of an imine between an N-terminal peptide and a C-terminal peptide aldehyde and its subsequent reduction can lead to the secondary amino functionality **Ψ**[$CH_2$NH] connecting the two peptide segments.

The first reaction investigated was the model reaction between Boc-Aib-H **1** and H-L-Val-CONH-pClBn **2** (Boc, tert-butyloxycarbonyl; NH-pClBn, para-chlorobenzylamino). For the synthesis of the C-terminal peptide aldehydes, the corresponding Boc-amino (i.e., Boc-Aib-OH) acid was converted in its Weinreb amide derivative [i.e., Boc-Aib-N(OMe)Me], and then chemically transformed in the aldehyde (i.e., Boc-Aib-H, **1**), by selective reduction with LiAlH4 (1 eq.) in THF, with a 44% yield over the two steps. The condensation reaction of **1** and **2** in $CHCl_3$ resulted in the formation of the corresponding stable Shiff-base product Boc-Aib-**Ψ**[CH=N]-L-Val-NH-pClBn **3** (Figure 1). Crystals of Boc-Aib-**Ψ**[CH=N]-L-Val-NH-*p*ClBn were grown from ethyl acetate/*n*-hexane through the vapor diffusion technique and the molecular structure of **3**, determined by single-crystal X-ray diffraction analysis, is highlighted in Figure 1. To the best of our knowledge, there is no precedent of crystallographic characterization of an imino surrogate for a peptide bond between two amino acids.

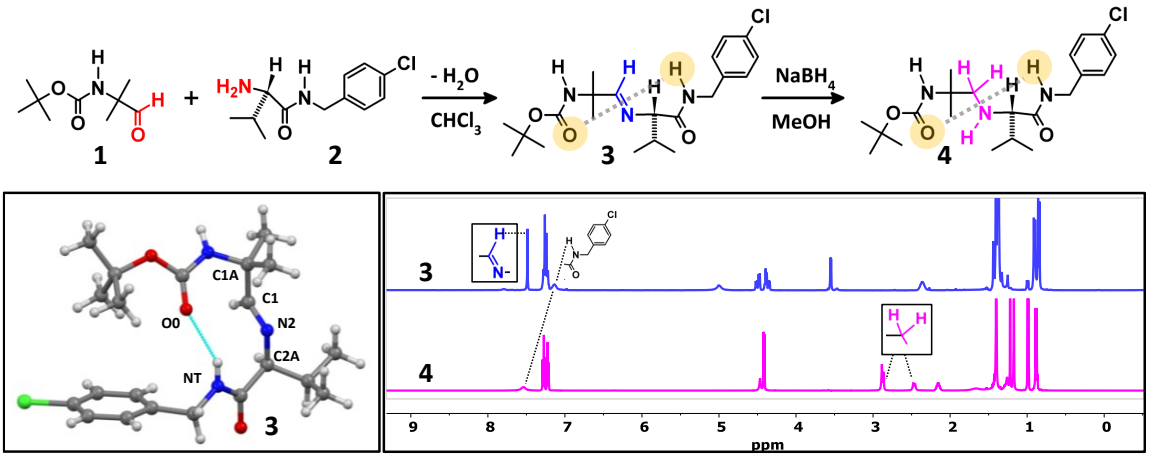


*Figure 1: top) Reaction scheme for the synthesis of imine **3** and its reduction to amine **4**. (bottom left) X-ray diffraction structure of **3**. (bottom right) $^1$H-NMR traces of **3** and **4**.*

The imino moiety is found in the *E* configuration without significant deviation from the ideal *trans* planarity. The *pseudo*peptide backbone is folded in a β-turn conformation stabilized by an intramolecular N-H→O=C hydrogen bond between the *p*-Cl-benzylamide N-H group and the urethane carbonyl oxygen which closes a ten-atom pseudocycle ($C_{10}$ structure). The values of the ϕ,ψ, backbone torsion angles adopted by the (*pseudo*) Aib and L-Val residues [$\phi_1,\psi_1$ = 51.7(4)°, -128.2(3)°; $\phi_2,\psi_2$ = -101.8(3)°, 8.0(4)°] are close to those typical for the *i*+1 and *i*+2 corner positions of a regular type-II′ β-turn conformation.[3] It is worth noting that the overwhelmingly preferred conformation of the regular Aib residue in peptides is $3_{10}$-/α-helical,[4] whereas *semi*-extended (or polyproline II) conformations, which include the *i*+1 corner position of type-II (II′) β-turns, are scarcely populated.5 Conceivably, lack of the C=O group in the *pseudo*-Aib residue might modify the energetic profile of the conformational map with respect to that of the parent compound along the ψ coordinate, but the preference for ϕ values close to ±60° can be retained. In the packing mode, an intermolecular hydrogen bond is observed between the (urethane) N1-H1 group and a (x-1/2, y+1/2, z) symmetry equivalent of the (amide) O2 carbonyl oxygen atom, generating rows of molecules along the *a* direction.

The subsequent reduction of the imino group in **3** with $NaBH_4$ in MeOH afforded its amino (secondary amine) surrogate **4**. The NMR analysis shown in Figure 1 confirms the occurrence of the two reactions (Figure 1). Following the formation of imine, we see the characteristic peak at about 7.5 ppm of imine (**3**), which disappears upon reduction giving way to the aliphatic peaks at about 2.5 and 2.9 ppm.

Our aim was to use this synthetic strategy to connect two ordered peptide sequences, introducing a secondary amine in the backbone. Thus, to explore the effect of the introduction of the secondary amine backbone modification in more structured foldamers, we started connecting two domains of various length based on the helicogenic L-Ala-Aib motif to investigate how the amino linker affects the conformational properties of this foldamers.

A set of Boc-(L-Ala-Aib)$_n$-H ($n$ = **1**, **2**, **4**; **6'-8'**) and H-(L-Ala-Aib)$_n$-OMe ($n$ = **1**, **2**, **4**; **6''-8''**) were synthesized and combined under reductive conditions to form the amino surrogate foldamers Boc-(L-Ala-Aib)$_n\Psi$[CH$_2$NH]-(L-Ala-Aib)$_n$-OMe ($n$ = **1**, **2**, **4**; **6-8**), as well as the *pseudo*dipeptide Boc-Aib$\Psi$[CH$_2$NH]-L-Ala-OMe **5**, too short to give rise to an intramolecularly H-bonded (Scheme 1).

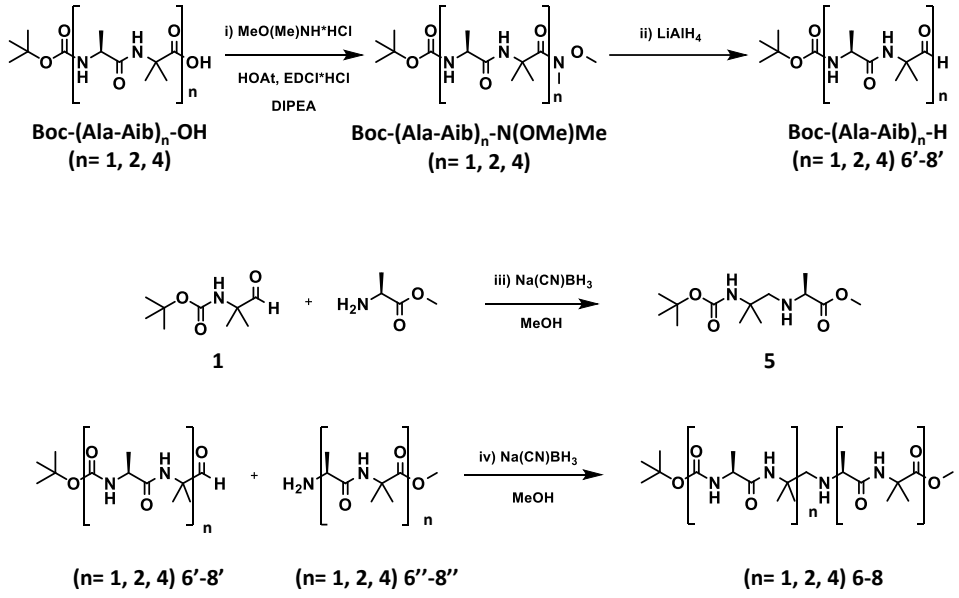


*Scheme 1: Synthesis of amino surrogate pseudopeptides* ***5-9****. Reagent and conditions: i) N,O-Dimethylhydroxylamine hydrochloride, EDC*HCl, HOAt, DIPEA, CH$_3$CN, r.t., 8h; ii) LiAlH$_4$ (2eq.), THF, r.t., 20 min; iii) and iv) Na(CN)BH$_3$, CH$_3$COOH (2 eq.), MeOH, r.t., 2h.*

For the synthesis of the -(L-Ala-Aib)$_n$- fragments for this study, we synthetized a series of Boc-(L-Ala-Aib)$_n$-OMe and Boc-(L-Ala-Aib)$_n$-OH oligomers (Scheme 1, see also Scheme S1 and S2 in Experimental Section). Thus, the amine partner H-(L-Ala-Aib)$_n$-OMe ($n$ = **1**, **2**, **4**; **6''-8''**) were obtained from deprotection of the parent peptide Boc-(L-Ala-Aib)$_n$-OMe ($n$ = **1**, **2**, **4**; **6''-8''**); for the synthesis C-terminal peptide aldehydes Boc-(L-Ala-Aib)$_n$-H ($n$ = **1**, **2**, **4**; **6'-8'**), in the same

fashion as the synthesis of **1**, the corresponding Boc-amino acid was converted in its Weinreb amide derivative [i.e., Boc–(L-Ala-Aib)$_n$-N(OMe)Me], and then reduced to the aldehyde.

As expected, in the short oligomers **5** and **6** the ECD spectra does not show the feature of a helical conformation. The short and flexible *pseudo*dipeptide **5**, lacking amide bonds, displayed a moderately weak positive band with maximum at 207 nm, while the longer *pseudo*tetrapeptide **6** displayed a ECD profile characterized by a positive maximum shifted at 202 nm, followed by a negative band at 225 nm. The longer analogues **7** and **8** have ECD spectra consistent with the expected helical structure but with an apparent partial loss of helicity compared to their parent peptides (Figure 2). Analysis of the $^1$H-NMR spectra also shows diagnostic features for the increase in the helical content in the **5**-**8** set (Figure 2C).

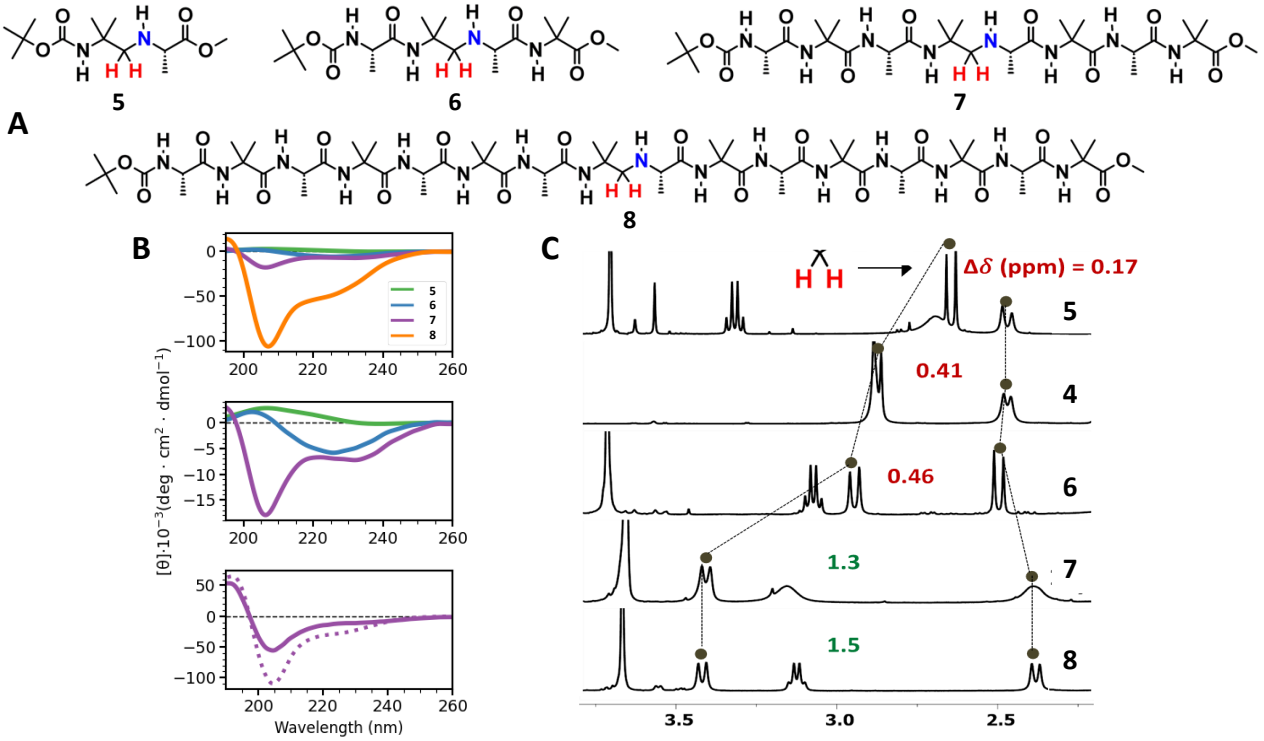


*Figure 2: (A) Chemical structure of L-Ala-Aib based synthesized foldamers* ***5-8****. (B) Comparison of ECD spectra of synthesized compounds* ***5-8*** *in MeOH (0.3 mM) (top and centre) and of* ***7*** *and the parent peptide Boc-(L-Ala-Aib)$_4$-OMe (purple dotted line) in CH$_3$CN (0.3 mM) (bottom). (C) $^1$H-NMR traces comparing Ψ[CH$_2$NH] methylene protons resonance of compound* ***4-8****.*

When the -CH$_2$NH- peptide bond surrogate is within a chiral molecule, the two methylene protons are diasterotopic. In the flexible *pseudo*dipeptide **5** the separation between the proton signals of the two methylene protons (Δδ) is 0.17 ppm, whereas it increases to 0.41 ppm in the case of the

*pseudo*tripeptide **4**, long enough to populate a β-turn conformation. In the series of foldamers **6-8**, increases from 0.46 ppm to 1.3 ppm and 1.5 ppm as the total main-chain length increases from four to eight and sixteen residues, respectively. These results support the view that a high population of folded conformation is achieved at the level of the longest oligomer investigated.

Precursors **7'**, **8'** and foldamer **8** were also characterized by X-ray diffraction analysis.

In the crystal state, the peptide aldehyde Boc-(L-Ala-Aib)$_2$-H **7'** is folded into two consecutive, intramolecularly H-bonded type-III β-turns which give rise to an incipient $3_{10}$-helix (Figure 3). Conversely, Boc-(L-Ala-Aib)$_4$-H **8'** is fully α-helical, featuring five consecutive N-H···O=C intramolecular H-bonds of the i+4 → i type (α-turn or $C_{13}$ structure).[9] The C-terminal $C_{13}$ structure, characterized by a rather elongated H-bond, encompasses a $C_{10}$ structure, in that the N8-H8 group is H-bonded to both the O4 and O5 carbonyl oxygen atoms (Figure 3).

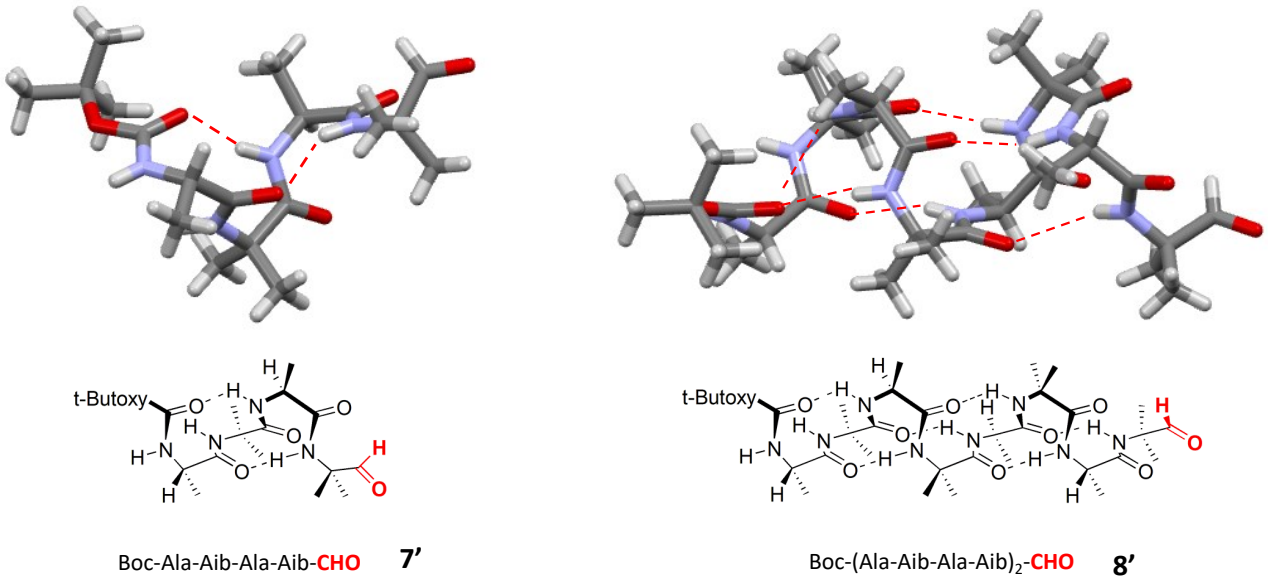


*Figure 3: X-Ray structure and chemical structure of compounds **7'** and **8'**. H-bonds are indicated by dashed lines.*

The X-ray diffraction structure of Boc-(L-Ala-Aib)$_4$Ψ[CH$_2$NH]-(L-Ala-Aib)$_4$-OMe **8** is illustrated in Figure 4. According to our analysis, the secondary amine N9 atom carries two H-atoms. In addition to the cationic foldamer, one hydroxide anion and two co-crystallized water molecules (not shown) compose the asymmetric unit. The conformation adopted by foldamer **8** is largely α-helical in its C-terminal half, whereas the N-terminal half shows a mixed $3_{10}$-/α-helical character. Specifically, starting from the N-terminus, two intramolecularly H-bonded $C_{10}$ structures, having the NH groups

of residues 3 and 4 as the donors and the urethane carbonyl oxygen O0 and the peptide carbonyl oxygen O1 as the acceptors, are observed. The orientation of the N5-H5 group toward O1 would be appropriate for the formation of a $C_{13}$ structure as well.

However, the H5···O1 separation, 2.70 Å, exceed the commonly accepted limit for the occurrence of an N-H···O=C H-bond accepted limit for the occurrence of an N-H···O=C H-bond.[6] Then, two consecutive $C_{13}$ structures (N6-H6···O2 and N7-H7···O3) are followed by two $C_{10}$ structures, N8-H8···O5 and N9-H9B···O6. This latter interaction involves, as the donor, one of the two H-atoms of the protonated secondary amine. The second H-atom on N9 is intermolecularly H-bonded to the co-crystallized hydroxide anion. The intramolecular H-bonding scheme continues with two $C_{13}$ structures (N10-H10···O6 and N11-H11···O7). There is no possibility for the N12-H12 group to form a $C_{13}$ structure because the *pseudo* Aib residue at position 8 lacks the carbonyl group. Conversely, N12-H12 is involved in a $C_{10}$ structure of which O9 is the acceptor, although the interaction is rather elongated and distorted.

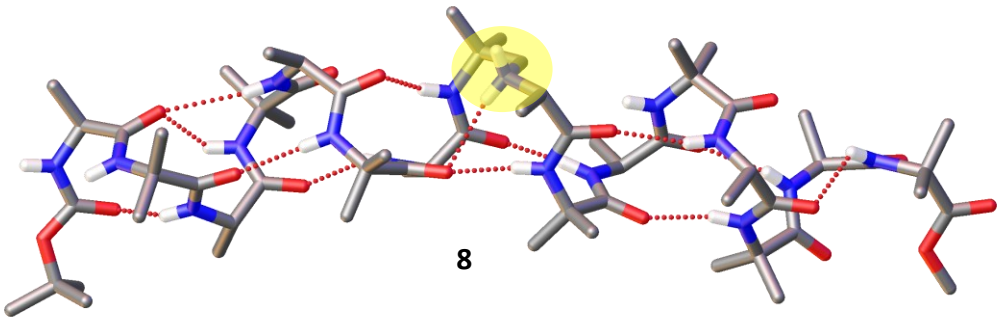


*Figure 4 Figure 16: X-Ray structure of compound* ***8****. H-bonds are indicated by dashed lines, Ψ[CH₂NH] linkage highlited in yellow.*

The α-helical pattern is restored with three additional $C_{13}$ structures (N13-H13···O9, N14-H14···O10, and N15-H15···O11), and terminates with a N16-H16→O13 $C_{10}$ structure. The average values of the backbone torsion angles for residues 1–7 are $\phi = -59.2°$, $\psi = -39.1°$, and those averaged over residues 9–15 are $\phi = -60.1°$, $\psi = -42.7°$, quite close to the values obtained from a statistical analysis of high-resolution crystal structures of α-helical peptides ($\phi = -63°$, $\psi = -42°$).[7] At the -Aib(8)Ψ[CH₂NH]-L-Ala(9)- junction, the values of the backbone torsion angles are $\phi_8 = -59.9(5)°$, $\psi_8 = -57.7(5)°$, "ω"$_8$ = 169.3(3)°, $\phi_9 = -52.6(5)°$, $\psi_9 = -56.0(5)°$. Overall, the Ψ[CH₂NH] modification seems to be tolerated within a helical backbone. In particular, the torsion angle about the C8–N9 single bond deviates by

less than 10° from the *trans* planarity typical for a regular peptide bond. However, the $\psi_8$ and $\psi_9$ values are significantly larger than those in a peptide α-helix, inducing a bending in the molecular shape. Indeed, angle between the two lines connecting the $C^{\alpha}$ atoms of residues 1 and 7 on one side, and of residues 7 and 15 on the other side (which can be considered as an approximation of the axis of the respective helical segment) is 33°.

Based on the X-ray structure of foldamer **8,** we decided to build up a three-dimensional catalytic centre around the secondary amine generated through reductive amination (Scheme 2). For this purpose, we planned to develop a general synthetic strategy where series of fragments with appropriate functional side chain (in the way to eventually assists the catalytic function of the novel secondary amine), will be combined directly to readily form the desired catalytic centre (Scheme 2). Foldamer **9** was synthetized starting from the peptide aldehyde Z-(L-Ala-Aib)$_2$-H which was combined under reductive conditions with $H_2N$-Dap$^{(Boc)}$-(L-Ala-Aib)$_2$-OMe (Scheme 2). In this foldamer, obtained after removal of the Dap side chain Boc protecting group, primary and secondary amines are spaced by two carbon atoms and reciprocally oriented according to the secondary structure.

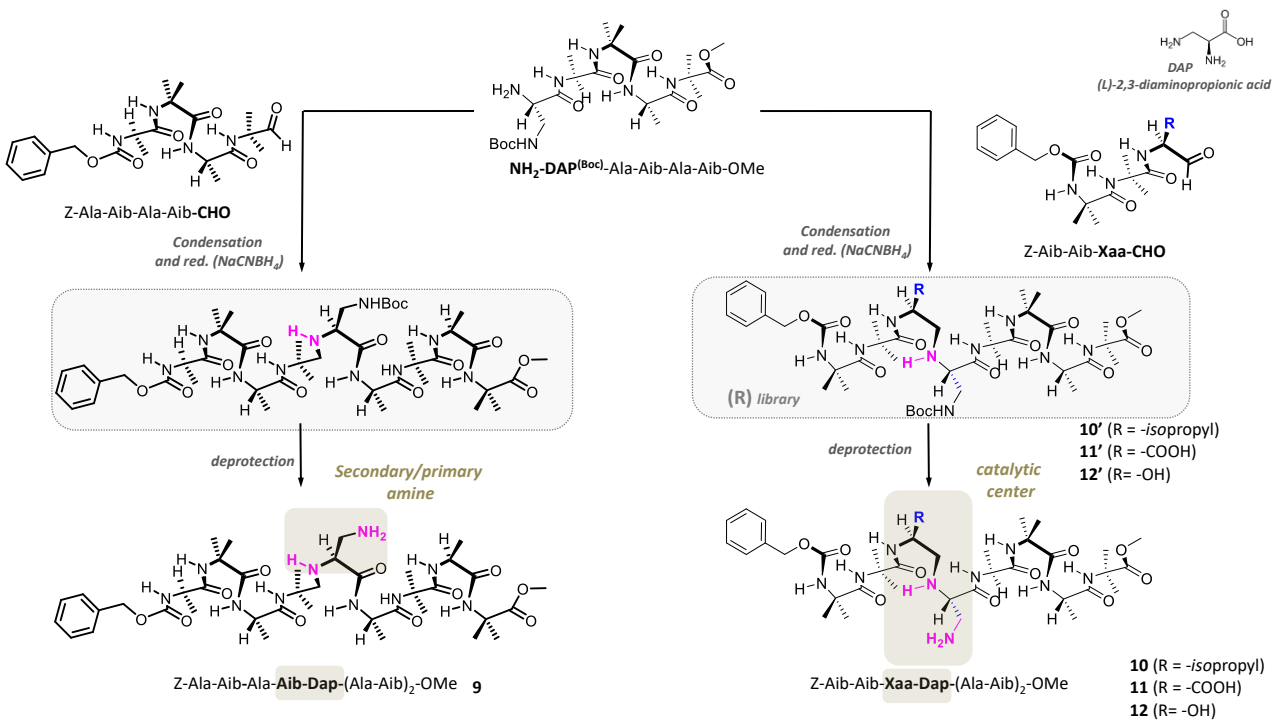


*Scheme 2: Synthesis of catalytic peptide foldamers* ***9-12****. Reagent and conditions: (condensation and reduction) Na(CN)BH$_3$, CH$_3$COOH (2 eq.), MeOH, r.t., 2h. (deprotection) 50% TFA in CH$_2$Cl$_2$, r.t., 20 min.*

To expand the general strategy to form a variety of 3D-catalytic centres, Z-Aib-Aib-(Aaa)-H (Aaa= Val, Asp and Ser) were combined with $H_2N$-$Dap^{(Boc)}$-(L-Ala-Aib)$_2$-OMe to form foldamers **10-12** after deprotection (Scheme 2). These tree foldamers are characterized by an identical length and primary sequence, thus identical 3D-folding, while they differ each other for the chemical nature of the assisted chemical functionality introduced nearby the primary/secondary amines catalytic centre.

Foldamers **10-12** share with foldamer **7** the same tetrapeptide -(L-Ala-Aib)$_2$ C-terminal motif while the N-terminal part is shorter but relatively richer in helicogenic Aib residues. The far-UV CD spectrum of **11-12** recorded in aqueous buffer showed features resembling the CD spectrum of **7-8.** Despite the different solvent and sequences, the spectrum is characterized by a negative maximum located at 205 nm and a shoulder around 230 nm of much less intensity (Figure 5A and B). Moreover, sequential αNH($i$) → αNH($i$+1) (and βCH$_3$($i$) → αNH($i$+1)), characteristic of a helical conformation, are seen in the NOESY spectra of foldamers in the more structured regions (Aib$_1$ → Aib$_2$, Aib$_2$ → Xaa$_3$ and Aib$_6$ → Ala$_7$, Ala$_7$ → Aib$_8$) (Figure 5D). We can suppose that the resemblance in the CD signature of **10-12** and **7-8** along with the structural similarity of foldamers **10-12** and foldamer **7** is diagnostic of similar 3D-helical folding.

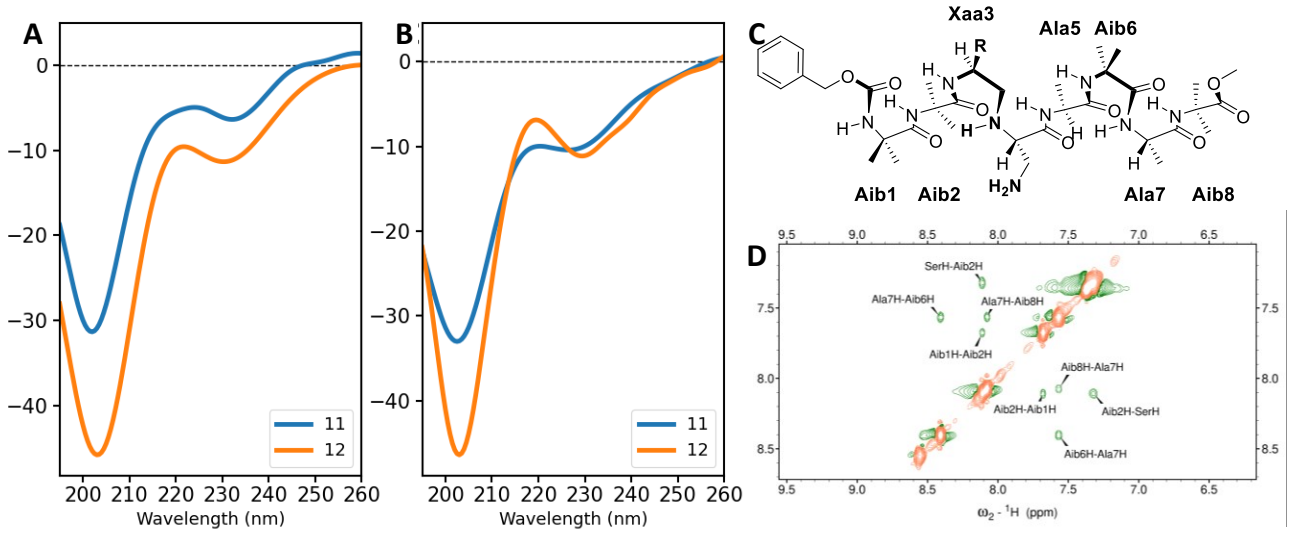


*Figure 5 (A-B) Comparison of ECD spectra of compound **11** and **12** in buffer (0.3 mM) at pH 6.4 (A) and 7.3 (B). (C) Chemical structure of the generic foldamer Z-(Aib)$_2$-Xaa-[CH$_2$NH]-Dap-(L-Ala-Aib)$_2$-OMe with numbered residues. (D) NH→NH section of ROESY spectrum of foldamer **12** (Xaa=Ser) in CD$_3$OH at 25°C.*

As a first example of chemical reactivity, we compared our foldamer performances to those recently published by Gellman and co-workers. In their studies, well-folded foldamers were able to activate

both ends of a linear dialdehyde precursor thus to orient the termini for reaction (via imine/enamine intermediate), therefore acting as a powerfully template for a ring closure through carbon-carbon bond formation. We selected the linear dialdehyde showed in Scheme 3. For the synthesis of dialdehyde **15,** we decided to oxidize its respective diol (**14**); the diol was synthetized through nucleophilic substitution with 1,9-nonanediol from the dibenzylbromide **13**.

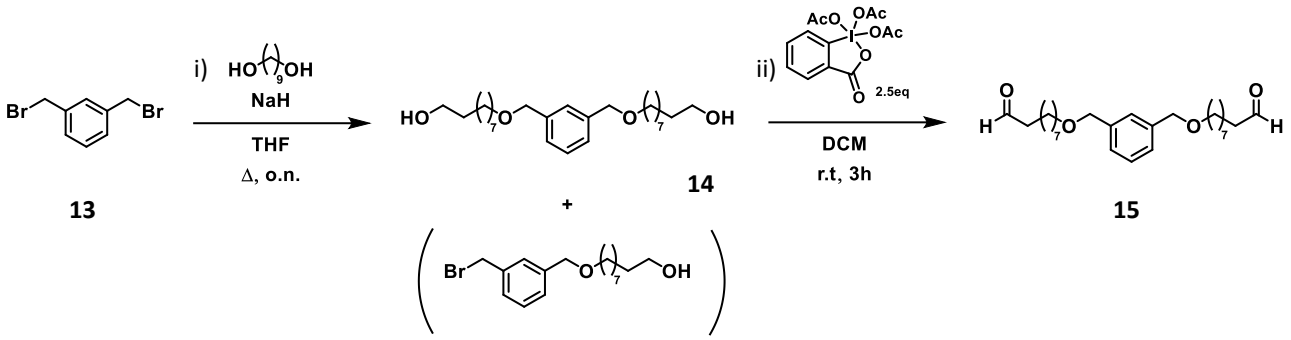


*Scheme 3: Synthesis of linear dialdehyde substrate (**15**) for macrocyclization reaction. Reagents and conditions: i) 1,9-nonanediol (2eq.), NaH (0.5 eq), THF, reflux, overnight. ii) Dess–Martin periodinane (2.5 eq), DCM, r.t., 3 h.*

To obtain diol **14,** 1,3-Bis(bromomethyl)benzene (**13**) was added dropwise to a solution of an excess of 1,9-nonanediol (2eq.) and NaH (0.5eq) in THF at room temperature and then refluxed overnight. The reaction was monitored by TLC, following the conversion of the dibromide. After evaporation of the organic solvent, the product was obtained as a white solid after *flash* chromatography. In these reaction conditions, we observed only partial conversion of the dibromide and the formation of a dominant by-product. After purification, the main by-product of the reaction resulted to be the mono-substituted compound. Some attempts of improving the yield of the reaction, such as changing the metal hydride, the stoichiometry and reaction times, were unsuccessful and the best yield in **14** was obtained in the conditions reported prior. The Dess–Martin periodinane (DMP), a hypervalent iodine compound, is a widely used oxidant for the chemo-selective and mild oxidation of alcohols to the corresponding carbonyl compounds under neutral conditions. It was also shown that for diols with a carbon tether longer than three atoms oxidation with DMP led exclusively to the corresponding dialdehydes in excellent yields, without the competitive cyclic acetal formation. Therefore, diol **14** was oxidized under standard conditions,[8] obtaining the desired di-aldehydes product **15** after flash chromatography.

To gain insight on the capabilities of the catalytic foldamer set **9-12**, we tested its selectivity in promoting cyclization of dialdehyde **15** (Figure 6). We choose reaction conditions similar to those reported for similar studies: aqueous isopropanol as solvent and an acid/base couple of additives, in our case acetic acid and triethylamine. The cyclic product was not observed in the control reaction with pyrrolidine and n-butylamine (10 mol %), which catalysed only slowly the formation of a mixture of linear compounds. The presence of foldamer **10'** lacking the secondary amino moiety and hindered at the Ψ[$CH_2NH$] junction was also not effective in catalysing both the intra- and the intermolecular reactions.

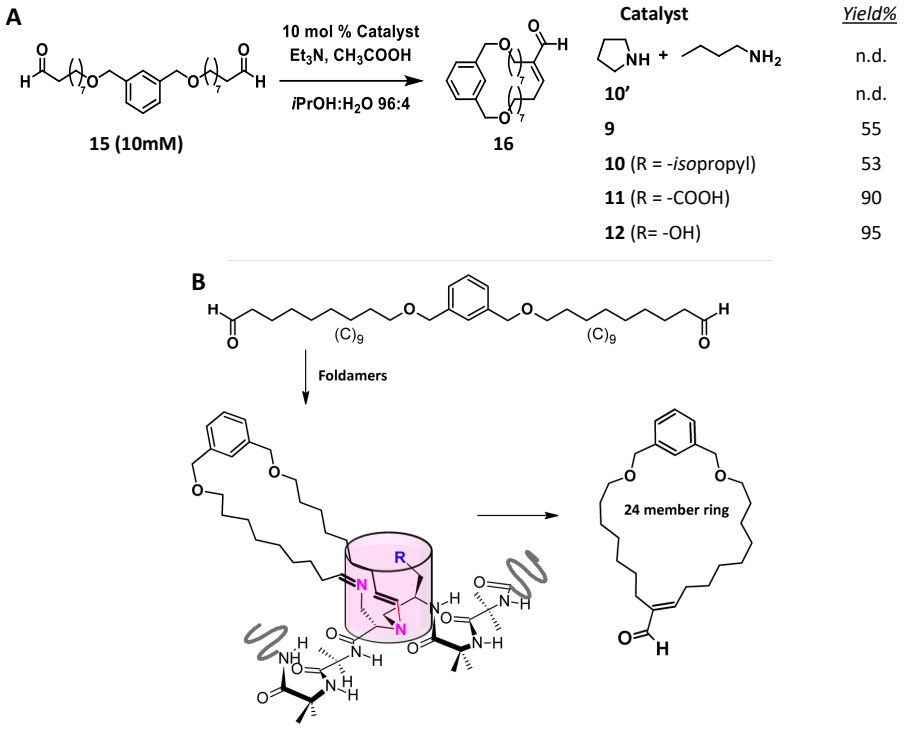


*Figure 6 (A) Macrocyclization experiments of dialdehyde **15;** the yield is referred to the cyclic product (**16**). (B) Proposed intermediate for the Intramolecular aldol reaction catalysed by foldamers **9-12**, in the pink cylinder is highlighted the action of the "active site" of the foldamer.*

The product of the foldamer-catalysed reactions was characterized through MS and NMR spectroscopy. From a comparison of the $^1$H-NMR spectra of the linear dialdehyde (**15**) and product (**16**), the nature of the enal product is suggested by the appearance of a triplet in the double-bond region of the spectra, with an integration ratio with the aldehyde proton of 1:1 (Figure 7). The configuration of the 24-membered ring cyclic *E*-enal (**16**) was confirmed through selective 1D-NOE

experiments: irradiating the alkene proton ($H_b$, red arrow), a negative NOE effect is observed for the aldehyde proton ($H_a$, blue circle, Figure 7).

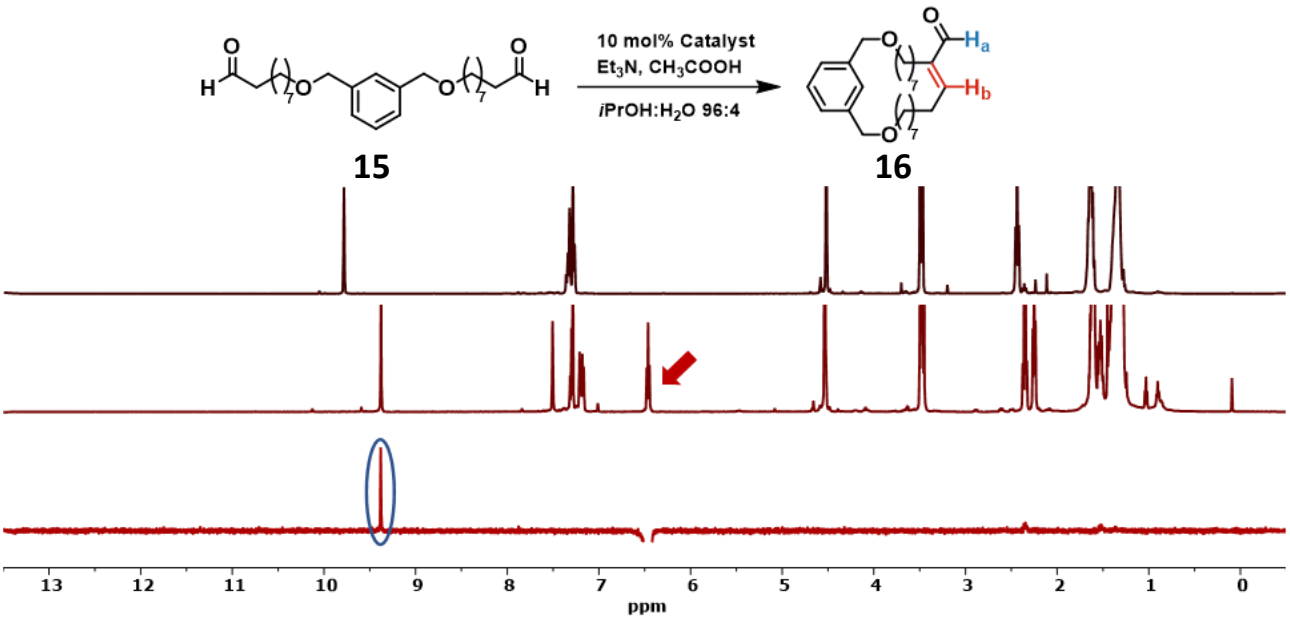


*Figure 7 $^1$H-NMR spectra of dialdehyde (**15**, top spectrum) and cyclic enal (**16**, centre spectrum) in $CDCl_3$. The bottom trace is the 1D-NOESY spectrum acquired irradiating the alkene proton (Hb) proton of **16**.*

Unfortunately, we were not able to detect possible intermediates to elucidate the reaction mechanism.

Foldamer **9** and **10** which are different only for length (and contained an aliphatic side chain) displayed the same reactivity by affording respectively 55 and 53% yield in the cyclic condensate product (Figure 6). Interestingly, foldamers **11** and **12** in the same reaction condition improved the yields up to 90 and 95 % respectively. Thus, the presence of a carboxylic group (Asp) or a hydroxyl group (Ser) seem to assist both the catalytic centre to achieve a faster chemical conversion of the substrate.

Peptide foldamers **9-12** were shown to adopt a helical conformation that could display the catalytic primary amine–secondary amine diad along the helix turn. This arrangement could template the ring closure, promoting the aldol reaction that form the macrocycle, suggesting a dual covalent catalysis through an enamine-iminium intermediate (Figure 6).

# Experimental Section

## General Methods

*High-Performance Liquid Chromatography.* The HPLC measurements were performed using an Agilent 1200 apparatus (Palo Alto, CA), equipped with a UV detector at various wavelength and a column Agilent extend-C18 (stationary phase). Eluants: A= 9:1 $H_2O/CH_3CN$, 0.05 % TFA; B= 1:9 $H_2O/CH_3CN$, 0.05 % TFA.

*Nuclear Magnetic Resonance.* $^{1}H$ NMR, $^{13}C$ NMR, and 2D-NMR spectra were recorded at 25°C on Bruker Avance400 or 500 MHz instruments. $^{1}H$ and $^{13}C$ spectra were referenced relative to the solvent residual peaks and chemical shifts (δ) reported in ppm downfield of tetramethylsilane ($CDCl_3$ δ H: 7.26 ppm, δ C: 77.16 ppm; $CD_3CN$ δ H: 1.94 ppm; DMSO δ H: 2.50 ppm). The multiplicity of a signal is indicated as br, broad; s, singlet; d, doublet; t, triplet; m, multiplet.

*Mass Spectrometry.* ESI-MS experiments and UPLC-MS experiments were performed using an ACQUITY UPLC H-Class System with Xevo G2-XS QTof (Waters, USA).

*Fourier Transform-Infrared Spectroscopy.* FT-IR absorption spectra were recorded with a ATi Perkin Elmer Spectra RX1 FT-IR spectrometer. The ῡ maxima for the main absorption bands are given.

*Melting point.* Melting point of the compounds were determined using a Leitz Laborlux 12 microscope equipped with a Mavotherm 32 thermometer (sensor: NiCr-Ni thermocouple; resolution: 0.1 K; inherent deviation: 199°C ± 0.5% meas. val.).

## Synthesis and characterization of compounds

### Materials

N,N-diisopropylethylamine (DIPEA), trifluoroacetic acid (TFA), triethylamine (TEA), L-amino acids methyl ester hydrochloride, N-(3-Dimethylaminopropyl)-N′-ethylcarbodiimide hydrochloride (EDC·HCl), N,O-dimethylhydroxylamine hydrochloride, lithium aluminum hydride ($LiAlH_4$), sodium cyanoborohydride ($NaCNBH_4$), 4-chlorobenzylamine, Boc-L-amino acids, were obtained from Merck. 1-hydroxy-7-aza-1,2,3-benzotriazole (HOAt) was purchased from GL Biochem (Shanghai).

The deuterated solvents DMSO-$d_6$, $CDCl_3$, $CD_3OD$ and $CDCN_3$ were purchased from Euriso-Top (France).

### General procedure for reductive amination

Peptide aldehyde (1 mmol) was dissolved in dry MeOH (15mL). The amino component (1.5 eq) and $NaCNBH_3$ (2 eq.) dissolved in the minimum amount of MeOH were added to the solution sequentially. Acetic acid (2 eq.) was added to the reaction and the mixture was stirred for 2h at room temperature. Then, the solvent was removed under reduced pressure. The residue was dissolved in EtOAc and washed with NaHCO3 (5% aqueous solution) and brine, dried over anhydrous $Na_2SO_4$, filtered and concentrated. The peptide were purified *via* flash chromatography using DCM/MeOH as eluant.

### General procedure for foldamer deprotection and Boc removal

The protected peptide was dissolved in a TFA/DCM 1:1 (v/v) mixture and the removal of protecting groups was followed by HPLC. At the end of the reaction, the solution was evaporated to dryness, the crude residue was dissolved in milliQ water and lyophilized.

Synthesis of compounds **3** and **4**

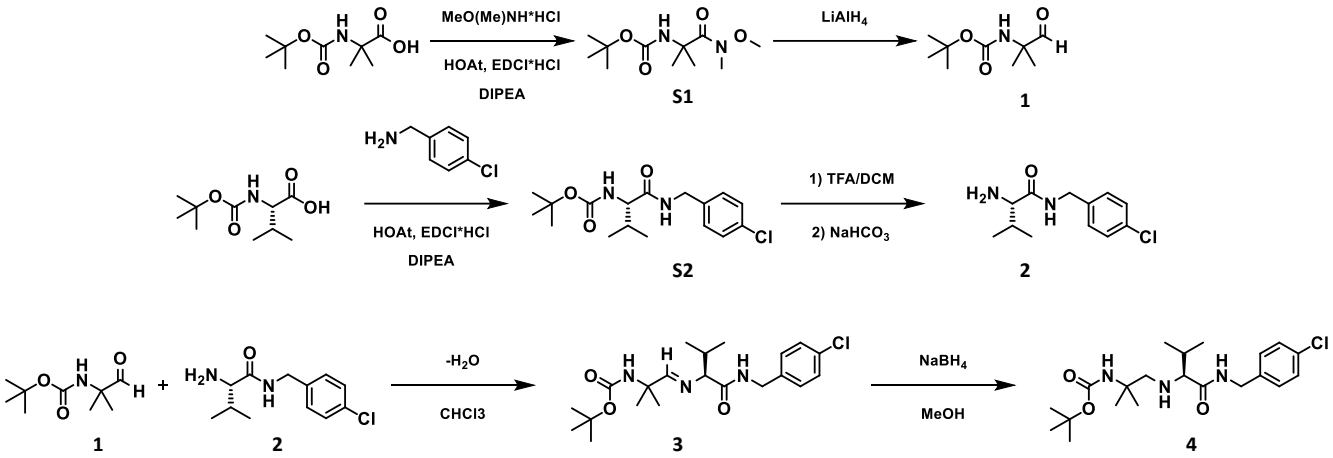


**Scheme S1**: Synthesis of compounds **3** and **4.**

Synthesis of Boc-Aib-N($OCH_3$)$CH_3$ **(S1)**

Boc-Aib-OH (1 g, 5 mmol) was dissolved in dry dichloromethane and HOAt (0.669 g, 5 mmol) and EDC·HCl (0.943 g, 5 mmol) were added. Then N,O-dimethylhydroxylamine hydrochloride (0.975 g, 10 mmol) was added to the reaction and DIPEA was used to reach basic pH. The reaction was allowed to stir at room temperature for 12 hours, then the solvent was removed under reduced pressure. The residue was dissolved in ethyl acetate, washed with $KHSO_4$ (5% aqueous solution), NaHCO3 (5% aqueous solution) and brine, dried over anhydrous $Na_2SO_4$, filtered and concentrated. Colourless solid, 78% yield, 0.960 g, m.p. 96-98°C.

$^1$H NMR (400 MHz, $CDCl_3$) δ 5.28 (br, 1H), 3.67 (s, 3H), 3.19 (s, 3H), 1.53 (s, 6H), 1.42 (s, 9H).

$^{13}$C{$^1$H} NMR (101 MHz, CDCl3) δ 174.7, 154.4, 60.6, 56.7, 33.9, 28.4, 24.7.

MS (ESI-TOF): $[M+H]^+$ calc. for $C_{11}H_{22}N_2O_5$ = 247.1652 m/z; found = 247.1654 m/z.

FT-IR $\nu_{max}$ 3094, 2988, 1733, 1706.

Synthesis of Boc-Aib-H **(1)**

Boc-Aib-N($OCH_3$)$CH_3$ (0.8 g, 3.25 mmol) was dissolved in dry tetrahydrofuran and $LiAlH_4$ (0.246 g, 6.5 mmol) was added. The reaction was followed by TLC. Once the reaction was over, $KHSO_4$ 5% was added dropwise to the reaction mixture, and ethyl acetate and brine were used to dilute the solution. The organic phase was separated, dried over anhydrous $Na_2SO_4$, filtered and concentrated

under reduced pressure. The crude aldehyde was obtained as a colorless oil. The product was purified *via* flash chromatography (eluant: chloroform/methanol 97/3).

Colourless solid, 56% yield, 0.340 g.

$^{1}$H NMR (400 MHz, $CDCl_3$) δ 9.39 (s, 1H), 5.21 (br, $J$ = 80.2 Hz, 1H), 1.38 (s, 9H), 1.26 (s, 6H).

$^{13}$C{$^{1}$H} NMR (101 MHz, $CDCl_3$) δ 201.0, 154.9, 125.4, 30.3, 28.2, 21.8.

MS (ESI-TOF): $[M+H]^+$ calc. for $C_9H_{17}NO_3$ = 188.1281 m/z; found = 188.1280 m/z.

Synthesis of Boc-Val-NH-$CH_2$-Ph-Cl **(S2)**

Boc-Val-OH (1 g, 4.6 mmol) was dissolved in dry dichloromethane and HOAt (0.626 g, 4.6 mmol) and EDC·HCl (0.882 g, 4.6 mmol) were added. Then 4-chlorobenzylamine (1.303 g, 9.2 mmol) was added to the reaction and DIPEA was used to reach basic pH. The reaction was allowed to stir at room temperature for 12 hours, then the solvent was removed under reduced pressure. The residue was dissolved in ethyl acetate, washed with $KHSO_4$ (5% aqueous solution), NaHCO3 (5% aqueous solution) and brine, dried over anhydrous $Na_2SO_4$, filtered and concentrated.

Colourless solid, 69% yield, 1.081 g.

$^{1}$H NMR (400 MHz, $CDCl_3$) δ 7.21 (dd, $J$ = 33.1, 8.3 Hz, 4H), 6.94 (s, 1H), 5.27 (d, $J$ = 8.8 Hz, 1H), 4.36 (qd, $J$ = 15.1, 5.9 Hz, 2H), 3.96 (t, $J$ = 7.8 Hz, 1H), 2.17 – 2.05 (m, 1H), 1.40 (s, 9H), 0.94 (dd, $J$ = 10.1, 6.9 Hz, 6H).

$^{13}$C{$^{1}$H} NMR (101 MHz, $CDCl_3$) δ 171.9, 156.1, 136.8, 133.1, 128.9, 128.7, 79.9, 60.2, 42.6, 30.7, 28.3, 19.3, 18.0.

MS (ESI-TOF): $[M+H]^+$ calc. for $C_{17}H_{25}ClN_2O_3$ = 341.1626 m/z; found = 341.1628 m/z.

Synthesis of $NH_2$-Val-NH-$CH_2$-Ph-Cl **(2)**

Boc-Val-NH-$CH_2$-Ph-Cl (1 g, 2.93 mmol) was dissolved in a TFA/dichloromethane (1:1) solution and removal of Boc- group was followed by TLC. After evaporation of the solvent, the residue was dissolved in dichloromethane and washed with $NaHCO_3$ (5% aqueous solution), dried over anhydrous $Na_2SO_4$, filtered and concentrated. The product was purified *via* flash chromatography (eluants: $CH_2Cl_2$/MeOH 9:1).

Colourless solid, 92% yield, 0.649 g.

$^{1}$H NMR (400 MHz, $CDCl_3$) δ 7.73 (br, 1H), 7.31 (d, $J$ = 8.4 Hz, 2H), 7.24 (d, $J$ = 8.3 Hz, 2H), 4.44 (qd, $J$ = 14.9, 6.1 Hz, 2H), 3.31 (d, $J$ = 3.6 Hz, 1H), 2.45 – 2.31 (m, 1H), 1.43 (br, 2H), 1.01 (d, $J$ = 7.0 Hz, 3H), 0.84 (d, $J$ = 6.9 Hz, 3H).

$^{13}$C{$^{1}$H} NMR (101 MHz, $CDCl_3$) δ 174.4, 137.3, 133.1, 129.1, 128.7, 60.1, 42.4, 30.8, 19.7, 16.0.

MS (ESI-TOF): $[M+H]^+$ calc. for $C_{12}H_{17}ClN_2O$ = 241.1102 m/z; found = 241.1128 m/z.

Boc-Aib-CH=NH-Val-NH-$CH_2$-Ph-Cl **(3)**

$^{1}$H NMR (400 MHz, $CDCl_3$) δ 7.51 (s, 1H), 7.27 (q, J = 8.4 Hz, 4H), 7.16 (s, 1H), 5.04 – 5.00 (m, 1H), 4.52 (dd, J = 15.1, 6.1 Hz, 1H), 4.39 (dd, J = 15.1, 5.8 Hz, 1H), 3.57 (d, J = 3.9 Hz, 1H), 2.44 – 2.35 (m, 1H), 1.47 – 1.37 (m, 15H), 0.93 (d, J = 6.8 Hz, 3H), 0.87 (d, J = 6.9 Hz, 3H).

$^{13}$C{$^{1}$H} NMR (101 MHz, $CDCl_3$) δ 172.5, 169.9, 154.9, 137.5, 129.3, 129.2, 128.9, 128.8, 78.1, 55.1, 42.5, 42.4, 31.9, 30.8, 30.5, 28.5, 28.4, 25.2, 19.8, 17.3.

MS (ESI-TOF): $[M+Na]^+$ calc. for $C_{21}H_{32}ClN_3O3$ = 432.2024 m/z; found = 432.2023 m/z.

Boc-Aib-$CH_2$-NH-Val-NH-$CH_2$-Ph-Cl (4)

$^{1}$H NMR (400 MHz, $CDCl_3$) δ 7.54 (s, 1H), 7.28 (d, J = 8.4 Hz, 2H), 7.22 (d, J = 8.4 Hz,2), 4.47 (s, 1H), 4.41 (d, J = 6.1 Hz, 2H), 2.91 – 2.84 (m, 2-3H), 2.47 (d, J = 11.5 Hz, 1H), 2.15 (pd, J = 6.9, 4.8 Hz, 1H), 1.66 (bs, 1H), 1.43 (dd, J = 12.7, 7.1 Hz, 1H), 1.40 (s, 9H), 1.22 (s, 3H), 1.17 (s, 3H), 0.99 (d, J = 6.9 Hz, 3H), 0.88 (d, $J$ = 6.8 Hz, 3H).

MS (ESI-TOF): $[M+H]^+$ calc. for $C_{21}H_{34}ClN_3O_3$ = 412.2289m/z; found = 412.2381 m/z.

Synthesis of foldamers **5-8**

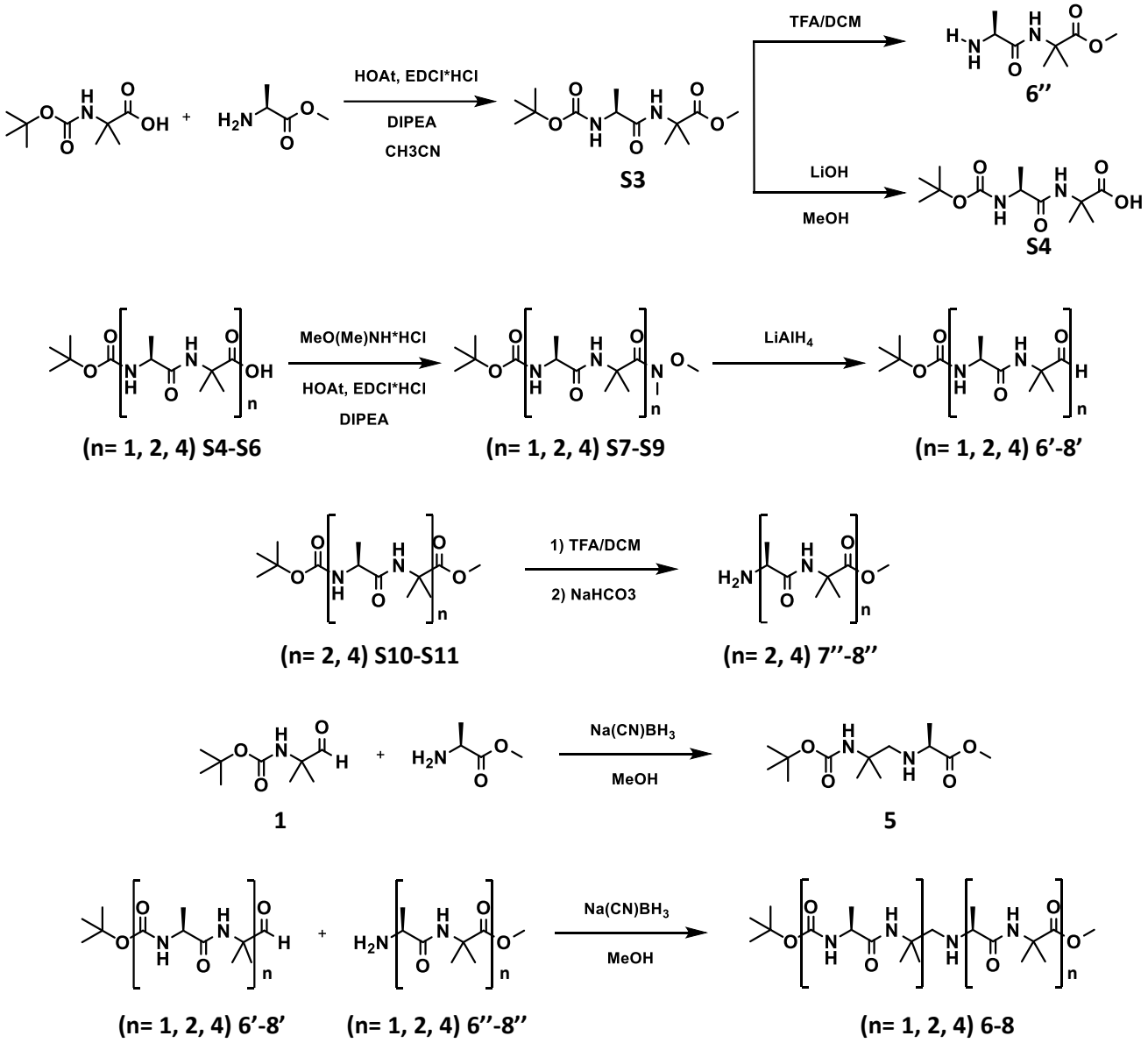


**Scheme S2**: Synthesis of foldamers **5-8.**

Synthesis of Boc-Ala-Aib-COOMe **(S3)**

Boc-Ala-OH (7,5 g, 39.6 mmol) and HOAt (5.99 g, 43,9 mmol) were dissolved in 180mL of dry $CH_3CN$. The suspension was cooled to 0 °C and EDC·HCl (8.43 g, 43.9 mmol) was added. After complete dissolution, HCl·H-Aib-COOMe (8 g, 52 mmol) was added and DIPEA was used to reach basic pH. The reaction mixture stirred overnight at r.t. The solvent was removed under reduced pressure and the residue dissolved in EtOAc. The organic phase was washed with $KHSO_4$(aq) 5%,

$NaHCO_3$(aq) 5%, brine, dried over $NaSO_4$, filtered and concentrated. The product was obtained as a white solid after precipitation from EtOAc/hexane (9.1 g, 79% yield).

$^{13}C\{^1H\}$ NMR (101 MHz, $CDCl_3$) δ 174.9, 172.1, 155.8, 80.22, 56.5, 52.7, 50.1, 28.4, 24.9, 24.8, 18.1.

### Synthesis of Boc-Ala-Aib-OH **(S4)**

Boc-Ala-Aib-COOMe (1.4 g, 4.86 mmol) was dissolved in 15 mL of MeOH and a solution of $LiOH \cdot H_2O$ (612 mg, 14.58 mmol) in 15 mL of water was added. The solution was stirred at 35°C until complete conversion (TLC). The organic solvent was removed under reduced pressure and the aqueous phase was acidified with $KHSO_4$. The compound was extracted using EtOAc (3v). The organic phase was washed with $KHSO_{4(aq)}$ 5% and brine, dried over anhydrous $Na_2SO_4$, filtered and concentrated under reduced pressure. The crude product was used for the following reactions without any further purification.

### Synthesis of $NH_2$-Ala-Aib-COOMe **(6")**

Boc-Ala-Aib-COOMe was dissolved in a TFA/DCM 1:1 (v/v) mixture and the removal of Boc-protecting group was followed by TLC. At the end of the reaction, the solution was evaporated to dryness and the crude product was used for the following reactions without any further purification.

### General procedure for Boc-$(Ala\text{-}Aib)_n$-COOH **(S5-S6)**

2-Chlorotrityl chloride resin (1.6 mmol/g) was added to a vessel. The resin was swelled in DMF and then the first Fmoc-amino acid (2 eq. relative to the resin) was dissolved in DMF and DIPEA (4 eq. relative to the carboxylic acid) was added. This mixture was added to the resin and stirred for 2 h. At the end of this time, the mixture was filtered and the resin was washed with DMF, DCM and DMF. For successive couplings, a solution of the amino acid Fmoc-AA-OH (3 eq.), HATU (3 eq.), HOAt (2.7 eq) and DIPEA (6 eq.) in DMF was added to the resin and stirred for 1h and 30 minutes. The resin was filtered, and washed with DMF, DCM and DMF. Iterative cycles of Fmoc deprotection and coupling were carried out with 20% piperidine solution in DMF. Unreacted sites were capped by treatment with an 18:4:1 DMF/$Ac_2O$/DIPEA mixture for 20 minutes. For the last coupling, Boc-Ala-OH was used. Cleavage of the peptide sequence from the resin was performed with a mixture of

hexafluoroisopropanol/DCM 1:4 (v/v); the filtrated was collected and evaporated under reduced pressure. The residue was triturated in cold $Et_2O$, centrifuged and lyophilized.

Boc-(Ala-Aib)$_2$-COOH **(S5)**

$^1$H NMR (400 MHz, $CDCl_3$) δ 8.00 (br, 1H), 7.65 (s, 1H), 7.63 (s, 1H), 7.40 (s, 1H), 5.96 (s, 1H), 4.40 – 4.26 (m, 1H), 4.00 – 3.84 (m, 1H), 1.55 (d, J = 9.8 Hz, 12H), 1.45 (s, 9H), 1.39 (dd, J = 17.5, 7.2 Hz, 6H).

$^{13}$C{$^1$H} NMR (101 MHz, $CDCl_3$) δ 176.3, 175.1, 174.1, 173.6, 157.0, 81.0, 56.7, 52.3, 49.9, 26.4, 25.1, 24.6, 23.9, 17.0, 16.7.

Boc-(Ala-Aib)$_4$-COOH **(S6)**

$^1$H NMR (400 MHz, $CDCl_3$) δ 7.80 (d, J = 5.3 Hz, 1H), 7.75 (s, 1H), 7.68 (d, J = 5.2 Hz, 1H), 7.61 (s, 1H), 7.58 (s, 1H), 7.54 (s, 1H), 7.49 (d, J = 8.0 Hz, 1H), 6.47 (d, J = 3.1 Hz, 1H), 4.53 (p, J = 7.3 Hz, 1H), 4.04 – 3.92 (m, 2H), 3.83 (qd, J = 7.2, 3.0 Hz, 1H), 1.63 (d, J = 5.3 Hz, 6H), 1.57 (s, 3H), 1.54 – 1.44 (m, 30H), 1.42 (d, J = 7.3 Hz, 3H), 1.35 (d, J = 7.2 Hz, 3H).

$^{13}$C{$^1$H} NMR (101 MHz, $CDCl_3$) δ 177.8, 177.0, 175.8, 175.6, 175.0, 175.0, 174.8, 173.7, 157.5, 80.9, 57.4, 56.9, 56.5, 56.4, 53.5, 53.2, 53.0, 49.1, 28.4, 27.7, 27.0, 26.9, 25.4, 24.4, 23.0, 22.9, 22.8, 16.8, 16.6, 16.6.

MS (ESI-TOF): $[M+H]^+$ calc. for $C_{33}H_{58}N_8O_{11}$ = 743,4298 m/z; found = 743.4815 m/z.

Synthesis of Boc-Ala-Aib-N($OCH_3$)$CH_3$ **(S7)**

Boc-Ala-Aib-OH (1.8 g, 6.56 mmol) was dissolved in dry dichloromethane and HOAt (0.89 g, 6.56 mmol) and EDC·HCl (1.26 g, 6.56 mmol) were added. Then N,O-dimethylhydroxylamine hydrochloride (0.96 g, 9.8 mmol) was added to the reaction and DIPEA was used to reach basic pH. The reaction was allowed to stir at room temperature for 12 hours, then the solvent was removed under reduced pressure. The residue was dissolved in ethyl acetate, washed with $KHSO_4$ (5% aqueous solution), NaHCO3 (5% aqueous solution) and brine, dried over anhydrous $Na_2SO_4$, filtered and concentrated.

The product was obtained as a white solid after precipitation from EtOAc/hexane (1.75 g, 84% yield).

$^{1}$H NMR (400 MHz, $CDCl_3$) δ 7.20 (s, 1H), 5.19 – 5.12 (m, 1H), 4.19 – 4.04 (m, 1H), 3.67(s, 3H), 3.19 (s, 3H), 1.63 – 1.57 (m, 6H), 1.41 (s, 9H), 1.31 (d, J = 7.0 Hz, 3H).

$^{13}$C{$^{1}$H} NMR (101 MHz, $CDCl_3$) δ 174.3, 171.3, 155.5, 60.8, 57.5, 50.5, 34.0, 28.4, 28.4, 23.5, 23.29, 18.9, 18.7.

Synthesis of Boc-Ala-Aib-H **(6')**

Boc-Ala-Aib-N($OCH_3$)$CH_3$ (1 g, 3.15 mmol) was dissolved in dry tetrahydrofuran and $LiAlH_4$ (239 mg, 6.3 mmol) was added. The reaction was followed by TLC. Once the reaction was over, $KHSO_4$ 5% was added dropwise to the reaction mixture, and ethyl acetate and brine were used to dilute the solution. The organic phase was separated, dried over anhydrous $Na_2SO_4$, filtered and concentrated under reduced pressure. The crude aldehyde was obtained after washing with $Et_2O$/hexane (0.5 g, 60% yield).

$^{1}$H NMR (400 MHz, $CDCl_3$) δ 9.36 (s, 1H), 6.84 (s, 1H), 5.05 (d, J = 7.5 Hz, 1H), 4.19 – 4.13 (m, 1H), 1.44 (s, 9H), 1.39 – 1.31 (m, 9H).

Synthesis of Boc-(Ala-Aib)$_2$-N($OCH_3$)$CH_3$ **(S8)**

Boc-(Ala-Aib)$_2$-OH (0.5 g, 1.2 mmol) was dissolved in dry dichloromethane and HOAt (0.158 g, 1.2 mmol) and EDC·HCl (0.220 g, 1.2 mmol) were added. Then N,O-dimethylhydroxylamine hydrochloride (0.230 g, 2.3 mmol) was added to the reaction and DIPEA was used to reach basic pH. The reaction was allowed to stir at room temperature for 12 hours, then the solvent was removed under reduced pressure. The residue was dissolved in ethyl acetate, washed with $KHSO_4$ (5% aqueous solution, NaHCO3 (5% aqueous solution) and brine, dried over anhydrous $Na_2SO_4$, filtered and concentrated.

Colourless solid, 87% yield, 0.478 g

$^{1}$H NMR (400 MHz, $CDCl_3$) δ 7.37 (s, 1H), 7.32 (d, $J$ = 8.1 Hz, 1H), 6.70 (s, 1H), 5.39 (br, 1H), 4.55 – 4.41 (m, $J$ = 7.3 Hz, 1H), 3.93 (dd, $J$ = 7.1, 3.4 Hz, 1H), 3.68 (s, 3H), 3.23 (s, 3H), 1.59 (d, $J$ = 3.7 Hz, 6H), 1.56 (s, 3H), 1.47 (s, 9H), 1.46 (s, 3H), 1.41 (t, $J$ = 7.4 Hz, 6H).

$^{13}$C{$^{1}$H} NMR (101 MHz, $CDCl_3$) δ 173.4, 173.2, 171.4, 156.6, 81.3, 60.6, 56.8, 56.6, 52.7, 49.3, 31.6, 28.2, 27.4, 25.0, 24.7, 23.8, 22.7, 17.8, 17.1, 14.1.

MS (ESI-TOF): $[M+Na]^+$ calc. for $C_{21}H_{39}N_5O_7$ = 496,2742m/z; found = 496.2739 m/z.

Synthesis of Boc-(Ala-Aib)$_2$-H **(7')**

Boc-(Ala-Aib)$_2$-N(OCH$_3$)CH$_3$ (0.4 g, 0.84 mmol) was dissolved in dry tetrahydrofuran and LiAlH$_4$ (0.064 g, 1.7 mmol) was added. The reaction was followed by TLC. Once the reaction was over, KHSO$_4$ 5% was added dropwise to the reaction mixture, and ethyl acetate and brine were used to dilute the solution. The organic phase was separated, dried over anhydrous Na$_2$SO$_4$, filtered and concentrated under reduced pressure. The crude aldehyde was obtained as a colorless oil. The product was purified *via* flash chromatography (eluant: CHCl$_3$/MeOH 97/3). Colourless solid, 96% yield, 0.334 g

$^1$H NMR (400 MHz, CDCl$_3$) δ 9.40 (s, 1H), 7.68 (s, 1H), 7.52 (d, $J$ = 7.5 Hz, 1H), 6.93 (s, 1H), 5.88 (s, 1H), 4.63 – 4.20 (m, $J$ = 7.4 Hz, 1H), 3.94 – 3.77 (m, 1H), 1.59 (s, 3H), 1.48 – 1.41 (m, 15H), 1.38 (d, $J$ = 7.3 Hz, 3H), 1.36 (s, 3H), 1.33 (s, 3H).

$^{13}$C{$^1$H} NMR (101 MHz, CDCl$_3$) δ 201.6, 174.0, 173.3, 156.9, 81.1, 59.2, 56.7, 53.2, 49.4, 28.4, 28.2, 27.7, 23.4, 21.4, 21.3, 17.3, 16.8.

MS (ESI-TOF): [M+H]$^+$ calc. for C$_{19}$H$_{34}$N$_4$O$_6$ = 415.2551 m/z; found = 415.2534 m/z.

Synthesis of Boc-(Ala-Aib)$_4$-N(OCH$_3$)CH$_3$ **(S9)**

Boc-(Ala-Aib)$_4$-OH (600 mg, 0.8 mmol) was dissolved in dry dichloromethane and HOAt (109 mg, 0.8 mmol) and EDC·HCl (155 mg, 0.8 mmol) were added. Then N,O-dimethylhydroxylamine hydrochloride (117 mg, 1.2 mmol) was added to the reaction and DIPEA was used to reach basic pH. The reaction was allowed to stir at room temperature for 12 hours, then the solvent was removed under reduced pressure. The residue was dissolved in ethyl acetate, washed with KHSO$_4$ (5% aqueous solution), NaHCO3 (5% aqueous solution) and brine, dried over anhydrous Na$_2$SO$_4$, filtered and concentrated.

Colourless solid, 85% yield, 540 mg

$^1$H NMR (400 MHz, CDCl$_3$δ 7.79 (d, J = 5.0 Hz, 1H), 7.72 – 7.55 (m, 3H), 7.51 (d, J = 7.3 Hz, 3H), 7.40 (d, J = 7.7 Hz, 1H), 6.68 (s, 1H), 4.40 – 4.30 (m, 1H), 3.95 (q, J = 7.2 Hz, 3H), 3.88 – 3.77 (m, 1H), 3.65 (s, 3H), 3.23 (s, 3H), 1.63 – 1.33 (m, 45H).

$^{13}$C{$^1$H} NMR (101 MHz, CDCl$_3$) δ 176.7, 176.7, 176.6, 175.0, 174.9, 174.7, 174.5, 172.6, 157.4, 80.6, 77.0, 60.5, 60.4, 56.8, 56.5, 56.3, 56.1, 55.5, 53.4, 52.8, 52.8, 49.8, 49.6, 31.6, 28.3, 27.4, 25.2, 23.3, 23.2, 22.8, 17.5, 16.5, 14.2, 14.1.

Synthesis of Boc-(Ala-Aib)$_4$-H **(8')**

Boc-(Ala-Aib)$_4$-N(OCH$_3$)CH$_3$ (0.5 g, 0.64 mmol) was dissolved in dry tetrahydrofuran and $LiAlH_4$ (0.049 g, 1.3 mmol) was added. The reaction was followed by TLC. Once the reaction was over, $KHSO_4$ 5% was added dropwise to the reaction mixture, and ethyl acetate and brine were used to dilute the solution. The organic phase was separated, dried over anhydrous $Na_2SO_4$, filtered and concentrated under reduced pressure. The crude aldehyde was obtained as a colorless oil. The product was purified *via* flash chromatography (eluant: $CHCl_3$/EtOH 98/2 to 90/10).

Colourless solid, 90% yield, 0.416 g.

$^1$H NMR (400 MHz, $CDCl_3$) δ 9.27 (s, 1H), 7.85 (s, 1H), 7.76 (d, J = 4.8 Hz, 1H), 7.60 – 7.51 (m, 3H), 7.45 (d, J = 7.5 Hz, 1H), 7.00 (s, 1H), 5.75 (s, 1H), 4.42 (p, J = 7.4 Hz, 1H), 4.03 – 3.94 (m, 2H), 3.93 – 3.85 (m, 1H), 1.65 – 1.31 (m, 45H).

$^{13}$C{$^1$H} NMR (101 MHz, $CDCl_3$) δ 202.2, 176.9, 176.4, 175.4, 175.0, 174.5, 174.4, 174.0, 157.3, 81.3, 77.2, 59.3, 57.0, 56.7, 56.5, 53.5, 53.0, 52.9, 49.6, 28.4, 28.3, 27.8, 27.4, 27.3, 23.3, 23.0, 22.9, 21.5, 21.4, 17.3, 16.9, 16.7, 16.6. ricontrolla

MS (ESI-TOF): $[M+H]^+$ calc. for $C_{33}H_{58}N_8O_{10}$ = 727,4349 m/z; found = 727.4382 m/z.

Synthesis of Boc-(Ala-Aib)$_2$-COOMe **(S10)**

The peptide was synthetized following 2-Chlorotrityl chloride resin (1.6 mmol/g) was added to a vessel. The resin was swelled in DMF and then the first Fmoc-amino acid (2 eq. relative to the resin) was dissolved in DMF and DIPEA (4 eq. relative to the carboxylic acid) was added. This mixture was added to the resin and stirred for 2 h. At the end of this time, the mixture was filtered and the resin was washed with DMF, DCM and DMF. For successive couplings, a solution of the amino acid Fmoc-AA-OH (3 eq.), HATU (3 eq.), HOAt (2.7 eq) and DIPEA (6 eq.) in DMF was added to the resin and stirred for 1h and 30 minutes. The resin was filtered, and washed with DMF, DCM and DMF. Iterative cycles of Fmoc deprotection and coupling were carried out with 20% piperidine solution in DMF. Unreacted sites were capped by treatment with an 18:4:1 DMF/$Ac_2O$/DIPEA mixture for 20 minutes. For the last coupling, Boc-Ala-OH was used. Cleavage of the peptide sequence from the resin was performed with a mixture of DIPEA/MeOH/DMF 1:5:5 (v/v) stirring

overnight; the filtrated was collected and evaporated under reduced pressure. The residue was triturated in cold $Et_2O$, centrifuged and lyophilized.

MS (ESI-TOF): $[M+H]^+$ calc. for $C_{20}H_{36}N_4O_7$ = 445,2657 m/z; found = 445.2649 m/z.

Synthesis of $NH_2$-(Ala-Aib)$_2$-COOMe **(7")**

Boc-(Ala-Aib)$_2$-COOMe was dissolved in a TFA/DCM 1:1 (v/v) mixture and the removal of Boc-protecting group was followed by TLC. At the end of the reaction, the solution was evaporated to dryness, the crude residue was dissolved in DCM and washed with $NaHCO_3$ 5%. The organic phase was dried over anhydrous $Na_2SO_4$, filtered and concentrated. The product was purified *via* flash chromatography (eluants: $CH_2Cl_2$/MeOH 9:1).

$^1$H NMR (400 MHz, $CDCl_3$) δ 7.85 (s, 1H), 7.26 (s, 1H), 6.76 (d, $J$ = 8.0 Hz, 1H), 4.55 – 4.43 (m, $J$ = 7.2 Hz, 1H), 3.73 (s, 3H), 3.50 (q, $J$ = 6.9 Hz, 1H), 1.95 (br, 2H), 1.51 (s, 3H), 1.39 – 1.25 (m, 15H).

$^{13}$C{$^1$H} NMR (101 MHz, $CDCl_3$) δ 176.0, 175.3, 173.8, 171.6, 56.4, 56.2, 52.5, 50.8, 48.8, 29.7, 28.8, 25.7, 25.3, 24.8, 24.4, 21.3, 17.4.

Synthesis of Boc-(Ala-Aib)$_4$-COOMe **(S11)**

Peptide Boc-(Ala-Aib)$_4$-COOMe was synthesized using standard solid phase 9-fluorenylmethoxycarbonyl (Fmoc) chemistry on a 2-chlorotrityl chloride resin. For each step, Fmoc deprotection was performed by mixing the resin in a piperidine/N,N-dimethylformamide (DMF) (2:8, *v/v*) solution for 10 minutes (2x), then washing with DMF, MeOH and DCM. For all of the amino acid couplings we used the following protocol: 5.0 eq. (relative to the resin loading) of Fmoc-protected amino acid were activated externally with 4.9 eq. of O-Benzotriazole-N,N,N',N'-tetramethyluronium hexafluorophosphate (HBTU) and 10 eq. of diisopropylethylamine (DIPEA) in DMF (2.5 ml/mmol of amino acid). This mixture was then added to a peptide chamber containing the resin and mixed for 3 hours. The resin was then drained and rinsed with MeOH, and DCM, then allowed to dry. As a last coupling, Boc-Ala-OH (5.0 eq.) was used instead of Fmoc-amino acid residue. Cleavage of the peptide sequence from the resin was performed with a mixture of

DIPEA/MeOH/DMF 1:5:5 (v/v) stirring overnight; the filtrated was collected and evaporated under reduced pressure. The residue was triturated in cold $Et_2O$, centrifuged and lyophilized.

$^1$H NMR (400 MHz, DMSO) δ 8.35 (s, 1H), 7.91 (d, $J$ = 4.6 Hz, 1H), 7.73 (s, 1H), 7.61 (d, $J$ = 5.7 Hz, 1H), 7.56 (s, 1H), 7.53 (s, 1H), 7.29 (d, $J$ = 7.7 Hz, 1H), 7.16 (d, $J$ = 4.9 Hz, 1H), 4.13 – 4.03 (m, 1H), 4.00 – 3.84 (m, 3H), 3.55 (s, $J$ = 15.8 Hz, 3H), 1.44 – 1.33 (m, 33H), 1.30 (d, $J$ = 7.2 Hz, 6H), 1.23 (d, $J$ = 7.3 Hz, 6H).

$^{13}$C{$^1$H} NMR (101 MHz, DMSO) δ 176.2, 175.7, 174.7, 174.3, 174.2, 174.0, 173.7, 172.0, 156.4, 79.1, 56.4, 56.3, 56.1, 55.3, 52.2, 51.7, 51.2, 48.9, 28.6, 26.5, 26.3, 26.0, 25.2, 25.2, 24.6, 24.4, 24.0, 17.7, 17.6, 17.4, 17.2, 16.9.

MS (ESI-TOF): $[M+H]^+$ calc. for $C_{34}H_{60}N_8O_{11}$ = 757.4454m/z; found = 757.4417 m/z.

Synthesis of $NH_2$-(Ala-Aib)$_4$-COOMe **(8")**

Boc-(Ala-Aib)$_4$-COOMe was dissolved in a TFA/DCM 1:1 (v/v) mixture and the removal of Boc-protecting group was followed by TLC. At the end of the reaction, the solution was evaporated to dryness, the crude residue was dissolved in DCM and washed with $NaHCO_3$ 5%. The organic phase was dried over anhydrous $Na_2SO_4$, filtered and concentrated. The product was purified *via* flash chromatography (eluants: $CH_2Cl_2$/MeOH 9:1).

$^1$H NMR (400 MHz, $CDCl_3$) 8.15 (s, 1H), 7.77 (s, 1H), 7.63 (d, J = 3.9 Hz, 1H), 7.60 (d, J = 4.9 Hz, 1H), 7.56 (s, 1H), 7.51 – 7.45 (m, 2H), 4.24 (p, J = 7.5 Hz, 1H), 3.97 – 3.88 (m, 2H), 3.63 (s, 3H), 3.48 (q, J = 6.9 Hz, 1H), 2.31 (bs, 2H), 1.54 – 1.38 (m, 39H), 1.32 (d, J = 7.3 Hz, 3H), 1.25 (d, J = 6.9 Hz, 3H).

$^{13}$C{$^1$H} NMR (101 MHz, $CDCl_3$) δ 177.1, 176.9, 176.5, 175.5, 174.7, 174.4, 173.0, 56.8, 56.5, 56.2, 56.0, 55.9, 53.5, 52.9, 52.6, 52.2, 50.6, 49.9, 27.3, 27.0, 26.9, 25.1, 25.0, 23.5, 23.3, 22.9, 21.1, 17.2, 16.8, 16.5.

MS (ESI-TOF): $[M+H]^+$ calc. for $C_{29}H_{52}N_8O_9$ = 657.3930 m/z; found = 657.3932 m/z.

Synthesis of Boc-Aib**Ψ**[$CH_2$NH]-Ala-OMe **(5)**

This compound was prepared following general for reductive amination using aldehyde (**1**) and H-Ala-OMe as starting materials.

$^{1}$H NMR (400 MHz, $CDCl_3$) δ 5.10 (s, 1H), 3.72 (s, 3H), 3.32 (q, J = 7.0 Hz, 1H), 2.69 (bs, 2H), 2.64 (d, J = 11.8 Hz, 1H), 2.47 (d, J = 11.8 Hz, 1H), 1.43 (m, 9H), 1.33 – 1.22 (m, 9H).

$^{13}$C{$^{1}$H} NMR (101 MHz, $CDCl_3$) δ 176.3, 155.1, 77.2, 57.3, 57.3, 52.3, 51.9, 28.6, 25.5, 24.9, 19.3.

MS (ESI-TOF): $[M+H]^+$ calc. for $C_{13}H_{26}N_2O_4$ = 275,1965 m/z; found = 275.1961 m/z.

### Synthesis of Boc-(Ala-Aib)Ψ[$CH_2$NH]-(Ala-Aib)-OMe **(6)**

This compound was prepared following the general procedure for reductive amination using aldehyde (**6'**) and amine (**6"**) as starting materials.

$^{1}$H NMR (400 MHz, $CDCl_3$) δ 7.66 (s, 1H), 6.33 (s, 1H), 5.08 (d, J = 7.3 Hz, 1H), 4.00 (q, J = 6.6 Hz, 1H), 3.72 (s, 3H), 3.08 (q, *J* = 6.9 Hz, 1H), 2.95 (d, J = 11.8 Hz, 1H), 2.49 (d, J = 11.8 Hz, 1H), 2.03 (bs, 2H), 1.54 (d, J = 4.4 Hz, 6H), 1.43 (s, 9H), 1.36 – 1.25 (m, 12H).

$^{13}$C{$^{1}$H} NMR (101 MHz, $CDCl_3$) δ 175.4, 174.6, 172.5, 155.8, 80.2, 77.4, 58.9, 56.9, 56.0, 53.7, 52.7, 28.53, 28.5, 28.4, 25.9, 25.0, 24.8, 19.7, 17.9.

MS (ESI-TOF): $[M+H]^+$ calc. for $C_{20}H_{38}N_4O_6$ = 431,2864 m/z; found = 431.2990 m/z.

### Synthesis of Boc-(Ala-Aib)$_2$Ψ[$CH_2$NH]-(Ala-Aib)$_2$-OMe **(7)**

This compound was prepared following the general procedure for reductive amination using aldehyde (**7'**) and amine (**7"**) as starting materials.

$^{1}$H NMR (400 MHz, $CDCl_3$) δ 7.98 (s, 1H), 7.72 (d, J = 7.2 Hz, 1H), 7.66 (d, J = 5.4 Hz, 1H), 7.46 (s, 1H), 6.74 (s, 1H), 6.69 (s, 1H), 5.49 (s, 1H), 4.48 (p, J = 7.2 Hz, 1H), 3.99 – 3.84 (m, 2H), 3.66 (s, 3H), 3.41 (d, J = 10.6 Hz, 1H), 3.16 (bs, 1H), 2.38 (bs, 1H), 1.82 (bs, 2H), 1.59 (s, 3H), 1.52 (d, *J* = 8.2 Hz, 6H), 1.50 – 1.29 (m, 36H).

MS (ESI-TOF): $[M+H]^+$ calc. for $C_{34}H_{62}N_8O_{10}$ = 743.4662 m/z; found = 743.4672 m/z.

### Synthesis of Boc-(Ala-Aib)$_4$Ψ[$CH_2$NH]-(Ala-Aib)$_4$-OMe **(8)**

This compound was prepared following the general procedure for reductive amination using aldehyde (**8'**) and amine (**8"**) as starting materials.

$^1$H NMR (400 MHz, $CDCl_3$) δ 8.40 (s, 1H), 8.31 (s, 1H), 7.77 – 7.72 (m, 2H), 7.64 (d, J = 4.7 Hz, 1H), 7.59 – 7.56 (m, 2H), 7.52 – 7.43 (m, 5H), 7.10 (s, 1H), 6.80 (s, 1H), 6.06 (bs, 1H), 4.34 (p, J = 7.3 Hz, 1H), 4.08 – 3.93 (m, 4H), 3.93 – 3.83 (m, 2H), 3.68 (s, 3H), 3.43 (d, J = 10.0 Hz, 1H), 3.13 (q, J = 6.8 Hz, 1H), 2.38 (d, J = 10.0 Hz, 1H), 1.80 (s, 2H), 1.59 (s, 6H), 1.56 – 1.39 (m, 72H), 1.35 (d, J = 6.8 Hz, 3H).

MS (ESI-TOF): $[M+H]^+$ calc. for $C_{62}H_{110}N_{16}O_{18}$ = 1367,8257 m/z; found = 1367.8375 m/z.

Synthesis of foldamers **9-12**

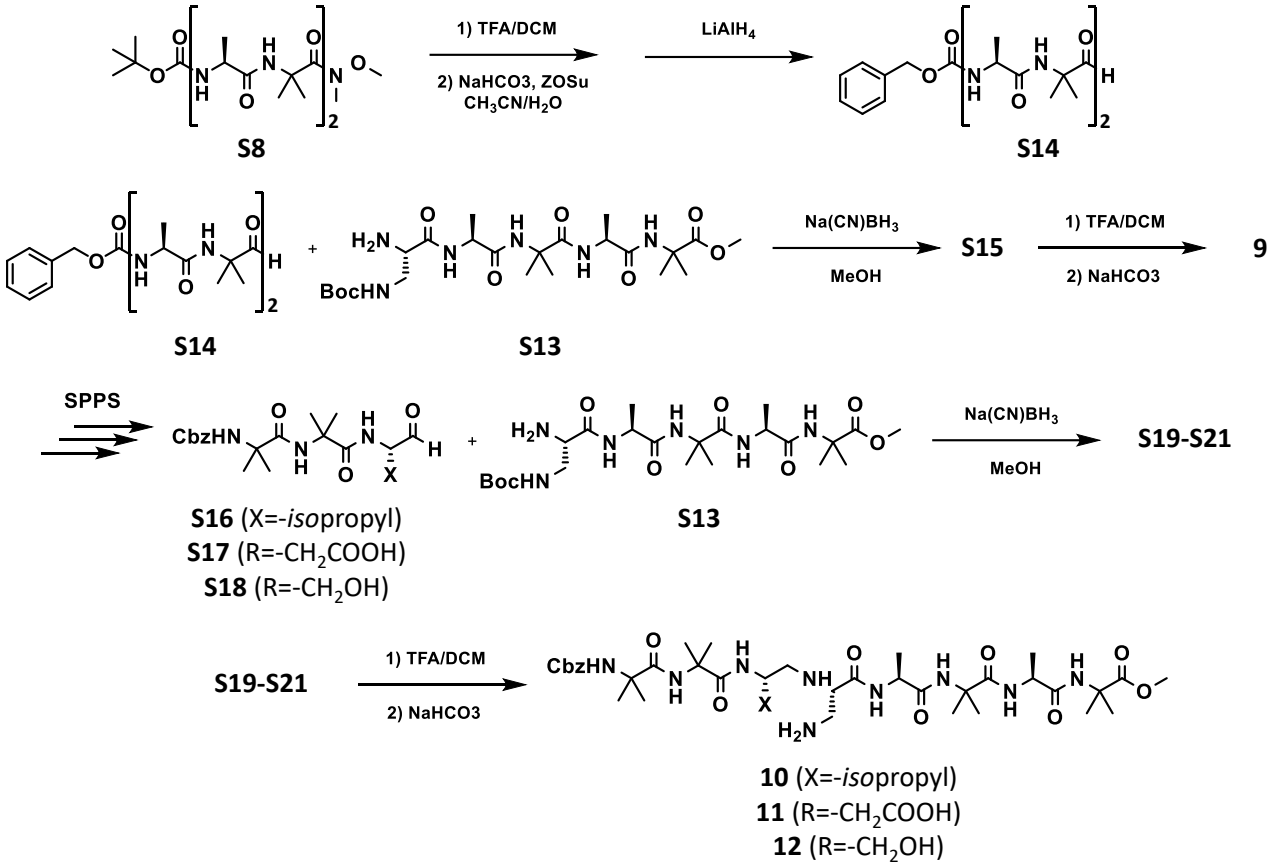


**Scheme S3**: Synthesis of foldamers **9-12.**

Synthesis of Z-Dap(Boc)-(Ala-Aib)$_2$-COOMe **(S12)**

Boc-(Ala-Aib)$_2$-COOMe (0.5 g, 1.12 mmol) was dissolved in a TFA/DCM 1:1 (v/v) mixture and the removal of Boc- protecting group was followed by TLC. At the end of the reaction, the solution was evaporated to dryness, the crude residue was dissolved in DCM and washed with $NaHCO_3$ 5%. The

organic phase was dried over anhydrous $Na_2SO_4$, filtered and concentrated. The product was used for the coupling reaction with Z-DAP(Boc)-OH ($N_\alpha$-Z-$N_\beta$-Boc-L-2,3-diaminopropionic acid, 0.57 g, 1.7 mmol), previously activated by means of HOAt (0.23 g, 1.7 mmol) and EDC·HCl (0.32 g, 1.7 mmol) in dry DCM. $NH_2$-(Ala-Aib)$_2$-COOMe in dry DCM was added to the active ester and DIPEA was used to reach basic pH. The reaction was allowed to stir at room temperature for 12 hours, then the solvent was removed under reduced pressure. The residue was dissolved in ethyl acetate, washed with $KHSO_4$ (5% aqueous solution), NaHCO3 (5% aqueous solution) and brine, dried over anhydrous $Na_2SO_4$, filtered and concentrated.

$^1$H NMR (400 MHz, $CDCl_3$) δ 7.40 – 7.28 (m, 6H), 7.19 (d, J = 9.8 Hz, 1H), 7.01 – 6.93 (m, 1H), 6.91 – 6.77 (m, 1H), 5.61 – 5.38 (m, 1H), 5.12 (q, J = 12.3 Hz, 2H), 4.41 – 4.32 (m, 1H), 4.19 – 4.03 (m, 2H), 3.66 (s, 3H), 3.55 – 3.41 (m, 2H), 1.51 (d, J = 4.4 Hz, 6H), 1.45 (d, J = 13.8 Hz, 15H), 1.38 (d, J = 7.2 Hz, 3H), 1.30 (d, J = 7.2 Hz, 3H).

MS (ESI-TOF): $[M+H]^+$ calc. for $C_{31}H_{48}N_6O_{10}$ = 665.3505 m/z; found = 665.3506 m/z.

Synthesis of $NH_2$-Dap(Boc)-(Ala-Aib)$_2$-COOMe **(S13)**

Z-Dap(Boc)-(Ala-Aib)$_2$-COOMe (1 g, 1.5 mmol) was dissolved in MeOH (30 ml, 0.05 M) under nitrogen atmosphere. Palladium on carbon (0.016 g, 0.15 mmol) was added and the reaction was stirred for 1 hr under nitrogen atmosphere. The reaction was followed by TLC. The solution was filtered on celite and the solvent was evaporated under reduced pressure to give the free amino-peptide as a colourless oil. The crude product was used for the following reactions without any further purification.

Synthesis of Z -(Ala-Aib)$_2$- H **(S14)**

Boc-(Ala-Aib)$_2$- N($OCH_3$)$CH_3$ (0.5 g, 1.05 mmol) was dissolved in a TFA/DCM 1:1 (v/v) mixture and the removal of Boc- protecting group was followed by TLC. At the end of the reaction, the solution was evaporated to dryness, the crude residue was dissolved in DCM and washed with $NaHCO_3$ 5%. The organic phase was dried over anhydrous $Na_2SO_4$, filtered and concentrated. The product was suspended in 15 mL of acetonitrile and the mixture was basified with $NaHCO_3$. A solution of Z-OSu (280 mg, 1.12mmol) in 5 mL of acetonitrile was added to the reaction and the mixture was stirred at room temperature for 12 hours, then the solvent was removed under reduced pressure. The residue was dissolved in ethyl acetate, washed with $KHSO_4$ (5% aqueous solution),

NaHCO3 (5% aqueous solution) and brine, dried over anhydrous $Na_2SO_4$, filtered and concentrated. The crude product was dissolved in dry tetrahydrofuran and $LiAlH_4$ (0.049 g, 1.3 mmol) was added. The reaction was followed by TLC. Once the reaction was over, $KHSO_4$ 5% was added dropwise to the reaction mixture, and ethyl acetate and brine were used to dilute the solution. The organic phase was separated, dried over anhydrous $Na_2SO_4$, filtered and concentrated under reduced pressure. The crude aldehyde was obtained as a colorless oil. The product was purified *via* flash chromatography (eluant: $CHCl_3$/EtOH 98/2 to 90/10).

$^1$H NMR (400 MHz, $CDCl_3$) δ 9.33 (s, 1H), 7.63 (d, J = 3.8 Hz, 1H), 7.35 – 7.26 (m, 5H), 7.20 (d, J = 7.9 Hz, 1H), 6.97 (s, 1H), 6.38 (s, 1H), 5.18 (d, J = 12.4 Hz, 1H), 5.04 (d, J = 12.4 Hz, 1H), 4.33 (p, J = 7.5 Hz, 1H), 3.95 – 3.85 (m, 1H), 1.53 (s, 3H), 1.38 (d, J = 7.2 Hz, 3H), 1.38 – 1.27 (m, 12H).

MS (ESI-TOF): $[M+H]^+$ calc. for $C_{22}H_{32}N_4O_6$ = 449,2395 m/z; found = 449,2360 m/z.

Synthesis of Z-(AlaAib)$_2$-$CH_2$-NH-Dap(Boc)-(Ala-Aib)$_2$-COOMe **(S15)**

This compound was prepared following the general procedure for reductive amination using amine (**S13**) and aldehyde (**S14**) as starting materials. The peptide was purified *via* flash chromatography using DCM/MeOH 95:5 as eluant.

$^1$H NMR (400 MHz, $CDCl_3$) δ 8.22 (s, 1H), 7.80 (s, 1H), 7.59 (s, 1H), 7.43 (s, 1H), 7.39 – 7.28 (m, 6H), 7.16 (s, 1H), 6.72 (s, 1H), 6.54 (s, 1H), 5.33 (s, 1H), 5.19 – 5.06 (m, 2H), 4.33 (p, J = 7.4 Hz, 1H), 4.00 – 3.89 (m, 2H), 3.89 – 3.79 (m, 1H), 3.65 (s, 3H), 3.47 – 3.31 (m, 2H), 3.26 – 3.11 (m, 1H), 2.41 – 2.23 (m, 1H), 2.04 (bs), 1.62 – 1.29 (m, 36H).

$^{13}$C{$^1$H} NMR (101 MHz, $CDCl_3$) δ 176.3, 175.6 174.8, 174.6, 173.8, 173.5, 173.0, 157.6, 156.1, 136.3, 128.8, 128.5, 128.1, 127.9, 79.4, 67.4, 64.5, 57.0, 56.7, 56.0, 54.2, 53.6, 53.3, 53.15, 52.3, 49.8, 28.5, 27.7, 27.4, 26.9, 25.3, 25.0, 24.9, 23.5, 17.4, 17.3, 17.1, 16.8.

Synthesis of Z-(AlaAib)$_2$-$CH_2$-NH-Dap-(Ala-Aib)$_2$-COOMe **(9)**

This compound was prepared following the general procedure for foldamer deprotection from compound (**S19**).

$^1$H NMR (400 MHz, DMSO-$d_6$) δ 8.59 (bs, 1H, $NH^{Ala}$), 8.40 (s, 1H, $NH^{Aib}$), 8.24 (s, 1H, $NH^{Aib}$), 7.95 (s, 1H, $NH^{Aib}$), 7.55 (d, J = 6.0 Hz, 1H, $NH^{Ala}$), 7.46 (d, J = 6.7 Hz, 1H, $NH^{Ala}$), 7.39 – 7.32 (m, 5H, $Ar^Z$), 7.30 (d, $J$ = 7.3 Hz, 2H, $NH^{Ala+Aib}$), 7.27 – 7.21 (m, 1H), 5.04 (dd, $J$ = 12.6, 3.8 Hz, 2H, $CH_2^Z$), 4.47 (bs, 1H) 4.30 (p, J = 7.1 Hz, 1H, H$\alpha^{Ala}$), 4.18 (p, J = 7.1 Hz, 1H, H$\alpha^{Ala}$), 4.00 (dq, J = 20.1, 6.9

Hz, 2H, $H\alpha^{Ala}$), 3.54 (s, 3H, COOMe), 3.12 (s, 2H), 2.91 (s, 2H), 1.37 – 1.27 (m, 20H, $\beta CH_3^{Aib}$), 1.31 – 1.24 (m, xH,$\beta CH_3^{Ala+Aib}$), 1.20 (d, J = 7.0 Hz, 3H, $\beta CH_3^{Ala}$), 1.17 (d, J = 7.0 Hz, 6H, $\beta CH_3^{Ala}$).

MS (ESI-TOF): $[M+H]^+$calc. for $C_{40}H_{66}N_{10}O_{11}$ = 863.2564 m/z; found = 863.5025 m/z.

General procedure for the synthesis of Z-$Aib_2$-AA-H **(S16-S18)**

Peptide Z-$Aib_2$-AA-H were synthesized using standard solid phase 9-fluorenylmethoxycarbonyl (Fmoc) chemistry on a Weinreb AM (N-Fmoc- N-methoxy-β-alanine) resin. Following removal of the Fmoc- group with 20% piperidine in DMF, the addition of the first amino acid (5 eq. relative to the resin loading) was achieved with HATU (5 eq. relative to resin loading) in DMF. DIPEA (10 eq. relative to the resin loading) was added immediately and the mixture was stirred for 3 hr. The resin was then drained and rinsed with MeOH, and DCM, then allowed to dry. For all of the amino acid couplings the following protocol was used: 5.0 eq. (relative to the resin loading) of Fmoc-protected amino acid activated externally with 4.9 eq. of HATU and 10 eq. of DIPEA in DMF (2.5 ml/mmol of amino acid). This mixture was then added to a peptide chamber containing the resin and mixed for 3 hours. The resin was then drained and rinsed with MeOH, and DCM, then allowed to dry. Removal of the Fmoc- group was performed with 20% piperidine in DMF. As a last coupling, Z-Aib-OH (5.0 eq.) was used instead of Fmoc-amino acid residue. For the reductive cleavage of the peptide sequence, the resin was swollen in THF, flushed with nitrogen and cooled to 0 °C. LiAlH4 (11 eq.) was added portion wise, and the mixture was allowed to stir for 3 h. The mixture was again cooled to 0 °C and diluted with EtOAc. The mixture was then quenched with saturated Rochelle's salt solution and allowed to stir for 15 min to ensure quenching. The mixture was then filtered and the resulting filtrate was extracted three times using EtOAc. The combined EtOAc fractions were concentrated in vacuo to yield the desired peptide aldehyde. The crude products were used for the following reactions without any further purification.

Synthesis of Z-$Aib_2$-Val-$CH_2$-NH-Dap(Boc)-$(Ala\text{-}Aib)_2$-COOMe **(S19)**

This compound was prepared following the general procedure for reductive amination using amine (**S13**) and aldehyde (**S16**) as starting materials.

$^1$H NMR (400 MHz, $CDCl_3$) δ 8.55 (d, J = 4.9 Hz, 1H), 7.56 (s, 1H), 7.46 (s, 1H), 7.40 – 7.26 (m, 6H), 6.84 (d, J = 9.7 Hz, 1H), 6.59 (s, 1H), 5.85 (s, 1H), 5.47 (t, J = 6.1 Hz, 1H), 5.25 (bs, 1H), 5.19 – 4.98 (m, 2H), 4.35 (p, J = 7.3 Hz, 1H), 4.02 (q, J = 6.7 Hz, 1H), 3.82 – 3.70 (m, 1H), 3.66 (s, 3H),

3.61 – 3.31 (m, 2H), 3.23 – 3.18 (m, 1H), 2.75 (d, J = 6.9 Hz, 2H), 2.09 (bs, 1H), 1.66 (dt, J = 13.3, 6.8 Hz, 1H), 1.56 – 1.32 (m, 39H), 0.91 – 0.80 (m, 6H).

$^{13}C\{^{1}H\}$ NMR (101 MHz, $CDCl_3$) δ 176.0, 175.4, 174.9, 174.6, 173.7, 173.4, 172.6, 156.5, 156.2, 136.2, 128.8, 128.5, 127.9, 127.8, 79.5, 67.1, 61.45, 57.2, 57.0, 55.9, 53.9, 52.4, 52.3, 50.1, 49.6, 41.7, 31.1, 28.7, 28.5, 27.2, 26.9, 25.4, 24.8, 23.9, 23.8, 23.7, 23.3, 19.9, 18.5, 17.3, 16.2.

MS (ESI-TOF): $[M+H]^+$ calc. for $C_{44}H_{73}N_9O_{12}$ = 920,5451 m/z; found = 920.5430 m/z.

Synthesis of Z-Aib$_2$-Asp(OtBu)-CH$_2$-NH-Dap(Boc)-(Ala-Aib)$_2$-COOMe **(S20)**

This compound was prepared following the general procedure for reductive amination using amine (**S13**) and aldehyde(**S17**) as starting materials.

MS (ESI-TOF): $[M+H]^+$ calc. for $C_{47}H_{77}N_9O_{14}$ = 992,5663 m/z; found = 992.5646 m/z.

Synthesis of Z-Aib$_2$-Val-CH$_2$-NH-Dap-(Ala-Aib)$_2$-COOMe **(10)**

This compound was prepared following the general procedure for foldamer deprotection from compound (**S19**).

$^{1}H$ NMR (400 MHz, DMSO-$d_6$) δ 8.84 (s, 1H, $NH^{Ala}$), 8.53 (s, 1H, $NH^{Ala}$), 8.40 (s, 1H), 8.04 – 7.97 (m, 2H), 7.41 – 7.29 (m, 5H, $Ar^{Z}$), 7.28 (d, J = 7.6 Hz, 1H, $NH^{Ala}$), 6.93 (d, J = 9.6 Hz, 1H, $NH^{Val}$), 5.17 (d, J = 12.9 Hz, 1H, $CH_2^{Z}$), 5.01 (d, J = 12.9 Hz, 1H, $CH_2^{Z}$), 4.33 (p, J = 6.8 Hz, 1H, $H\alpha^{Ala}$), 4.21 (p, J = 7.2 Hz, 1H, $H\alpha^{Ala}$), 4.05 (s, 1H, $H\alpha^{Dap}$), 3.95 – 3.84 (m, 1H, $H\alpha^{Val}$), 3.53 (s, 3H, COOMe), 3.44 – 3.36 (m, 1H, $H\beta^{Dap}$), 3.28 – 3.19 (m, 1H, $H\beta^{Dap}$), 3.09 – 3.05 (m, 1H, $\Psi[CH_2NH]^{Val}$), 2.86 – 2.74 (m, 1H, $\Psi[CH_2NH]^{Val}$), 1.67 (h, J = 6.5 Hz, 1H, $H\beta^{Val}$), 1.37 – 1.21 (m, 27H, $\beta CH_3^{Ala+Aib}$), 1.16 (d, J = 7.1 Hz, 3H), 0.74 (dd, J = 32.7, 6.7 Hz, 6H, $\gamma CH_3^{Val}$).

MS (ESI-TOF): $[M+H]^+$ calc. for $C_{39}H_{65}N_9O_{10}$ = 820,4927 m/z; found = 820.5004 m/z.

Synthesis of Z-Aib$_2$-Asp-CH$_2$-NH-Dap-(Ala-Aib)$_2$-COOMe **(11)**

This compound was prepared following the general procedure for foldamer deprotection from compound (**S20**).

MS (ESI-TOF): $[M+H]^+$ calc. for $C_{38}H_{61}N_9O_{12}$ = 836,4512 m/z; found = 836.4495 m/z.

Synthesis of Z-Aib$_2$-Ser-CH$_2$-NH-Dap-(Ala-Aib)$_2$-COOMe **(12)**

This compound was prepared following the general procedure for reductive amination using amine (**S13**) and aldehyde (**S18**) as starting materials, obtaining compound (**S21**) and then the general procedure for foldamer deprotection from compound (**S21**).

$^1$H NMR (400 MHz,CD$_3$OH) δ 8.56 (d, J = 5.2 Hz, 1H, NH$^{Ala}$), 8.41 (s, 1H, , NH$^{Aib}$), 8.11 (s, 1H, NH$^{Aib}$), 8.08 (s, 1H, NH$^{Aib}$), 7.68 (s, 1H, , NH$^{Aib}$), 7.56 (d, J = 7.3 Hz, 1H, NH$^{Ala}$), 7.41 – 7.26 (m, 6H, NH$^{Ser}$andAr$^Z$), 5.12(CH$_2^Z$), 4.33 – 4.17 (m, 2H, Hα$^{Ala}$), 4.06 – 4.01 (m, 1H, Hα$^{Ser}$), 3.66 (s, 3H, COOMe), 3.62 (t, J = 6.7 Hz, 1H, Hα$^{Dap}$), 3.52 – 3.46 (m, 2H, Hβ$^{Ser}$), 3.28 – 3.14 (m, 2H, Hβ$^{Dap}$), 2.97 (dd, J = 12.4, 4.2 Hz, 1H, Ψ[C*H*$_2$NH]$^{Ser}$), 2.75 (dd, J = 12.5, 9.4 Hz, 1H, Ψ[C*H*$_2$NH]$^{Ser}$), 1.48 – 1.39 (m, 19H), 1.41 – 1.36 (m, 8H, βCH$_3^{Ala+Aib}$), 1.35 (s, 3H), 1.31 (d, J = 7.2 Hz, 3H, βCH$_3^{Ala}$).

MS (ESI-TOF): [M+H]$^+$ calc. for C$_{37}$H$_{61}$N$_9$O$_{11}$ = 808,4563m/z; found = 808.4606 m/z.

Synthesis of dialdehyde substrate **(S22)**

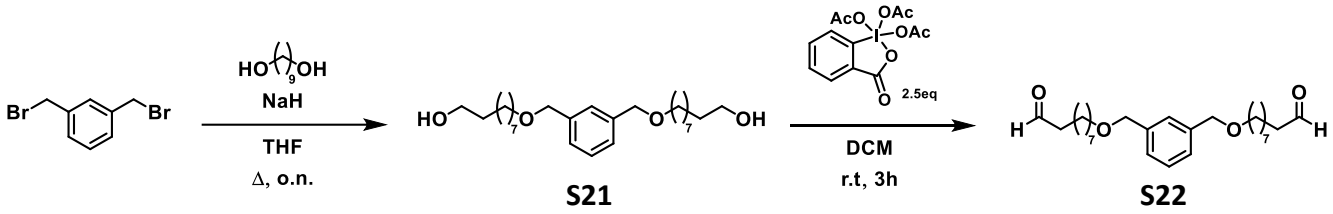


**Scheme S2**: Synthesis of dialdehyde **S22.**

Nonane-1,9-diol (4.8 g, 28 mmol), was dissolved in 14 mL of THF and then NaH was added (600 mg of a 60% dispersion in mineral oil, 14 mmol). 1,3-bis(bromomethyl)benzene (2 g, 7.6 mmol) in 8 mL of THF was added dropwise and the mixture was refluxed overnight. The solvent was removed under reduced pressure and the compound was purified *via* flash chromatography using DCM/MeOH 8:2 as eluant. Colorless solid, 44% yield, 1.44 g (**S21**)

$^1$H NMR (400 MHz, CDCl$^3$) δ 7.43 – 7.11 (m, 4H), 4.52 (s, 4H), 3.65 (t, J = 6.6 Hz, 4H), 3.48 (t, J = 6.6 Hz, 4H), 1.68 – 1.55 (m, 8H), 1.42 – 1.26 (m, 20H).

$^{13}$C{$^1$H} NMR (101 MHz, CDCl$_3$) δ 138.9, 128.5, 127.0, 126.9, 72.9, 70.7, 63.1, 32.9, 29.9, 29.7, 29.5, 29.5, 26.3, 25.9.

MS (ESI-TOF): [M'+H]$^+$ calc. for C$_{26}$H$_{46}$O$_4$ = 423.3469 m/z; found = 423.3458 m/z.

Diol **S21** (0.84 g, 2 mmol,), was dissolved in 6 mL dichloromethane. Dess-Martin periodinane (2.12 g, 5 mmol) was then added all at once. The reaction mixture was stirred under $N_2$ for 3 hours, at which point 24 mL diethyl ether was then added. The entire contents of the flask were combined with 37 mL saturated aqueous sodium bicarbonate containing sodium thiosulfate pentahydrate (25g/100mL). After stirring for 1 hour, the organic layer was removed. The aqueous layer was extracted 2 times with 24 mL diethyl ether. All the organic layers were then washed with $NaHCO_3$ (5% aqueous solution) (2X), and brine (1X). The organic layers were then dried with $Na_2SO_4$, filtered, and concentrated under vacuum. The light-yellow oil obtained was purified *via* flash chromatography using hexane/ EtOAc 8:2 as eluant. Colorless oil, 68% yield, 0.58 g (**S22**)

$^1$H NMR (400 MHz, $CDCl_3$) δ 9.76 (t, $J$ = 2.0 Hz, 2H), 7.35 – 7.22 (m, 4H), 4.49 (s, 4H), 3.46 (t, J = 6.6 Hz, 4H), 2.41 (td, J = 7.4, 1.8 Hz, 4H), 1.67 – 1.56 (m, 8H), 1.38 – 1.26 (m, 16H).

$^{13}$C{$^1$H} NMR (101 MHz, $CDCl_3$) δ 203.0, 138.9, 128.5, 127.0, 126.9, 72.9, 70.7, 44.0, 29.9, 29.4, 29.4, 29.2, 26.3, 22.2.

MS (ESI-TOF): $[M+Na]^+$ calc. for $C_{26}H_{42}O_4$ = 441.2975 m/z; found = 441.2947 m/z.

Under the conditions employed, large quantities of the methanolic di-hemiacetal were formed $[M'+Na]^+$ calc. for $C_{28}H_{50}O_6$ = 505.3499 m/z; found = 505.3506 m/z.

## Foldamer catalysed macrocyclization

Dialdehyde **S22** (104 mg, 0.25 mmol) was dissolved in isopropanol, followed under agitation by acetic acid (0.25 mmol, 14.3. µL, as 2mL of a 0.5M solution in isopropanol/water 96/4) and triethylamine (0.25 mmol, 34.8 µL, as 2mL of a 0.5M solution in isopropanol/water 96/4) for a total volume of 25mL. Added last was catalysts **9-12** (0.025 mmol). The reaction was allowed to stir at 30°C in a sand bath for 12 hours. The reaction mixture was analysed via HPLC (method used is 85-100 %B over 10 minutes, then 100%B for 4 minutes with an Eclipse XDB-C18 5µm, 4.6x150mm) and then the solvent was removed under reduced pressure. The residue was dissolved in EtOAc and washed with $KHSO_4$ (5% aqueous solution), NaHCO3 (5% aqueous solution) and brine, dried over anhydrous $Na_2SO_4$, filtered and concentrated.

Product **S23**: $^{1}$H NMR (400 MHz, $CDCl_3$) δ 9.35 (s, 1H), 7.48 (s, 1H), 7.33 – 7.12 (m, 3H), 6.44 (t, J = 7.6 Hz, 1H), 4.51 (d, J = 2.6 Hz, 4H), 3.45 (dt, J = 11.3, 6.3 Hz, 4H), 2.33 (q, J = 7.6 Hz, 2H), 2.23 (t, J = 7.5 Hz, 2H), 1.67-1.21 (m, 20H).

$^{13}C\{^{1}H\}$ NMR (101 MHz, $CDCl_3$) δ 195.6, 155.6, 143.9, 139.1, 139.1, 128.3, 127.0, 126.9, 126.9, 77.5, 77.2, 76.8, 72.9, 72.8, 70.2, 30.5, 29.9, 29.9, 29.8, 29.4, 29.3, 29.2, 29.10, 28.9, 28.8, 28.5, 28.5, 26.4, 26.0, 24.0.

MS (ESI-TOF): $[M+Na]^+$ calc. for $C_{26}H_{40}O_3$ = 423.2870 m/z; found = 423.2870 m/z.

Under the conditions employed, large quantities of the methanolic acetal were formed $[M'+Na]^+$ calc. for $C_{28}H_{46}O_4$= 469.3288 m/z; found = 469.3329 m/z.

## References


1 V. Martí-Centelles, M. D. Pandey, M. I. Burguete and S. V. Luis, *Chem. Rev.*, 2015, **115**, 8736–8834.

2 Z. C. Girvin, M. K. Andrews, X. Liu and S. H. Gellman, *Science.*, 2019, **366**, 1528–1531.

3 C. M. Venkatachalam, *Biopolymers*, 1968, **6**, 1425–1436.

4 C. Toniolo, M. Crisma, F. Formaggio and C. Peggion, *Biopolymers*, 2001, **60**, 396–419.

5 S. Aravinda, N. Shamala and P. Balaram, *Chem. Biodivers.*, 2008, **5**, 1238–1262.

6 C. Toniolo and E. Benedetti, *Crit. Rev. Biochem.*, 1980, **9**, 1–44.

7 M. Crisma, F. Formaggio, A. Moretto and C. Toniolo, *Biopolymers*, 2006, **84**, 3–12.

8 J. Roels and P. Metz, *Synlett*, 2001, 789–790.

9 A. Erkkilä and P. M. Pihko, *European J. Org. Chem.*, 2007, **2007**, 4205–4216.

# 4. Multivalent catalysts from a single peptide sequence inspired by hydrolytic enzymes

The design of synthetic equivalents of hydrolytic enzymes in both activity and range of chemical transformations continues to be a major challenge. As discussed in the previous chapter, enzymatic catalysis often depends on the proper spatial organization of two or more reactive groups within an active site which binds the substrate and stabilizes the transition state. For example, the catalytic action of serine peptidases depends on the interplay of a nucleophile, a general base, and an acid: in the classic trypsin family this catalytic triad is composed of serine, histidine, and aspartic acid residues. In the previous chapter, foldamer-based catalysts were reported as an attractive alternative to well-developed strategies involving small molecules or conventional peptides.[1,2]

Another approach in the design of synthetic equivalents of enzymes is the development of multivalent catalytic systems (see Section 1.3). The building up of the contributions of several weakly binding units into a strong binding is a process well-exploited by natural systems in recognition phenomena, such as protein-protein and protein-cell interactions. Indeed, catalytic systems should benefit from multivalency: from enhanced interaction to the transition states to cooperative interactions of different functional groups. In synthetic systems, this multivalent display of functional groups may originate from the repetition of identical building blocks held together by weak interactions (e.g., micellar aggregates) or by covalent bonding (e.g., polymers and functionalized nanoparticles). Peptides offer a unique scaffold for the development of multivalent catalytic systems. Their modular and programmable nature allows to expand their function by the insertion of functional moieties as modified building blocks or as capping ends at the N- and C-termini. A short peptide sequence containing the catalytic triad of reactive side chains – Ser, His and Asp – can be functionalized with moieties to achieve self-assembly, as well as polymerization or metal nanoparticle functionalization; thus, a wide array of multivalent catalytic systems is accessible from a single peptide motif.

As a first approach in the development of peptide-based multivalent catalytic system, we decided to investigate the formation of such systems from the assembly of functional units by dynamic covalent bonding. Dynamic formation of covalent bonds allows for error correction during the polymerization

processes of subunits, giving rise to the thermodynamically most stable object, and it could enable the synthesis of various homomeric sequences from a single sub-unit simply varying the reaction conditions. Disulfide-based chemistry was chosen because it was well investigated by Otto group and others, and it is well-suited for the generation of dynamic combinatorial libraries (DCLs) of macrocycles and foldamers in water.[3] Disulfide formation occurs readily by oxidation of thiols upon exposure to air. Exchange is achieved through $SN_2$ nucleophilic substitution under mild conditions.[4] The presence of the thiolate, which is a better nucleophile than the thiol, favours the process. Thus, the process usually requires base catalysis and is favoured at pH 7–9. In the presence of thiolate, thiol oxidation is sufficiently slow under standard conditions to allow equilibration to occur (Figure 1A). For poly(disulfides), highly specific interactions between building blocks (e.g. R=peptide group that is predisposed to β-sheet formation, Figure 1B) lead to selective formation of specific library members.[5] Otto group also showed that, in the chemical space explored so far for poly(disulfides), it is possible to locate a window for foldamer formation where the amphiphilic peptide side chains bear substituents that carry hydrogen-bonding functionalities near the 3,5-dimercaptobenzoic acid moiety (Figure 1B).[3]

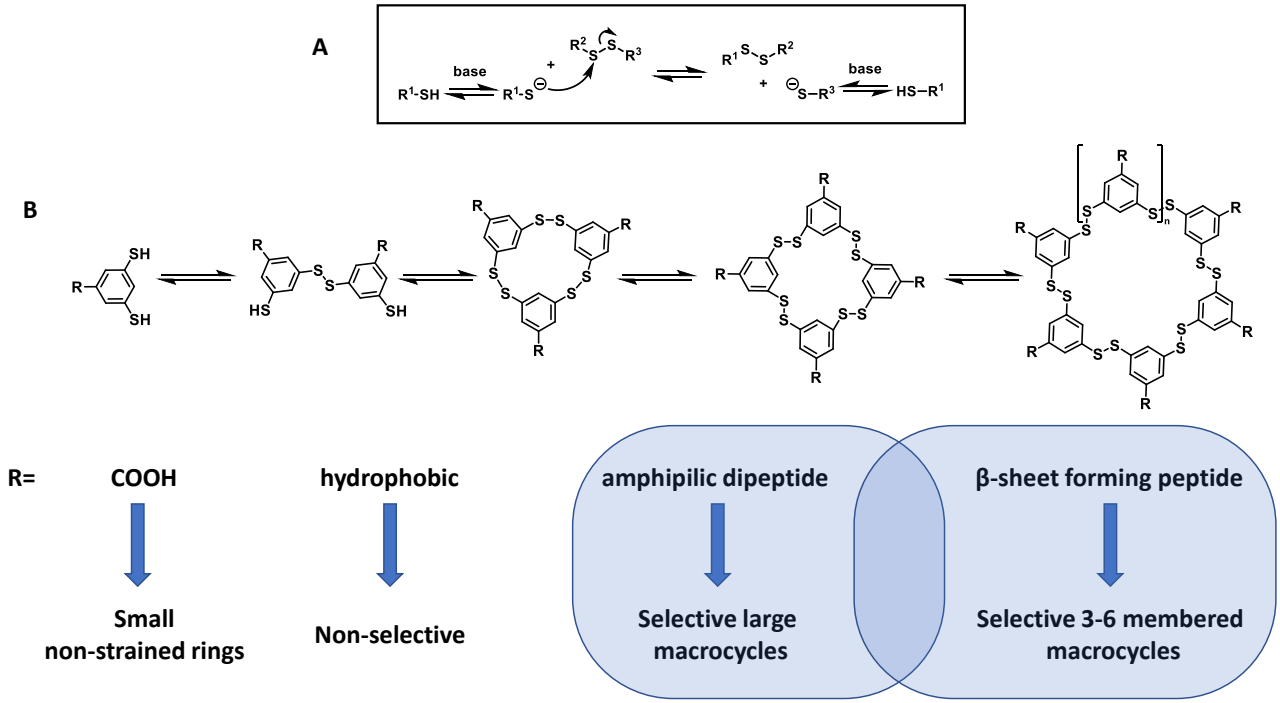


*Figure 1: (A) Schematic representation of the disulfide exchange reaction. (B) Schematic representation of DCLs of differently sized disulfide macrocycles formed from dithiol building blocks and product obtained depending on the substituent R.*

To explore the possibility of obtaining folded structures with well-defined conformations akin to those of biopolymers and displaying multiple reactive moieties, two peptidyl aryl-dithiols were synthesized (**1** and **2**, Figure 2, box). Both peptides contain a modified Phe residue linked to the backbone forming 1,3-dimercaptobenzene unit and the Asp, His and Ser triad. In peptide **2** a C-terminal Leu residue is used to increase the amphiphilicity of the system (Figure 2).

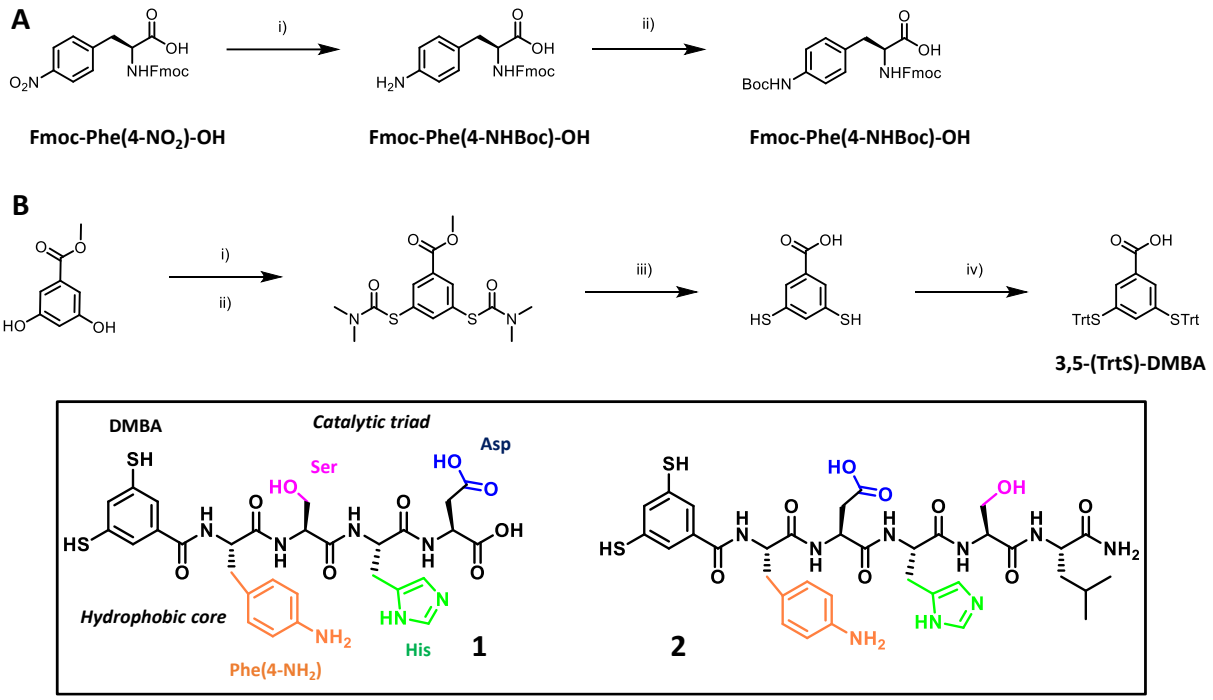


*Figure 2: (A) Synthesis of Fmoc-Phe(4-NHBoc)-OH. Reagents and conditions: i) Zn/HCl, $^{i}$PrOH/$H_2O$, Δ; ii) $Boc_2O$, $NaHCO_3$, $CH_3CN/H_2O$, r.t., o.n.; (B) Synthesis of 3,5-(TrtS)-DMBA. Reagents and conditions: i) $Me_2N$-C(S)-Cl, DABCO, r.t., DMF; ii) 240 °C, $Ph_2O$; iii) KOH, diethyleneglycol, 105 °C; iv) Trt-Cl, pyridine, $CH_3CN$, r.t.; (box) Chemical structure of peptidyl aryl-dithiols **1** and **2**.*

Peptides **1** and **2** were synthesized by solid phase peptide synthesis from Fmoc protected monomers. The modified Phe residue was obtained from Fmoc-Phe(4-$NO_2$)-OH, through reduction of the nitro group with Zn/HCl and subsequent protection of the side-chain amino group as *tert*-butoxycarbamate, i.e., Fmoc-Phe(4-NHBoc)-OH (Figure 2A). The tritylated 1,3-dimercaptobenzene (3,5-bis(tritylthio)-benzoic acid or 3,5-(TrtS)-DMBA, Figure 2B) unit was obtained from methyl 3,5-dihydroxybenzoate following protocols reported in the literature, with slight modifications in proportions of reagents and purification conditions .[6,7]

DCLs were generated by dissolving building blocks at a 3 mM concentration in buffered aqueous solution. Oxidation of the thiols into disulfides is done from the oxygen in the air and the formed

disulfides exchange with each other as long as residual thiolate is present. The product distribution of dynamic combinatorial libraries generated by **1** were analysed using high performance liquid chromatography/mass spectrometry (HPLC/MS). The libraries resulted to be dominated by small and medium sized three- and four-membered rings. Small non-strained rings are the common product of diluite DCLs due to the entropic contribution.

The libraries generated from monomer **2** were also dominated by small three- and four-membered rings, but a notable exception was represented by the library in Britton buffer 50mM at pH=8.5 (Figure 3A). After 10 days, the selective formation of a large 16-mer ring $\mathbf{(2)_{16}}$ was observed (Figure 3B).

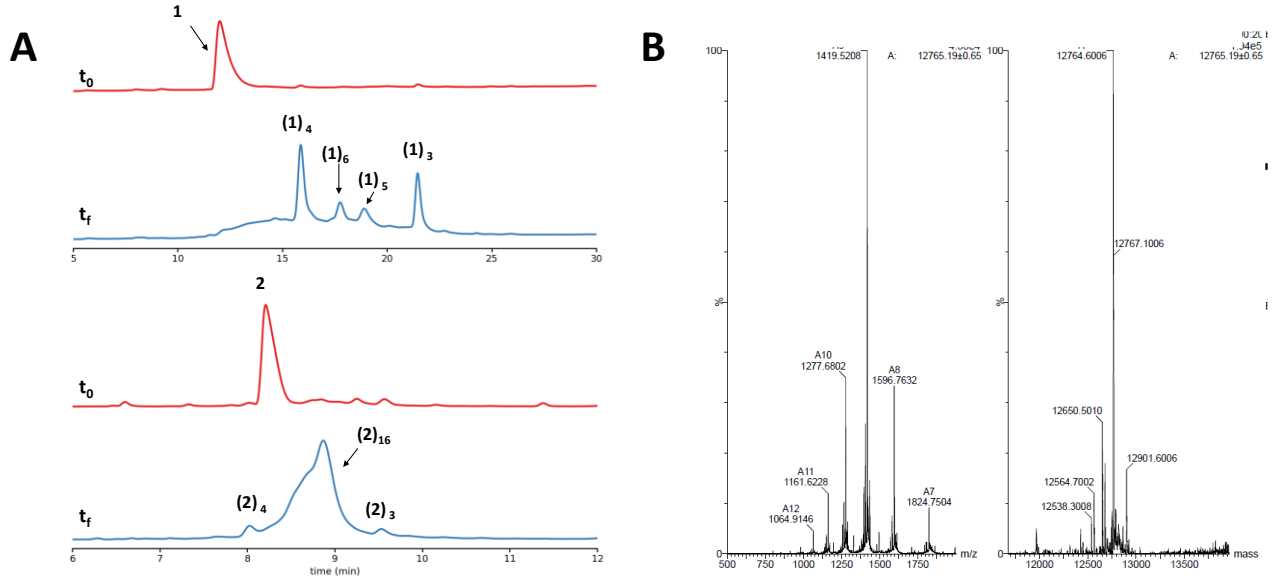


*Figure 3: (A) HPLC analyses of the DCL made from **1** (top) and **2** (bottom) (3.0 mM) in borate and britton buffer (50 mM, pH = 8.5): ($t_0$) immediately after dissolving and ($t_f$) after stirring for 10 days. **E:** Mass spectrum of $\mathbf{(2)_{16}}$.*

The selectivity of the formation of this 16-mer ring from building block **2** in this specific buffer suggests that the macrocyclic ring benefits from specific non-covalent interactions that occur more favourably in this buffer; the striking difference from libraries from **1** and **2** highlights also the subtle balance of multiple specific non-covalent interactions at play.

The shift of the product distribution of the library towards the prevalence of the single specie $\mathbf{(2)_{16}}$ also suggests the presence of a folded structure, where specific intramolecular non-covalent interactions allow an increase in stability compared to the disordered members of the library.

Further evidence of the folded nature of **(2)**$_{16}$ came by ECD analysis (Figure 4). Intense and distinct ECD bands were observed for **(2)**$_{16}$ in $H_2O/D_2O$, suggesting a defined folding of the molecule. The spectrum is characterized by an intense positive maximum at 273 nm (having a shoulder at 300 nm) followed by another less intense, oppositely signed, and structured band between 310 nm and 360 nm with two negative maxima at 327 nm and 346 nm. The shorter wavelength section of the spectrum is characterized by a negative maximum at 227 nm followed by two weaker bands of opposite sign at 243 nm (positive) and at 255 nm (negative).

A temperature dependent ECD experiment was used to evaluate the effect of temperature on the conformational freedom and the ECD spectra of compound **(2)**$_{16}$. The variable temperature ECD (VT-ECD) spectra were recorded in $H_2O/D_2O$ in the range from 20 to 80 °C in steps of 10 °C. The general ECD profile is retained during the heating process and the sign of the bands is maintained (Figure 4A).

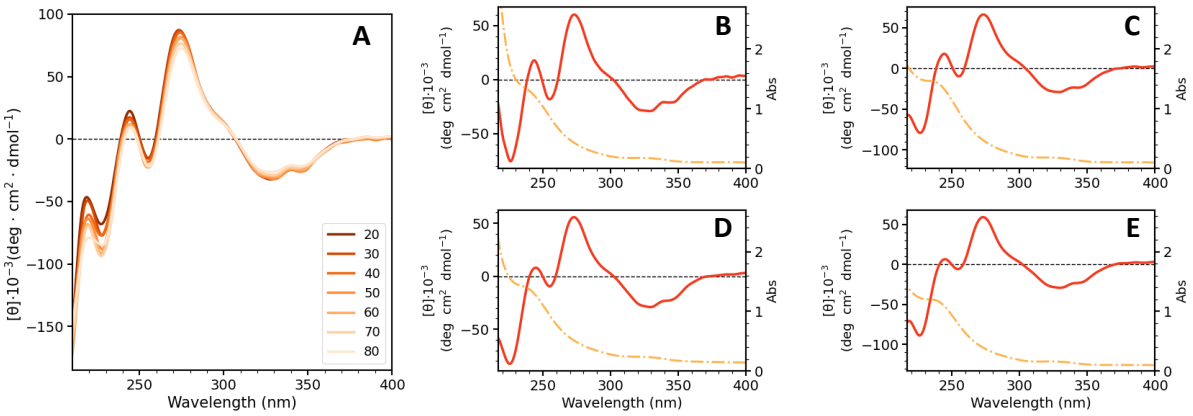


*Figure 4: (A) Change in the ECD spectra of foldamer (**2**)$_{16}$ upon heating, recorded in $H_2O/D_2O$ (concentration: 2 x $10^{-4}$ M). (B-E) ECD and UV spectra of foldamer (**2**)$_{16}$ at pH 6.1 (B, 10mM MES buffer), 7.2 (C, 10mM PBS buffer), 8.3 (D, 10mM Tris buffer) and 9.2 (E, 10mM borate buffer) (concentration: 2 x $10^{-5}$M).*

Upon heating at 80 °C, compound **(2)**$_{16}$ underwent a 20 % decrease in the intensity of the 273 nm band (as referred to the measurement at 20 °C), suggesting a certain thermal stability. The overall profile is maintained also at various pH, and it is interesting to note that the spectra recorded at 298 K in different buffers have the same intensity, suggesting that the conformational freedom of this foldamer is not affected by the environment (Figure 4B-E).

The possibility of obtaining hierarchic tertiary folded structures with defined helical domains through dynamic combinatorial chemistry it is still limited. In biopolymers, formation of disulfide bridges between cysteine residues is an important component of the stabilization against proteolytic enzymes and in the sorting of folded conformations through stabilization and coupling of secondary motifs.[8–10]

Recently, disulfide bridge formation was investigated in helical aromatic oligoamide foldamers.[11] Depending on the position of thiol-bearing side chains on the foldamer, intermolecular bridging serendipitously produced a two-helix bundle-like macrocyclic structure. Small, well-characterized, helical peptides could be used as building blocks to generate functional complex scaffolds. Although still limited, the understanding in the design of DCL based on helical modules is attractive to the de novo design of functional peptide covalent assemblies that mediate chemical reactions.

To this aim, we performed an exploratory study on the oligomerization of peptidyl aryl-dithiols containing an octapeptide -(L-Ala-Aib)$_4$ octapeptide sequence (Figure 5A).

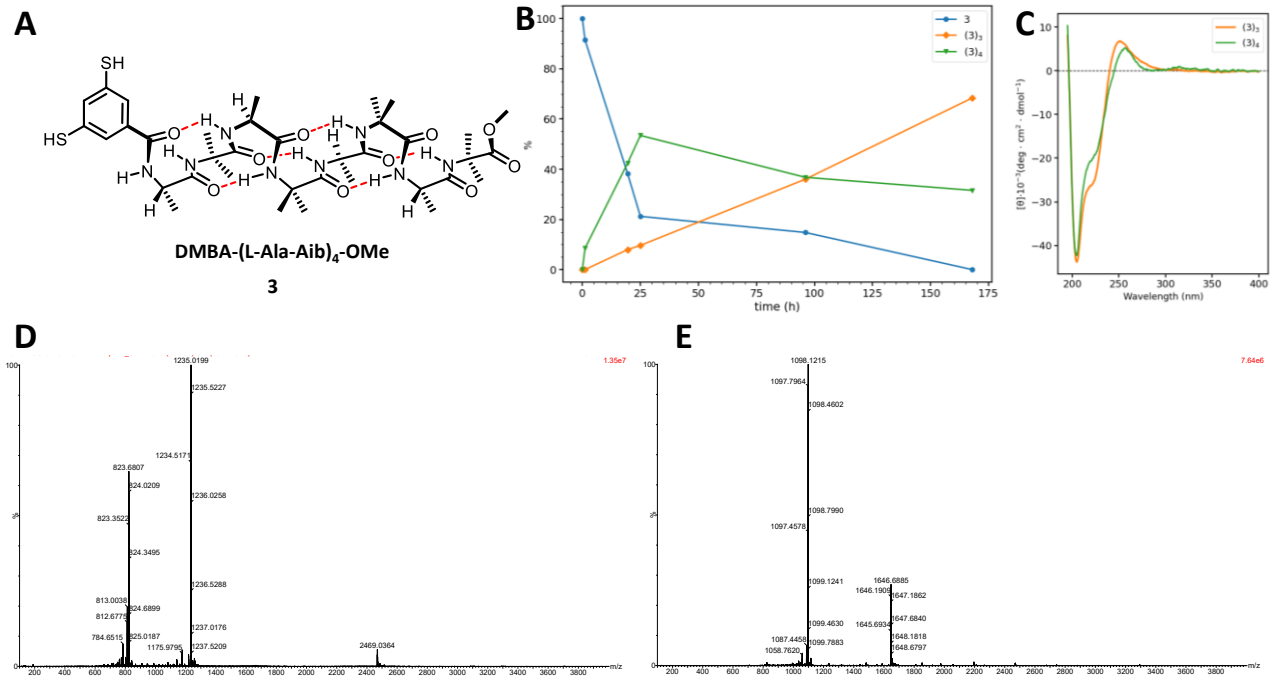


*Figure 5: (A) Chemical structure of the synthesized peptidyl aryl-dithiol with helical domain **3**. (B) Change of the product distribution with time for DCL made from building block **3** (3 mM in MeOH basified with $K_2CO_3$, pH ~8, stirred at 1200 rpm). (C) ECD spectra of **(3)$_3$** and **(3)$_4$** in $CH_3CN/H_2O$ (monomer concentration c 1x10$^{-3}$ M). (D) Mass spectrum of **(3)$_3$**. **(3)$_3$**: m/z calculated: 2469.0286 $[M+H]^+$,1235.0179 $[M+2H]^{2+}$, 823.6877 $[M+3H]^{3+}$; m/z observed: 2469.0364 $[M+H]^+$,1235.0199 $[M+2H]^{2+}$ , 823.6807 $[M+3H]^{3+}$. (E) Mass spectrum of **(3)$_4$**. **(3)$_4$**: m/z calculated: 1646.6881 $[M+2H]^{2+}$, 1098.1211 $[M+3H]^{3+}$; m/z observed: 1646.6885 $[M+2H]^{2+}$ , 1098.1215 $[M+3H]^{3+}$*

The -(L-Ala-Aib)$_4$- sequence is expected to give rise to a $3_{10}/\alpha$- helical structure of right-handed screw sense dictated by the L-configuration of the Ala residues.

As noted above, in the absence of any intra- or inter-molecular noncovalent interactions, DCLs of building blocks based on the 3,5-dimercaptobenzoic acid core are populated prevalently by small trimeric and tetrameric macrocycles. Indeed, the DCLs from 3 μM solution of building block showed three- and four-membered rings as the common products.

It is interesting to note that while the library produced almost selectively trimers and tetramers, their time evolution differs strongly. In the first hour of evolution, the tetramer emerged as the prevailing species. After a day, as the relative peak area of monomer lowers below 20%, the relative amounts of $\mathbf{(3)_4}$ starts to diminish in favour of trimer $\mathbf{(3)_3}$. Thus, $\mathbf{(3)_3}$ resulted as the prevailing product of the library after 6 days of agitation (Figure 5B). In the presence of excess template (e.g., the initial phase of the library) smaller oligomers are usually favoured over larger ones, because from a fixed amount of monomer it is possible to generate more of the former. The increase of the shorter oligomer $\mathbf{(3)_3}$ at the expense of $\mathbf{(3)_4}$ suggest the nature of $\mathbf{(3)_3}$ as the thermodynamically favoured product.[12]

Immobilized cooperative catalysts are highly desirable from economic and environmental points of view. A complex supramolecular system can be assembled from simple building blocks bearing catalytic functional groups that are brought in close proximity by non-covalent interactions. The presence of a multitude of reactive functional groups from the repetition of the build blocks could enable cooperativity in the catalytic process.

As highlighted in the Introduction (Section 1.3), metal nanoparticles covered by a monolayer of peptides were found to be an interesting example of self-assembled hydrolytic catalysts. A thiol group is typically employed to anchor the peptide ligands to the metal core in order to provide a strong bond with the metal. The packing of the ligands is strictly correlated with the size of the nanoparticles, with a tighter packing in small clusters. Gold nanoparticles are the most studied systems owing to their stability and ease of preparation and use, but silver nanoparticles could represent an interesting alternative due to the abundance and low cost of silver paired with desirable

physical properties. However, the development of silver-based systems is limited by their stability and susceptibility to oxidation. In recent years, Bigioni et al. reported a simple synthetic protocol for producing ultra-stable silver nanoparticles as silver thiolate clusters with *p*-mercaptobenzoic acid (*p*-MBA) as a ligand (Figure 6A).[13,14]

The reduction of a soluble precursor, in a semi-aqueous solution, in the presence of an alkali metal cations produces a single sized $M_4Ag_{44}$(*p*-MBA)$_{30}$ cluster. The final product is obtained through washing of the salts with DMF and protonation using an organic acid such as acetic or citric acid. Once protonated, the molecules are soluble in polar protic and aprotic solvents and their decay rate in solution is reported to be ~7 times slower than those of $Au_{25}(SG)_{18}$ (SG =glutathione) cluster solutions.

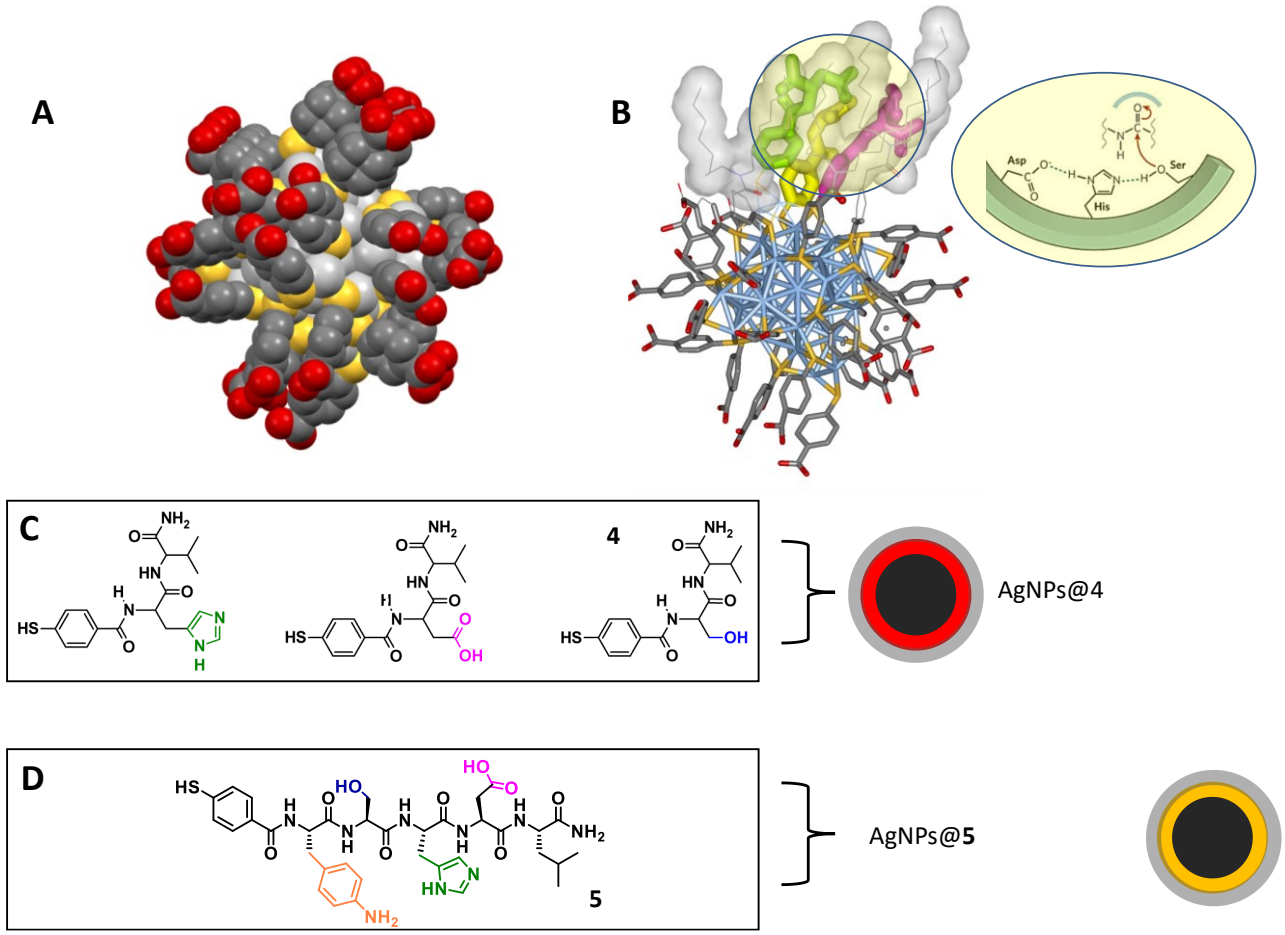


*Figure 6: (A) Space-filling view of $M_4Ag_{44}$(p-MBA)$_{30}$ cluster (Colour scheme: grey, carbon; red, oxygen; grey, exterior silver atoms in the mounts; gold, sulphur). (B) Illustrative representation of the $M_4Ag_{44}$(p-MBA)$_{30}$ cluster with modified ligands for hydrolytic catalysis. (C) Chemical structure of the synthesized ligand mixture **4** and corresponding nanoparticles AgNPs@**4**. (D) Chemical structure of the synthesized ligand mixture **5** and corresponding nanoparticles AgNPs@**5**.*

The capping ligands are arranged in a complex three-dimensional structure around an $Ag_{32}$ excavated-dodecahedral core with icosahedral symmetry; $\pi$-$\pi$ stacking (face-to-face and edge-to-face) of the aromatic ring of *p*-MBA ligands results in precise grouping of two and three ligands (Figure 6A). The substitution of the *p*-MBA ligand with peptidyl aryl-thiol ligands could afford a functionalized nanoparticle, with a proper spatial organization of reactive side-chains thanks to its defined geometry. In particular, we planned to mimic protease activity by the use of Ser/His/Asp containing ligands (Figure 6B). As a starting point, a set of molecules was synthesized, where the *p*-MBA ligand was functionalized at the carboxylic group with Ser, His and Asp and the short peptide capped as a L-valinamide to improve local hydrophobicity and aid interaction with the substrates (Figure 6C). Next, we synthesized a ligand related to compound **2**, but the bifunctional 3,5-dimercaptobenzoic acid unit was replaced with a *p*-MBA unit (Figure 6D). Compounds **4** and **5** were synthesized on a Rink-amide resin by solid phase peptide synthesis from Fmoc protected monomers.

The synthesis of silver nanoparticles as silver thiolate clusters was performed following the protocol reported in the literature with *p*-mercaptobenzoic acid (*p*-MBA),[14] but with **4** and **5** as ligands. The silver–thiolate precursor was formed from the combination of silver ions derived from $AgNO_3$ and *p*-MBA (or **4** and **5**), with an excess of ligand (2mmol/mmol$AgNO_3$) in a water-ethanol mixture. A cloudy light yellow precipitate is formed and it is solubilized by increasing the pH at around 12 with CsOH to obtain an homogenous starting mixture. The modulation of the pH can also be done with other metal hydroxides, such as the cheaper and more available NaOH, but we observed an increased stability of the final product using CsOH. Reduction with $NaBH_4$ (10 eq.) generates upon mixing for ~1 h a deep red solution of deprotonated $M_4Ag_{44}$(*p*-MBA)$_{30}$ nanoparticles. The final product is obtained through washing of the salts with DMF and protonation using an organic acid such as acetic or citric acid. Several cycles of protonation and precipitation with toluene are needed to obtain the fully protonated product which is then soluble in DMF e polar solvents. Coordinating solvent is essential to improve the life of the products, stabilizing the nanoparticles, therefore the samples were never completely dried during the process. The UV-Vis absorption spectrum of $M_4Ag_{44}$(*p*-MBA)$_{30}$ nanoparticles is highly structured and can be used to evaluate the progress and success and progress of the reaction (Figure 7).

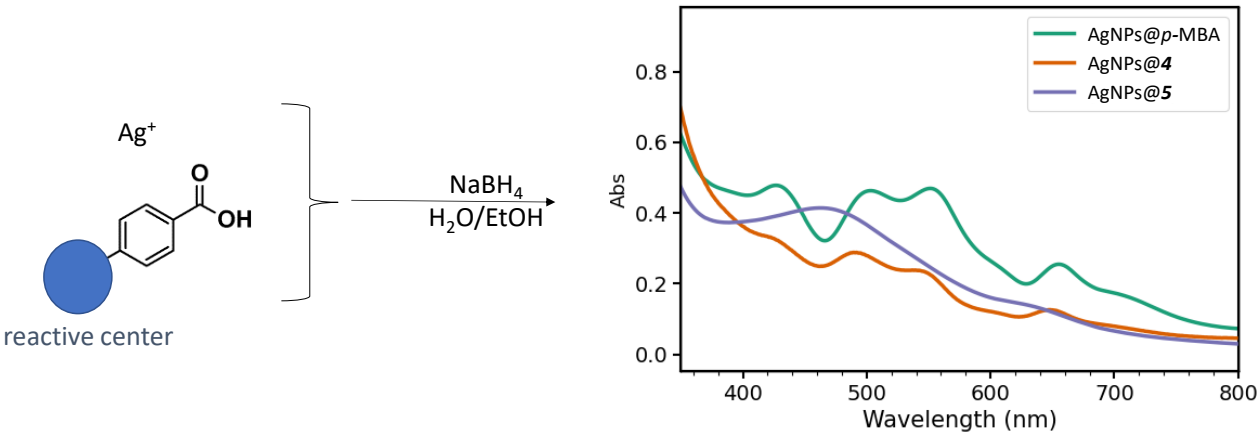


*Figure 7: Schematic representation of the synthetic procedure and absorption spectra of AgNPs@p-MBA, AgNPs@**4** and AgNPs@**5**.*

AgNPs@*p*-MBA and AgNPs@**4** nanoparticles showed near identical spectra (Figure 7). The spectrum of AgNPs@**4** was only slightly blue-shifted and showed all the sharp transitions observed with the $M_4Ag_{44}$(*p*-MBA)$_{30}$ molecular cluster, but with different relative peak intensities. In contrast, the spectrum of AgNPs@**5** shows a broad surface plasmon resonance peak located at 470 nm and another band as a shoulder at 635 nm blue-shifted compared to the secondary peak of AgNPs@**4** at 650 nm; the significant red-shift from 420 nm typical of large silver nanoparticles (>2 nm) suggests a small core diameter (~2 nm).[15,16] As in gold clusters, the optical features of silver clusters are strongly influenced by ligand-silver interactions, especially by the charge density of the sulfur atoms.[17,18] Therefore, modification of the *p*-MBA ligand with a peptidyl moiety could produce large deviations from the multiple sharp transitions observed for $M_4Ag_{44}$(*p*-MBA)$_{30}$. Small peptidyl moieties (**4**) seem to produce slight deviations in the optical properties of this clusters, while longer peptides such as **5** strongly influence the spectrum.

The same nanoparticles were further characterized by TEM analysis of samples dissolved in water. A size distribution analysis of AgNPs@**5** nanoparticle revealed that they had a mean diameter of 2.2 nm (SD 0.8) (Figure 8A). The spectrum of AgNPs@**5** shows a plasmon resonance peak located at 470 nm: this type of spectrum is similar to what has been reported aryl-thiol capped silver NPs of 2.1±0.7 nm mean diameter.[19]

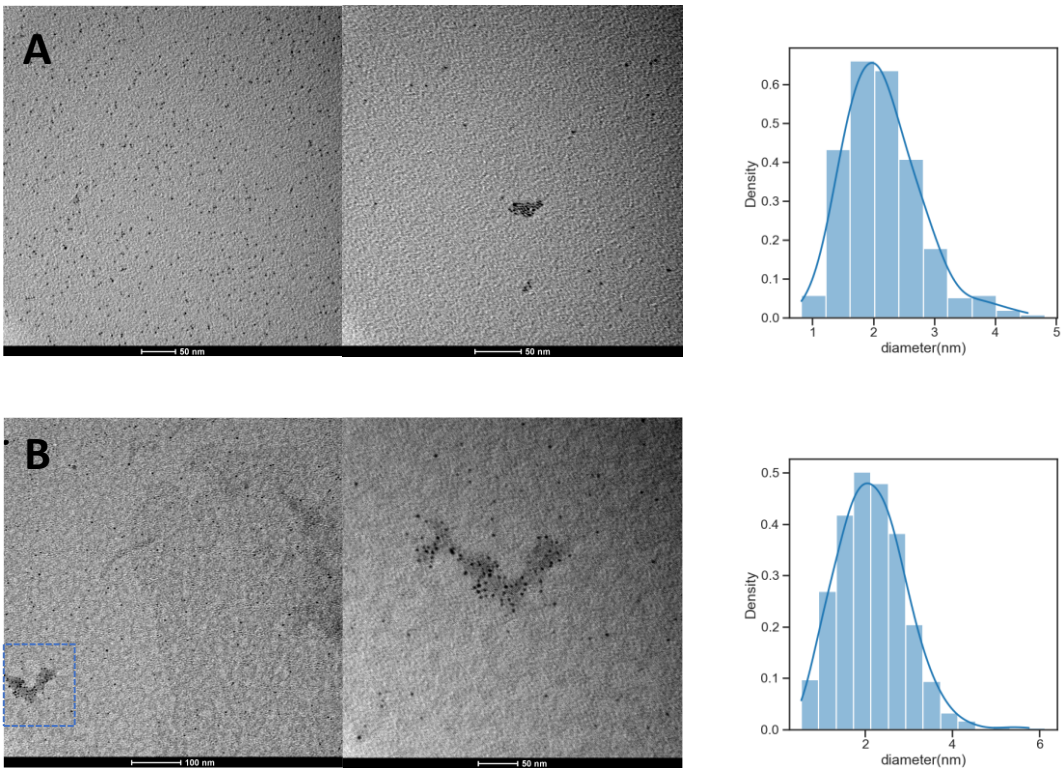


*Figure 8: (A) TEM images (left) of AgNPs@**5** and their size distribution (right). (B) TEM images (left) of AgNPs@**4** and their size distribution (right).*

TEM images of a sample from AgNPs@**4** solution revealed that the NPs had a mean diameter of 2.2 nm (SD 0.6) (Figure 8B). However, TEM observation might be overestimating the size and polydispersity of the nanoparticles given they possess an UV-Vis spectrum with multiple sharp transitions and the absence of a plasmon resonance. The low contrast of AgNP could result in a possible undercounting of particle with smaller dimensions.[20] Moreover, aggregation of smaller clusters due to concentration upon drying and then annealing under the microscope could also lead to overestimate particle dimensions.[19]

Development of small self-assembling peptides is an attractive method in the design of supramolecular catalysis. A short peptide able to self-assemble into multivalent supramolecular structure, driven by non-covalent interactions, is a simple way to achieve an increase in structural and functional complexity from a minimalist molecule.

The 1D and 2D assembly of small amphiphilic peptides of lead to the formation of supramolecular fibrillar networks that trap the solvent forming supramolecular gels. Gels can be considered

heterogeneous catalysts that possess some interesting features such as a large active surface exposed to the solvent and in most cases reversible formation (controlled through variation of temperature and concentration) which could result in a tunable activity.

Moreover, the disposition of the gelator molecules in self-assembled fibres is often ordered and can lead to cooperativity among different catalytic moieties surrounded by an organized hydrophobic microenviroment, resulting in enhanced catalytic efficiency compared to the single molecule (See Section 1.3).

In this work, we synthesized a short tetrapeptide, containing a Asp-His-Ser-Leu in analogy to **2** and **5**, and a N-terminal lipophilic tail (**6**, Figure 9). Next, we synthesized a ligand related to compound **6**, but the palmitoyl tail acid was replaced with acetyl unit to hinder its self-assembling ability (**7**, Figure 9). Compounds **6** and **7** were synthesized on a Rink-amide resin by solid phase peptide synthesis from Fmoc protected monomers and were characterized by 1D and 2D NMR and HPLC-MS spectrometry.

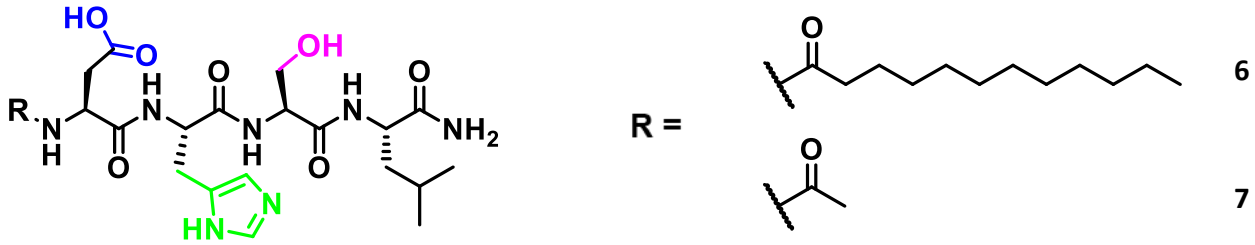


*Figure 9: Chemical structure of compounds **6** and **7***

The hydrophobicity of compound **6** was notable by the almost insolubility in buffer at physiological pH. The peptide was dissolved by heating and progressive cooling triggered fibrillization. Thus, depending on the concentration, self-sustaining gels were successfully obtained through a heat-cooling cycle. The minimum gelling concentration was found to be 2.6 mM, leading to a hydrogel with only 0.2 %w/w gelator.

The nanomorphology of the hydrogel was then analyzed by Transmission electron microscopy (TEM) analysis (Figure 10). The samples of peptide at concentrations around the minimum gelling concentration displayed dense networks of fibrils entangled in bundles of heterogeneous dimensions, with diameters spanning from 20 to hundreds of nm. The staining with uranyl acetate of the samples

of **6** revealed instead the presence of nanofibrils spanning several microns with a diameter of 20-30 nm.

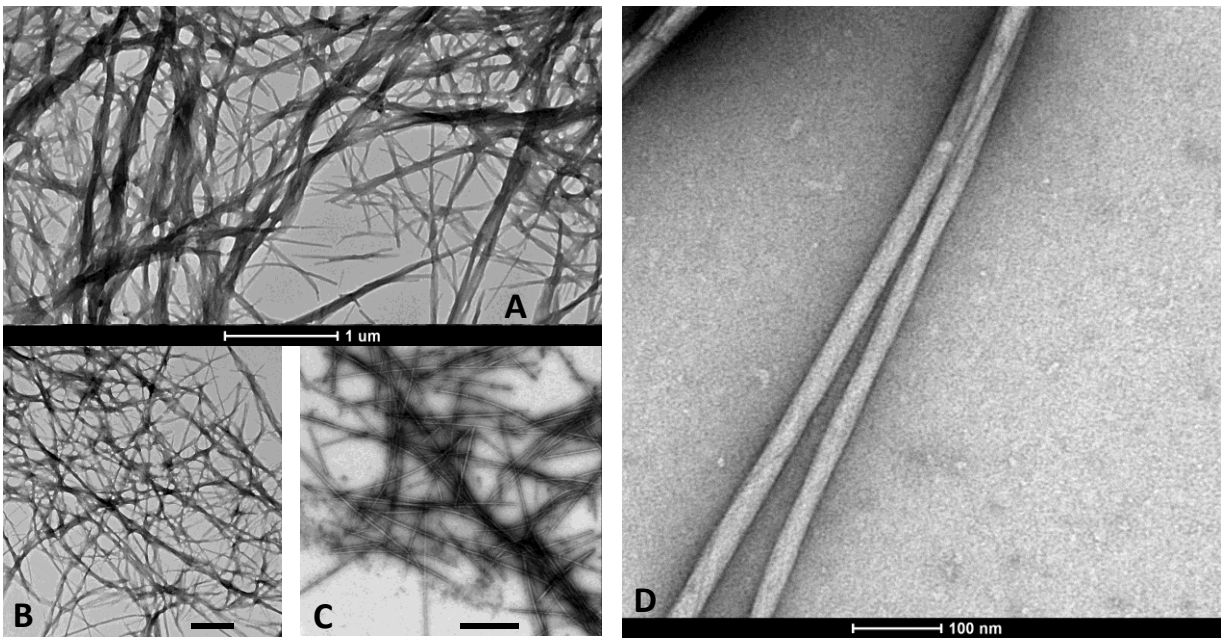


*Figure 10: (A and B) TEM (unstained) images of the fibrillar network obtained from peptide **6**. (C and D) TEM (stained with uranyl acetate) images of the thinner fibrils obtained from peptide **6**.*

The evaluation of the synthesized compounds as catalyst with esterase-like activity was performed observing the ability of the systems to promote the ester hydrolysis of para-nitrophenyl acetate *p*-NPA. The stability and optical properties of the silver nanoclusters dictated the set of conditions employed. The experiments were run in a quartz cuvette and followed by monitoring the increase in absorbance at 400 nm produced by the increase in concentration of *p*-nitrophenolate, by UV-Vis spectroscopy.

Given the strong absorbance of NP samples in the UV-Vis range, the concentration of the samples must remain under a certain value, in order to obtain a linear response from the instrument and an adequate precision in monitoring the formation *p*-nitrophenolate. Moreover, preliminary experiments also showed that while Ag NPs are stable around physiological pH, precipitation from solution is observed for values of pH higher than 8.5 and lower than 6.5. Therefore, the experiments were run in PBS buffer at pH 7.2 and using a concentration of nanoparticles corresponding to a concentration of Ser/His/Asp triads of 25 μM, as derived from TGA measurements of the ligand-to-metal ratio of the

nanoparticles. This value was the maximum concentration of reactive moieties achievable while maintaining a linear response from the instrument during the experiment.

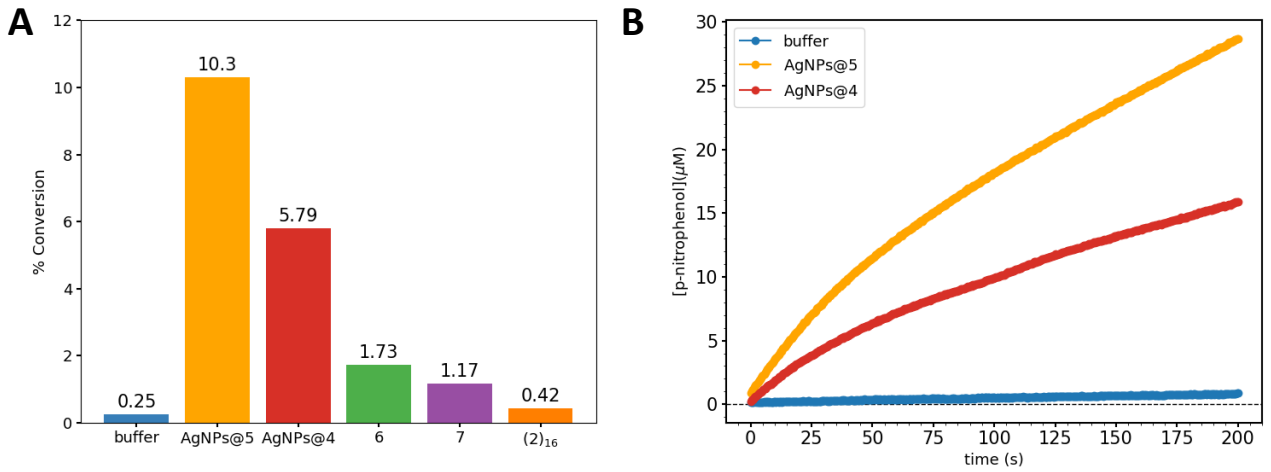


*Figure 11: (A-B) Evaluation of the synthesized compounds (8% mol) for the hydrolysis of p-NPA at pH 7.2 (40 mM PBS buffer). (A) Extent of pNPA hydrolysis, as judged by optical absorbance, upon incubation for 3 min. (B) Extent of pNPA hydrolysis over 200s with AgNPs@**4** and AgNPs@**5**.*

In these conditions, the data indicated a difference in extent of hydrolysis of *p*-NPA in the presence versus the absence of the various systems (Figure 11A). In peptide **7** and foldamer $\mathbf{(2)_{16}}$, the presence of Ser/His/Asp triad has little to no effect on the rate of hydrolysis of the substrate compared to that of the buffer alone. The formation of a supramolecular fiber network from **6** may be the reason for the small increase in the rate of hydrolysis relative to **7**. The only catalytic systems to show little, but not negligible, catalytic activity are AgNPs@**4** and AgNPs@**5.** Thus, the catalytic effect of AgNPs seems be related to the environment and disposition of the Ser–His–Asp in the nanosystem which allows catalytic cooperativity between side chains.

# Experimental Section

## Instruments and Methods

*Nuclear Magnetic Resonance.* 1H and 13C NMR spectra were recorded at room temperature on a Bruker AC-200 (200 MHz) and a Bruker Avance III 400 spectrometer (400.13 MHz 1H frequency and 100.62 MHz 13C frequency) instrument using TMS (tetramethylsilane) as the internal reference. The multiplicity of a signal is indicated as s, singlet; d, doublet; t, triplet; m, multiplet; and br, broad. Chemical shifts (δ) are expressed in ppm.

*FT-IR absorption.* FT-IR absorption spectra were recorded with a Perkin-Elmer 1720X spectrophotometer.

*Mass Spectrometry.* ESI-MS experiments and UPLC-MS experiments were performed using an ACQUITY UPLC H-Class System with Xevo G2-XS QTof (Waters, USA). HPLC-MS experiments were performed using an Agilent 1200 HPLC system with an Agilent 6120 Single Quadrupole.

*Transmission Electron Microscopy.* Samples were analyzed on a Jeol 300 PX TEM instrument. A glow discharged carbon coated grid was floated on a small drop of the nanosphere suspension and excess was removed by #50 hardened hatman filter paper. Image analysis was performed using Fiji.

### Synthesis of 3,5-bis(tritylthio)-benzoic acid

3,5-bis(tritylthio)-benzoic acid was synthesized according to a reported procedure. Methyl 3,5-dihydroxybenzoate (5.0 g, 29.7 mmol) was dissolved in anhydrous DMF (20 mL) under a nitrogen atmosphere and cooled to 0 °C. DABCO (13.3 g, 119 mmol) was added in portions. N,N-dimethylthiocarbamoyl chloride (14.7 g, 119 mmol) in DMF (20 mL) was added dropwise at 0 °C to the resulting suspension. The suspension was allowed to warm to room temperature and stirred for 24 h. The reaction mixture was poured into water (200 mL), filtered and the residue was washed with ethanol to give 8.8 g (28.3 mmol, 95%) a white crystalline powder. O-Thiocarbamate (8.0 g, 23.3 mmol) was suspended in diphenyl ether (100 mL) and heated under a nitrogen atmosphere to 230–240 °C. The reaction was monitored by TLC and after 3 days the reaction mixture was allowed to cool to 30–40 °C and it was poured into hexane and slowly allowed to cool to 4 °C overnight. The precipitate was filtrated and washed with hexane obtaining a light beige solid. Under a nitrogen atmosphere the product was suspended in a 1.75m solution (70 mL) of KOH in diethyleneglycol that had been purged through vacuum/$N_2$ cycles and the mixture was heated at 105 °C for 30 min. After the solution had cooled down to room temperature 500 mL of water (purged) was added followed by rapid addition of 10% HCl (55 mL). The precipitate was filtered, washed extensively with water and dried by azeotropic distillation with toluene under reduced pressure.

To a solution of 3,5-dimercaptobenzoic acid (1.6 g, 8.6 mmol) in degassed acetonitrile (180 mL) was added a solution of trityl chloride (7.2 g, 25.8 mmol) in degassed dichloromethane (60 mL), under a nitrogen atmosphere. Pyridine (1.38 mL, 17.2 mmol) was added, and the solution stirred for 20 hours at room temperature. The white precipitate was collected, washed with water and dried (4.7 g, 7 mmol, 80%). The $^1$H-NMR data were consistent with that reported in the literature, and the product was used without further purification.

$^1$H-NMR (400 MHz, $CDCl_3$) δ 7.35 – 7.29 (m, 12H), 7.27 (d, $J$ = 1.7 Hz, 2H), 7.23 – 7.14 (m, 18H), 7.02 (t, $J$ = 1.6 Hz, 1H).

### Synthesis of building block Fmoc-Phe(4-NHBoc)-OH

L-Phe(4-$NO_2$)-OH (6 g, 28 mmol) was suspended in 50 mL of acetone and the mixture was basified with $NaHCO_3$. A solution of Fmoc-OSu (9g, 27mmol) in 40 mL of acetone was added to the reaction

and the mixture was stirred overnight. The reaction was acidified with $KHSO_4$ to pH 4-5 and the precipitated was filtered off, washed with ethyl acetate, and dried. The reaction product (Fmoc-L-Phe(*p*$NO_2$)-OH) was reprecipitated from hot EtOAc and used without further purification. Fmoc-L-Phe(*p*$NO_2$)-OH (3.9 g, 24 mmol) was suspended in a 4:3 $^{i}$PrOH/$H_2O$ (100 mL) solvent mixture. Then, Zn dust and $HCl_{conc}$ (4eq) were added in small portions. The resulting suspension was stirred at reflux for 2 h, then the $^{i}$PrOH was removed at reduced pressure. The mixture was then refluxed in 20% hydrochloric acid for 6 h. After cooling the resulting suspension was neutralized with aqueous sodium acetate and filtered. The precipitate was washed with a cold mixture of 5:1 EtOH/$H_2O$ (40 mL) to remove the excess of Zn. The filtrate was suspended in toluene and water was removed by azeotropic distillation at reduced pressure. The solid (2.6 g, ~6.4 mmol) was dissolved in 80 mL of solvent mixture of $CH_3CN$/$H_2O$ (1:1 v/v) with $NaHCO_3$ (1.34 g, 16 mmol). $Boc_2O$ (1.26 g, 5.7 mmol) was dissolved in 25 mL of $CH_3CN$ and added to the solution of amino acid. The mixture was stirred at r.t. for 18 h. The organic solvent was removed under reduced pressure and the aqueous residue was acidified with HCl 1M. The precipitate was extracted with EtOAc (3v), then the organic phase was washed with water (2v) and brine. The organic layer was dried over $Na_2SO_4$, filtered and evaporated to dryness under reduced pressure. The product was recovered as a brown solid (4.4 g, 32% overall yield) and used without further purification.

### Synthesis of peptide **1**

2-Chlorotrityl chloride resin (1.6 mmol/g) was added to a vessel. The resin was swelled in DMF and then the first Fmoc-amino acid (2 eq. relative to the resin) was dissolved in DMF and DIPEA (4 eq. relative to the carboxylic acid) was added. This mixture was added to the resin and stirred for 2 h. At the end of this time, the mixture was filtered and the resin was washed with DMF, DCM and DMF. For successive couplings, a solution of the amino acid Fmoc-AA-OH (3 eq.), HATU (3 eq.), HOAt (2.7 eq) and DIPEA (6 eq.) in DMF was added to the resin and stirred for 1h and 30 minutes. Amino acids were introduced protected as Fmoc-Ser(tBu)-OH, Fmoc-Asp(tBu)-OH, Fmoc-His(Trt)-OH or Fmoc-Phe(4-NH-Boc)-OH.

The resin was filtered, and washed with DMF, DCM and DMF. Iterative cycles of Fmoc deprotection and coupling were carried out with 20% piperidine solution in DMF. For the last coupling, 3,5-bis(tritylthio)-benzoic acid was used. Cleavage of the peptide sequence from the resin was performed

with a mixture of 94% trifluoroacetic acid, 2.5% 2,2′-(Ethylenedioxy)diethanethiol (DODT), 1.25% water and 1.25% triisopropylsilane for 3 h; the filtrated was collected and evaporated under reduced pressure. The residue was triturated in cold $Et_2O$, centrifuged and lyophilized. Crude peptide was purified using flash column chromatography and lyophilized.

MS (ESI-Quad): $[M]^+$ calc. $C_{29}H_{33}N_7O_9S_2$= 688.185 m/z; found = 688.22 m/z.

### General Procedure for the synthesis of peptides by SPPS on Fmoc-Rink amide Resin

The peptides were prepared using standard solid-phase peptide synthesis (SPPS) and Fmoc chemistry on a Fmoc-Rink amide resin. The dry resin was swelled with DMF for 30-45 minutes before use and the Fmoc-protecting group on the resin was removed with a solution of 20% piperidine in DMF.

After linking the first amino acid (Fmoc-Gly-OH) to the resin, the latter was capped with a solution of DMF/$Ac_2O$/DIPEA (20:2:1). In each step, the Fmoc-protecting group was removed with a solution of 20% piperidine in DMF. For successive couplings, a solution of the amino acid Fmoc-AA-OH (3 eq.), *N*-diisopropylcarbodiimide (DIC, 3 eq.), ethyl cyano(hydroxyimino)acetate (Oxyma, 3 eq.) in DMF was added to the resin and stirred for 1h and 30 minutes. Amino acids were introduced protected as Fmoc-Ser(tBu)-OH, Fmoc-Asp(tBu)-OH, Fmoc-His(Trt)-OH or Fmoc-Phe(4-NH-Boc)-OH. The resin was filtered, and washed with DMF, DCM and DMF. Iterative cycles of Fmoc deprotection and coupling were carried out with 20% piperidine solution in DMF. Unreacted sites were capped by treatment with an 18:4:1 DMF/$Ac_2O$/DIPEA mixture for 20 minutes.

After the last coupling, cleavage of the peptide sequence from the resin was performed with a mixture of trifluoroacetic acid and suitable scavengers for 3 h; the filtrated was collected and evaporated under reduced pressure. The residue was triturated in cold $Et_2O$, centrifuged and lyophilized. Crude peptides were purified using flash column chromatography, if needed, and lyophilized.

### Synthesis of **2**

Compound **2** was synthetized according to the general procedure for the synthesis of peptides by SPPS on Fmoc-Rink amide resin. For the last coupling, 3,5-bis(tritylthio)-benzoic acid was used. Cleavage of the peptide sequence from the resin was performed with a mixture of 94% trifluoroacetic acid, 2.5% 2,2′-(Ethylenedioxy)diethanethiol (DODT), 1.25% water and 1.25% triisopropylsilane for

3 h; the filtrated was collected and evaporated under reduced pressure. The residue was triturated in cold $Et_2O$, centrifuged and lyophilized. The crude peptide was purified using flash column chromatography and lyophilized.

$^1$H NMR (400 MHz, $D_2O$) δ 8.59 (d, $J$ = 6.5 Hz, 1H, $NH^{His}$), 8.52 (d, $J$ = 7.2 Hz, 1H, $NH^{Asp}$), 8.49 – 8.39 – 8.34 (m, 1H, $Ar(C2)^{His}$), 8.25 (d, $J$ = 7.5 Hz, 1H, $NH^{Phe}$), 8.21 – 8.14 (m, 2H, $NH^{Leu}$, $NH^{Ser}$), 7.43 – 7.35 (m, 1H, $CONH_2^{Leu}$), 7.32 – 7.25 (m, 2H, Ar), 7.24 – 7.18 (m, 3H, Ar), 7.14 – 7.12 (m, 2H, Ar), 7.05 (s, 1H, $Ar(C4)^{His}$), 6.98 – 6.91 (m, 1H, $CONH_2^{Leu}$), 4.35 – 4.28 (m, $\alpha H^{Ser}$), 4.22 – 4.15 (m, $\alpha H^{Leu}$), 3.78 – 3.66 (m, 2H, $\beta CH_2^{Ser}$), 3.24 – 2.89 (m, 4H, $\beta CH_2^{His}$ and $\beta CH_2^{Phe}$), 3.02 (ddd, $J$ = 15.2, 8.8, 5.0 Hz, 3H, $\beta CH_2^{Asp}$), 2.81 – 2.53 (m, 3H, $\beta CH_2^{Asp}$), 1.87 (s, 1H), 1.60 – 1.42 (m, 3H, $\beta CH_2^{Leu}$ and $\gamma CH^{Leu}$), 0.78 (d, $J$ = 5.9 Hz, 3H, $\delta CH_3^{Leu}$), 0.73 (d, $J$ = 5.9 Hz, 3H, $\delta CH_3^{Leu}$).

MS (ESI-Quad): $[M+H]^+$ calc. $C_{35}H_{45}N_9O_9S_2$= 800.29 m/z; found = 800.30 m/z.

Synthesis of **3**

3,5-bis(tritylthio)-benzoic acid (98 mg, 0.14 mmol) was dissolved in a mixture of $CH_3CN$:DMF=10:1 (5.5 mL) and HOAt (20 mg, 0.14 mmol) and EDC·HCl (28 mg, 0.14 mmol) were added. After 10 min $H_2N$-$(AU)_4$-$NH(CH_2)_{15}$-$CH_3$ (79mg, 0.12mmol) was added to the reaction mixture, and DIPEA was used to reach basic pH. The reaction was stirred overnight at 40°C. The solvent was removed under reduced pressure and the residue dissolved in DCM. The organic phase was washed with $KHSO_4$ (5%), $NaHCO_3$ (5%) and brine, dried over $MgSO_4$, filtered, and concentrated to dryness. Removal of the Trt protecting group was performed with 4 mL of a mixture of 95% trifluoroacetic acid, 2.5% triisopropylsilane and 2.5% water. The removal of the Trt was followed by TLC and, at the end of the reaction, the solution was evaporated to dryness, the crude residue was triturated in cold $Et_2O$, centrifuged and purified by flash chromatography.

MS (ESI-Quad): $[M+Na]^+$ calc. $C_{36}H_{56}N_8O_{10}S_2$= 825.363 m/z; found = 825.3593 m/z.

Synthesis of **4**

Mixture **4** was synthetized according to the general procedure for the synthesis of peptides by SPPS on Fmoc-Rink amide resin. For the second coupling an equimolar mixture of Fmoc-Ser(tBu)-OH, Fmoc-Asp(tBu)-OH, Fmoc-His(Trt)-OH was used. Cleavage of the peptide sequence from the resin was performed with a mixture of 95% trifluoroacetic acid, 2.5% triisopropylsilane and 2.5% water, the resin was filtered and washed with DCM; the filtrated was collected and evaporated under

reduced pressure. The residue was triturated in cold $Et_2O$, centrifuged,lyophilized andused without further purification.

Synthesis of **5**

Compound **5** was synthetized according to the general procedure for the synthesis of peptides by SPPS on Fmoc-Rink amide resin. For the last coupling, 4-(tritylthio)-benzoic acid was used. Cleavage of the peptide sequence from the resin was performed with a mixture of 95% trifluoroacetic acid, 2.5% triisopropylsilane and 2.5% water, the resin was filtered and washed with DCM; the filtrated was collected and evaporated under reduced pressure. The residue was triturated in cold $Et_2O$, centrifuged and lyophilized.

$^1$H NMR (400 MHz, $D_2O$) δ 8.59 (d, J = 6.6 Hz, 1H, $NH^{His}$), 8.56 – 8.49 (m, 1H, $NH^{Asp}$), 8.43 – 8.39 (m, 1H, $Ar(C2)^{His}$), 8.33 (d, J = 7.5 Hz, 1H, $NH^{Phe}$), 8.31 – 8.20 (m, 2H, $NH^{Leu}$, $NH^{Ser}$), 7.46 (bs, 1H, $CONH_2^{Leu}$), 7.44 (d, J = 8.4 Hz, 2H, Ar), 7.38 – 7.19 (m, 6H, Ar), 7.10 (s, 1H, $Ar(C4)^{His}$), 7.00 (bs, 1H, $CONH_2^{Leu}$), 4.40-4.18 (m, $\alpha H^{Leu}$, $\alpha H^{Ser}$), 3.83 – 3.75 (m, 2H, $\beta CH_2^{Ser}$), 3.28 – 3.01 (m, 4H, $\beta CH_2^{His/Phe}$), 2.86 – 2.56 (m, 2H, $\beta CH_2^{Asp}$), 1.67 – 1.38 (m, 3H, $\beta CH_2^{Leu}$ and $\gamma CH^{Leu}$), 0.84 (d, J = 6.1 Hz, 3H, $\delta CH_3^{Leu}$), 0.79 (d, J = 6.2 Hz, 3H, $\delta CH_3^{Leu}$).

MS (ESI-Quad): $[M+H]^+$ calc. $C_{35}H_{45}N_9O_9S$= 768,31 m/z; found = 768.36 m/z.

Synthesis of **6**

Compound **6** was synthetized according to the general procedure for the synthesis of peptides by SPPS on Fmoc-Rink amide resin. For the last coupling, lauric acid was used. Cleavage of the peptide sequence from the resin was performed with a mixture of 95% trifluoroacetic acid, 2.5% triisopropylsilane and 2.5% water, the resin was filtered and washed with DCM; the filtrated was collected and evaporated under reduced pressure. The residue was triturated in cold $Et_2O$, centrifuged and lyophilized.

$^1$H NMR (400 MHz, DMSO-$d_6$) δ 8.67 (s, 1H, $Ar(C2)^{His}$), 8.17 (d, $J$ = 7.3 Hz, 1H, $NH^{Asp}$), 8.15 – 8.06 (m, 3H, $NH^{His}$), 7.97 (d, $J$ = 7.1 Hz, 1H, $NH^{Ser}$), 7.29 – 7.19 (m, 2H, , $Ar(C2)^{His}$, $CONH_2^{Leu}$), 7.10 – 6.98 (bs, $CONH_2^{Leu}$), 4.60 – 4.42 (m, 2H, $\alpha H^{His}$, , $\alpha H^{Asp}$), 4.32 – 4.14 (m, 2H, $\alpha H^{Ser}$, $\alpha H^{Leu}$), 3.70 – 3.51

(m, 2H, βCH$_2^{Ser}$), 3.32 (bs, water), 3.13 – 2.87 (m, 2H, βCH$_2^{His}$), 2.64 (dd, $J$ = 16.6, 5.3 Hz, 1H, βCH$_2^{Asp}$), 2.08 (t, $J$ = 7.4 Hz, 2H), 1.78 – 1.37 (m, 5H), 1.23 (s, 16H), 0.90 – 0.80 (m, 6H, δCH$_3^{Leu}$).

MS (ESI-Quad): $[M+H]^+$ calc. $C_{31}H_{53}N_7O_8$= 652.40 m/z; found = 652.40 m/z.

Synthesis of **7**

Compound **7** was synthetized according to the general procedure for the synthesis of peptides by SPPS on Fmoc-Rink amide resin. After the Fmoc deprotection of the last amino acid, a solution of $Ac_2O$ (10 mmol), DIPEA (2.6 mmol) in 20mL DMF was added to the vessel and shaken for 30 min (x 2). The resin was filtered and washed with DMF and DCM. Cleavage of the peptide sequence from the resin was performed with a mixture of 95% trifluoroacetic acid, 2.5% triisopropylsilane and 2.5% water, the resin was filtered and washed with DCM; the filtrated was collected and evaporated under reduced pressure. The residue was triturated in cold $Et_2O$, centrifuged and lyophilized.

$^1$H NMR (400 MHz, $D_2O$) δ 8.49 (m, 2H, Ar(C2)$^{His}$), 8.31 – 8.24 (m, 2H, NH$^{Leu}$, NH$^{Asp}$), 8.22 (d, $J$ = 6.8 Hz, NH$^{Ser}$), 7.46 (s, 1H, CONH$_2^{Leu}$), 7.17 (s *1*H, Ar(C4)$^{His}$), 6.99 (s, 1H, CONH$_2^{Leu}$), 3.80 – 3.71 (m, 2H, βCH$_2^{Ser}$), 3.28 – 2.95 (m, 2H, βCH$_2^{His}$), 2.69 (qd, $J$ = 17.0, 6.8 Hz, 1H, βCH$_2^{Asp}$), 1.88 (s, 3H, Ac), 1.65 – 1.40 (m, 3H, βCH$_2^{Leu}$ and γCH$^{Leu}$), 1.07 (s, 0H), 0.82 (d, $J$ = 6.1 Hz, 3H, δCH$_3^{Leu}$), 0.76 (d, $J$ = 6.1 Hz, 3H, δCH$_3^{Leu}$).

MS (ESI-Quad): $[M+H]^+$ calc. $C_{21}H_{33}N_7O_8$= 512.25 m/z; found = 512.30 m/z.

General procedure for the synthesis of silver nanoparticles

Silver nanoparticles were synthesized according to a reported procedure.

$AgNO_3$ was dissolved in water to a 12mM concentration. An 83 mM solution of ligand was added to aqueous solution (2 mol ligand/mol $AgNO_3$). The pH of the suspension was then raised using aqueous CsOH (50% w/v) or NaOH (2 M) to 12. To the precursor solution, aqueous 278 mM NaBH4 (10 mol/mol $AgNO_3$) were slowly added dropwise with stirring and allowed to incubate for at least one hour, or overnight. The colour of the solution developed as reported from light yellow solution to dark red (or dark orange for ligand **5**) upon reduction and remained unchanged. Moreover, the optical absorption spectrum of the solutions was in agreement with the final nanoparticles spectrum. The product was cleaned first by centrifuging to remove any solids and then precipitating the

clusters with DMF. The final product was prepared by cycles of dissolution of the precipitate into a 1% acetic acid solution in DMF and precipitation with toluene. The resulting solid was further purified by size-exclusion chromatography through gel filtration (Sephadex G-50) and eluted with water.

### Buffer preparation

In DCLs generation, and in kinetic and spectrophotometric experiments, the buffer employed are:

- acetate buffer pH 5.4

- 4-Morpholineethanesulfonic acid (MES) pH 6.1

- Phosphate-buffered saline (PBS) pH 7.2

- Tris(hydroxymethyl)aminomethane (TRIS) pH 8.3

- Britton–Robinson buffer (BRB) pH 8.5

- borate buffer pH 8.5 and pH 9.2

Buffer solutions were prepared by dissolving a weighted amount of buffering agents in mQ water. The pH was adjusted using 1M NaOH or 1M HCl and mQ water was added to reach the proper volume.

### Library preparation

Building blocks **1** and **2** were dissolved in 3 mM concentration in Britton buffer (50mM, pH=8.5) or borate buffer (50mM pH 8.5). Where necessary, the pH of the solution was adjusted by the addition of 1.0 M NaOH. All the libraries were set up in a glass vial with screw cap. All the vials were equipped with a cylindrical stirrer, stirred at 1,200 r.p.m. and maintained at 27°C.

An aliquot of 25 µL was taken into a HPLC vial insert and diluted with 50 µL of double distilled water. HPLC analyses were performed on an Agilent 1200 apparatus (Palo Alto, CA), equipped with a UV detector. UV absorbance was monitored at 226 nm. The analyses were performed at ambient conditions, with a flow rate of 1 mL/min.

For DCLs of peptide **1** the analyses were performed using an Agilent Zorbax RX-C18 5µm (4.6x250mm) column and the following linear gradient:

| time | 0 | 30 | 31 | 32 | 33 | 35 |
|---|---|---|---|---|---|---|
| %B | 0 | 20 | 100 | 100 | 0 | 0 |

For DCLs of peptide **2** the analyses were performed using an Agilent Eclipse XDB-C18 5µm (4.6x150mm) column and the following linear gradient:

| time | 0 | 10 | 11 | 12 | 13 | 15 |
|---|---|---|---|---|---|---|
| %B | 0 | 30 | 100 | 100 | 0 | 0 |

Building block **3** was dissolved in 3 mM concentration in MeOH basified with $K_2CO_3$(pH ~8). An aliquot of 25 µL was taken into a HPLC vial and diluted with 50 µL reagent grade MeOH. HPLC analyses were performed on the previous apparatus. The analyses were performed at ambient conditions, with a flow rate of 1 mL/min, using an Agilent Eclipse XDB-C8 5µm (4.6x150mm) column.

For DCLs of peptide **3** the analyses were performed using the following linear gradient:

| time | 0 | 15 | 18 | 20 | 23 |
|---|---|---|---|---|---|
| %B | 35 | 100 | 100 | 35 | 35 |

CD spectroscopy

Spectra were recorded on a Jasco J-715 spectrometer with a Peltier temperature controller. Quartz cuvette (Hellma, Müllheim, Germany) with a 0.1 and 1 cm path length were used for the measurements.

VT-ECD spectra were acquired at different temperatures from 20 °C to 80°C using a ramp rate of 2° $min^{-1}$ and waiting for 15 min at every temperature before measuring. Spectra were obtained as

averages of three measurements from 210 to 400 nm with a scanning speed of 100 nm $min^{-1}$ and a bandwidth of 1 nm. A quartz cuvette with a 0.1 cm path length was used for the measurements.

### General procedure for hydrolysis experiments

Substrates solutions for hydrolysis experiments were prepared dissolving *p*-NPA in 4 ml of a THF solution. Experiments were run in a quartz cuvette at pH 7.2(40 mM PBS buffer) and followed by UV-Vis spectroscopy at 25°C while stirring, with substrate (*p*-NPA) concentration of 250 µM and catalyst concentration of 25 µM (10%mol). The cuvette was placed in a Shimadzu model UV-2501 PC spectrophotometer and the hydrolysis of the substrates was monitored at 400 nm.

## References


1 Z. C. Girvin and S. H. Gellman, *J. Am. Chem. Soc.*, 2020, 142, 17211–17223.

2 M. Pollastrini, G. Marafon, J. Clayden and A. Moretto, *Chem. Commun.*, 2021, **57**, 2269–2272.

3 C. G. Pappas, P. K. Mandal, B. Liu, B. Kauffmann, X. Miao, D. Komáromy, W. Hoffmann, C. Manz, R. Chang, K. Liu, K. Pagel, I. Huc and S. Otto, *Nat. Chem. 2020 1212*, 2020, **12**, 1180–1186.

4 D. A. Keire, E. Strauss, W. Guo, B. Noszal and D. L. Rabenstein, *J. Org. Chem.*, 1992, **57**, 123–127.

5 J. W. Sadownik, E. Mattia, P. Nowak and S. Otto, *Nat. Chem.*, 2016, **8**, 264–269.

6 J. M. A. Carnall, C. A. Waudby, A. M. Belenguer, M. C. A. Stuart, J. J.-P. Peyralans and S. Otto, *Science.*, 2010, **327**, 1502–1506.

7 P. T. Corbett, J. K. M. Sanders and S. Otto, *Chem. - A Eur. J.*, 2008, **14**, 2153–2166.

8 M. Matsumura and B. W. Matthews, 1991, pp. 336–356.

9 S. Cheek, S. S. Krishna and N. V. Grishin, *J. Mol. Biol.*, 2006, **359**, 215–237.

10 W. J. Wedemeyer, E. Welker, M. Narayan and H. A. Scheraga, *Biochemistry*, 2000, **39**, 4207–4216.

11 C. Tsiamantas, X. de Hatten, C. Douat, B. Kauffmann, V. Maurizot, H. Ihara, M. Takafuji, N. Metzler-Nolte and I. Huc, *Angew. Chemie Int. Ed.*, 2016, **55**, 6848–6852.

12 P. T. Corbett, J. Leclaire, L. Vial, K. R. West, J.-L. Wietor, J. K. M. Sanders and S. Otto, *Chem. Rev.*, 2006, **106**, 3652–3711.

13 A. Desireddy, B. E. Conn, J. Guo, B. Yoon, R. N. Barnett, B. M. Monahan, K. Kirschbaum, W. P. Griffith, R. L. Whetten, U. Landman and T. P. Bigioni, *Nature*, 2013, **501**, 399–402.

14 B. E. Conn, A. Desireddy, A. Atnagulov, S. Wickramasinghe, B. Bhattarai, B. Yoon, R. N.

Barnett, Y. Abdollahian, Y. W. Kim, W. P. Griffith, S. R. J. Oliver, U. Landman and T. P. Bigioni, *J. Phys. Chem. C*, 2015, **119**, 11238–11249.

15 I. Chakraborty and T. Pradeep, *Chem. Rev.*, 2017, **117**, 8208–8271.

16 J. P. Wilcoxon, J. E. Martin and P. Provencio, *J. Chem. Phys.*, 2001, **115**, 998–1008.

17 H. Grönbeck, M. Walter and H. Häkkinen, *J. Am. Chem. Soc.*, 2006, **128**, 10268–10275.

18 O. M. Bakr, V. Amendola, C. M. Aikens, W. Wenseleers, R. Li, L. Dal Negro, G. C. Schatz and F. Stellacci, *Angew. Chemie Int. Ed.*, 2009, **48**, 5921–5926.

19 M. R. Branham, A. D. Douglas, A. J. Mills, J. B. Tracy, P. S. White and R. W. Murray, *Langmuir*, 2006, **22**, 11376–11383.

20 Z. L. Wang, *J. Phys. Chem. B*, 2000, **104**, 1153–1175.

# 5. Self- and co-assembly of amphiphilic peptide foldamers

As shown in Section 1.1, peptide amphiphile (PA) molecules consist of a peptide sequence conjugated to a fatty acid and have found increasing interest in the development of peptide-based supramolecular materials. As discussed in Section 1.3 and Section 4, peptide supramolecular materials are attractive potential supramolecular catalysts. Supramolecular materials often present organized microenvironments that can affect catalytic performance promoting, for example, the cooperative action of ordered catalytic moieties.

We designed and synthetized a set of amphiphilic peptides characterized by different recognition sequences and studied their self- and co-assembly behaviour, in order to develop a modular platform for the creation of peptide-based supramolecular catalysts (Figure 1).

The peptides are characterized by a common domain which consists in a helicoidal spacer made of an -(L-Ala-Aib)$_4$-octapeptide **1** sequence (Aib: α-aminoisobutyric acid, which has been reported to favour a $3_{10}$-/α-helical structure of right-handed screw sense dictated by the L-configuration of the Ala residues), linked in its N-terminus with a lipophilic tail **2** (hexadecylamine). As hydrophilic heads we chose an RGD-binding sequence **3** (a well-known cell adhesion sequence found in fibronectine), and an arginine-rich sequence **4** (a well-known cell-penetrating motif).

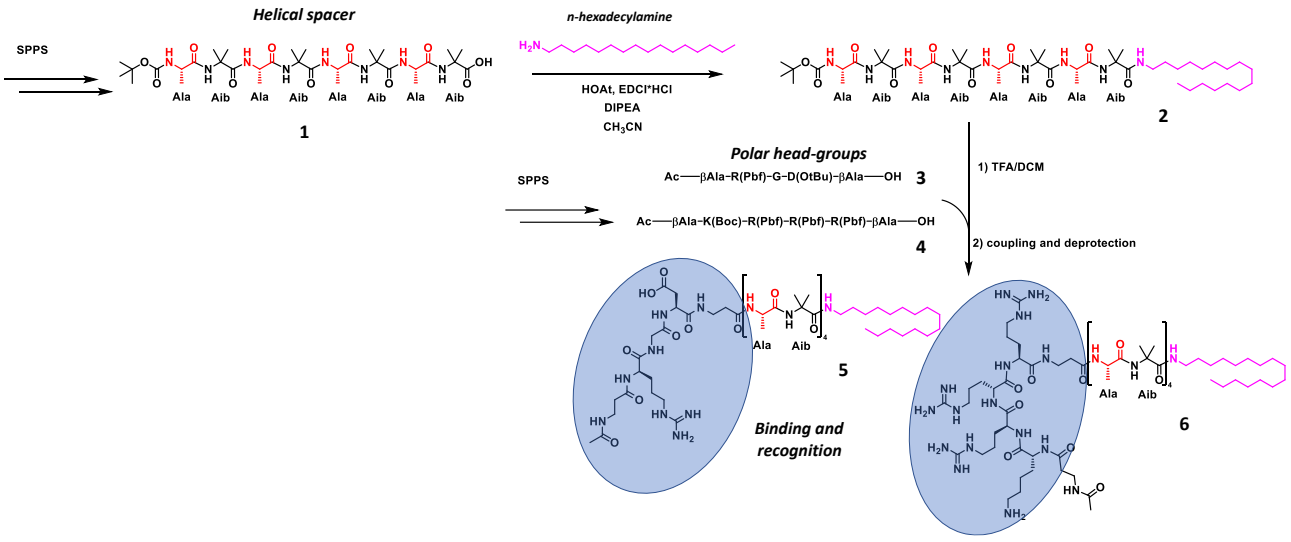


*Figure 1: Chemical structure and synthesis of helical peptide amphiphiles **1-6**.*

Peptides were synthetized by the combination of solid phase peptide synthesis (SPPS) with solution synthesis (Figure 1). Both Boc-(L-Ala-Aib)$_4$-OH (**1**) and the protected epitope sequences (**3** and **4**) were synthetized separately by SPPS. Then, the coupling of the carboxylic acid end of the spacer with hexadecylamine was performed in solution and the resulting peptide (**2**) was deprotected and coupled with the hydrophilic heads. Removal of the protecting groups afforded the final amphiphilic peptide foldamers **5** and **6**.

The consequences of conjugating the Ac-βAla-L-Arg-Gly-L-Asp-βAla- polar head group to the -(L-Ala-Aib)$_4$ helical spacer in **5** were studied using $^1$H and 2D-NMR (ROESY) experiments in $CD_3OH$ (9 mM, Figure 2).

As expected from the structure of peptide **5**, sequential αNH($i$)→αNH($i$+1) correlations, characteristic of a well-developed helical conformation,[1] and sequential αCH($i$)→αNH($i$+1) and βCH3($i$)→αNH($i$+1) correlations are seen in the ROESY spectra in the spacer region.

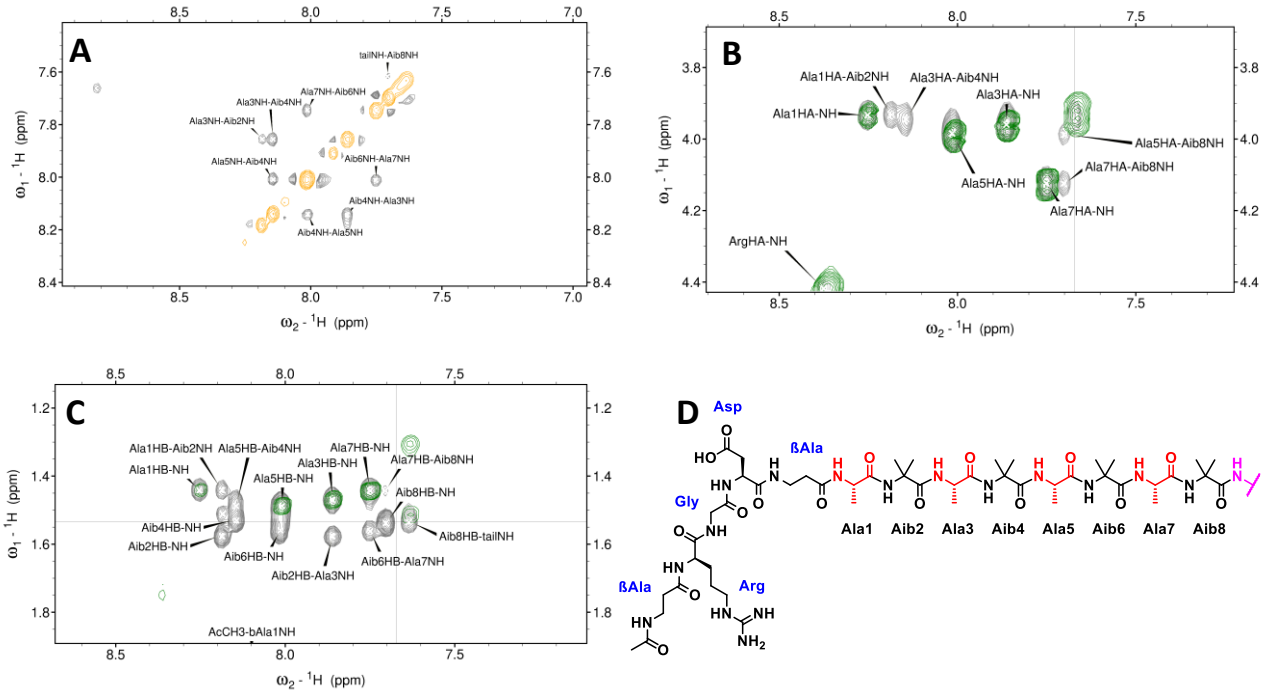


*Figure 2: (A) NH → NH region of the ROESY spectra of peptide **5**; (B) βCH3 αCH → αNH region of the ROESY spectra of peptide **5**; (C) βCH3 → αNH region of the ROESY spectra of peptides **5**; (D) chemical structure of peptide **5**.*

We also measured the J(αNH-αCH) coupling constants for the six non-Aib Cα-substituted residues. For the Ala residues in the core region of the spacer, the experimental values are compatible with helical structures, as they range between around 4.7 and 6.5 Hz. In the N-terminal region of **5** the

measured values for the L-Arg and L-Asp residues suggest a less structured conformation, as they range between 6.5 and 7.6 Hz. These finding suggest that the -(L-Ala-Aib)$_4$ is folded into a helical conformation that does not extend through the β-peptide linker (βAla) to the N-terminal RGD polar head.

Next, to further understand the role played by the polar head and the helical spacer on the conformation of the amphiphilic peptides, we recorded a series of ECD curves for peptides **2** and **5** in MeOH at different concentration of $H_2O$ (Figure 3).

Compound **2** exhibits a spectrum indicative of a right-handed, mixed $3_{10}$-/α-helix, characterized by two negative maxima at 224 nm and 206 nm, with an ellipticity ratio $R = [\theta]_{222}/[\theta]_{208} \approx 0.5$ . Compared to its shorter analogue, compound **5** displays a similar ECD spectrum, but characterized by a more intense 224 nm maximum ($R \approx 0.7$) and an overall increase (almost two-fold) in the intensity of the spectrum. This finding was unexpected based on the NMR analysis and suggests that the polar head group of compound **5** could also be involved to a certain degree in the helical conformation of the molecule.

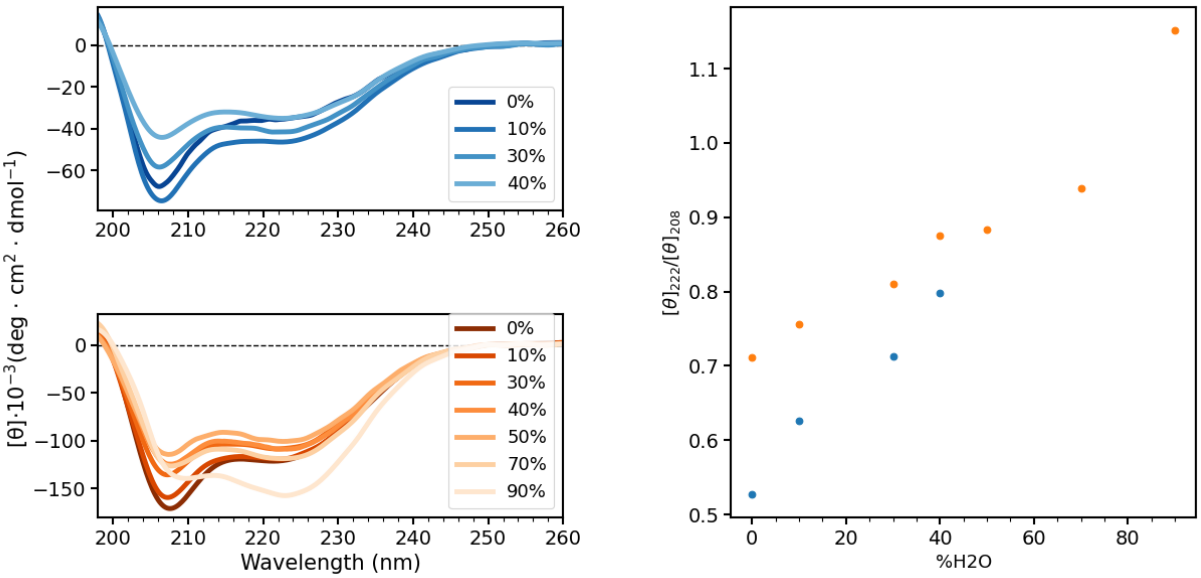


*Figure 3: (left) ECD spectra in MeOH (0.3 mM) of **2** (blue) and **5** (red) with increasing %v/v content of H2O; (right) $R = [\theta]_{222}/[\theta]_{208}$ values extrapolated from the spectra.*

After increasing the water content of the mixtures, both peptide **2** and functionalized peptide **5** underwent an increase in the ellipticity ratio. The analysis of the ratio between the ellipticities of the

negative Cotton effects at 222 nm (peptide n $\rightarrow \pi^*$ transition) and near 210 nm (parallel component of the split peptide $\pi \rightarrow \pi^*$ transition) value can be diagnostic for $3_{10}$-helix ($R \approx 0.4$) and an α-helix ($R \approx 1$) content; however, it is affected by several factors, including environmental (solvent) changes, 3D-structural factors, such as incomplete α-helix formation. In this case, we are inclined to ascribe this variation in the ellipticity ratio more to the formation of supramolecular assembled species in the organic/water solvent mixture, than to an increase in α-helix content. This hypothesis was corroborated, for compound **2**, when we were able to obtain single crystal suitable for X-ray diffraction analyses to further characterize the conformational properties of the octapeptide. The crystals were obtained from a slow concentration of in **2** in aqueous solution, thus, we could assume that the crystal packing may represent the self-assemble structure of **2** in water.

The molecular structure of Boc-(L-Ala-Aib)$_4$-NH-HexDec, as determined by single crystal X-ray diffraction, is illustrated in Figure 4.

Bond distances and bond angles are in general agreement with typical values for the Boc group,[2] the peptide unit,[3] the amide bond,[4] and the Aib residue.[5,6]The values of the ω torsion angles internal to the peptide chain are within ±5° from the exact *trans*-planarity (ω = 180°) and slightly larger (but far from exceptional)[7,8] deviations characterize the N-terminal urethane [$\omega_0 = -170.2(3)°$] and the C-terminal amide [$\omega_T = -171.9(5)°$] groups.

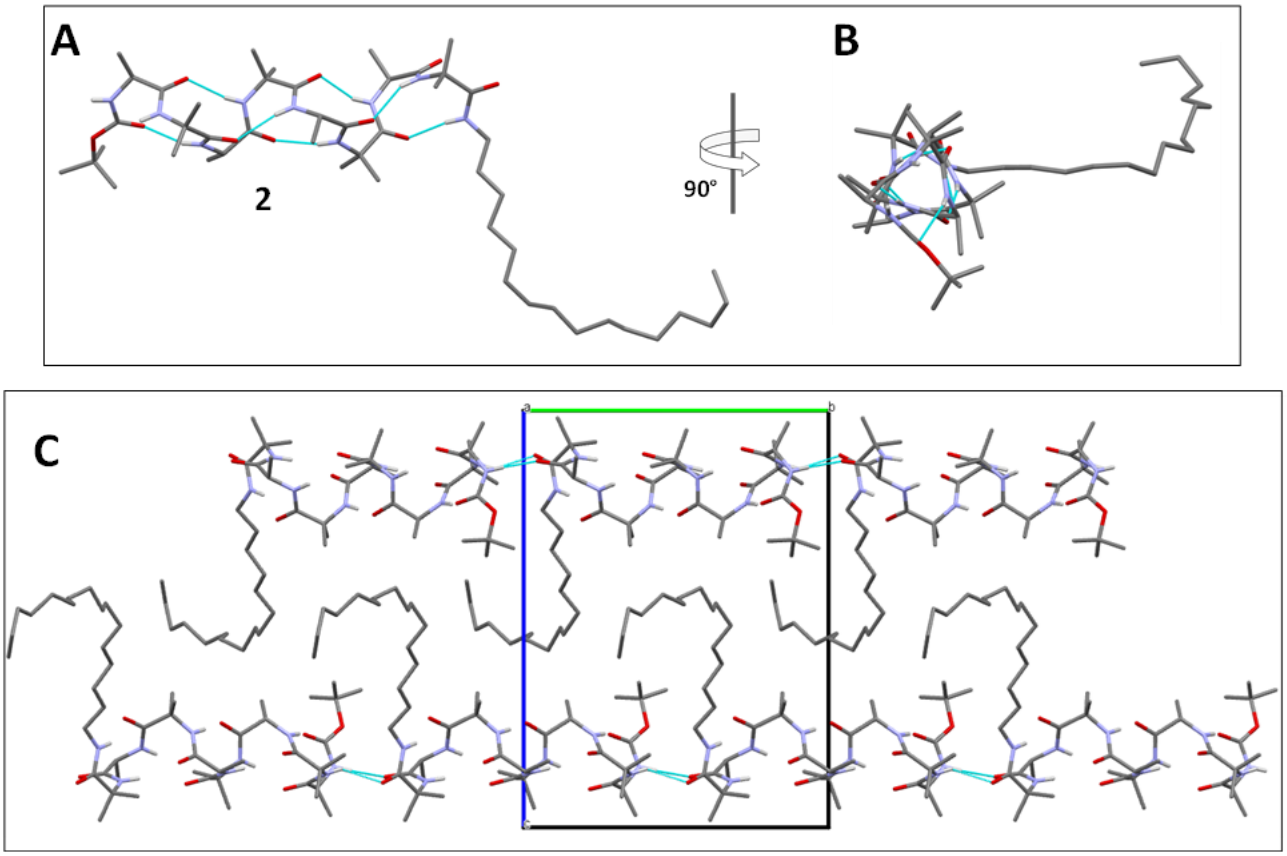


*Figure 4: (A,B) X-Ray diffraction structure of Boc-(L-Ala-Aib) 4 -NH-Hxd. Only the major occupancy conformer of the disordered hexadecyl chain is shown. Most of the H-atoms are omitted for clarity. The intramolecular N-H…O=C H-bonds are indicated by dashed lines. (C) Packing mode of Boc-(L-Ala-Aib) 4 -NH-Hxd as viewed down the a axis.*

The peptide backbone is folded in a right-handed $3_{10}$-helical conformation,[9,10] stabilized by seven, consecutive C=O···H-N intramolecular H-bonds of the $i \leftarrow i+3$ ($C_{10}$) type[11,12] (Figure 4A). The related N···O and H···O distances are in the ranges 2.972(5) - 3.105(6) Å and 2.13 - 2.31 Å, respectively, and the N-H···O angles vary from 153.2° to 170.7°. The possible concomitant occurrence of at least some intramolecular H-bonds of the α-helical $i \leftarrow i+4$ ($C_{13}$) type[12] is definitely ruled out, as all of the O($i$) ···N($i$+4) distances are longer than 4.33 Å.

The values of the ϕ,ψ torsion angles, as averaged for the eight residues, are –56.6°, –30.0°, thus matching those typical for a peptide $3_{10}$-helix (–57°, –30°).[10] Deviations from the average by individual ϕ or ψ values do not exceed ±8°, an indication of the regularity of the $3_{10}$-helix formed.

It is worth recalling that peptides combining Aib and protein α-amino acid residues in their sequences in general give rise to $3_{10}$-helices in the case of relatively short oligomers, while to α-helices as the main-chain length increases.[13] Interestingly, among the terminally protected / blocked peptides

featuring a strict alternation of Aib and L-Ala residues so far characterized in the crystal state, the present octapeptide amide represents one of the longest example of a fully $3_{10}$-helical conformation.[14–17]

The C-terminal hexadecyl chain is characterized by significant disorder. The long hexadecyl amino tail protrudes from the helical envelope. Its segment proximal to the peptide moiety, from NT to CT6, is quite linearly arranged and it is almost perpendicular to the peptide helix axis. The value of 86° of the torsion angle about the CT6-CT7 bond causes a bending of the chain which then proceeds irregularly up to CT16, featuring additional kinks at the level of the CT11-CT12 and CT14-CT15 bonds. The overall shape of the hexadecyl tail can be described as a loose hook.

In the crystal, the peptide helix axis of the molecule taken as the asymmetric unit lays parallel to the *ab* plane, roughly oriented along the [1,-1,0] direction. In the packing mode, two intermolecular H-bonds are observed, connecting respectively the N1-H and N2-H groups to the O7 and O8 carbonyl oxygen atoms of a (x-1, y+1, z) translationally equivalent molecule, thus giving rise to infinite rows of molecules connected head-to-tail (Figure 4C). These rows are arranged in layers parallel to the *ab* plane (Figures X2 and X3). In each layer, all of the hexadecyl chains protrude from the same side. Layers stack along the *c* direction, alternating the face-to-face close approach of two "bald" sides with the approach from a longer distance of two "hairy" sides. Each helical peptide molecule is about 18 Å in length, 7 Å in diameter, and carries a single hexadecyl tail. As a consequence, the interdigitation of the hexadecyl chains in the packing is unavoidably loose, thus accounting for their disorder. The overall supramolecular organization, as illustrated in Figures 4C, is somehow reminiscent of that of multiple phospholipid bilayers, despite obvious differences arising from the nature of the "head", the number of lipid tails per molecule, the relative size of head and tail, and the bent rather than linear disposition of the latter. In the present case, the overall thickness of a bilayer corresponds to the *c* axis length (21.104 Å), and the lipid-like interior is ≅ 7 Å.

This study revealed that peptide **2** self-assembled into liposomal structures (that may be called "*peptosome*" structures), with average dimensions of around 50-100 nm (Figure 5). We hypothesized that the morphology of the nanostructures could be structurally like the supramolecular organization of **2** in its crystal packing, with a two-layered disposition of the molecules with the hydrophobic tails

pointing toward the centre in a phospholipid bilayer fashion. This disposition is also reminiscent to other structures formed by (Ala-Aib)$_4$-based peptides in water, in which the hydrophobic tails are packed in the core of the fibres with the hydrophilic head laying on the surface.[18]

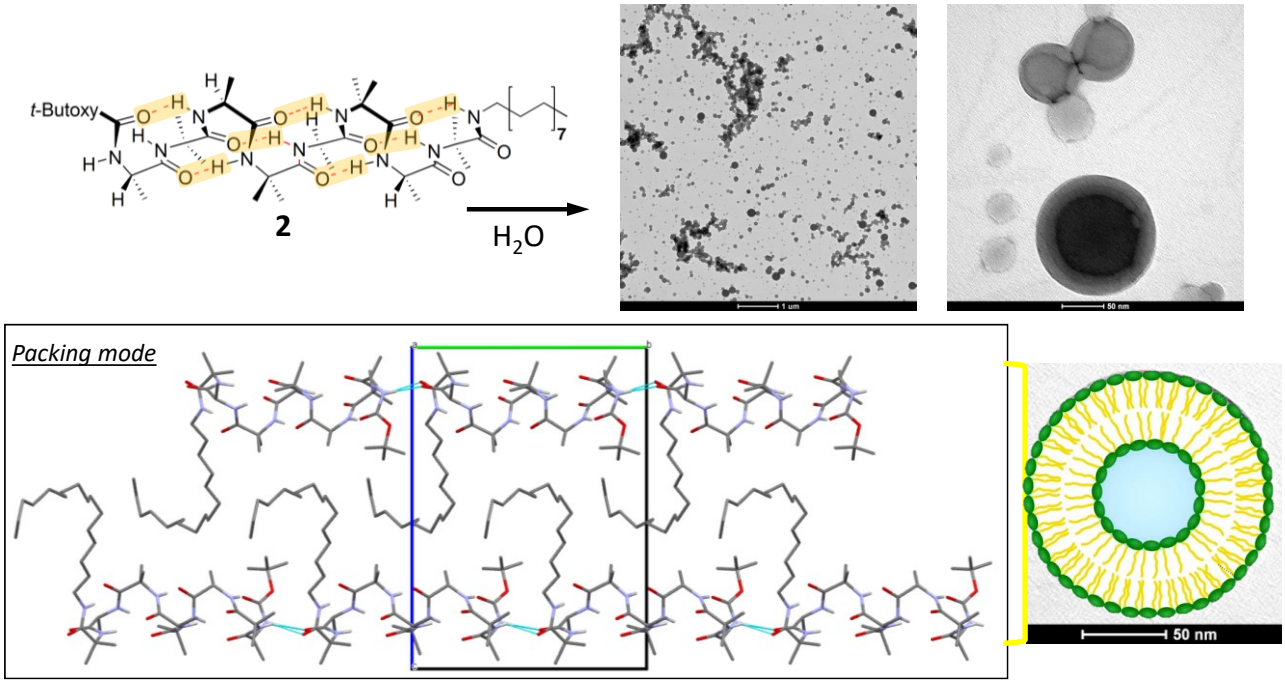


*Figure 5: (Top) Chemical structure and TEM images of liposomal like structures obtained from aqueous self-assembly of peptide amphiphiles* ***2*** *(bottom) Packing mode of* ***2*** *that highlight an ordered confinement of the hydrophobic tail and schematic cartoon representation of the "peptosome" structure.*

Self-assembled structures formed by **5** in water were obtained and successively characterized by transmission electron microscopy (TEM, Figure 6). This study revealed that peptide **5** self-assembled into tubular structure with a diameter up to 500 nm and lengths up to 200 μm. These fibres showed the presence of a hollow interior filled by water, as detected by the formation of bubbles upon heating under the microscope beam.

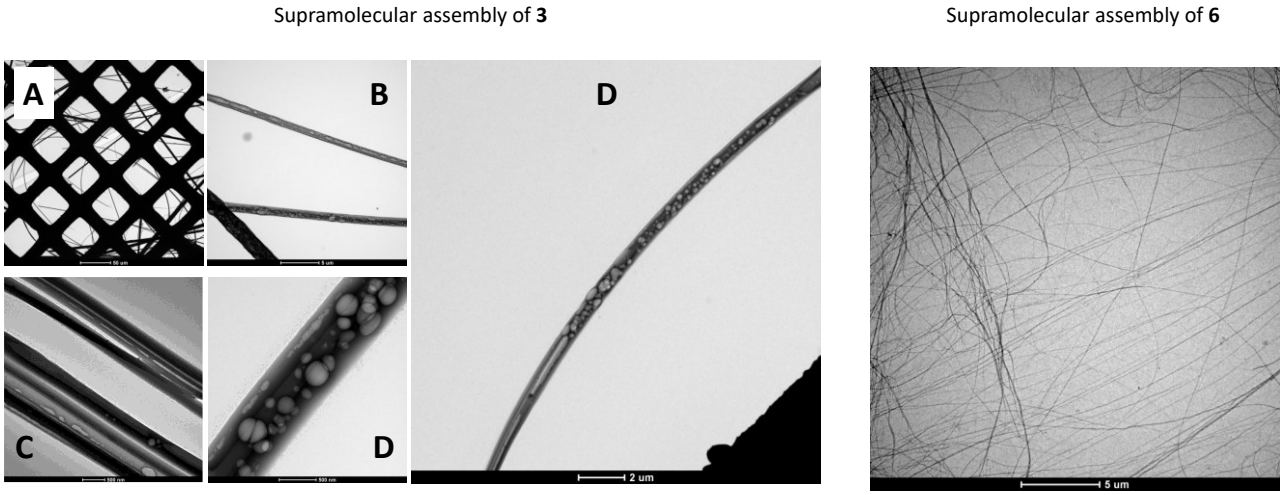


*Figure 6: (left, A-D): TEM images of tubular structure obtained from self-assembly of **5**. **Right**: TEM images of tubular structure obtained from self-assembly of **6**.*

The self-assembled structures formed by **6** in water (Figure 6) revealed the formation of long filaments up to 20 μm characterized by a very thin diameter (10-20 nm).

Therefore, the difference of the structure formed by **3** and **4** relates to the presence of the binding sites, that drive the supramolecular aggregation process toward an axial direction.

We then run two components co-assembly experiments by mixing **2/5**, or **2/6**, or **5/6** (TEM, Figure 7 D, E and F respectively). The results of the experiments involving **2** show the occurrence of a co-assembly process that produces spherical structures, larger than those formed only by **2** (around 100 nm).

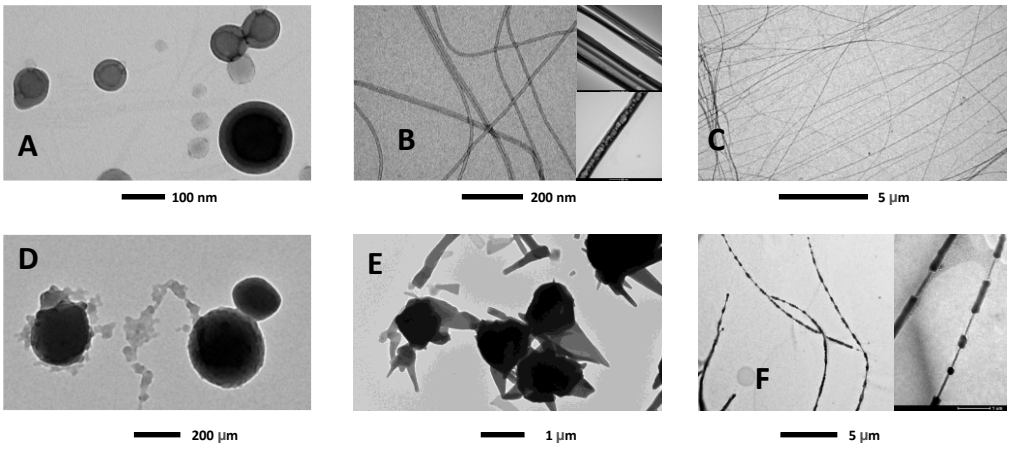


*Figure 7: Top: TEM images of structures obtained from self-assembly of peptide amphiphiles **2** (**A**), **5** (**B**) and **6** (**C**). Bottom: Structure formed by the co-assembly of **2/5** (**D**), **2/6** (**E**) and **5/6** (**F**).*

In these aggregates, peptides **5** and **6** might have been incorporated and probably ordered; a more irregular surface could suggest a partial leaking of the peptides **5** and **6** content. In the last case, we attempted to run different experiments in the way to carry out the **5** *plus* **6** co-assembly. The most relevant co-assembly result was found when fiber from **5** were used as template for **6** assembly. A water solution of **5** was added to a diluted solution of fibres from **6** and, after an ageing period, it could be recognized that **5** starts to grow over the **6** filaments. Thus, a hierarchical co-assembled system is formed where tubular structures **5** are formed over the thinner templating structure of **6,** probably mediated by a head-to-head binding sites recognition.

In summary, we reported the modular synthesis of novel peptide amphiphiles characterized by an -(L-Ala-Aib)$_4$ helical spacer. The self-assembly in water of such amphiphilic systems led to the formation of liposomal-like, fibrillar or tubular nanostructures depending on the nature of the hydrophilic head. In conclusion, the modularity of such peptides allowed us to explore a large self-assembly space and may be interesting for the development of peptide-based supramolecular catalysts. Moreover, future developments could involve a further study of the recognition phenomena between these amphiphilic peptide systems and the preparation of organized nanostructures for the delivery of "cargo" drugs through multifunctional liposomal-like systems.

# Experimental Section

## General Methods

*High-Performance Liquid Chromatography.* The HPLC measurements were performed using an Agilent 1200 apparatus (Palo Alto, CA), equipped with a UV detector at various wavelength and a column Agilent extend-C18 (stationary phase). Eluants: A= 9:1 $H_2O/CH_3CN$, 0.05 % TFA; B= 1:9 $H_2O/CH_3CN$, 0.05 % TFA.

*Nuclear Magnetic Resonance.* $^1H$ NMR, $^{13}C$ NMR, and 2D-NMR spectra were recorded at 25°C on Bruker Avance400 or 500 MHz instruments. $^1H$ and $^{13}C$ spectra were referenced relative to the solvent residual peaks and chemical shifts (δ) reported in ppm downfield of tetramethylsilane ($CDCl_3$ δ H: 7.26 ppm, δ C: 77.16 ppm; $CD_3CN$ δ H: 1.94 ppm; DMSO δ H: 2.50 ppm). The multiplicity of a signal is indicated as br, broad; s, singlet; d, doublet; t, triplet; m, multiplet.

*Mass Spectrometry.* Mass spectra by electrospray ionization (ESI), collected in the positive mode, were performed on Perseptive Biosystem Mariner ESI-ToF5220 spectrometer (Foster City, CA).

*Fourier Transform-Infrared Spectroscopy.* FT-IR absorption spectra were recorded with a ATi Perkin Elmer Spectra RX1 FT-IR spectrometer. The ῡ maxima for the main absorption bands are given.

## Synthesis and characterization of compounds

### Materials

N,N-diisopropylethylamine (DIPEA), trifluoroacetic acid (TFA), triethylamine (TEA), L-amino acids methyl ester hydrochloride, N-(3-Dimethylaminopropyl)-N′-ethylcarbodiimide hydrochloride (EDC·HCl), N,O-dimethylhydroxylamine hydrochloride, lithium aluminum hydride ($LiAlH_4$), sodium cyanoborohydride ($NaCNBH_4$), 4-chlorobenzylamine, Boc-L-amino acids, were obtained from Merck. 1-hydroxy-7-aza-1,2,3-benzotriazole (HOAt) was purchased from GL Biochem (Shanghai).

The deuterated solvents DMSO-$d_6$, $CDCl_3$, $CD_3OD$ and $CDCN_3$ were purchased from Euriso-Top (France).

### General procedure for deprotection and Boc removal

The protected peptide was dissolved in a TFA/DCM 1:1 (v/v) mixture and the removal of protecting groups was followed by HPLC. At the end of the reaction, the solution was evaporated to dryness, the crude residue was dissolved in milliQ water and lyophilized.

### Synthesis of Boc-(Ala-Aib)$_4$-COOMe

Peptide Boc-(Ala-Aib)$_4$-COOMe was synthesized using standard solid phase 9-fluorenylmethoxycarbonyl (Fmoc) chemistry on a 2-chlorotrityl chloride resin. For each step, Fmoc deprotection was performed by mixing the resin in a piperidine/N,N-dimethylformamide (DMF) (2:8, *v/v*) solution for 10 minutes (2x), then washing with DMF, MeOH and DCM. For all of the amino acid couplings we used the following protocol: 5.0 eq. (relative to the resin loading) of Fmoc-protected amino acid were activated externally with 4.9 eq. of O-Benzotriazole-N,N,N',N'-tetramethyluronium hexafluorophosphate (HBTU) and 10 eq. of diisopropylethylamine (DIPEA) in DMF (2.5 ml/mmol of amino acid). This mixture was then added to a peptide chamber containing the resin and mixed for 3 hours. The resin was then drained and rinsed with MeOH, and DCM, then allowed to dry. As a last coupling, Boc-Ala-OH (5.0 eq.) was used instead of Fmoc-amino acid residue. Cleavage of the peptide sequence from the resin was performed with a mixture of

DIPEA/MeOH/DMF 1:5:5 (v/v) stirring overnight; the filtrated was collected and evaporated under reduced pressure. The residue was triturated in cold $Et_2O$, centrifuged and lyophilized.

MS (ESI-TOF): $[M+H]^+$ calc. for $C_{34}H_{60}N_8O_{11}$ = 757.4454m/z; found = 757.4417 m/z.

$^1$H NMR (400 MHz, DMSO) δ 8.35 (s, 1H), 7.91 (d, $J$ = 4.6 Hz, 1H), 7.73 (s, 1H), 7.61 (d, $J$ = 5.7 Hz, 1H), 7.56 (s, 1H), 7.53 (s, 1H), 7.29 (d, $J$ = 7.7 Hz, 1H), 7.16 (d, $J$ = 4.9 Hz, 1H), 4.13 – 4.03 (m, 1H), 4.00 – 3.84 (m, 3H), 3.55 (s, $J$ = 15.8 Hz, 3H), 1.44 – 1.33 (m, 33H), 1.30 (d, $J$ = 7.2 Hz, 6H), 1.23 (d, $J$ = 7.3 Hz, 6H).

$^{13}$C{$^1$H} NMR (101 MHz, DMSO) δ 176.2, 175.7, 174.7, 174.3, 174.2, 174.0, 173.7, 172.0, 156.4, 79.1, 56.4, 56.3, 56.1, 55.3, 52.2, 51.7, 51.2, 48.9, 28.6, 26.5, 26.3, 26.0, 25.2, 25.2, 24.6, 24.4, 24.0, 17.7, 17.6, 17.4, 17.2, 16.9.

Synthesis of Boc-(Ala-Aib)$_4$-OH **(1)**

Boc-(Ala-Aib)$_4$-OMe (0.25 g, 0.33 mmol) was dissolved in MeOH (5 mL) and a solution of $LiOH \cdot H_2O$ (0.07 g, 1.67 mmol) in water (5 mL) was added. The solution was stirred at r.t. and the reaction was followed by HPLC until complete conversion. The organic solvent was removed under reduced pressure and the aqueous phase was acidified with $KHSO_4$. The compound was extracted using EtOAc (3v). The organic phase was washed with $KHSO_{4(aq)}$ 5% and brine, dried over anhydrous $Na_2SO_4$, filtered and concentrated under reduced pressure. The crude product was used for the following reactions without any further purification.

**Boc-(Ala-Aib)$_4$-OH** as a waxy solid (0.2 g, 0.27 mmol, 81%).

MS (ESI-TOF): $[M+H]^+$ calc. for $C_{33}H_{58}N_8O_{11}$ = 743.4298 m/z; found = 743.4815 m/z.

$^1$H NMR (400 MHz, $CDCl_3$) δ 7.80 (d, J = 5.3 Hz, 1H), 7.75 (s, 1H), 7.68 (d, J = 5.2 Hz, 1H), 7.61 (s, 1H), 7.58 (s, 1H), 7.54 (s, 1H), 7.49 (d, J = 8.0 Hz, 1H), 6.47 (d, J = 3.1 Hz, 1H), 4.53 (p, J = 7.3 Hz, 1H), 4.04 – 3.92 (m, 2H), 3.83 (qd, J = 7.2, 3.0 Hz, 1H), 1.63 (d, J = 5.3 Hz, 6H), 1.57 (s, 3H), 1.54 – 1.44 (m, 30H), 1.42 (d, J = 7.3 Hz, 3H), 1.35 (d, J = 7.2 Hz, 3H).

$^{13}C\{^{1}H\}$ NMR (101 MHz, $CDCl_3$) δ 177.8, 177.0, 175.8, 175.6, 175.0, 175.0, 174.8, 173.7, 157.5, 80.9, 57.4, 56.9, 56.5, 56.4, 53.5, 53.2, 53.0, 49.1, 28.4, 27.7, 27.0, 26.9, 25.4, 24.4, 23.0, 22.9, 22.8, 16.8, 16.6, 16.6.

General procedure for SPPS of polar heads **3** and **4**

The peptide was synthetized following 2-Chlorotrityl chloride resin (1.6 mmol/g) was added to a vessel. The resin was swelled in DMF and then the first Fmoc-amino acid (5 eq. relative to the resin) was dissolved in DMF and DIPEA (4 eq. relative to the carboxylic acid) was added. This mixture was added to the resin and stirred for 1 h. At the end of this time, the mixture was filtered and the resin was washed with DMF, DCM and DMF. Unreacted sites were capped by treatment with an 80:15:5 DCM/MeOH/DIPEA mixture for 20 minutes. After filtering, the resin was washed with DCM. Then, the resin was treated with DMF. Iterative cycles of Fmoc deprotection and coupling were carried out with 20% piperidine solution in DMF (2x20min). For successive couplings, a solution of the amino acid Fmoc-AA-OH (3 eq.), HATU (3 eq.), HOAt (2.7 eq) and DIPEA (9 eq.) in DMF was added to the resin and stirred for 1h and 30 minutes. The resin was filtered and washed with DMF, DCM and DMF. After the Fmoc deprotection of the last amino acid, a solution of $Ac_2O$ (10 mmol), DIPEA (2.6 mmol) in 20mL DMF was added to the vessel and shaken for 30 min (x 2). The resin was filtered, and washed with DMF and DCM.

Cleavage of the peptide sequence from the resin was performed with a mixture of HFIP/DCM 3:7 (v/v), the resin was filtered and washed with DCM; the filtrated was collected and evaporated under reduced pressure. The residue was triturated in cold $Et_2O$, centrifuged and lyophilized.

Ac-*β*AR(Pbf)GD(O$^t$Bu)*β*A-OH (**3**)

MS (ESI-TOF): $[M+H]^+$ calc. $C_{37}H_{58}N_8O_{12}S$= 839.3968 m/z; found = 839.3990 m/z.

$^{1}H$ NMR (400 MHz, DMSO-$d_6$) δ 12.20 (s, 1H), 8.17 (t, $J$ = 5.6 Hz, 2H), 8.12 (d, $J$ = 7.3 Hz, 1H), 8.07 (d, $J$ = 8.3 Hz, 1H), 7.88 (t, $J$ = 5.6 Hz, 1H), 7.82 (t, $J$ = 5.6 Hz, 1H), 6.69 (s, 0H), 6.40 (s, 0H), 4.54 (q, $J$ = 8.1 Hz, 2H), 4.18 (q, $J$ = 7.5 Hz, 2H), 3.79 – 3.60 (m, 3H), 3.21 (dp, $J$ = 13.3, 7.2 Hz, 7H), 3.02 (q, $J$ = 6.5 Hz, 2H), 2.96 (s, 3H), 2.63 (dd, $J$ = 15.8, 5.8 Hz, 1H), 2.45 (d, $J$ = 22.2 Hz,

9H), 2.36 (t, $J$ = 7.1 Hz, 4H), 2.29 (t, $J$ = 7.0 Hz, 3H), 2.00 (s, 4H), 1.77 (s, 3H), 1.70 – 1.54 (m, 1H), 1.41 (s, 8H), 1.36 (s, 10H).

$^{13}$C NMR (101 MHz, DMSO) δ 172.8, 172.1, 170.9, 170.1, 169.3, 169.2, 168.6, 157.5, 156.1, 137.3, 131.4, 124.3, 116.3, 86.3, 80.2, 52.6, 49.4, 42.5, 42.0, 37.6, 35.3, 35.2, 35.0, 33.7, 28.3, 27.6, 22.6, 22.1, 18.9, 17.6, 12.3.

Ac-$\beta$AK(Boc)R(Pbf)R(Pbf)R(Pbf)$\beta$A-OH (**4**)

MS (ESI-TOF): $[M+H]^+$ calc. $C_{37}H_{58}N_8O_{12}S$= 1655.7994 m/z; found = 1655.7993 m/z.

$^1$H NMR (400 MHz, DMSO-$d_6$) δ 12.23 (s, 1H), 8.05 (d, $J$ = 7.9 Hz, 2H), 7.94 (dt, $J$ = 15.7, 5.8 Hz, 3H), 7.82 (d, $J$ = 5.9 Hz, 1H), 6.77 – 6.57 (m, 2H), 6.40 (s, 2H), 5.16 (m, 1H), 4.27 – 4.09 (m, 2H), 3.26 – 3.19 (m, 2H), 3.08 – 2.98 (m, 4H), 2.96 (s, 6H), 2.92 – 2.82 (m, 2H), 2.48 (s, 6H), 2.43 (s, 6H), 2.36 – 2.20 (m, 3H), 2.01 (s, 6H), 1.78 (s, 2H), 1.72 – 1.55 (m, 3H), 1.41 (s, 17H), 1.36 (s, 6H).

Synthesis of Boc-(Ala-Aib)$_4$-NH(CH$_2$)$_{15}$-CH$_3$ **(2)**

Boc-(Ala-Aib)$_4$-OH (0.2 g, 0.27 mmol) was dissolved in dry CH$_3$CN (5 mL) and HOAt (0.040 g, 0.29 mmol) and EDC·HCl (0.057 g, 0.29 mmol) were added. After 10 min hexadecylamine (0.13 g, 0.54 mmol) was added to the reaction mixture, and DIPEA was used to reach basic pH. After 1.5 hours the solvent was removed under reduced pressure. The crude product was purified by flash chromatography (eluant: DCM/MeOH 93:7) to give 0.21 g (80% yield)of Boc-(Ala-Aib)$_4$-NH(CH$_2$)$_{15}$-CH$_3$ as a whithe solid.

MS (ESI-TOF): $[M+H]^+$ calc. for $C_{33}H_{58}N_8O_{11}$ = 966.6962 m/z; found = 966.7015 m/z.

$^1$H NMR (400 MHz, CDCl$_3$) δ 7.80 (d, $J$ = 5.0 Hz, 1H, $\mathbf{NH_{Ala2}}$), 7.62 (s, 1H, $\mathbf{NH_{Aib2}}$), 7.60 (d, J = 4.9 Hz, 1H, $\mathbf{NH_{Ala3}}$), 7.51 (s, 1H, $\mathbf{NH_{Aib3}}$), 7.43 (s, 1H, $\mathbf{NH_{Aib4}}$), 7.40 (d, $J$ = 6.9 Hz, 1H, $\mathbf{NH_{Ala4}}$), 7.36 (s, 1H, $\mathbf{NH_{Aib1}}$), 7.29 – 7.20 (m, 1H, $\mathbf{NH_{tail}}$), 6.39 (s, 1H, $\mathbf{NH_{Ala1}}$), 4.27 (p, J = 7.2 Hz, 1H, $H^{\alpha}_{Ala4}$), 4.05 – 3.93 (m, 2H, $H^{\alpha}_{Ala3}$ and $H^{\alpha}_{Ala3}$), 3.87 (qd, J = 7.3, 2.8 Hz, 1H, $H^{\alpha}_{Ala1}$), 3.24 – 3.09 (m, 2H, $H^{\alpha}_{tail}$), 1.61 – 1.42 (m, 42H, Aib and Ala CH$_3$), 1.40 (d, $J$ = 7.3 Hz, 3H, $H^{\beta}_{Ala1}$), 1.34 – 1.22 (m, 10H, tail), 0.87 (t, $J$ = 6.7 Hz, 28H, CH$_3$-tail).

.

Synthesis of $NH_2$-(Ala-Aib)$_4$-$NH(CH_2)_{15}$-$CH_3$

Boc-(Ala-Aib)$_4$-$NH(CH_2)_{15}$-$CH_3$ (150mg, 0.15 mmol) was dissolved in 4.2mL of a TFA/DCM 1:1 (v/v) mixture and the removal of Boc- protecting group was followed by TLC. At the end of the reaction, the solution was evaporated to dryness, the crude residue was triturated in cold $Et_2O$, centrifuged and lyophilized.

Synthesis of Ac-$\beta$AR(Pbf)GD(OtBu)$\beta$A(AU)$_4$-$NH(CH_2)_{15}$-$CH_3$

Ac-$\beta$AR(Pbf)GD(O$^t$Bu)$\beta$A-OH(0.156 g, 0.18 mmol) was dissolved in a mixture of $CH_3CN$:DMF=10:1 (5.5 mL) and HOAt (0.027 g, 0.2 mmol) and EDC·HCl (0.039 g, 0.2 mmol) were added. After 10 min $H_2N$-(AU)$_4$-$NH(CH_2)_{15}$-$CH_3$ was added to the reaction mixture, and DIPEA was used to reach basic pH. The reaction was stirred overnight at 40°C. The solvent was removed under reduced pressure and the residue dissolved in DCM. The organic phase was washed with $KHSO_4$ (5%), $NaHCO_3$ (5%) and brine, dried over $MgSO_4$, filtered, and concentrated to dryness. The crude product was purified by flash chromatography (eluant: DCM/MeOH 9:1) to give 0.10 g (0.06 mmol, 38%) of Ac-$\beta$AR(Pbf)GD(O$^t$Bu)$\beta$A(AU)$_4$-$NH(CH_2)_{15}$-$CH_3$ as a white solid and used as it is.

Synthesis of Ac-$\beta$ARGD$\beta$A(AU)$_4$-$NH(CH_2)_{15}$-$CH_3$ **(5)**

The removal of the protecting groups was obtained treating Ac-$\beta$AR(Pbf)GD(O$^t$Bu)$\beta$A(AU)$_4$-$NH(CH_2)_{15}$-$CH_3$ with an 1:1 TFA/$CH_2Cl_2$ mixture (4 mL) at r.t. under stirring with TIPS and $H_2O$ for 2 hours. Then the solvent was evaporated, the residue washed with $Et_2O$, dissolved in MeOH, reprecipitated in cold $Et_2O$ and centrifuged.

MS (ESI) calcd for $C_{64}H_{116}N_{17}O_{16}^+$ $[M+H]^+$ *m/z* 1378.8780, found 1378.8759.

$^1$H NMR (400 MHz, DMSO-$d_6$) δ 11.47 (s, 0H), 8.57 – 8.41 (m, 1H), 8.34 (d, $J$ = 4.2 Hz, 1H), 8.31 (s, 1H), 8.20 (d, $J$ = 7.4 Hz, 1H), 7.92 (s, 1H), 7.86 (t, $J$ = 5.7 Hz, 1H), 7.80 – 7.75 (m, 2H), 7.70 (s, 1H), 7.40 (d, $J$ = 6.7 Hz, 1H), 7.35 (s, 1H), 7.20 (t, $J$ = 5.8 Hz, 3H), 4.43 – 4.35 (m, 1H), 4.30 – 4.20 (m, 1H), 4.02 – 3.93 (m, 2H), 3.87 (dt, $J$ = 7.9, 4.1 Hz, 2H), 3.74 (qd, $J$ = 16.9, 5.6 Hz, 2H), 3.48 (dt, $J$ = 13.7, 6.9 Hz, 1H), 3.22 (q, $J$ = 7.1 Hz, 2H), 3.11 (dq, $J$ = 11.8, 6.1 Hz, 3H), 2.99 (dp, $J$ = 19.5, 6.2 Hz, 2H), 2.56 – 2.47 (m, 3H), 2.43 – 2.27 (m, 4H), 1.78 (s, 3H), 1.44 – 1.18 (m, 61H), 0.84 (t, $J$ = 6.7 Hz, 3H).

$^1$H NMR (400 MHz, Methanol-$d_3$) δ 8.80 (d, $J$ = 7.6 Hz, 1H, $\mathbf{NH_{Asp}}$), 8.35 (d, $J$ = 7.0 Hz, 1H, $\mathbf{NH_{Arg}}$), 8.23 (d, $J$ = 3.0 Hz, 1H, $\mathbf{NH_{Ala1}}$), 8.17 (s, 1H, $\mathbf{NH_{Aib1}}$), 8.13 (s, 1H, $\mathbf{NH_{Aib2}}$), 8.08 (t, $J$ = 6.2 Hz, 1H, $\mathbf{NH_{\beta Ala1}}$), 8.02 – 7.95 (m, 2H, $\mathbf{NH_{Ala3}}$ and $\mathbf{NH_{Aib3}}$), 7.84 (d, $J$ = 5.1 Hz, 1H, $\mathbf{NH_{\mathit{Ala2}}}$), 7.73 (d, $J$ = 6.5 Hz, 1H, $\mathbf{NH_{\mathit{Ala4}}}$), 7.68 (s, 1H, $\mathbf{NH_{\mathit{Aib4}}}$), 7.69 – 7.58 (m, 2H, $\mathbf{NH_{\mathit{Tail}}}$ and $\mathbf{NH_{\mathit{\beta Ala2}}}$ and $\mathbf{NH_{\mathit{Gly}}}$), 4.48 – 4.42 (m, $H^{\alpha}_{Asp}$), 4.42 – 4.36 (m, $H^{\alpha}_{Arg}$), 4.15 – 4.08 (m, $H^{\alpha}_{Ala4}$), 4.05 (d, J = 16.5 Hz, 1H, , $H^{\alpha}_{Gly}$), 4.00 – 3.89 (m, 3H, $H^{\alpha}_{Ala1,2,3}$), 3.75 (d, $J$ = 16.8 Hz, 1H, $H^{\alpha}_{Gly}$), 3.43 (dq, $J$ = 13.6, 6.8 Hz, 2H), 3.35 – 3.26 (m, 10H, solvent residual peak and $H^{\delta}_{Arg}$), 3.23 – 3.09 (m, 3H, $H^{\delta}_{Arg}$, 2.80 (dd, $J$ = 16.5, 4.2 Hz, 1H, $H^{\beta}_{Asp}$), 2.53 (dd, J = 16.5, 5.3 Hz, 1H, $H^{\beta}_{Asp}$), 2.50 – 2.37 (m, 4H, $H^{\beta}_{\beta Ala1}$and $H^{\beta}_{\beta Ala2}$), 2.18 – 2.08 (m, 1H, $H^{\gamma}_{Arg}$), 1.92 (s, 3H, $CH_3$-acetamide), 1.83 – 1.62 (m, 3H, $H^{\beta}_{Arg}$ and $H^{\gamma}_{Arg}$), 1.55 (d, $J$ = 5.9 Hz, 6H, $H^{\beta}_{Aib1}$), 1.59 – 1.41 (m, 36H, Aib and Ala $CH_3$), 0.93 – 0.84 (m, 3H, $CH_3$-tail).

Synthesis of Ac-***β***AK(Boc)R(Pbf)R(Pbf)R(Pbf)***β***A-$(AU)_4$-$NH(CH_2)_{15}$-$CH_3$

Ac-***β***AK(Boc)R(Pbf)R(Pbf)R(Pbf)***β***A-OH (250 mg, 0.1 mmol) was dissolved in a mixture of $CH_3CN$:DMF=10:1 (4 mL) and HOAt (14 g, 0.1 mmol) and EDC·HCl (19 mg, 0.1 mmol) were added. After 10 min $H_2N$-$(AU)_4$-$NH(CH_2)_{15}$-$CH_3$ was added to the reaction mixture, and DIPEA was used to reach basic pH. The reaction was stirred overnight at 40°C. The solvent was removed under reduced pressure and the residue dissolved in DCM. The organic phase was washed with $KHSO_4$ (5%), $NaHCO_3$ (5%) and brine, dried over $MgSO_4$, filtered, and concentrated to dryness. The crude product was purified by flash chromatography to give 69 mg (0.06 mmol, 41%) of Ac-***β***AR(Pbf)GD(O$^t$Bu)***β***A$(AU)_4$-$NH(CH_2)_{15}$-$CH_3$.

MS (ESI-TOF): $[M+2H]^{2+}$ calc. for $C_{120}H_{199}N_{25}O_{26}S_3$ = 1252.2163m/z; found = 1252,7166 m/z.

$[M+3H]^{3+}$ calc. for $C_{120}H_{199}N_{25}O_{26}S_3$ = 835.1466 m/z; found = 835.4113 m/z.

Synthesis of Ac-***β***A$KR_3$***β***A-$(AU)_4$-$NH(CH2)_{15}$-$CH_3$ **(6)**

The removal of the protecting groups was obtained treating Ac-***β***AK(Boc)R(Pbf)R(Pbf)R(Pbf)***β***A-$(AU)_4$-$NH(CH_2)_{15}$-$CH_3$ with an 1:1 TFA/$CH_2Cl_2$ mixture (4 mL) at r.t. under stirring with TIPS and $H_2O$ for 2 hours. Then the solvent was evaporated, the residue washed with $Et_2O$, dissolved in MeOH, reprecipitated in cold $Et_2O$ and centrifuged

MS (ESI-TOF): $[M+2H]^{2+}$ calc. for $C_{76}H_{143}N_{25}O_{15}$ = 824.0671 m/z; found = 824.0659 m/z.

$[M+3H]^{3+}$ calc. for $C_{76}H_{143}N_{25}O_{15}$ = 549.7138 m/z; found = 549.7166 m/z.

$^{1}$H NMR (400 MHz, DMSO-$d_6$) δ 8.58 – 8.15 (m, 6H), 8.10 – 7.71 (m, 9H), 7.51 – 7.10 (m, 15H), 6.82 – 6.70 (m, 1H), 4.30 – 4.12 (m, 2H), 4.11 – 4.00 (m, 2H), 4.03 – 3.80 (m, 5H), 3.20 – 2.90 (m, 10H), 2.90 – 2.71 (m, 4H), 2.47 – 2.23 (m, 4H), 1.79 (s, 5H), 1.72 – 1.49 (m, 12H), 1.46 – 1.28 (m, 35H), 1.27 – 1.13 (m, 28H), 0.85 (s, 3H).

## References


1 Kurt Wüthrich, *NMR of Proteins and Nucleic Acids*, Wiley, 1991.

2 E. Benedetti, C. Pedone, C. Toniolo, G. Némethy, M. S. Pottle and H. A. Scheraga, *Int. J. Pept. Protein Res.*, 2009, **16**, 156–172.

3 T. Ashida, Y. Tsunogae, I. Tanaka and T. Yamane, *Acta Crystallogr. Sect. B Struct. Sci.*, 1987, **43**, 212–218.

4 P. Chakrabarti and J. D. Dunitz, *Helv. Chim. Acta*, 1982, **65**, 1555–1562.

5 Y. Paterson, S. M. Rumsey, E. Benedetti, G. Nemethy and H. A. Scheraga, *J. Am. Chem. Soc.*, 1981, **103**, 2947–2955.

6 G. Valle, M. Crisma, F. Formaggio, C. Toniolo and G. Jung, *Liebigs Ann. der Chemie*, 1987, **1987**, 1055–1060.

7 R. A. Engh and R. Huber, *Acta Crystallogr. Sect. A Found. Crystallogr.*, 1991, **47**, 392–400.

8 D. E. Tronrud and P. A. Karplus, *Acta Crystallogr. Sect. D Biol. Crystallogr.*, 2011, **67**, 699–706.

9 C. Toniolo and E. Benedetti, *Trends Biochem. Sci.*, 1991, **16**, 350–353.

10 M. Crisma, F. Formaggio, A. Moretto and C. Toniolo, *Biopolymers*, 2006, **84**, 3–12.

11 C. M. Venkatachalam, *Biopolymers*, 1968, **6**, 1425–1436.

12 C. Toniolo and E. Benedetti, *Crit. Rev. Biochem.*, 1980, **9**, 1–44.

13 C. Toniolo, M. Crisma, F. Formaggio and C. Peggion, *Biopolymers*, 2001, **60**, 396–419.

14 E. Longo, A. Moretto, F. Formaggio and C. Toniolo, *Chirality*, 2011, **23**, 756–760.

15 V. Pavone, E. Benedetti, B. Di Biasio, C. Pedone, A. Santini, A. Bavoso, C. Toniolo, M. Crisma and L. Sartore, *J. Biomol. Struct. Dyn.*, 1990, **7**, 1321–1331.

16 E. Benedetti, B. Di Blasio, V. Pavone, C. Pedone, A. Santini, A. Bavoso, C. Toniolo, M. Crisma and L. Sartore, *J. Chem. Soc., Perkin Trans. 2*, 1990, 1829–1837.

17 K. Otoda, Y. Kitagawa, S. Kimura and Y. Imanishi, *Biopolymers*, 1993, **33**, 1337–1345.

18 E. Longo, M. Crisma, F. Formaggio, C. Toniolo and A. Moretto, *Polym. J.*, 2013, **45**, 516–522.

# Conclusions

In this thesis, it was shown that a foldamer-based approach to catalyst development represents an attractive alternative to well-developed strategies involving small molecules or conventional peptides.

In summary, as reported in Chapter 2, it has been possible to obtain a short peptide foldamer that acts as a catalyst for the hydrolysis of esters and in which the esterase activity is triggered by the use of light. The reported catalyst is based on a fumaramide chromophore linking a Ser residue to a helical domain that contains within its sequence the residues His and Asp. The photoisomerization of the linker brings together a "catalytic triad", triggering esterase activity that is absent in the starting isomer. Apparently, the foldamer activity depends on the cooperative action of the hydroxyl–imidazole–carboxyl group interactions, suggesting a mechanism analogue to its enzyme equivalents. The absence of a burst phase and the high pH required to the catalytic activity suggest that the initial Ser acylation step is rate determining, while still dependent on the proximity of His and Asp residues. These results highlight the importance of the presence of both a proper three-dimensional arrangement of the catalytic moieties and a hydrophobic environment to boost the catalytic activity of synthetic catalysts inspired by hydrolytic enzymes. Further work is needed for the optimization of the local chemical environment around the "catalytic triad" to achieve better catalytic performances and broaden the applicability of the system.

Furthermore, as reported in Chapter 3, a new reductive amination approach for the synthesis of amine/amide foldameric systems has been effective in the creation of helical foldamers containing catalytic triads. This strategy makes the creation of this catalytic systems reasonably easy to perform and it could be suitable for combinatorial approaches as it does involve the formation of a "catalytic site" through a reductive amination/deprotection step between peptide fragments. We made use of helical foldamers obtained with this approach to efficiently template the C-C bond macrocyclization of a linear dialdehyde compound. Further work is needed to explore and broaden the catalytic systems generated through this approach.

On the other hand, more work is required to understand and better exploit the potential of the peptide-based multivalent catalysts explored in Chapter 4. Self-sorting from dynamic combinatorial libraries based on a peptidyl aryl-dithiol monomer showed to be a viable route to the one-pot

selective formation of a large multivalent macrocycle with a foldamer-like behaviour. Unfortunately, the foldamer showed little catalytic activity in the hydrolysis of an activated ester such as *p*-nitrophenyl acetate. Since catalysis is linked to molecular recognition, the next step of the investigation will be focused on the use of a transition-state analogue (TSA) to verify if a correlation exists between the thermodynamic amplification of library members in the presence of a TSA and the efficiency in ester hydrolysis.

The catalysts based on silver nanoparticles with modified *p*-mercaptobenzoic acid as ligands showed little but promising activity and suggested a new strategy for the development of an efficient multivalent catalytic system. Further work is needed for the development of suitable ligands to increase the performance of the system.

In the last chapter, it was presented a modular approach for the creation of supramolecular catalysts from peptide amphiphiles made mainly of Aib and L-Ala residues. The peptides were able to self-assemble producing different structures, from fibres to liposomal-like ("peptosomes") structures, depending on the nature of the polar heads. The results of these experiments allowed to gain knowledge on the self- and co-assembly behaviour of such systems and suggested new strategies for reaching the final goal. The next step will be focused on the exploration of the obtained "peptosomes" as catalytic nanoreactors and on the study of the incorporation of catalytically active monomers in the reported supramolecular structures through co-assembly.